THE FILM BOILING OF DROPS

UNDER PRESSURE

By

THOMAS ROBERT RHODES II

Bachelor of Science
Oklahoma State University
Stillwater, Oklahoma
May, 1966

Master of Science
Oklahoma State University
Stillwater, Oklahoma
July, 1967

Submitted to the Faculty of the Graduate College
of the Oklahoma State University
in partial fulfillment of the requirements
for the Degree of
DOCTOR OF PHILOSOPHY
May, 1976

THE FILM BOILING OF DROPS

UNDER PRESSURE

Thesis Approved:

Thesis Adviser

Dean of the Graduate College

PREFACE

The effects of elevated pressure on the Leidenfrost phenomenon were studied for small drops. Drop diameter histories were determined photographically for water and Freon-114. The pressure range covered reduced pressures from 1/8 to 1 for Freon-114 and atmospheric for water. The experimental results were compared to those predicted by the Gottfried-Lee-Bell model.

I am indebted to Dr. Kenneth J. Bell for not only his help and advise, but most of all, his long suffering patience. The help provided by the members of my Advisory Committee and the staff of the School of Chemical Engineering is gratefully acknowledged.

The initial support for this research was appreciatively received from the United States Army Research Office, Durham, North Carolina.

The greatest thanks are for my wife, Rita, and family whose encouragement, help, and patience made my graduate studies possible.

TABLE OF CONTENTS

LIST OF TABLES

LIST OF FIGURES

NOMENCLATURE

A_D	Area of drop, ft^2
A_P	Area of plate, ft^2
C_P	Mean heat capacity, BTU/lb ^oF
Eb	Total emissive power of a black body, BTU/hr ft^2
Eb_w	Total emissive power of the wall, BTU/hr ft^2
E_D	Total emissive power of the drop, BTU/hr ft^2
F	Configuration factor, dimensionless
F_{DP}	Configuration factor for the drop to the plate
F_{DW}	Configuration factor for the drop to the wall
F_{pD}	Configuration factor for the plate to the drop
g	Acceleration of gravity, ft/hr^2
g_c	Proportionality constant, lbm ft/lb_f hr^2
G_D	Total irradiation of the drop, BTU/hr ft^2
G_P	Total irradiation of the plate, BTU/hr ft^2
h	Heat transfer coefficient, BTU/hr ft^2 ^oF
J_D	Total radiosity of the drop, BTU/hr ft^2
J_P	Total radiosity of the plate, BTU/hr ft^2
K	Thermal conductivity, BTU/hr ft ^oF
L	Length, ft
P	Excess pressure beneath the drop, lb_f/ft^2
$P(\theta')$	Excess pressure beneath the drop at angle θ', lb_f/ft^2
q_{min}	Heat flux at the minimum temperature difference for stable film boiling, BTU/hr ft^2

q''_{net} Net heat flux, BTU/hr ft^2

Q_c Rate of heat transfer due to conduction, BTU/hr

Q_{R1} Rate of heat transfer due to radiation to the bottom of the drop, BTU/hr

Q_{R2} Rate of heat transfer due to radiation to the top of the drop, Btu/hr

R Radius, ft

R_0 Initial value of the radius at each time step, ft

R_i Value of radius used in intergration sequence, ft

t_i Time at a given step in integration routine, hr

T_{Avg} Arithmetic average of the plate and drop temperature, ^oF

T_P Plate temperature, ^oF

T_{sat} Saturation temperature of the drop, ^oF

T_W Temperature of the wall, ^oF

T Temperature a large distance from the wall, ^oF

ΔT Difference between the plate and saturation temperature, ^oF

θ Angle, radians

V* Dimensionless volume defined by Baumeister (4), dimensionless

V_r Radial velocity, ft/hr

$\overline{V}_r$ Average radial velocity, ft/hr

V_θ Angular velocity, radians/hr

W1 Mass flow rate from bottom of drop, lb/hr

W2 Mass flow rate from top of drop, lb/hr

Z Distance from plate to drop, ft

Greek Letters

α_D Absorptance of the drop, dimensionless

δ Distance from plate in vapor gap, ft

δ_1 Distance from plate in bottom of drop, ft

ε_D Emissivity of the drop, dimensionless

ε_P Emissivity of the plate, dimensionless

ε_W Emissivity of the wall, dimensionless

λ Latent heat, Btu/lb

λ' Latent heat corrected for superheat, Btu/lb

μ Viscosity, $lb_m/ft\ hr$

ν Kinematic viscosity, ft^2/hr

ρ Reflectance, dimensionless

ρ_L Density of the liquid, lb_m/ft^3

ρ_V Density of the vapor, lb_m/ft^3

σ Surface tension, lb_f/ft

Subscripts

D Drop

P Plate

Sat Saturation condition

W Wall

i Dummy subscript

0 Original value

∞ Value at ∞

CHAPTER I

INTRODUCTION

The first scientific investigation of the film boiling of discrete liquid masses was by J. G. Leidenfrost (24), a German doctor, in 1756. Leidenfrost noted that small spherical droplets formed on a hot smooth iron spoon took a relatively long time to evaporate. In his honor, the stable film boiling of discrete masses is termed the Leidenfrost Phenomenon. The surface temperature at which the minimum heat flux occurs on the pool boiling curve is termed the Leidenfrost Point.

Drew and Mueller (6) first described the similarities between the Leidenfrost Phenomenon and the pool boiling curve. Figure 1 illustrates a typical pool boiling curve (the solid line) and a typical droplet lifetime curve (the dashed line). The pool boiling curve has been discussed in detail by Drew and Mueller. However, a general description with the accepted names of each region and a brief description of their mechanisms is sufficient to illustrate the similarities.

Region I is termed the free convective regime. The heat transfer is governed by natural convection and no phase changes occur at the solid-liquid interface. Nucleate boiling occurs in Region II. This region is characterized by bubble formation at preferred sites on the hot surface and by high heat fluxes. Region III is termed the transitional film boiling regime where nucleate boiling occurs concurrently with an unstable vapor film which partly masks the hot surface. Stable

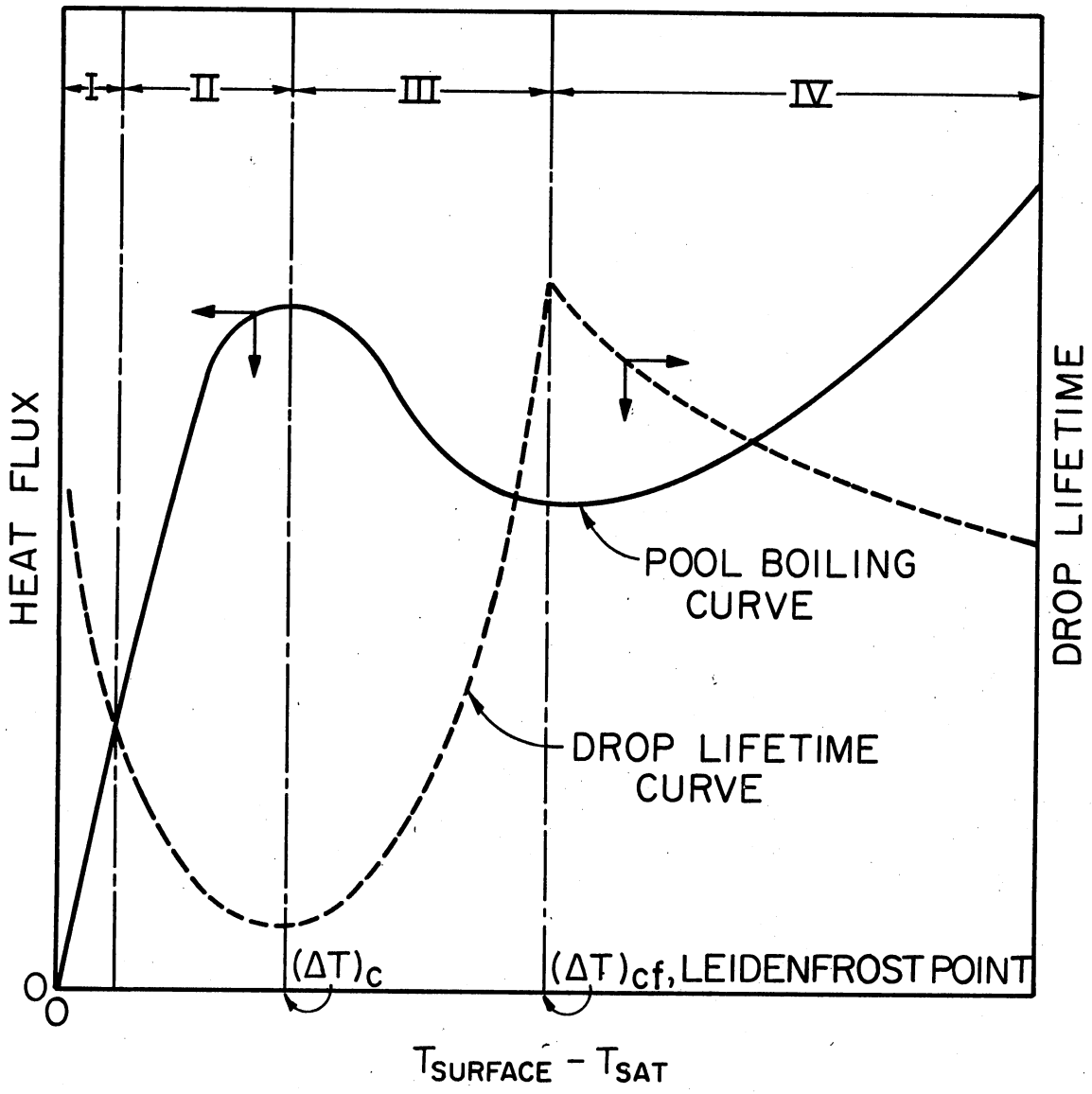

Figure 1. Typical Boiling Curves

film boiling occurs in Region IV. A vapor film separates the liquid phase from the heated surface and bubbles of vapor rise periodically through the liquid mass.

Two critical points occur on the pool boiling curve: The first critical point, $(\Delta T)_c$, is the temperature difference corresponding to the maximum heat flux and is the upper limit for stable nucleate boiling. The second critical point occurs at $(\Delta T)_{cf}$. This is the lowest temperature difference at which stable film first occurs and is termed the minimum heat flux in pool boiling. The minimum heat flux on the pool boiling curve is often called the Leidenfrost Point.

The dashed line in Figure 1 illustrates the time behavior of a drop placed on a heated surface. In the free convection regime the drop wets and spreads over the surface evaporating at the liquid-vapor interface. Due to low temperature differences the drop may take a relatively long time to evaporate. In Region II, the nucleate boiling regime, the drop receives a comparatively higher flux, hence has a more rapid evaporation rate and a shorter evaporation time. The evaporation time reaches a minimum at the point of maximum heat flux. As temperature difference increases the vapor generation at the solid-liquid interface increases and partly blankets the interface. This results in a lowered heat flux to the drop and, hence, a longer evaporation time. As the temperature difference increases to that of the Leidenfrost Point the drop and heated surface are separated by a film of vapor. Heat is conducted through the vapor film and drop slowly evaporates. The maximum lifetime of the drop occurs at this point. As the temperature difference is increased further the heat flux to the drop increases.

This is due to increased conduction and to thermal radiation. The drop lifetime decreases from the maximum at the Leidenfrost Point.

The general behavior of the lifetime curve is relatively independent of the size of the liquid mass as shown by Patel (26). The Leidenfrost Point $(\Delta T)_{cf}$ and ΔT_c for nucleate boiling are independent of mass. The lifetime of a drop is, however, directly related to the initial mass present.

The Leidenfrost Phenomenon is a special case of film boiling. If the heated surface becomes partially covered with liquid through some set of circumstances, the liquid will continue to evaporate, supported on a film of its own vapor. The excess pressure generated by vapor flow beneath the mass integrated over the bottom surface provides the force necessary for support. As a large discrete mass of liquid evaporates the mass goes through three relatively distinct regimes as seen in Figure 2. The first regime is the extended mass regime. This regime is typified by a bubbly appearnace and an amorphous shape caused by vapor bubbles breaking through the liquid. The thickness of the liquid is relatively constant where the surface is bubble free. The action of the bubble breakthrough serves to enhance the heat transfer rate. As the liquid mass evaporates further, bubble breakthrough diminishes and finally stops, and a new regime appears.

In this new regime the liquid mass becomes a recognizable drop. The shape of the drop is similar to a prolate spheroid with a flattened bottom. A characteristic sometimes observed with this regime is oscillatory behavior. The drop will vibrate to form multiple-sided geometric patterns, and will change patterns as the size decreases.

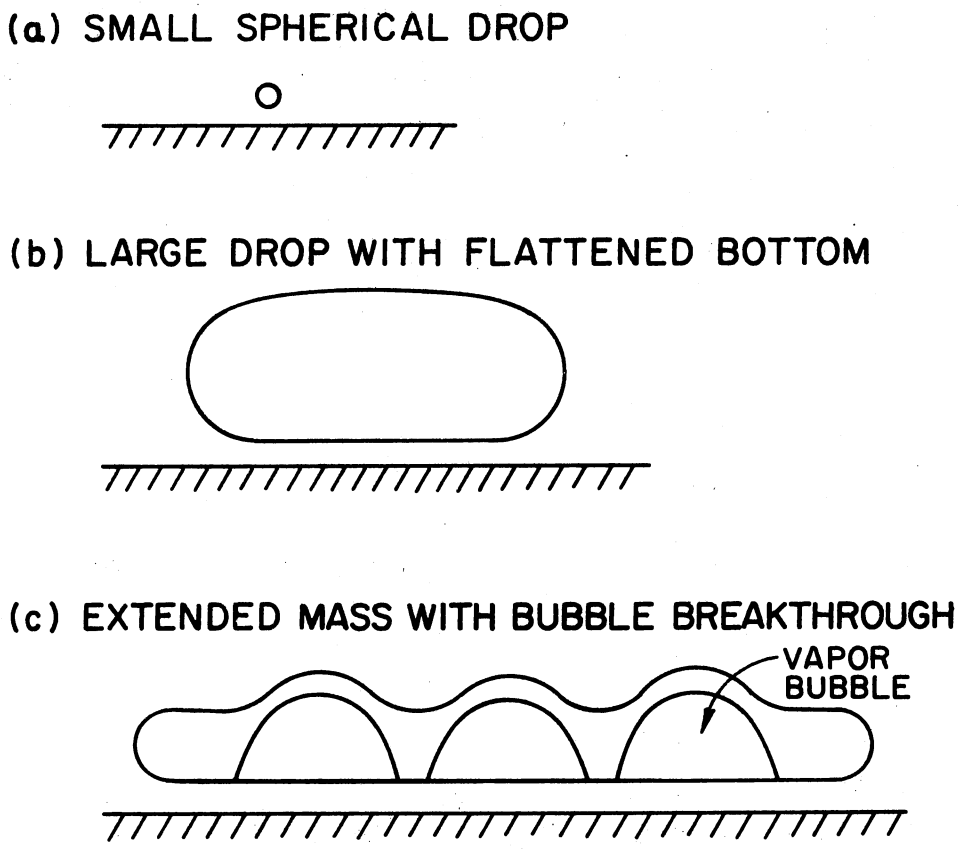

Figure 2. Drop Size Regimes

As the drop evaporates further the vibrations dampen and the drop enters its last regime.

In the last regime the drop becomes spherical in shape. The drop usually remains quiescent on the surface until the liquid has totally evaporated. However, due to perturbations in the liquid flow field beneath the drop will sometimes start dancing vertically on the heated surface, in some cases reaching heights many times its diameter. Also observed in some drops is lateral movement on the surface. Many experimenters use a heated surface with a slight depression in the center to discourage the lateral movement. As the droplet gets very small and close to the end of its lifetime it sometimes will evaporate quite explosively with a discernible popping sound.

Many investigators have studied each phase of the film boiling of discrete masses. Mathematical models and correlations have been obtained for lifetimes and heat transfer coefficients.

Purpose

The purpose of this work is to determine the effect of pressure on the film boiling of small droplets. The pressure effect is important in several applications, among which are:

1) Vaporization of fuel drops in internal combustion engines;
2) Spray and fog cooling in nuclear reactors;
3) Cooling of cryogenic equipment and transfer lines;
4) Mist flow heat transfer in boiler tubes;
5) Cooling of rocket nozzles by injection of a liquid spray.

Goals

The goal of this investigation was to experimentally determine the behavior of small drops undergoing stable film boiling under pressure. The liquids used are water and Freon-114. The study covered a pressure range from atmospheric to approximately 500 psi. specific goals were:

1) Experimental determination of droplet lifetime curves.
2) Photographic determination of droplet diameters as a function of time.
3) Comparison of the results of goals 1 and 2 to the behavior predicted by the Gottfried-Lee-Bell model.

CHAPTER II

LITERATURE SURVEY

Until recently the bulk of the boiling research was performed at atmospheric pressure. The effect of pressure on pool boiling and the boiling of discrete masses has only been the subject of recent research. Due to changing technologies more attention has been given to boiling under pressures up to and in one case exceeding the critical pressure.

Pool Boiling

In the literature there is an increasing amount of work on pool boiling under pressure. Starting with the work of Farber and Scorah (14), subsequent investigators (7, 14, 22, 31, 32) have increased the range of pressure substantially and expanded the scope to fluids other than water.

Farber and Scorah (14) studied the pool boiling of water from a series of wire surfaces, these being nickel, tungsten, chromel A, and chromel C, over a pressure from 0 to 100 psig. Their results generally indicate that the Leidenfrost Point decreases with increasing pressure, over the range of pressures and surfaces covered. They also noted that each surface material had distinctive maximum and minimum heat fluxes at each pressure studied.

Kovalev (22) investigated the minimum heat fluxes in the pool boiling of water. The author made his study on polished nichrome wires

2.0 - 2.5 mm in diameter. The point of interest is the large pressure range of the data, 1.0 - 100 atmospheres. The correlation for the minimum heat flux (q_{min}) for the range of pressures studied is:

$$q_{min} = 18.5 \times 10^3 \times p^{0.48} \text{ kcal/m}^2\text{hr} .$$

where p is the pressure in atmospheres.

Sciance and Colver (31) investigated the film boiling of methane, ethane, propane, and butane between one atmosphere and the critical pressure. The boiling occurred on a horizontal gold-plated cylinder 0.811 inches in diameter in a pool of liquid. The cylinder was heated electrically and the surface temperature was measured by thermocouples inside the cylinder. The minimum heat flux for film boiling was measured over a reduced pressure range 0.05 - 0.8. The experimental results were compared to Berenson's (10) expression for the minimum heat flux. The order of magnitude agreement was quite good. But, below reduced pressures of 0.4 the expression under-predicts the heat flux. Above a reduced pressure of 0.5 the equation over-predicts the data.

The temperature difference, ΔT_{min}, at the minimum heat flux were also measured by Sciance and Colver. These results were compared to Berenson's equation for the minimum temperature difference for stable film boiling. The minimum temperature difference peak in the reduced pressure range of 0.2 - 0.3. As will be seen, this behavior is similar to other systems.

Film Boiling of Discrete Masses

Atmospheric Pressure

Much progress has been made in the study of film boiling of drop-

lets since Leidenfrost (24) first recorded his observations. Until recently the bulk of the work on drops has been at atmospheric pressure (3, 5, 6, 16, 17, 18, 20, 21, 23, 24, 26, 30, 36). A survey by Ball (9) covers much of the literature on the film boiling of discrete masses up to 1967. Since that time investigators have studied the film boiling of LNG and cryogenic fluids (6, 19, 20, 21). The film boiling of drops under pressure has been explored only recently as discussed later.

Mathematical models and correlations of drop behavior have been proposed and tested by several authors (4, 17, 28, 36). Gottfried, Lee and Bell (17) presented a model for the behavior of small drops undergoing film boiling. Satcunanathan (28) has proposed a model applicable to flat bottomed drops. Wachters et al. (36) derived a mathematical model for the behavior of flat and concave bottomed drops. Baumeister, Hamill, and Schoessow (4) presented a generalized correlation for vaporization times of drops on a hot plate in film boiling. The correlation covers the three different regimes of drop size. However, the effect of mass transfer is neglected in the correlation. A discussion of the actual mass transfer effects follows.

Effect of Mass Transfer. The first quantitative analysis of the effect of mass transfer on droplet lifetime was described by Gottfried, Lee and Bell (17). In Chapter IV of the present work a detailed explanation of the Gottfried-Lee-Bell model is presented. Wachters (36) has presented a qualitative description of mass transfer effects for flat bottomed drops. Schoessow and Baumeister (29) have modified the work of Gottfried et al. to arrive at an a priori semiquantitative method of predicting whether mass transfer is important. A more detailed description of these works follows.

Wachters et al. (36) studied the evaporation of water drops in saturated and dry atmospheres. The studies were conducted on a concave gold plate. The drops were photographed at short intervals to study the volume and rate of change of volume as a function of time. The results of the experimental work were compared to mathematical models for the saturated atmosphere case.

Two basic drop geometries were considered in the mathematical models: a flat bottom and a slightly concave bottom. Also, included in the models was the effect of circulation within the drop. The data followed more closely the behavior predicted by the flat bottom model than the concave model. The authors' explanation was that due to vibration the concave bottomed drop had a time averaged bottom surface that was essentially flat.

In Wachters' investigation of drops boiling in a nonsaturated atmosphere, the drops evaporated much faster than in a saturated atmosphere. Thus, the evaporation rate in the unsaturated case is higher than the saturated case and therefore the heat transfer rate must also be larger than the saturated case. Wachters concludes that the distance between the drop and hot surface must be closer for the unsaturated case than in the saturated case. The evaporation rate on the top and sides of the drop must be larger than the saturated case since the total evaporation rate is larger.

Wachters reports another experiment carried out in a dry air atmosphere. The plate was cooled from a temperature above the boiling point to a value below, with the drop remaining suspended above the plate. The author's explanation was that as the plate temperature dropped below the boiling point diffusion of vapor from the bottom

surface provided the mass flow necessary to maintain the drop above the surface. The pressure gradient necessary for drop support is maintained by diffusion as opposed to bulk flow when the plate temperature is above the boiling point. Wachters points out that the plate surface must be extremely smooth for the phenomenon to occur. Otherwise, the drop will contact the irregularities of the surface and go into nucleate boiling. The authors were able to cool the plate to a temperature of 75°C in a dry atmosphere and maintain a water drop floating above the plate. Wachters (36) states

> This may be in fact occur as long as the drop temperature is higher than the wet bulb temperature associated with the surrounding atmosphere and this will be the case as long as the solid surface temperature is above that point. However, when the temperature of the solid surface is decreased below the wet bulb temperature the concentration gradient across the outer rim of the drop bottom disappears, so that the spherical state will not be maintained (pg. 932).

Due to the previous phenomenon, Wachters et al. have questioned the previous definitions of the Leidenfrost Point. Their conclusion is as follows

> Hence, it appears that the definition of a critical temperature for the occurrence of the spheroidal state is rather difficult. The best definition would be one considering the collapse of a completely quiet drop. In that case the critical temperature for the certain liquid would only depend upon the roughness of the surface (pg. 933).

Schoessow and Baumeister (29) have investigated the film boiling of water droplets evaporating in air, nitrogen, argon, helium, and steam. The tests were conducted on a stainless steel plate inside a cylindrical tank.

An expression, N_{DC}, based on the Gottfried-Lee-Bell model was derived to predict the importance of diffusion. N_{DC} is basically the ratio of diffusive mass transfer to the mass evaporated due to

conduction into the drop. The value of N_{DC} increases as the drop size decreases or as the temperature difference between the plate and the drop decreases.

The decrease in vaporization time due to the diffusion contribution agreed fairly well with the effect predicted from N_{DC}. The argon, air and nitrogen data fell close together due to the similar diffusivities of the systems. The evaporation time in a helium atmosphere was more rapid (as would be expected due to the higher diffusivity) than for the other systems studied.

Film Boiling of Drops Under Pressure

Since 1962 when Adadevoh (1) completed his work, several workers have investigated the vaporization of drops on hot surfaces under pressure, notably Temple-Pediani (33), Nikolayev et al. (26), and most recently Emmerson (13). A more detailed description of these investigations follows.

Temple-Pediani (33) investigated the lifetimes of fuel drops evaporating under pressures up to 69 atmospheres. The drop behavior throughout the boiling range at conditions above and below the critical temperatures and pressures is described. The primary interest of the investigation was the behavior of the fuel drops (n-hexane, n-hexadecane and α-methyl naphthalene) as they contacted the hot surfaces in internal combustion engines. The author also did subsidiary tests to examine the effects of the plate material on evaporation of the drops at atmospheric pressure.

The equipment used by Temple-Pediani in the study was basically similar to previous investigators. A pressure chamber held a stainless

steel disc with a depression machined in the surface to hold the drop in view during evaporation. The chamber was pressurized with nitrogen. The temperature of the disc was measured with chromel-alumel thermocouples. The disc had a surface roughness of 8 microinches. View ports were provided for illumination, motion pictures and viewing.

Temple-Pediani's results at subcritical pressures are similar to previous investigators. The drops show a minimum lifetime at temperature differences corresponding to the maximum heat flux in nucleate boiling. There is a maximum lifetime of the drop in stable film boiling corresponding to the Leidenfrost Point.

In the supercritical region the droplet lifetime falls with increasing temperature difference until the critical temperature is reached. At a surface temperature of approximately 60^{o}C above the critical for the fuels studied the drop lifetime becomes independent of further increases in surface temperature.

In the tests of surface material the aluminum and stainless steel plates had the same Leidenfrost Point. However, the fused quartz plate had a much higher Leidenfrost Point than the metal plates.

The film boiling of n-pentane and n-hexane droplets on a hot plate under pressure was studied by Nikolayev, Bychenkov and Skripov (25). The studies were conducted over a pressure range from 1 atmosphere to a reduced pressure of 0.8 in a saturated vapor atmsophere. Various plate materials were used, including copper, brass, stainless steel and aluminum.

The results of the study show that the evaporation rate for n-hexane was a maximum at a reduced pressure of approximately 0.25. The authors

did not present any evaporation rate data for n-pentane. The data presented for n-hexane was for the brass plate only.

Emmerson (13) investigated the film boiling of water drops in a nitrogen atmosphere up to a pressure of 75 psia. Included in the investigation was the effect of plate materials of different thermal diffusivities, these being stainless steel, monel and brass.

For the brass and stainless steel surfaces the temperature difference at which the lifetime of the drops was a maximum increased with increasing pressure. For a monel surface the temperature difference for maximum lifetime was almost constant over the pressure range, increasing only slightly. The maximum evaporation time was found to be substantially independent of the thermal diffusivity of the surface. Emmerson found that the experimental lifetime plate temperature data agreed closely with Baumeister's (4) correlation for vaporization times.

CHAPTER III

EXPERIMENTAL EQUIPMENT AND PROCEDURES

To conduct the experiments a test system was designed and constructed; it is shown schematically in Figure 3. The test system may be broken down into the following subsystems: the experimental cell, the inert gas pressurizing system, the temperature and pressure measuring systems, the sample injection system, and the photographic recording system.

The experimental cell was designed for operating conditions of 1000 psia and 500^{o}C. The main body and split ring were machined from 316 stainless steel forgings. The test cell lid was fabricated from 410 stainless steel plate. Detailed drawings of these parts are found in Figures 4 and 5.

A depression two inches in diameter with a slope of one degree towards the center was machined on the inside bottom of the main body to keep the droplet in sight. Five thermocouple wells were drilled to within one sixty-fourth of an inch from the inner surface of the bottom of the cell. Slots were milled from the thermowells to one side of the cell as seen in Figure 5. Holes were drilled and tapped in the side of the cell for the nitrogen inlet and outlet, sample line cooling jacket, and gas thermocouple. An O-ring groove was machined at the top of the main chamber to seal the lid. The O-ring was Parker Seal Company type 77-545 Viton-A as were the O-rings in the lid. The main body was

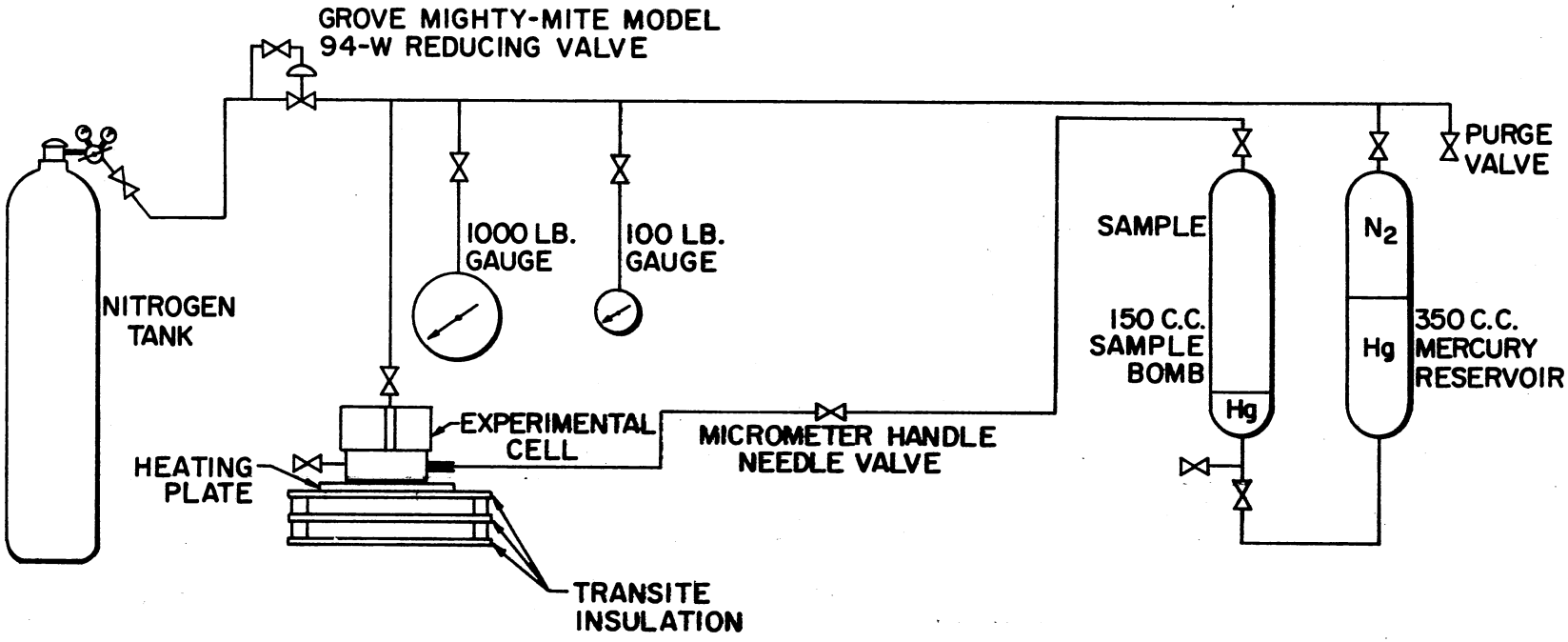

Figure 3. Schematic Drawing of Test System

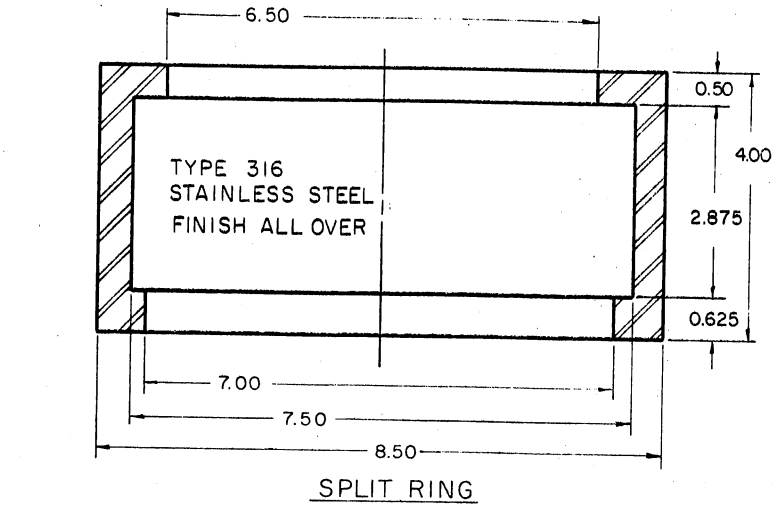

SPLIT RING

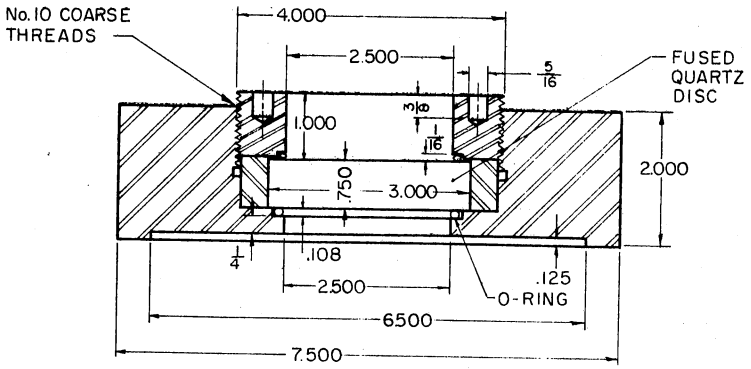

LID

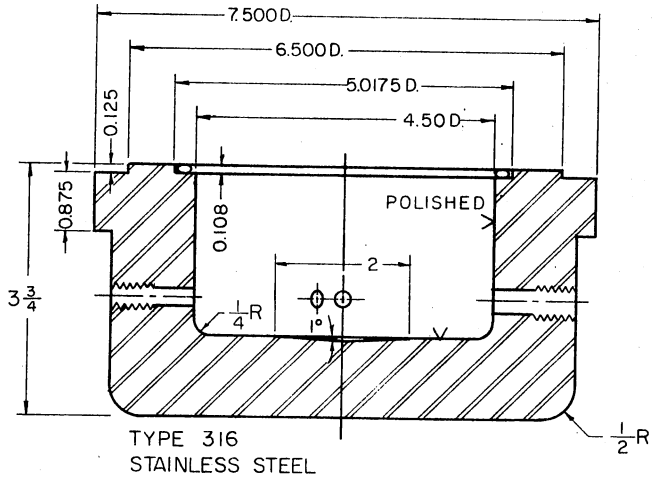

MAIN CHAMBER

Figure 4. Test Cell

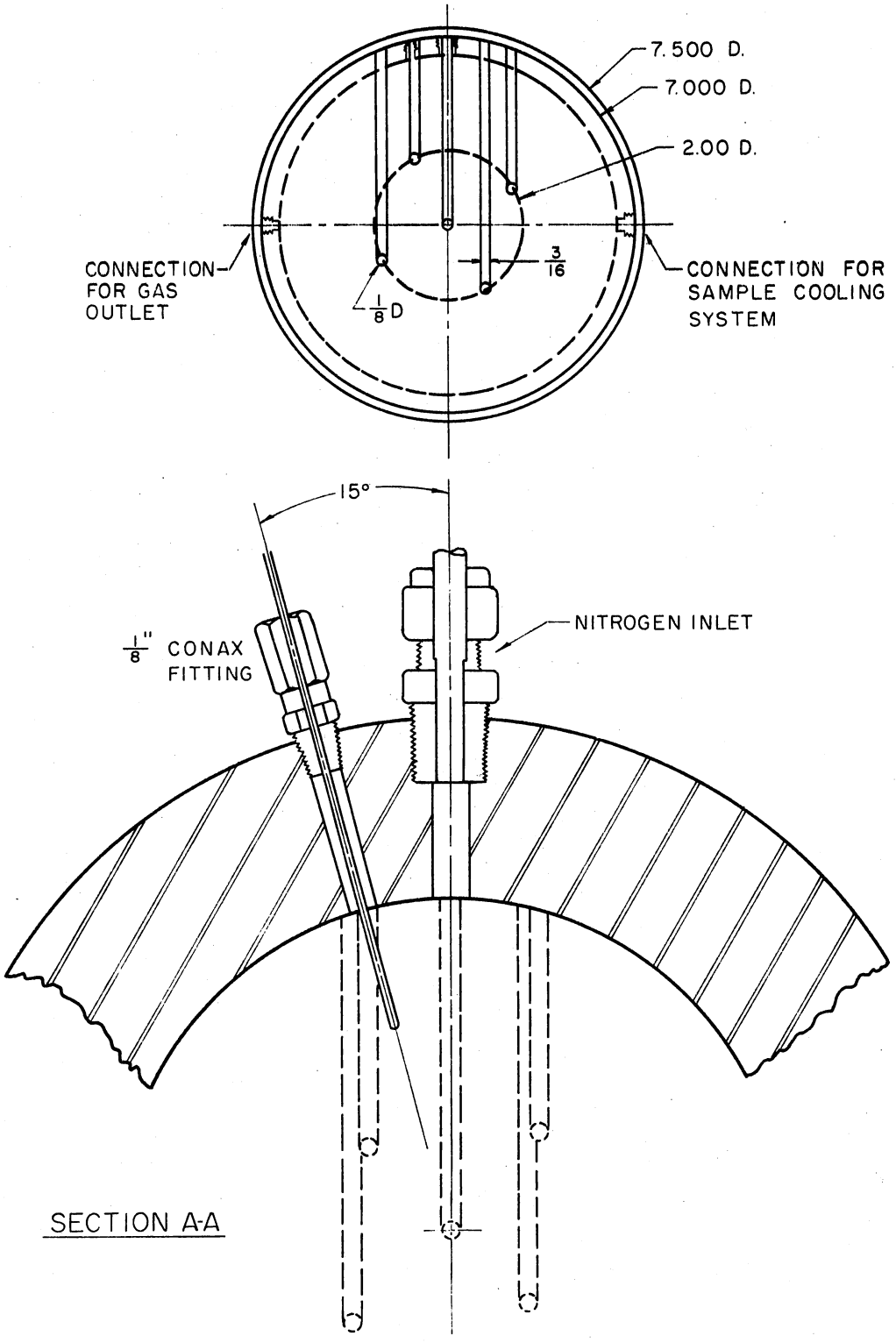

Figure 5. Detailed Views of Test Cell

originally plated with chrome, but the chrome in the test area failed by flaking and had to be removed. The metal in the area of the depression was polished to a 2-4 microinch finish as measured by a profilometer.

The entire cell was then heated in the presence of oxygen to convert the highly reflective surface of the depression to a dull golden brown oxidized surface. The oxidation left the surface as smooth as before but most importantly the area where the drop would evaporate offered good contrast for the photographic recording.

The lid also held the sight glass through which the evaporating droplets were observed. The sight glass was a fused quartz disc obtained from General Electric. The disc was pitch polished and then etched in a twenty percent solution of hydrofluoric acid. The disc was sealed in the lid by means of two Viton-A O-rings as seen in Figure 5. A steel ring was used to center the disc and to prevent the retaining nut from being screwed onto the surface of the quartz.

The split retaining ring was used to hold the lid to the main chamber. However, the O-ring must be compressed until the two halves will slide over the retaining lips. This assured a tight seal between the lid and the main chamber as long as there was no compression set in the O-rings.

The test cell was centered on two Hevi-Duty #54-KSS flat electric heating units. The units were controlled by a 20 ampere 120 volt Powerstat. To thermally insulate the bottom of the heating unit from the table three sheets of transite, separated by air gaps, were used. The top sheet had three adjustable screws for leveling the test cell.

The sample injection system was designed to prevent the sample from vaporizing while passing through the wall of the cell. The sample line,

which runs from the top of the sample bomb to the interior of the test cell, was the inside "pipe" in a double pipe heat exchanger. Swagelock tees and male connectors were used as connections for the jacket of the exchanger. A drawing of the exchanger may be found in Figure 6. The end of the sample line was tapered to accept standard hypodermic needles. To control the flow rate through the sample line so that a droplet would form slowly, a Whitey model 22RS4 micrometer handle needle valve was used. The valve was able to regulate the flow very precisely due to its small orifice diameter, 0.02 inches.

To force the liquid through the sample line, the system shown schematically in Figure 3 was used. The mercury slug was used to keep the nitrogen, which was at 10 psi higher pressure than the test cell, from diffusing into the liquid. The volume of the sample bomb was 150 cc, while that of the mercury reservoir was about 350 cc.

The inert gas pressurizing system utilized dry nitrogen to pressurize the test cell. A Matheson regulator was used on the gas cylinder for primary regulation. A Grove Mighty-Mite, model 94-SW, regulator was used as a secondary control to stabilize fluctuations in the primary regulator. To control the flow of nitrogen through the test cell a micrometer handle valve was used on the exit line from the test cell. A flow rate, as measured by a bubble flow meter, of 25 standard cubic centimeters per minute was used.

Chromel-Alumel thermocouples, 0.015 inches in diameter, were used for the temperature measurements because of their stability over the temperature range, their high voltage differential per degree, and their availability. Saureisen cement was used to hold the thermocouples in the walls and slots. The bead of the thermocouple was in contact with

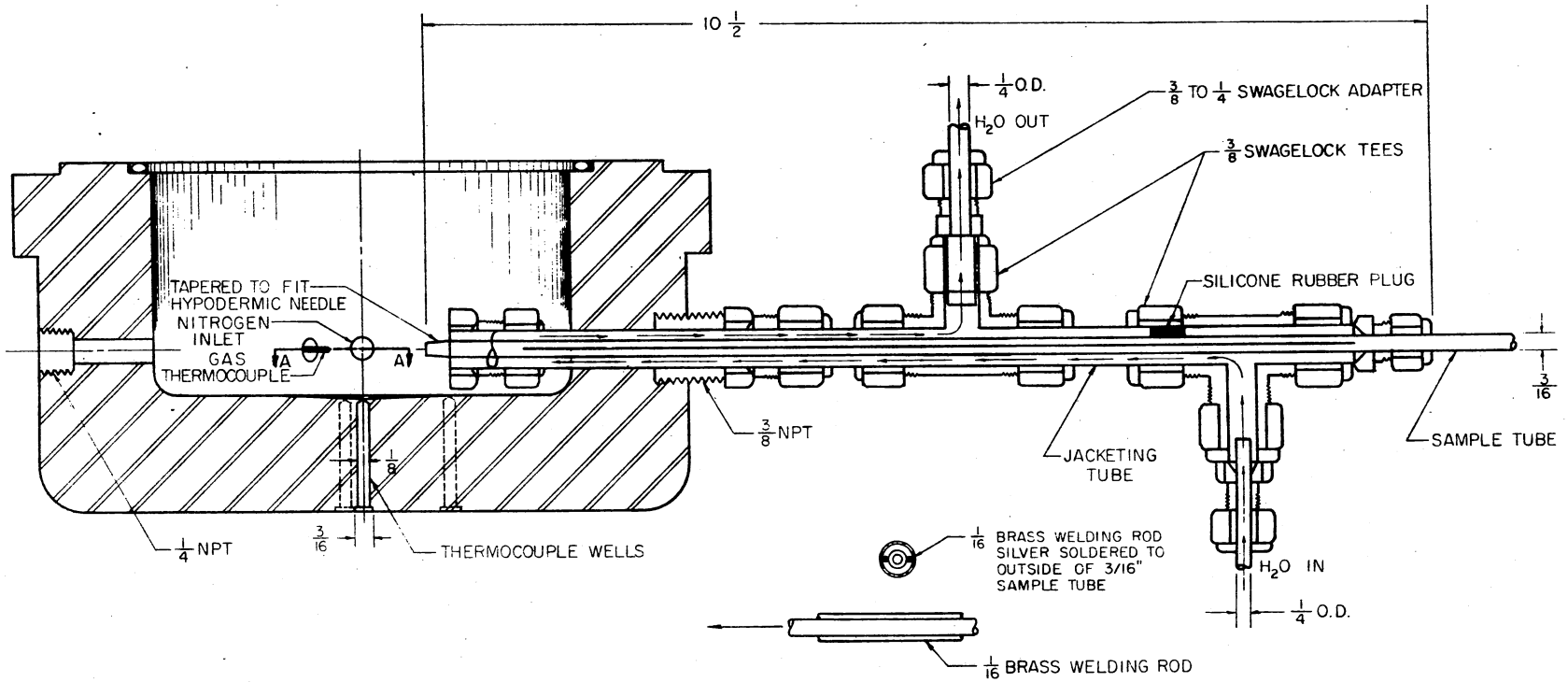

Figure 6. Cooling System for Test Cell

the metal to give a faster response time. The thermocouple was measured by a Leeds and Northrup model 8687 potentiometer in conjunction with an ice bath reference junction.

Pressure measurements were made on two gauges, a 1000 psig ACCO Helicoid and a 100 psig Marsh, for the high and low ranges, respectively. The gauges were calibrated by a deadweight tester, the results of which may be found in Appendix I.

To photographically record the data a system shown schematically in Figure 5 was used. A Bolex H16 Rex movie camera with a 50 mm lens and a 5 mm extension ring was used to film the drops during vaporization. A variable speed electric drive (12 to 32 fps) was used to maintain a constant film speed.

For observation purposes two right angle prisms in a holder were used. The movie camera was aimed into one prism while the light source and observer utilized the other prism.

The observer used a low power telescope to magnify the vaporizing drop. With the aid of the telescope the observer could actuate the control switch of the camera motor and light source.

For the protection of the observer, bullet resistant glass was installed between the observer and the experimental apparatus.

To analyze the data a Vanguard Instruments Corporation model M7-3-1 motion analyzer was used. The film from the experimental run was placed in the transport system of the motion analyzer. The image on the film is magnified and projected onto a ground glass screen. Direct measurements may be made on the projected image by means of precision moveable crosshairs. The crosshairs have essentially full range of the screen in the x and y direction and their position is read to the nearest 0.001

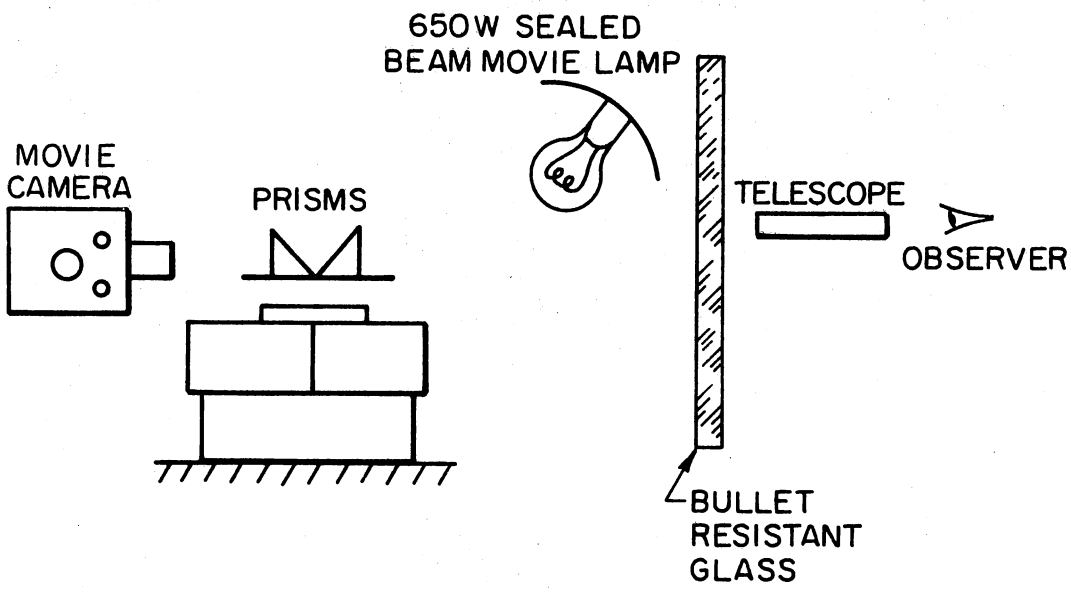

Figure 7. Schematic of Visual Observation System

inches. Measurements of the projected diameter of each drop is made for the x and y directions and averaged. The magnification of the drop image is determined from the image of a scale placed on the edge of the surface where the drop was evaporating. Comparison of the length of the projected image of the scale to the actual length gives the magnification.

The Vanguard motion analyzer also provides a direct readout of each frame number. Thus, as the film passes through the transport system, each frame may be located from the initial frame number. Knowing the frame numbers and the number of frames per second the camera was running, time intervals between each frame can be determined. Thus, from the Vanguard motion analyzer the diameter history of a drop could be reconstructed from the images on the movie film.

An analysis of the sources of error is found in Appendix M. The uncertainties associated with the drop diameter and time measurements are discussed.

Experimental Procedure

Prior to heating the test cell, the surface where the drops evaporate was cleaned with jeweler's rouge and Kimwipes, then rinsed with alcohol and dried. This procedure was necessary to insure that no foreigh material was present to interfere with a drop during its lifetime.

The mercury reservoir was pressurized to approximately 10 psi over the pressure at which the run was made. This pressure differential was found to give the best control of the formation of a droplet.

Next, the test cell was assembled, and the pressurizing nitrogen was admitted through the inlet valve. Flow of nitrogen out of the cell was regulated by a micrometer handle needle valve. The Powerstat was turned on, and the cooling media started. After the desired temperature was attained, a drop was formed on the end of the needle and allowed to fall to the surface. Prior to the drop leaving the needle the movie light and movie camera were started. After the drop evaporated, the camera and light were stopped; and the temperature read on the potentiometer. The temperature was recorded and the same procedure was repeated with another drop.

CHAPTER IV

THEORETICAL DEVELOPMENT

The development of the mathematical and physical model closely parallels the formulation of Gottfried-Lee-Bell as presented by Lee (23). The primary differences are in the analysis of the radiant heat transfer and the technique of solving the differential equation.

For the mathematical analysis of the drop, several assumptions are advantageous.

1. The drop has a spherical shape throughout its lifetime.
2. The drop is quiescent.
3. The drop is at the saturation temperathre throughout its lifetime.
4. The drop remains supported on a film of nonabsorbing/emitting vapor and does not touch the surface at any time.
5. The temperature and velocity profiles associated with the drop and vapor film are fully developed at all times throughout the history of the drop.

Several physical phemonena are postulated to occur simultaneously at the surface of the drop. On the lower half of the drop heat is conducted through the vapor film from the plate to the drop. Thermal radiation from the plate and the surroundings supplies heat to the entire surface of the drop. Molecular diffusion is assumed to occur into a stagnant medium from the upper half of the drop.

The basic philosophy of the model is to write the governing conservation equations for the physical phenomena occurring at the surface of the drop.

By applying the simplifying assumptions and the geometrical configuration shown in Figure 8 to the conservation equations, a model can be constructed to predict the lifetime and history of the drop. The following analysis is basically the same in logic and nomenclature as given by Lee (23).

Mass Balance:

$$4\pi R^2 \rho_L \frac{dR}{dT} = -(W_1 + W_2) \tag{1}$$

where W_1 and W_2 are the overall rates at which mass leaves the lower and upper surfaces, respectively. W_1 and W_2 are implicit functions of R and must be determined from the physical phenomena occuring at their respective surfaces.

Overall Heat Balance:

$$Q_c + Q_{R1} + Q_{R2} = W_1 \lambda' + W_2 \lambda \tag{2}$$

The heat balance can be written from the heat transfer model depicted in Figure 9. As heat is conducted through the vapor film the vapor in contact with the surface is superheated to the plate temperature. Thus, on the lower half of the drop part of the heat from conduction is used to superheat the vapor and part is used to provide the latent heat of vaporization, λ. λ' is the sum of these two effects.

$$\lambda' = \lambda + C_p(T_{Avg} - T_{Sat}) = \lambda + C_p(T_p - T_{Sat}) / 2 \tag{3}$$

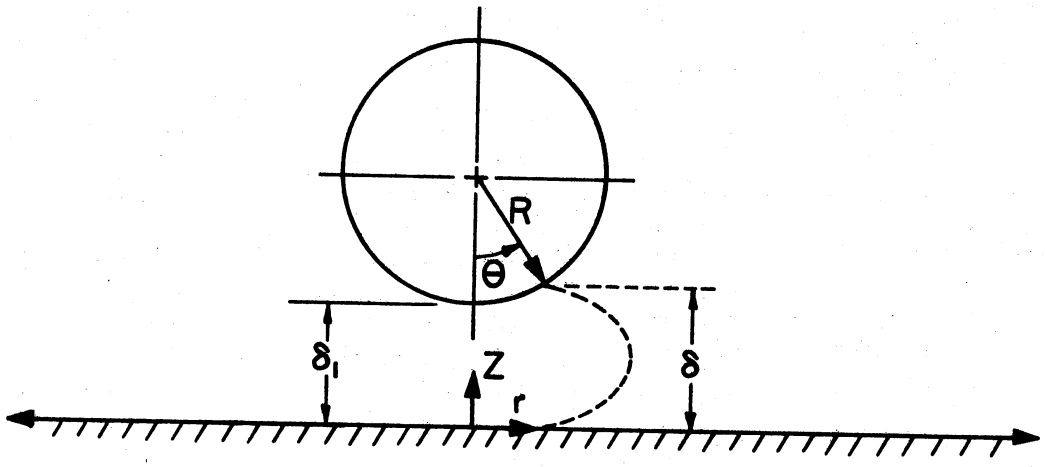

$$\delta = \delta_1 + R(1-\cos\theta)$$

$$r = R\sin\theta$$

$$dr = R\cos\theta\, d\theta$$

$$Ap = \pi r^2$$

$$dAp = 2\pi r\, dr = 2\pi R^2 \sin\theta\cos\theta\, d\theta$$

Figure 8. Geometry of Model

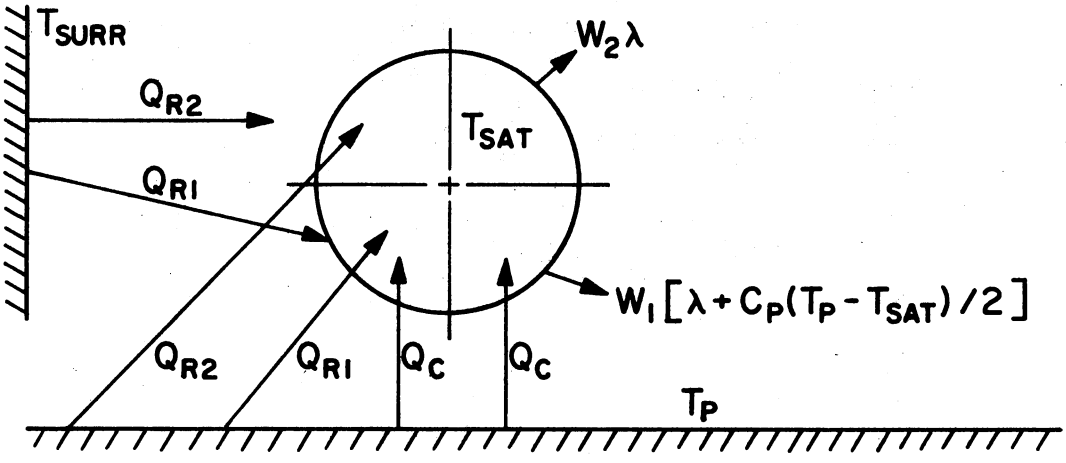

Figure 9. Heat Transfer Mechanism for the Model

Q_c is the amount of heat due to conduction through the vapor film to the bottom half of the drop. Q_{R1} and Q_{R2} represent heat inputs to the lower and upper halves of the drop, respectively, due to the thermal radiation from the plate and the surroundings. Mathematical expressions for Q_c, Q_{R1}, and Q_{R2} are derived in following sections.

Flow Field Beneath the Drop

The flow field between the drop and the heated surface provides the pressure gradient necessary to support the drop. The flow between the drop and plate is caused by the vapor generated due to heat conduction to the bottom of the drop. To analyze the vapor flow in the gas between the drop and the plate the Navier-Stokes equations (11) for a Newtonian fluid in laminar flow with constant properties can be written as follows:

Monentum Balance

r-component.

$$\rho\left[\frac{\partial V_r}{\partial t} + V_r\frac{\partial V_r}{\partial r} + \frac{V_\theta}{r}\frac{\partial V_r}{\partial \theta} - \frac{V_\theta}{r} + V_z\frac{\partial V_r}{\partial z}\right] = -\frac{\partial p}{\partial r} + \rho g_r$$

$$+ \mu\left[\frac{\partial}{\partial r}\left(1/r\,\frac{\partial (rV_r)}{\partial r}\right) + 1/r^2\,\frac{\partial^2 V_r}{\partial \theta^2} - \frac{2}{r^2}\frac{\partial^2 V_\theta}{\partial \theta^2} + \frac{\partial^2 V_r}{\partial z^2}\right] \qquad (4)$$

Z-component.

$$\rho\left[\frac{\partial V_z}{\partial t} + V_r\frac{\partial V_z}{\partial r} + \frac{V_\theta}{r}\frac{\partial V_z}{\partial \theta} + V_z\frac{\partial V_z}{\partial z}\right] = -\frac{\partial P}{\partial z} + \rho g_z$$

$$+ \mu\left[1/r\,\frac{\partial}{\partial r}\left(\frac{r\partial V_z}{\partial r}\right) + 1/r^2\,\frac{\partial^2 V_z}{\partial \theta^2} + \frac{\partial^2 V_z}{\partial z^2}\right] \qquad (5)$$

The θ component of the Navier-Stokes equations is omitted since there is no fluid motion in the θ direction or outside forces to induce such motion.

Equations (4) and (5) are too complex for solution; additional simplification is necessary. The equations may be simplified by an order of magnitude analysis as found in Appendix K.

The results of the order of magnitude analysis yield a simplified form of Equation (4) as follows:

$$g_c \frac{dP}{dr} = \mu \frac{\partial^2 V_r}{\partial z^2} \tag{6}$$

Equation (6) can be integrated with respect to Z with boundary conditions of $V_r = 0$ at $Z = 0$ and $Z = \delta$. The resulting velocity profile is

$$V_r = \frac{gc}{2\mu} \left(\frac{dP}{dr}\right) (Z^2 - \delta Z) \tag{7}$$

Mass Balance

A mass balance on the vapor flowing beneath the drop may be written for any angle θ. Consider an annulus of height δ, thickness dr, and radius r with an incompressible vapor flowing. The material balance between the limits $0 \leq r \leq R$ is

$$W_1 (\theta) = \rho 2\pi r \delta \overline{V}_r \tag{8}$$

where $\overline{V}_r$ is the average radial velocity as found by the following equation

$$\overline{V}_r = 1/\delta \int_0^{\delta} \overline{V}_r dZ \tag{9}$$

Substituting Equation (7) into Equation (9) and integrating yields

$$\overline{V}_r = \frac{\delta^2 g_c}{12\mu}\left(-\frac{dP}{dr}\right) \tag{10}$$

Substituting Equation (10) into Equation (8) and making use of the geometrical relations in Figure (7) yields

$$W_1(\theta) = \frac{\pi\rho g_c}{6\mu}\left(-\frac{dP}{dr}\right)(\delta_1 + R - R\cos\theta)^3 R\sin\theta \tag{11}$$

Equation (11) can be integrated to give the pressure distribution under the drop

$$\int_{P(\theta)}^{P(\theta')} -dP = \frac{6\mu}{\pi\rho g_c}\int_o^{\theta'} \frac{W_1(\theta)\cos\theta d\theta}{(\delta_1+R-R\cos\theta)^3\sin\theta} \tag{12}$$

where $P(\theta')$ is the excess pressure existing under the drop and $P(0)$ is the excess pressure at bottom center of the drop. Utilizing the fact that $P(\pi/2) = 0$, then $P(0)$ may be found from the following integral,

$$P(0) = \frac{6\nu}{\pi g_c}\int_o^{\pi/2} \frac{W_1(\theta)\cos\theta d\theta}{\sin\theta(\delta_1+R-R\cos\theta)^3} \tag{13}$$

Combining Equation (13) with (12) gives

$$P(\theta') = \frac{6\nu}{\pi g_c}\int_{\theta'}^{\pi/2} \frac{W_1(\theta)\cos\theta d\theta}{\sin\theta(\delta_1+R-R\cos\theta)^3} \tag{14}$$

The net upward force due to the excess pressure is found by

$$\int_{A_p} P(\theta')dAp = 2\pi R^2\int_o^{\pi} P(\theta')\sin(\theta')\cos(\theta')d\theta' \tag{15}$$

The drop has been assumed to be quiescent on the plate; thus the upward force must be balanced by the weight of the drop as given by

$$\frac{4}{3}\pi R^3(\rho_L-\rho_V)g = 2\pi R^2 \int_o^{\pi/2} P(\theta')\sin(\theta')\cos(\theta')d\theta \tag{16}$$

Simplifying (16) yields

$$R = \frac{3}{2(\rho_L-\rho_V)g} \int_o^{\pi/2} P(\theta')\sin(\theta')\cos(\theta')d\theta \tag{17}$$

Combining Equations (17) and (14) yields

$$R = \frac{9\nu}{\rho g(\rho_L-\rho_V)} \int_o^{\pi/2} \left[\int_{\theta'}^{\pi/2} \frac{W_1(\theta)\cos\theta d\theta}{\sin\theta(\delta_1+R-R\cos\theta)^3} \right] \sin\theta' \cos\theta' d\theta' \tag{18}$$

$W_1(\theta)$ is a function of R that is yet to be determined. An analysis of the heat and mass transfer processes occurring at the surface of the drop will give an expression for $W_1(\theta)$.

The mechanism for vapor generation on the bottom half of the drop may be hypothesized as being an effective heat conduction. At the angular position θ', $W_1(\theta')$ may be represented by an expression as follows:

$$\frac{d[W_1(\theta')]}{dAp} = \frac{1}{\lambda'} K_E \frac{(T_p-T_{sat})}{\delta} \tag{19}$$

Substituting the previous relation for dAp, δ and integrating gives

$$W_1(\theta') = \frac{2\pi R}{\lambda'} \int_o^{\theta'} \frac{K_E(T_p - T_{sat})\sin\theta\cos\theta d\theta}{(\delta_1/R+1-\cos\theta)}$$

$$= \frac{2\pi r\ K_E(T_p - T_{sat})}{\lambda'} \int_o^{\theta'} \frac{\sin\theta\cos\theta d\theta}{\delta_1/R+1-\cos\theta} \qquad (20)$$

The value of K_E, the effective thermal conductivity for the hypothetical heat conduction mechanism, is determined from the heat balance equation (2).

Equation (20) can now be combined with Equation (18) and give the following equation

$$R^3 = \frac{18\nu K_E\ \Delta T}{g(\rho_L - \rho_V)\lambda'} * \text{INTA}\ (\delta_1/R) \qquad (21)$$

where

$$\text{INTA} = \int_o^{\pi/2} \sin\theta''\cos\theta'' I_2(\delta_1/R, \theta'')d\theta \qquad (22)$$

where

$$I_2 = \int_o^{\theta''} \frac{\cos\theta I_1(\delta_1/R,\ \theta')d\theta}{\sin\theta(\delta_1/R+1-\cos\theta)} \qquad (23)$$

finally, where

$$I_1 = \int_o^{\theta'} \frac{\sin\theta\cos\theta d\theta}{\delta_1/R+1-\cos\theta} \qquad (24)$$

The integrals in Equations (22), (23), and (24) have been evaluated numerically by Lee (23). The results of the integrations are as follows:

INTA (δ_1/R) between the limiting values of .0198 and 11,213,855

$$\text{Ln}(\delta_1/R) = 1.383204 - .398007\text{Ln}(\text{INTA}) - .010403 [\text{Ln}(\text{INTA})]^2 + .0003547 [\text{Ln}(\text{INTA})]^3 \quad (25)$$

Integral $I_1(\delta_1/R, \pi/2)$ can be evaluated analytically as follows for all values of δ_1/R.

$$I_1(\delta_1/R, \pi/2) = -1+(\delta_1/R+1) \text{ Ln } \left(\frac{\delta_1/R+1}{\delta_1/R}\right) \quad (26)$$

The total mass flow from the bottom half of the drop may be expressed as

$$W_1 = W_1(\delta_1/R, \pi/2) = \frac{2\pi R \, K_E(T_p - T_{sat})}{\lambda'} * I_1(\delta_1/R, \pi/2) \quad (27)$$

Mass Transfer Analysis

The mass transfer rate, W_2, from the upper half of the droplet can be evaluated by the following expression given by Froessling (15):

$$\frac{K_c R}{D_{AB}} = 1.0 + .3 \, Re^{\frac{1}{2}} Sc^{\frac{1}{2}} \quad (28)$$

for mass transfer from spheres. If the surrounding atmosphere is still or nearly so, the Reynolds number, Re, vanishes and Equation (28) reduces to:

$$K_c = D_{AB}/R \quad (29)$$

which corresponds to diffusion into an infinite stagnant medium.

The mass transfer coefficient K_c can be related to the mass transfer rate W_2 by

$$W_2 = K_c(\text{mol wt})(C_s - C_\infty)A_2 \tag{30}$$

where C is the concentration of the diffusing substance. The subscripts s and ∞ refer to values at the surface and a large distance away, respectively. If the surrounding atmosphere is vapor free at infinity then $C_\infty = 0$. Substituting Equation (29) into (30) and simplifying yields:

$$W_2 = \frac{D_{AB}}{R} C_s \text{ (mol wt) } A_z \tag{31}$$

However, the molar concentration, C_s, times the molecular weight of the diffusing species is the density of the vapor, P_v, at the surface. Substituting the surface area of a hemisphere for A_2 reduces equation (31) to

$$W_2 = D_{AB}\, \rho_v\, 2\pi R \tag{32}$$

The value of the mass transfer rate due to diffusion, W_2, from the upper half of the drop can now be determined from Equation (32). The values of W_2 obtained from Equation (32) are used in the evaluation of the material and heat balances.

Conduction and Radiation Heat Transfer Analysis

The heat transfer to the lower half of the drop is by convective-conductive and radiant transport. From the analysis of these transport

mechanisms, Q_c, Q_{R1}, and Q_{R2} are evaluated for use in Equation (2).

Let q_c be the heat flux through the vapor gap beneath the drop. Assuming the conduction to be in the Z direction only, q_c is found from Fourier's Law

$$q_c = K \cdot \frac{(T_p - T_{sat})}{\delta} \tag{33}$$

or in terms of the total heat Q_c

$$Q_c = \int_{AP} \frac{K\Delta T}{\delta} dAp = K\Delta T \; 2\pi R \int_0^{\pi/2} \frac{\sin\theta\cos\theta d\theta}{(\delta_1/R+1-\cos\theta)}$$

$$= K\Delta T \; (2\pi R) \left[-1 + (\frac{\delta_1}{R} + 1) \; \text{Ln} \; (\frac{\delta_1/R + 1}{\delta \; 1/R})\right] \tag{34}$$

Radiant Heat Transfer Analysis

Due to the temperature of the plate and the walls of the test cell radiant heat transfer must be taken into account. To calculate the amount of heat input due to radiation, configuration factors for each half of the drop and the wall temperature must be determined as shown in Appendix L.

To analyze the heat input to the droplet due to radiation the following relations for the drop and the plate can be written

$$G_D A_D = J_p A_p F_{pD} \tag{35}$$

$$G_p A_p = J_D A_D F_{Dp} \tag{36}$$

where G is the total irradiation, A is the area, J is the total radiosity, and F is the configuration factor. The subscripts p and D

refer to the plate and droplet, respectively. To eliminate the areas in (35) and (36) reciprocity is used, i.e.

$$A_1 F_{12} = A_2 F_{21} \tag{37}$$

Equations (35) and (36) now reduce to

$$G_D = J_p F_{Dp} \tag{38}$$

$$G_p = J_D F_{pD} \tag{39}$$

The total radiosity, J, of the drop and the plate can be written as

$$J_p = \varepsilon_p E_{bp} + \rho_p G_p \tag{40}$$

$$J_D = \varepsilon_D E_{bD} + \rho_D G_D \tag{41}$$

where ε is the emissivity, ρ the reflectivity, and Eb is the blackbody total emissive power from the Stefan-Boltzmann equation.

The net heat flux to the drop $\dot{q}''_{net}$ is expressed by

$$\dot{q}''_{net} = \alpha_D G_D - E_D \tag{42}$$

where α_D is the absorptance of the drop and E_D is the total emissive power of the drop. Equation (42) can be rewritten in terms of J_p and the blackbody emissive power of the drop as follows

$$\dot{q}''_{net} = \alpha_D \, Fdp \, Jp - \varepsilon_D \, Eb_D$$

substituting (40) for J_p yields

$$\dot{q}''_{net} = \alpha_D \, Fdp \, [\varepsilon_p \, Eb_p + \rho_p \, G_p] - \varepsilon_D \, Eb_D$$

If ρ_p approaches zero, which is reasonable since the surface is a dark oxidized stainless steel, the preceding equation reduces to

$$\dot{q}''_{net} = \alpha_D \, F_{Dp} \, \varepsilon_p \, Eb_p - \varepsilon_D Eb_D \tag{43}$$

To obtain the emissivity of the drop, ε_D, Kirchoff's Laws can be used for a gray body in thermal equilibrium, i.e.

$$\alpha_D = \varepsilon_D$$

Thus the final form of the relation of the net heat flux to the drop of the plate is

$$\dot{q}''_{net} = \alpha_D \, [F_{Dp} \, \varepsilon_p \, Eb_p - Eb_D] \tag{44}$$

The E's can be calculated from the temperatures of the plate and the droplet and the Stephan-Boltzmann equation. F_{Dp} is obtained from the previous analysis of the configuration factors. The values of ε_p is available from Weibelt (37). The value of α_D is found from integrating monochromatic values of $\alpha(\lambda)$ as shown in Appendix D.

A similar analysis for the heat transfer between the surrounding walls of the cell and the drop can be derived. The result is similar in form to the equation (44).

$$\dot{q}''_{net} = \alpha_D \, [F_{DW} \, \varepsilon_W \, Eb_W - Eb_D] \tag{45}$$

Equations (44) and (45) can be evaluated from the temperatures of the wall and the plate, the physical properties and the geometry of the

system. The analysis for the average wall temperature as a function of the plate temperature is found in Appendix C.

Computational Scheme

From the previous analysis the final form of Equation (1) is non-linear. Due to the non-linearity an analytical solution is impossible. To solve Equation (1) numerical methods must be used.

The functional form of Equation 1 is

$$\frac{dR}{dt} = -\frac{1}{4\pi R^2 \rho_L} \quad (W_1 + W_2) * F(R_1 t) \tag{46}$$

This equation is an ordinary first order differential equation. The equation can be solved by the method of Runge-Kutta with fourth order accuracy.

The Runge-Kutta method is an explicit method so that nothing is required other than the initial values of the variables R and t. The basic method of solution is as follows:

$$F = -\left[W_1(R_o) + W_2(R_o)\right] \;/\; \left[4\pi R_o^2 \rho_L\right]$$

$$B1 = \Delta t \cdot F(R_i,\ t_i)$$

$$B2 = \Delta t \cdot F(R_i + \tfrac{1}{2}B1,\ t_i + \tfrac{1}{2}\Delta t)$$

$$B3 = \Delta t \cdot F(R_i + \tfrac{1}{2}B2,\ t_i + \tfrac{1}{2}\Delta t)$$

$$B4 = \Delta t \cdot F(R_i + B3,\ t_i + \Delta t)$$

$$R_{i+1} = R_i + 1/6\ (B1 + 2 \cdot B_2 + 2 \cdot B3 + B4)$$

$$t_{i+1} = t_i + \Delta t$$

The process is repeated for each time increment, where in the next step R_{i+1}, t_{i+1} are substituted for R_i and T_i

Computational Sequence

The computational sequence is as follows:

1) The physical properties are read and the variables initialized.

2) The heat inputs QR_1 and QR_2 are calculated. The mass loss due to diffusion, W2, is also calculated.

3) From the information obtained in step 2, equations (2), (21), and (25) can be solved simultaneously by interval halving for the dimensionless distance off the plate, δ_1/R.

4) From the value of δ_1/R calculated in step 3, the rate of mass loss from the bottom surface, W_1, can be calculated.

5) The values of W_1 and W_2 are now known from steps 4 and 2, respectively.

6) The rate of change of drop radius is calculated from W_1 and W_2.

7) The rate of change of drop radius can then be integrated over the time increment by the method of Runge and Kutta as outlined previously. The results of the integration give the new value of the radius. These results are printed out.

8) With the new value of the radius the computational sequence starting with step 2 is repeated.

9) Steps 2 through 8 are repeated until the drop evaporates.

10) Step 1 is then repeated for a new drop and set of conditions. Again the whole process is repeated.

A discussion of the results predicted by the Gottfried-Lee-Bell model compared to the experimental data are found in Chapter V.

CHAPTER V

PRESENTATION AND DISCUSSION OF RESULTS

The theoretical model can be supported by comparing the experimental data to the calculated values. Droplet lifetime and instantaneous diameters are two types of experimental data that can be compared to the calculated values. A subtle and indirect test of the Gottfried-Lee-Bell model is the effect of increasing pressure on the physical properties and the effect on the computed values.

When the plate temperature exceeded the Leidenfrost Point and the drops were in stable film boiling the diameter as a function of time could be measured photographically. The experimental results are shown with the calculated values in Figures 10 through 18 for water and Freon-114. Only selected results are shown in the following figures, the remaining results are shown in Appendices F and G.

A total of 22 water drops were studied at atmospheric pressure over range of plate temperatures from 456^{o}F to 685^{o}F. Table I gives the range of parameters for Freon-114.

The instantaneous diameter versus time behavior of water is seen in Figures 10, 11 and 12. The remainder of the graphs are in Appendix F. From the results shown in Figures 10 and 11 the model overpredicts the diameter-time relationship as compared to the experimental data at the lower temperature differences. In Figure 12 the agreement between the model and the data is considerably better.

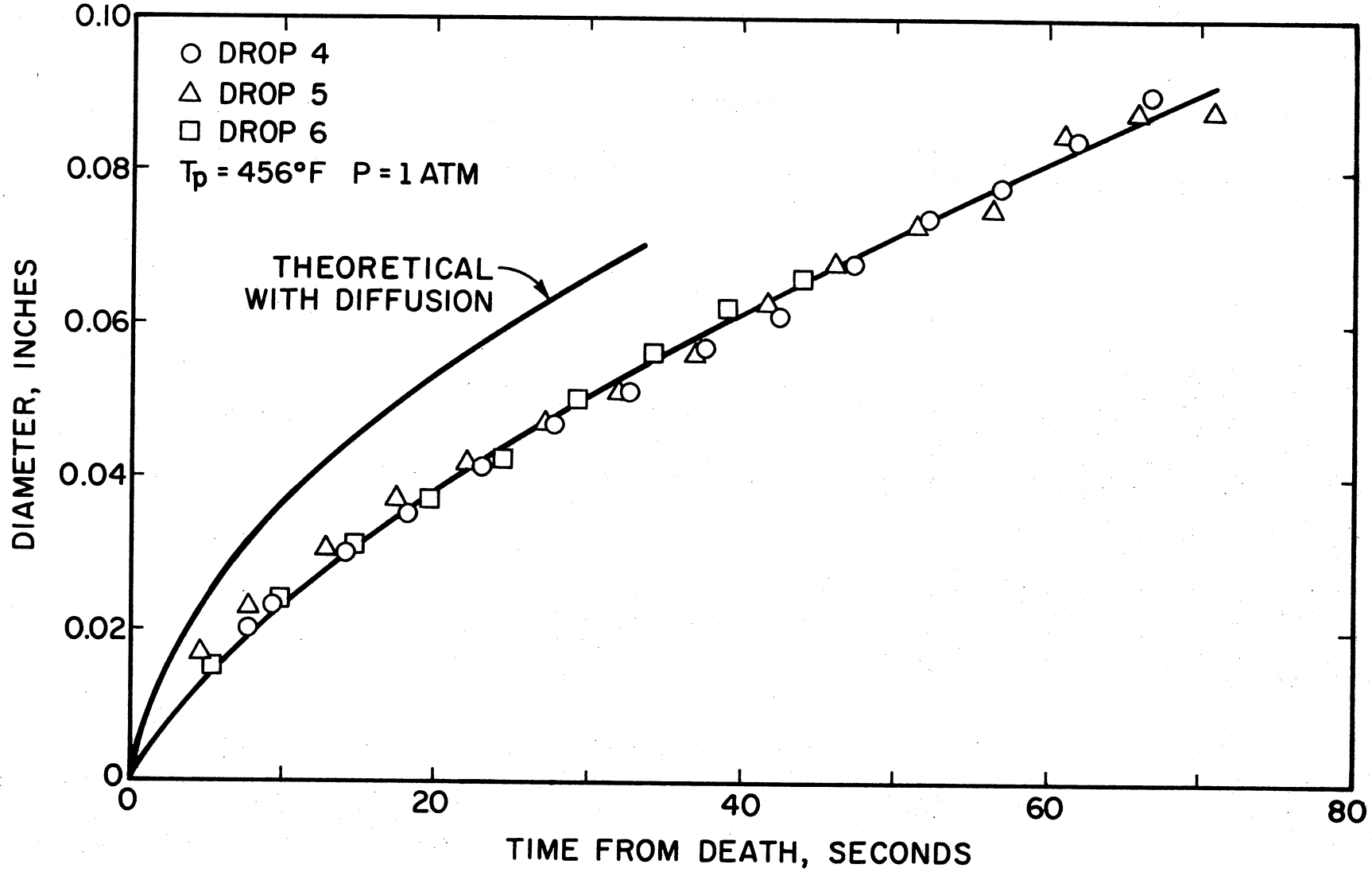

Figure 10. Water Drop Diameter History, $\Delta T = 244^{\circ}F$

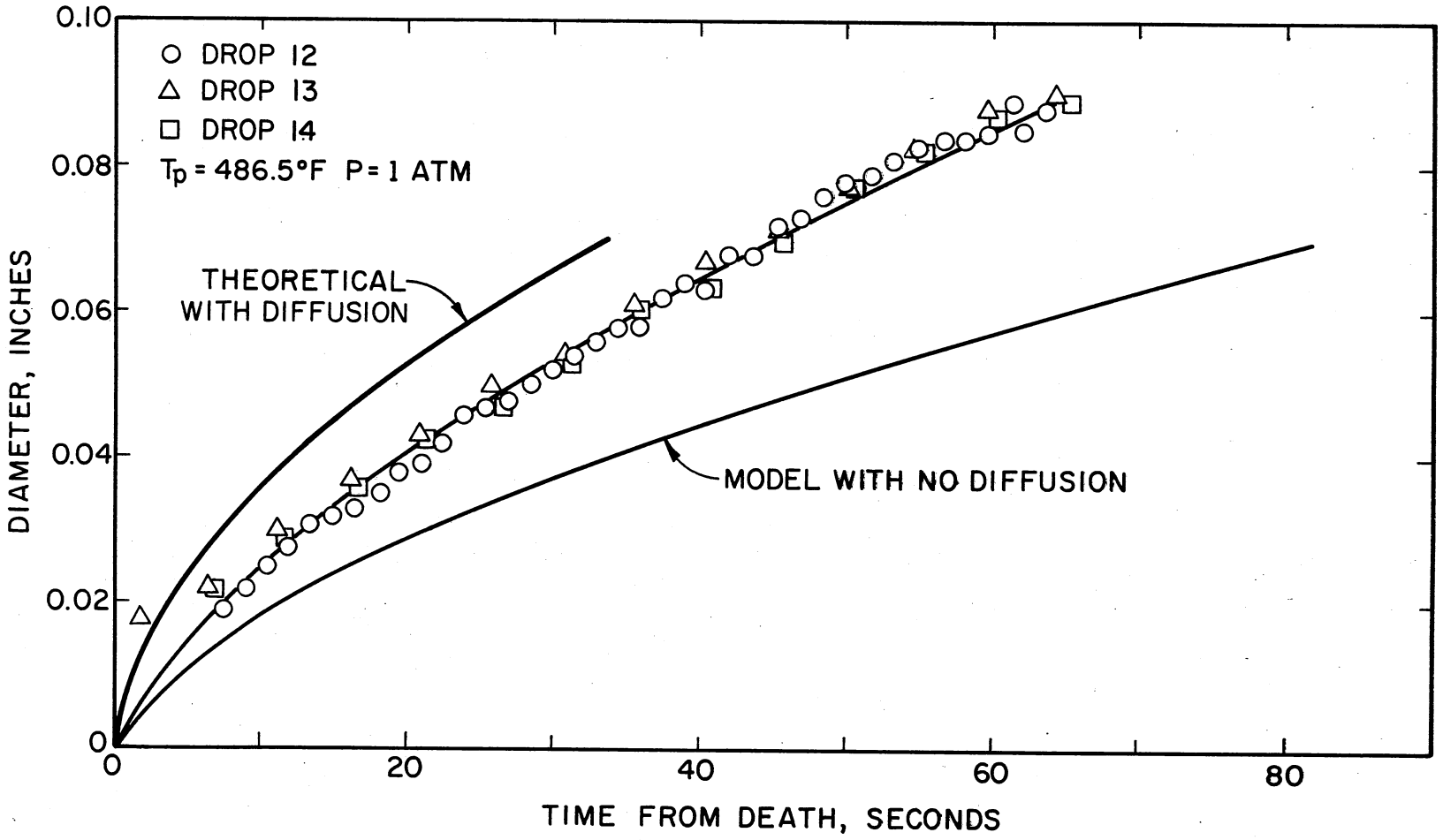

Figure 11. Water Drop Diameter History, $\Delta T = 264.5^{o}F$

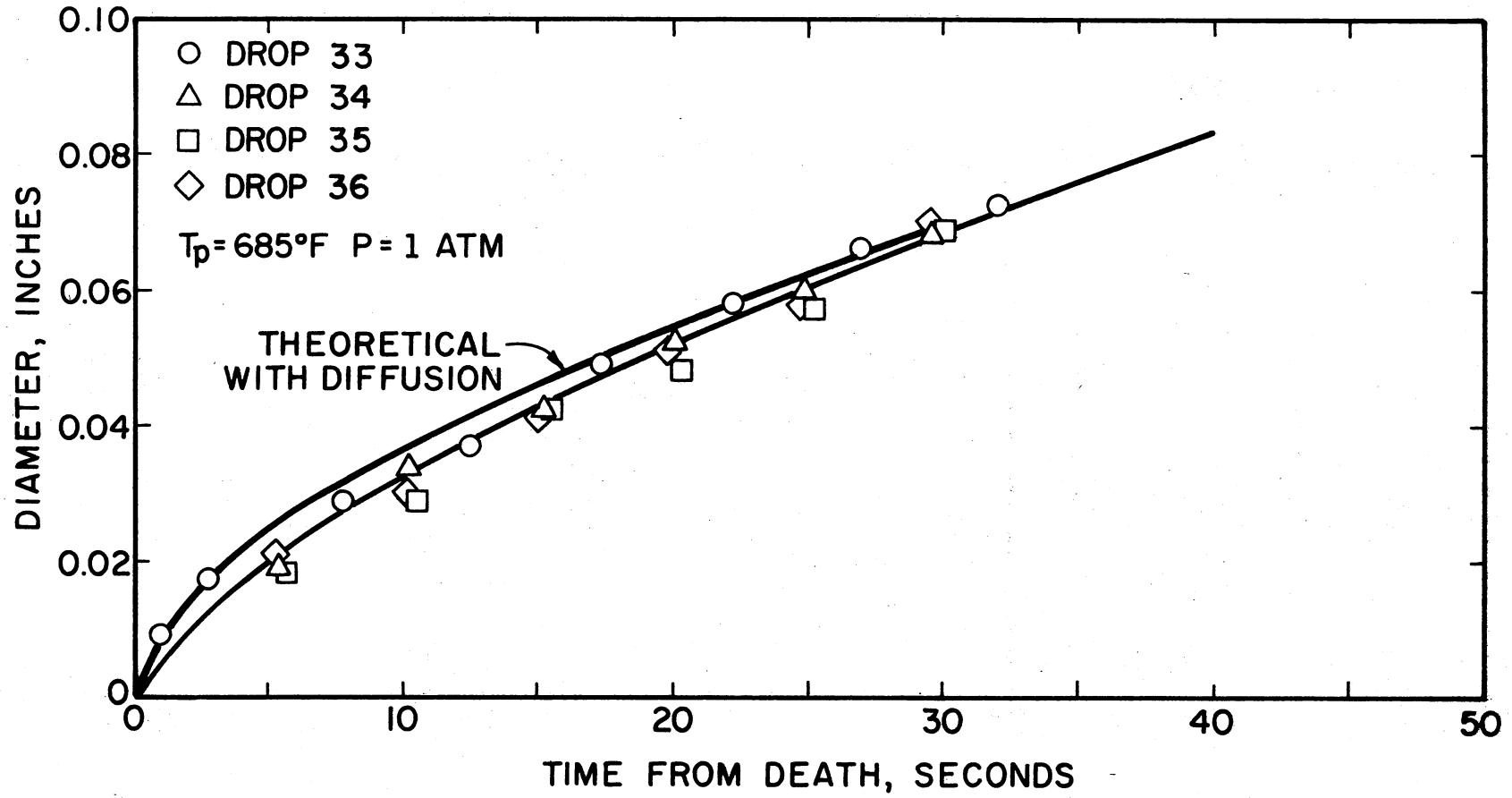

Figure 12. Water Drop Diameter History, $\Delta T = 463^{o}F$

TABLE I

RANGE OF PARAMETERS STUDIED FOR FREON-114

Reduced Pressure	Minimum Plate Temp., ^{o}F	Maximum Plate Temp., ^{o}F	Number of Drops Studied
1/8	222.8	485.6	32
1/4	257.0	524.3	31
1/3	261.5	462.2	24
1/2	279.5	516.2	40
3/4	330.8	498.2	16
1	316.4	425.0	17

The improvement at the higher temperature differences as in Figure 12 is possibly accounted for by the relative densities of steam and nitrogen. The molecular weight of water is 18 and nitrogen is 28. Thus, the nitrogen would be more dense than the steam at the same conditions. The density inversion would tend to promote the water vapor flowing up around the top half of the drop. The enshroudment of the drop would retard the diffusion process and cause longer evaporation times. As the plate temperature increases the nitrogen temperature follows, while the steam temperature remains constant. The nitrogen is less dense at the higher plate temperatures than at lower temperatures; thus the density inversion disappears. The water vapor no longer enshrouds the upper surface, diffusion occurs more readily, and the model and data come closer in agreement. The effect of removing the

diffusion term from the model is seen in Figure 11. As expected the data fell between the two limits, giving plausibility of the previous explanation.

From instantaneous diameter versus time behavior of Freon-114 is shown in Figures 13 through 18. The remainder of the data is shown in Appendix G. At the lower reduced pressures - 1/8, 1/4, 1/3, and 1/2 - the model tends to slightly underpredict the diameter history of the drops undergoing film boiling. At a reduced pressure of 3/4 the underprediction becomes more pronounced. The trend, however, reverses at Pr = 1. The model overpredicts the diameter-time relationship. A possible explanation of the discrepancy between the model and the data at high pressure may lie in the physical properties. Most of the physical properties are based on low pressure data. The properties have been extended to high pressures where the validity of the extension becomes quesionable, especially in the critical region. Thus, variances from the actual values may cause significant changes in the predicted behavior of droplet diameter history.

From the instantaneous diameter versus time curves crossplots of droplet lifetime versus temperature difference were made. These plots were constructed by picking a starting diameter and finding the drop lifetime at each plate temperature. The intersection of the horizontal line from the initial diameter with the experimental and computer curves gives the corresponding points on the lifetime curves at that particular plate temperature.

For water at one atmosphere the lifetime vs. temperature difference behavior is shown in Figure 19. As can be seen from the figure the agreement between theory and experiment is poor at the lower temperature

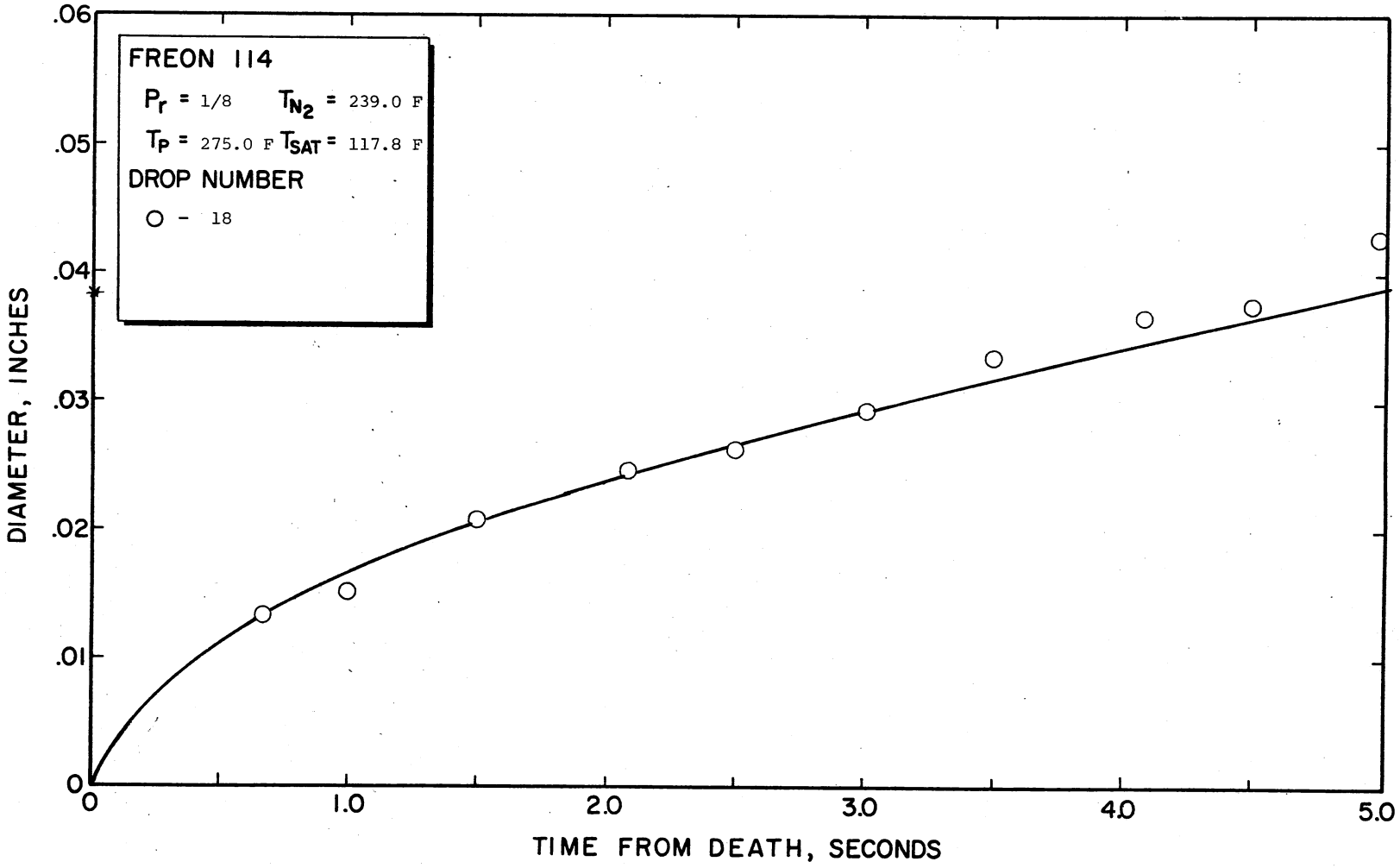

Figure 13. Freon-114 Drop Diameter History, P_r = 1/8, ΔT = 157.2°F

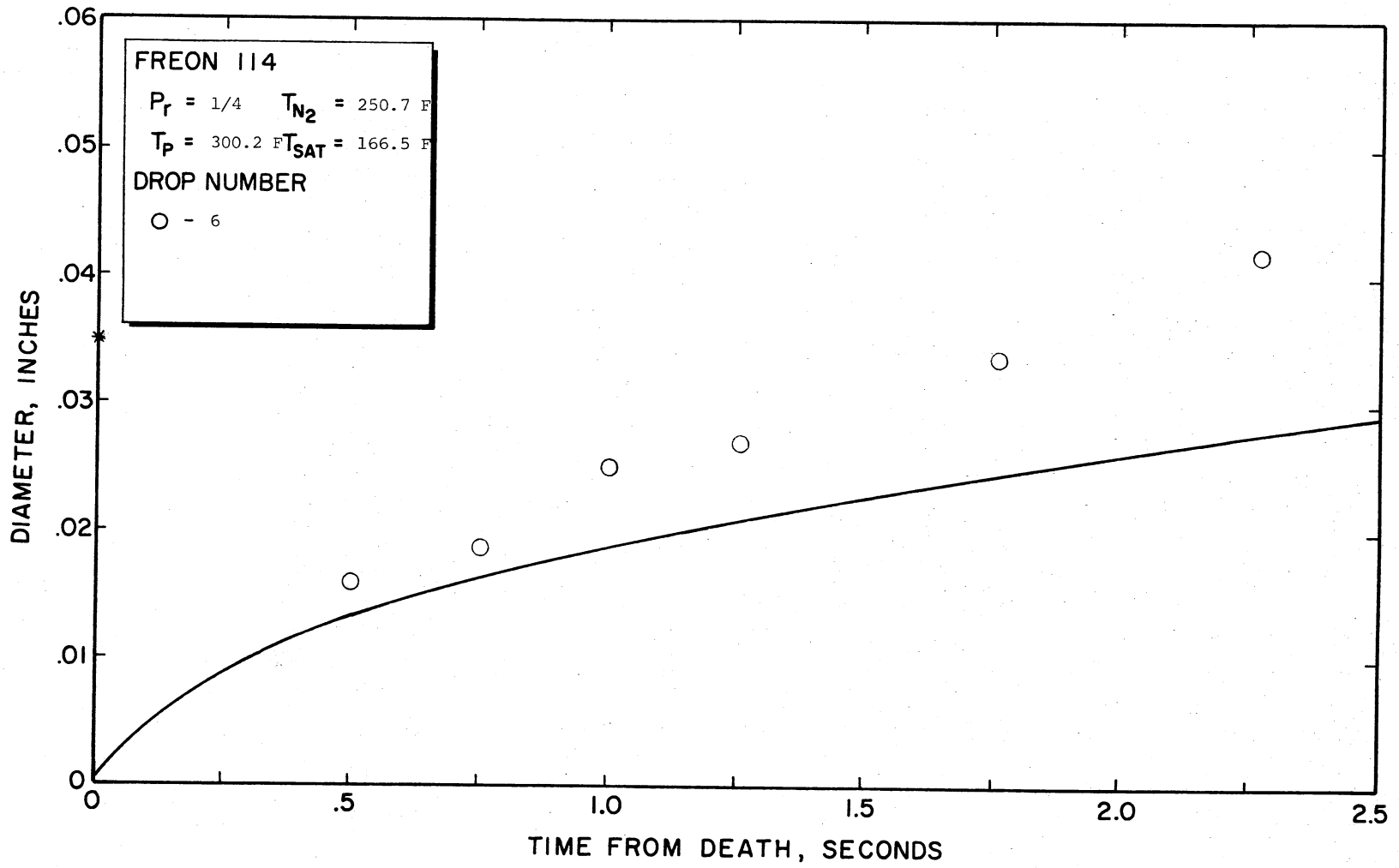

Figure 14. Freon-114 Drop Diameter History, P_r = 1/4, ΔT = 133.7°F

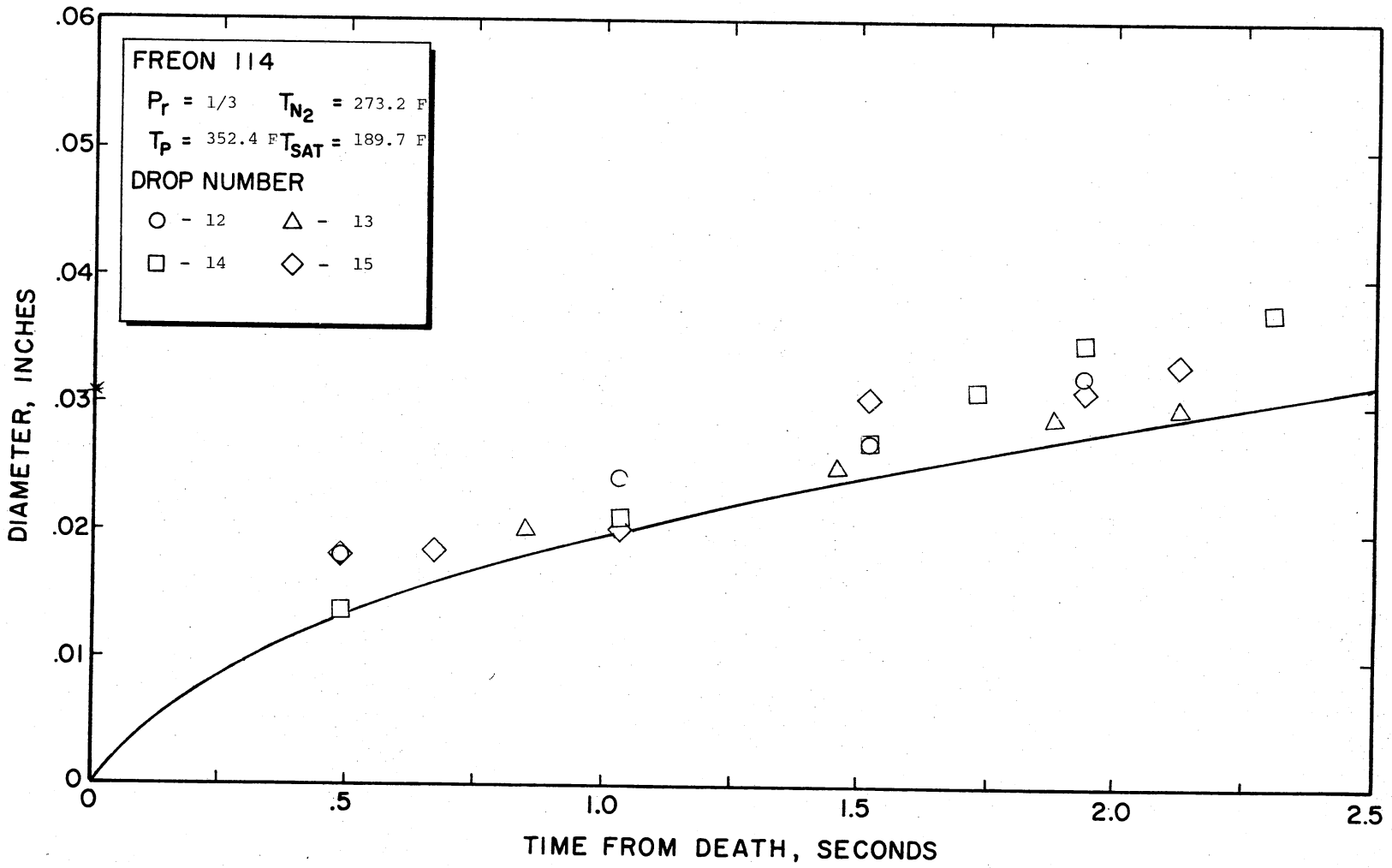

Figure 15. Freon-114 Drop Diameter History, P_r = 1/3, ΔT = 162.7°F

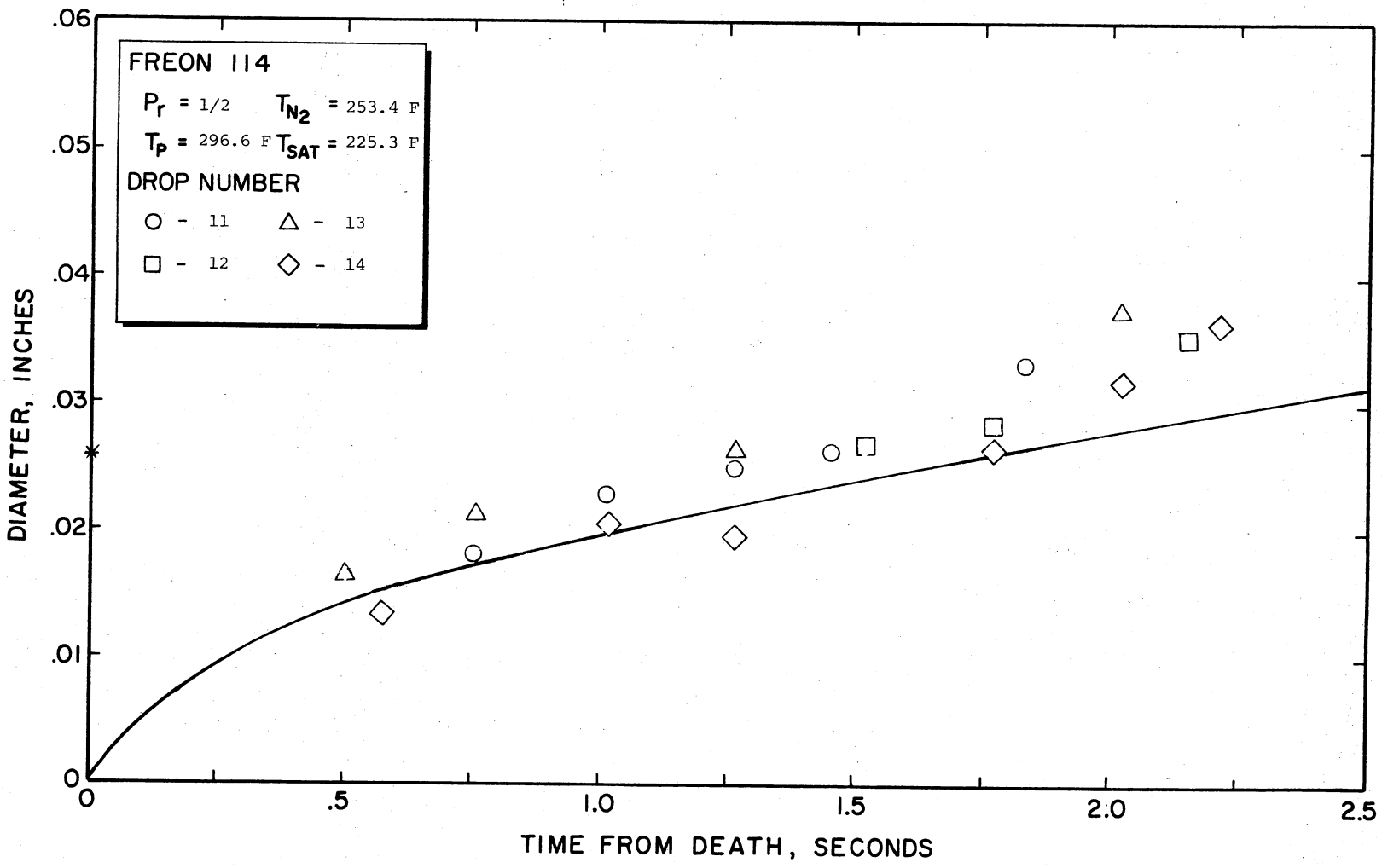

Figure 16. Freon-114 Drop Diameter History, P_r = 1/2, ΔT = 71.3°F

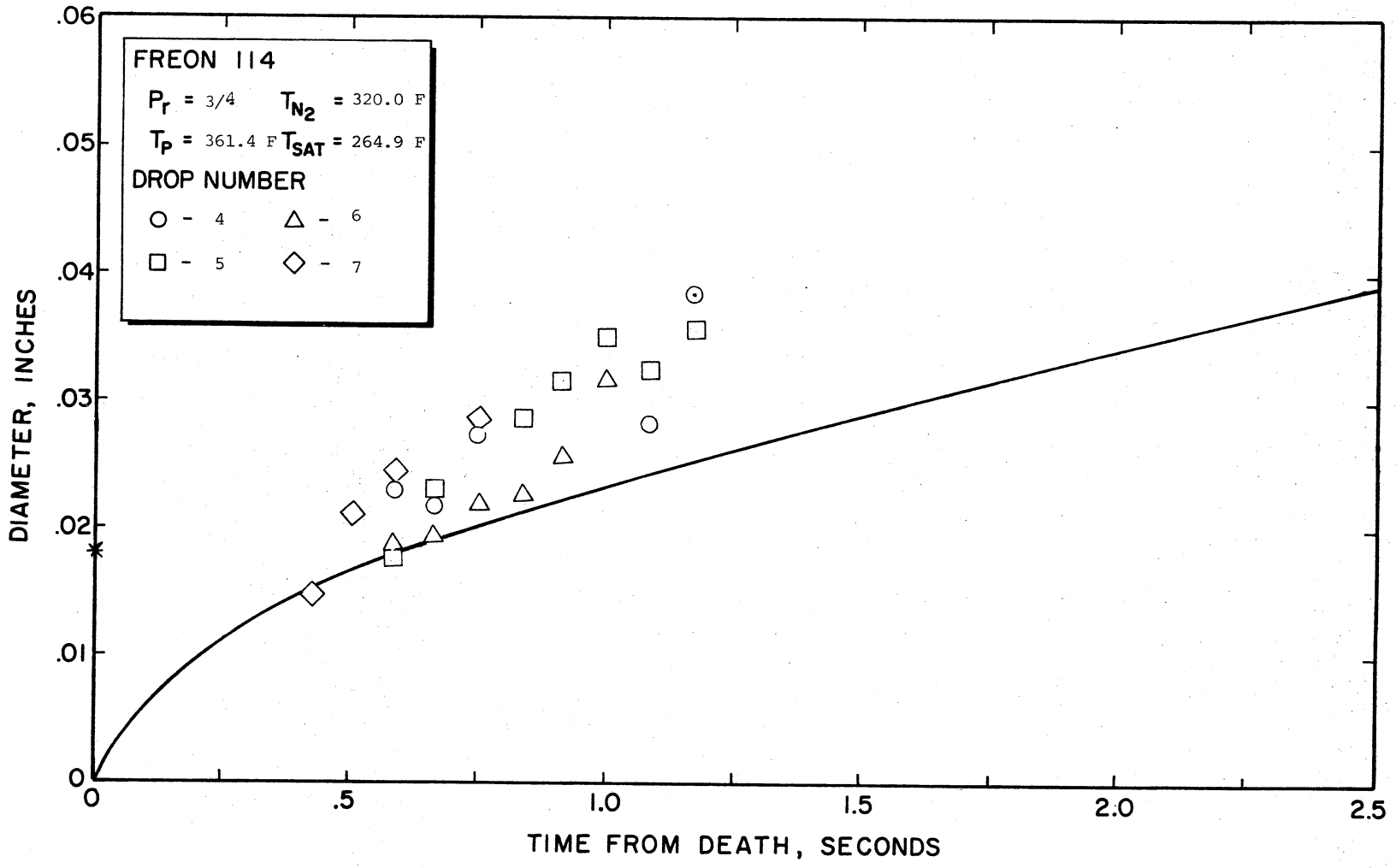

Figure 17. Freon-114 Drop Diameter History, P_r = 3/4, ΔT = 96.5°F

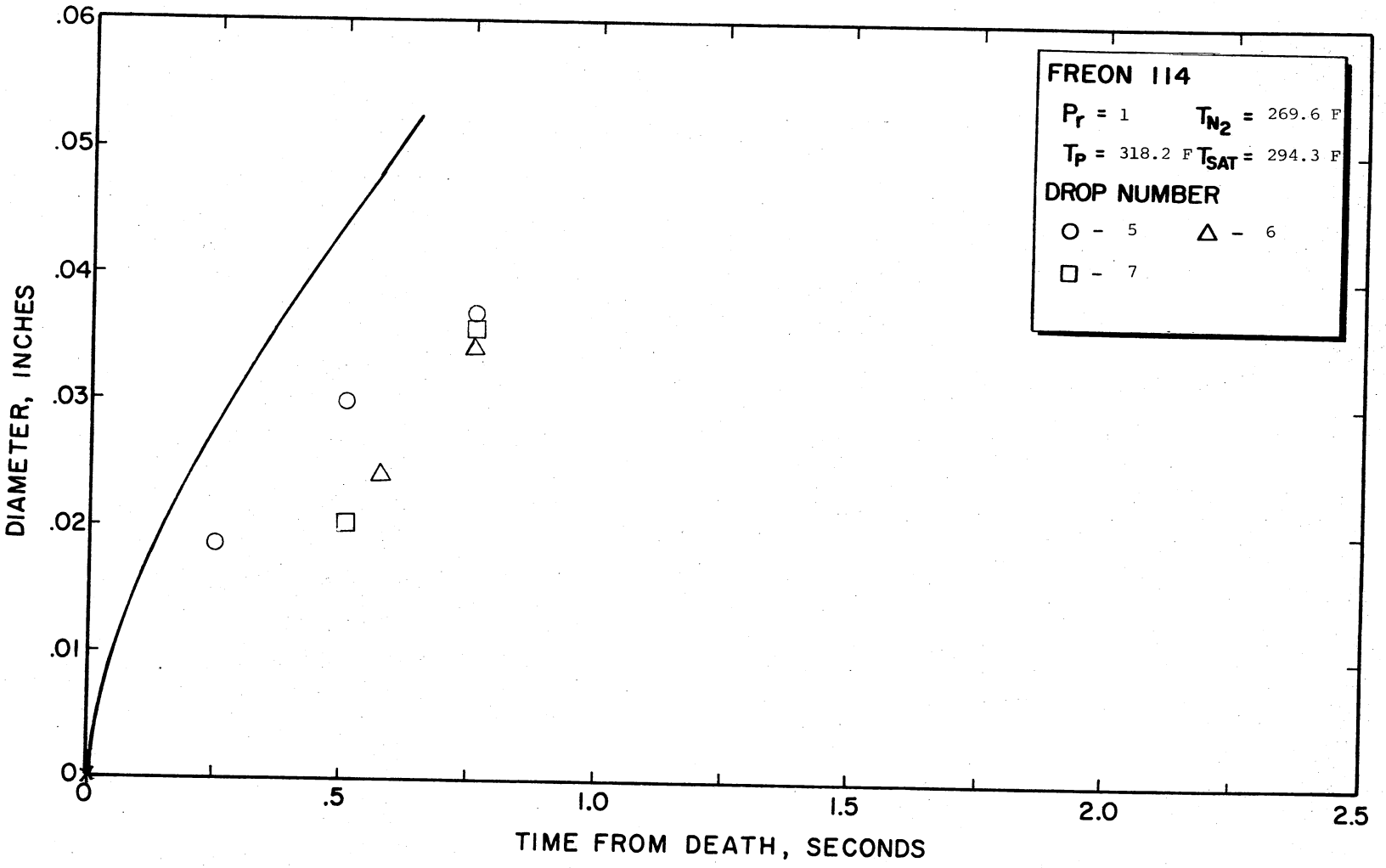

Figure 18. Freon-114 Drop Diameter History, $P_r = 1$, $\Delta T = 23.9^{o}F$

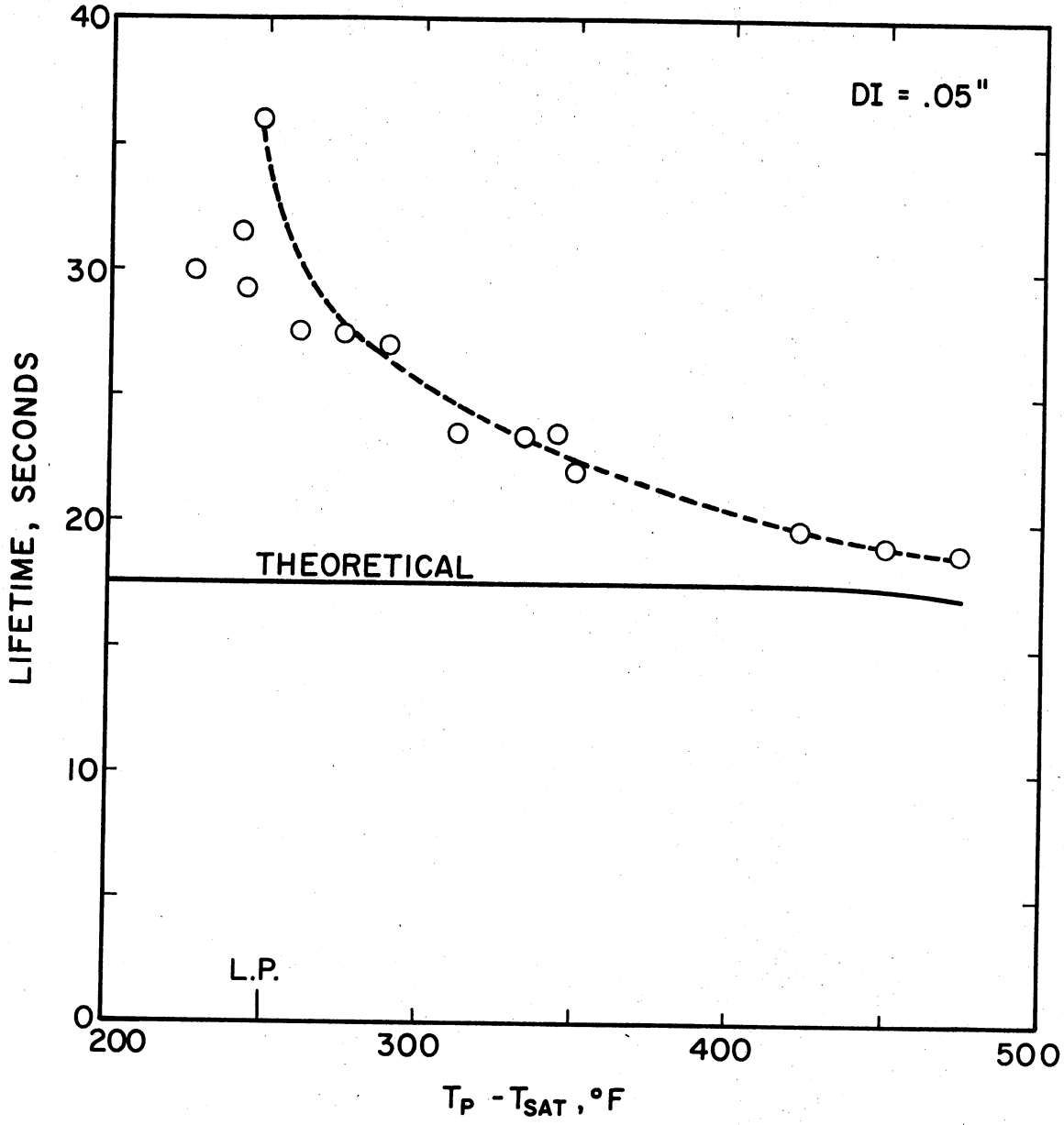

Figure 19. Water Drop Lifetime Curve

differences. At the upper temperature differences the agreement comes to within five percent. The behavior predicted by the model at the lower temperature differences is possibly caused by the density inversion as previously outlined.

The lifetime versus temperature difference behavior of Freon-114 drops is shown in Figures 20 through 25. The range of reduced pressures studied is from 1/8 to 1. The overall agreement between the experimental data and the model at reduced pressures of 1/8, 1/4, 1/3, and 1/2 is good. There is a tendency to overpredict the evaporation time at the higher temperature differences at reduced pressures of 1/4 and 1/3. At a reduced pressure of 3/4 the model substantially over-predicts the drop lifetimes. The opposite behavior occurs at $P_r = 1$. The model underpredicts substantially the drop lifetimes. In either case the data and model are not off by more than a factor or two. The explanation of this behavior probably lies with the prediction of the physical properties. Figure 26 shows the drop lifetime behavior for Freon-114 as a function of reduced pressure. The curves shown are those predicted by the model. As seen in the figure the lifetime curves decrease with increasing pressure.

Figure 27 shows the Reynolds number history of Freon-114 drops at various reduced pressures. The plate temperatures are maximum values from each experimental run. The maximum value of the Reynolds number was at a reduced pressure of 1 where the value was approximately 22. This is the highest value predicted by the model and is justification for the assumption of laminar flow in the gap between the drop and the plate. Turbulence would not be expected to be present except at Reynolds Numbers two orders of magnitude larger.

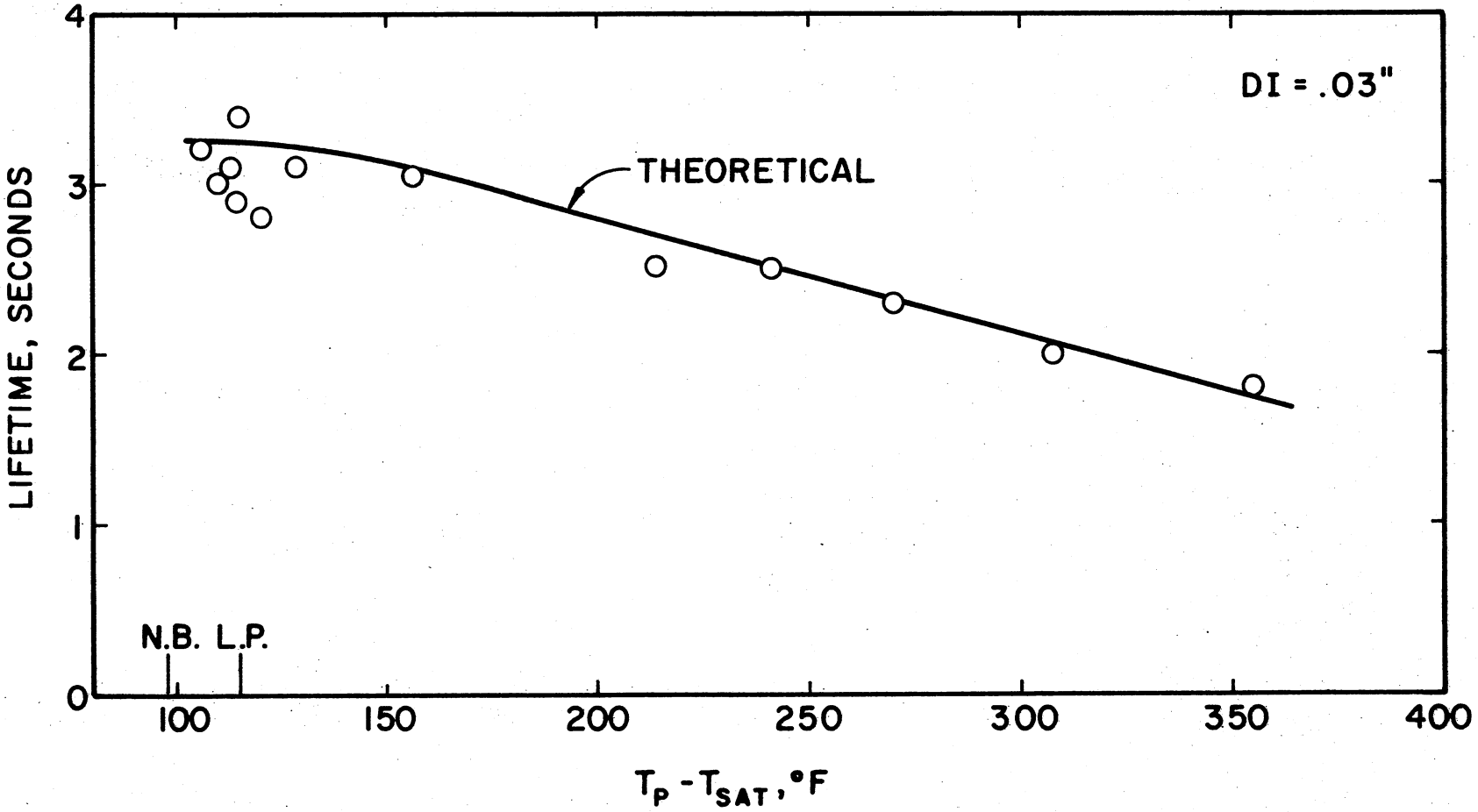

Figure 20. Freon-114 Drop Lifetime Curve, $P_r = 1/8$

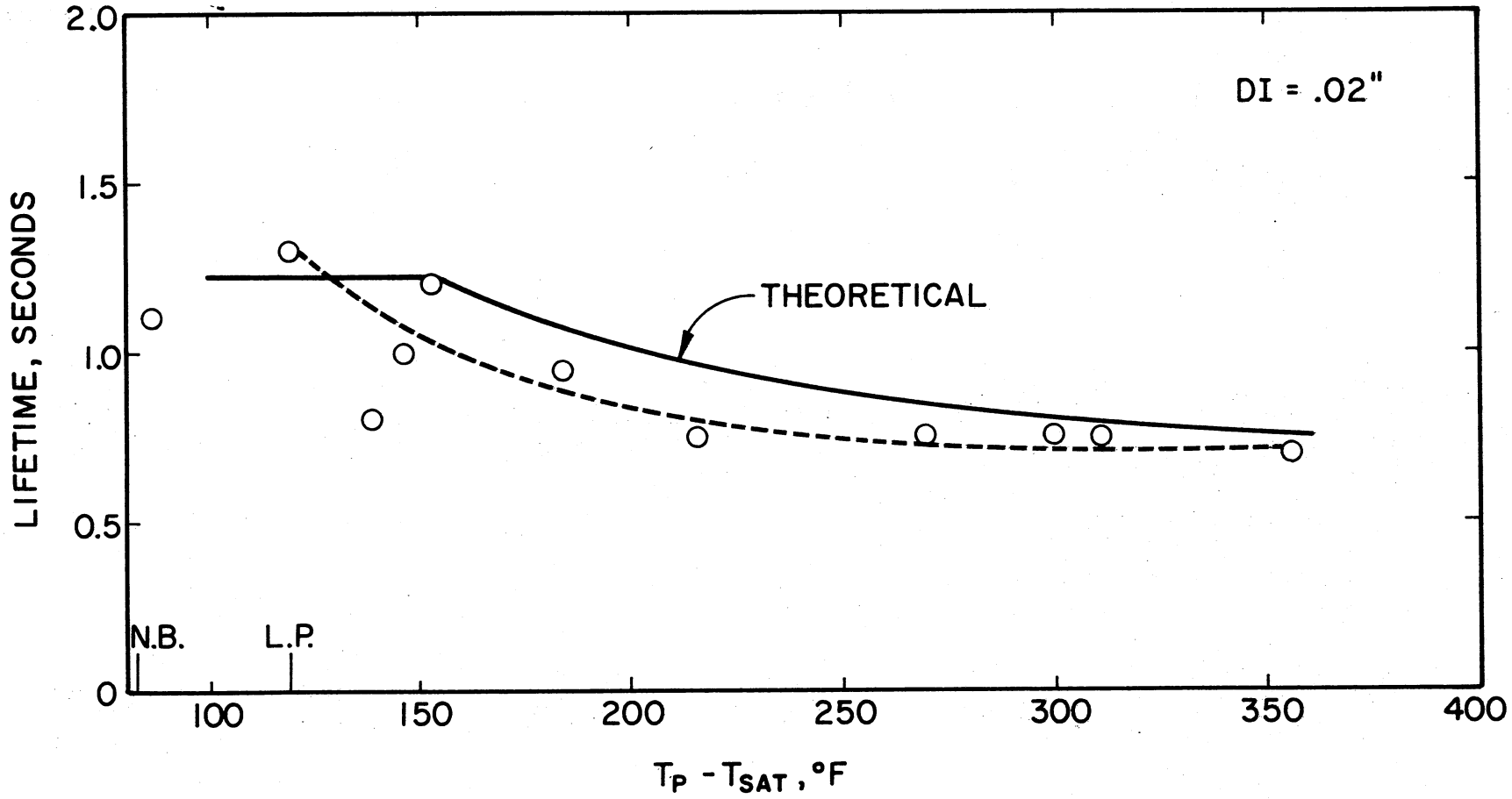

Figure 21. Freon-114 Drop Lifetime Curve, $P_r = 1/4$

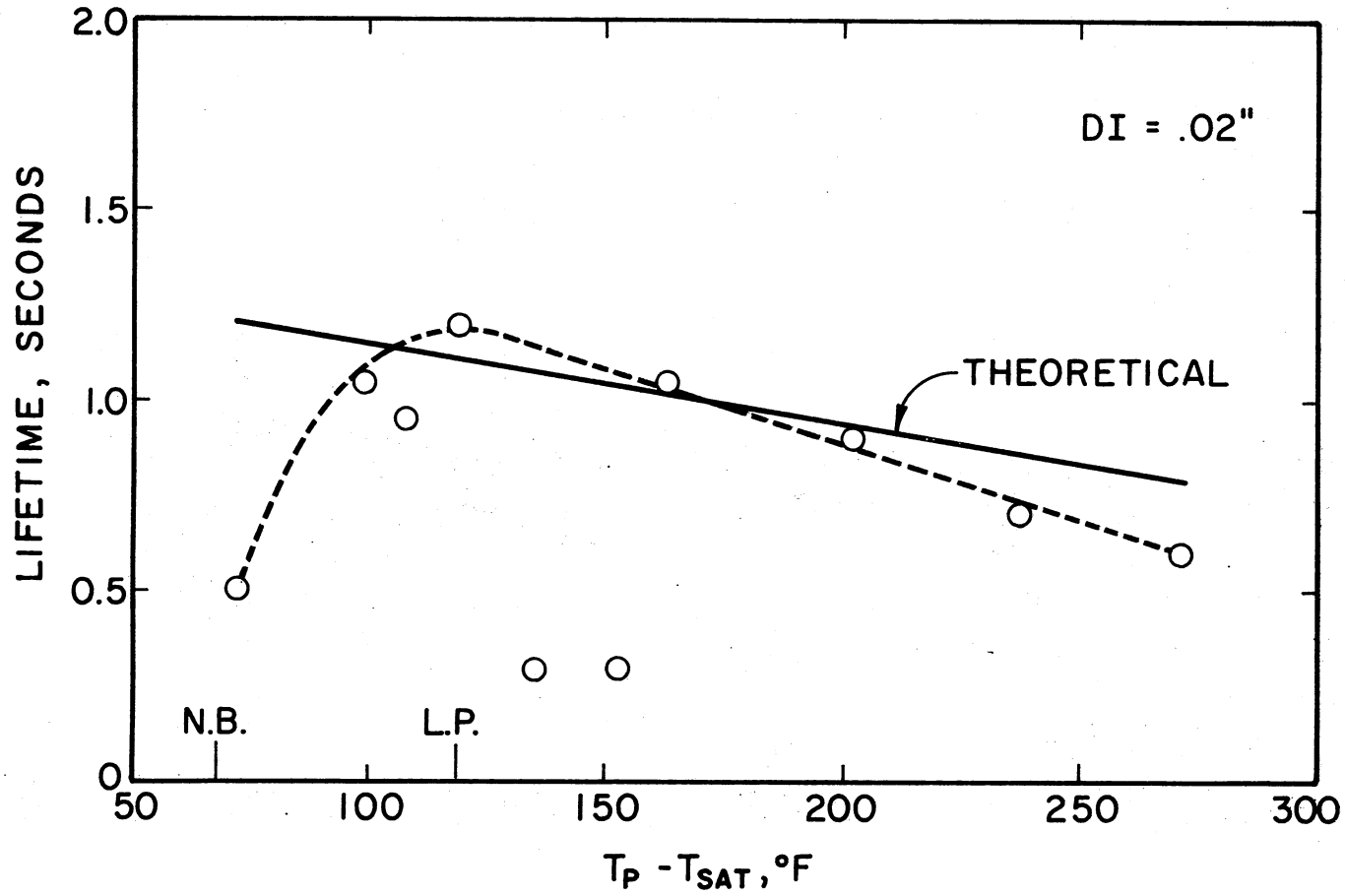

Figure 22. Freon-114 Drop Lifetime Curve, P_r = 1/3

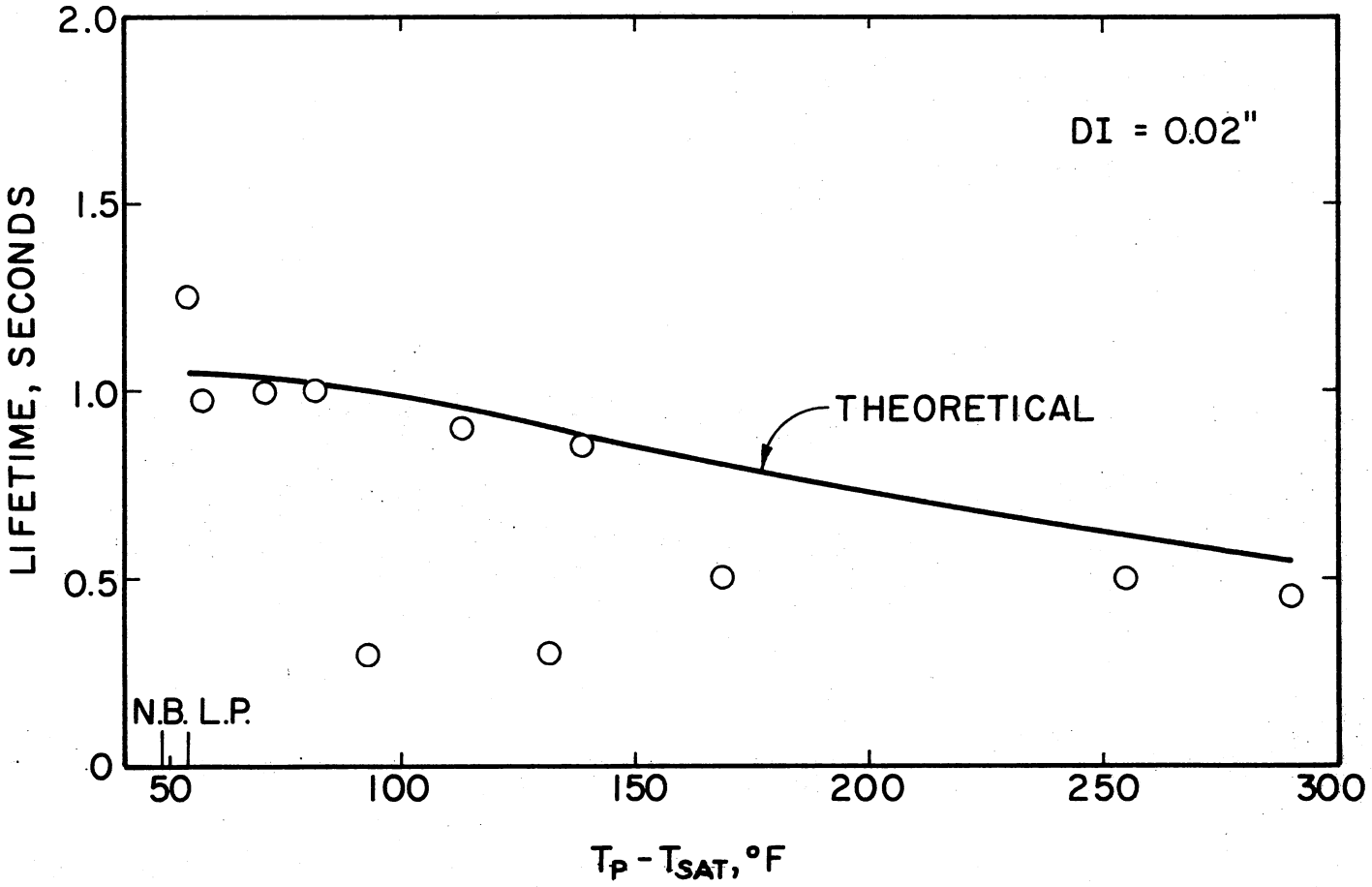

Figure 23. Freon-114 Drop Lifetime Curve, $P_r = 1/2$

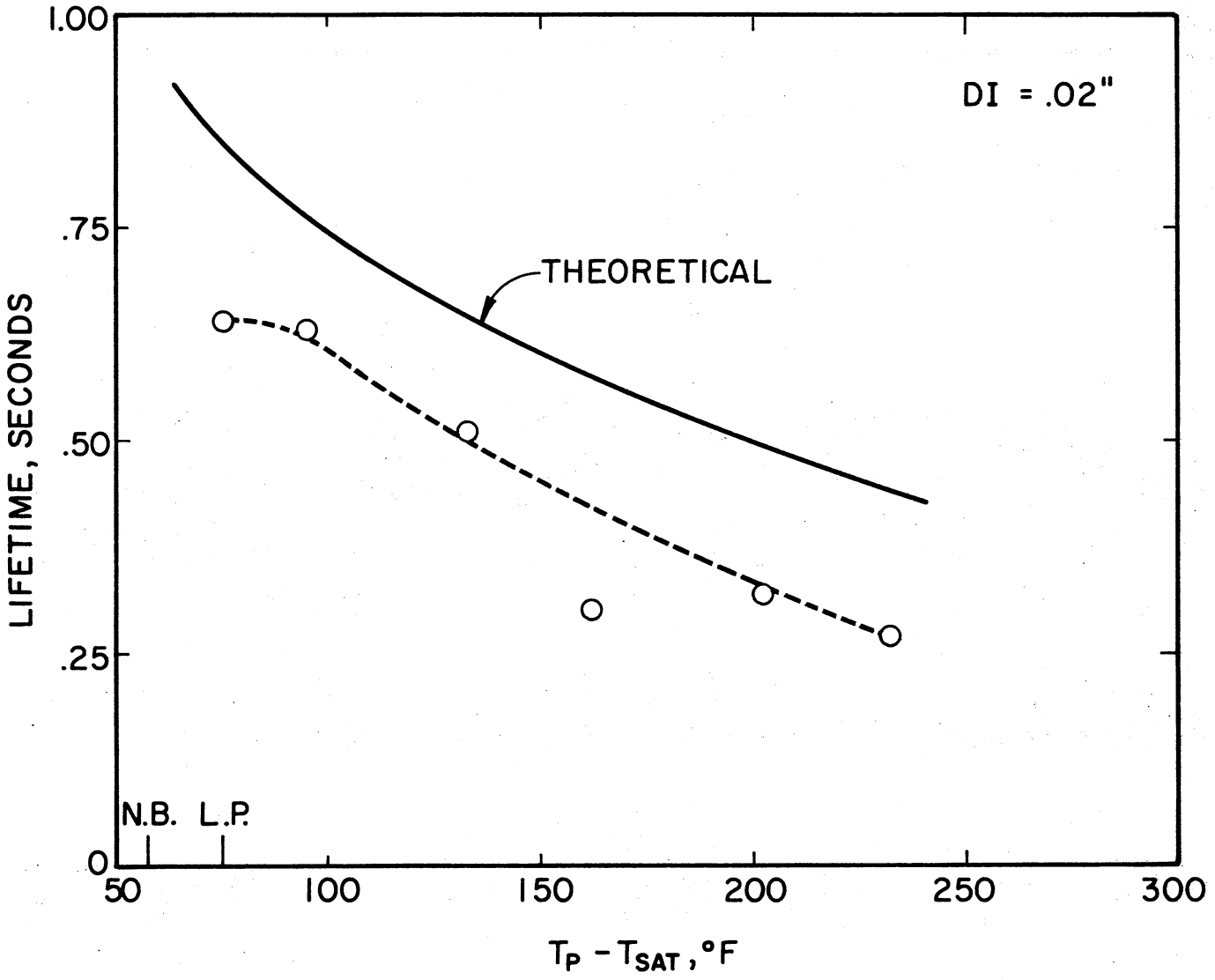

Figure 24. Freon-114 Drop Lifetime Curve, P_r = 3/4

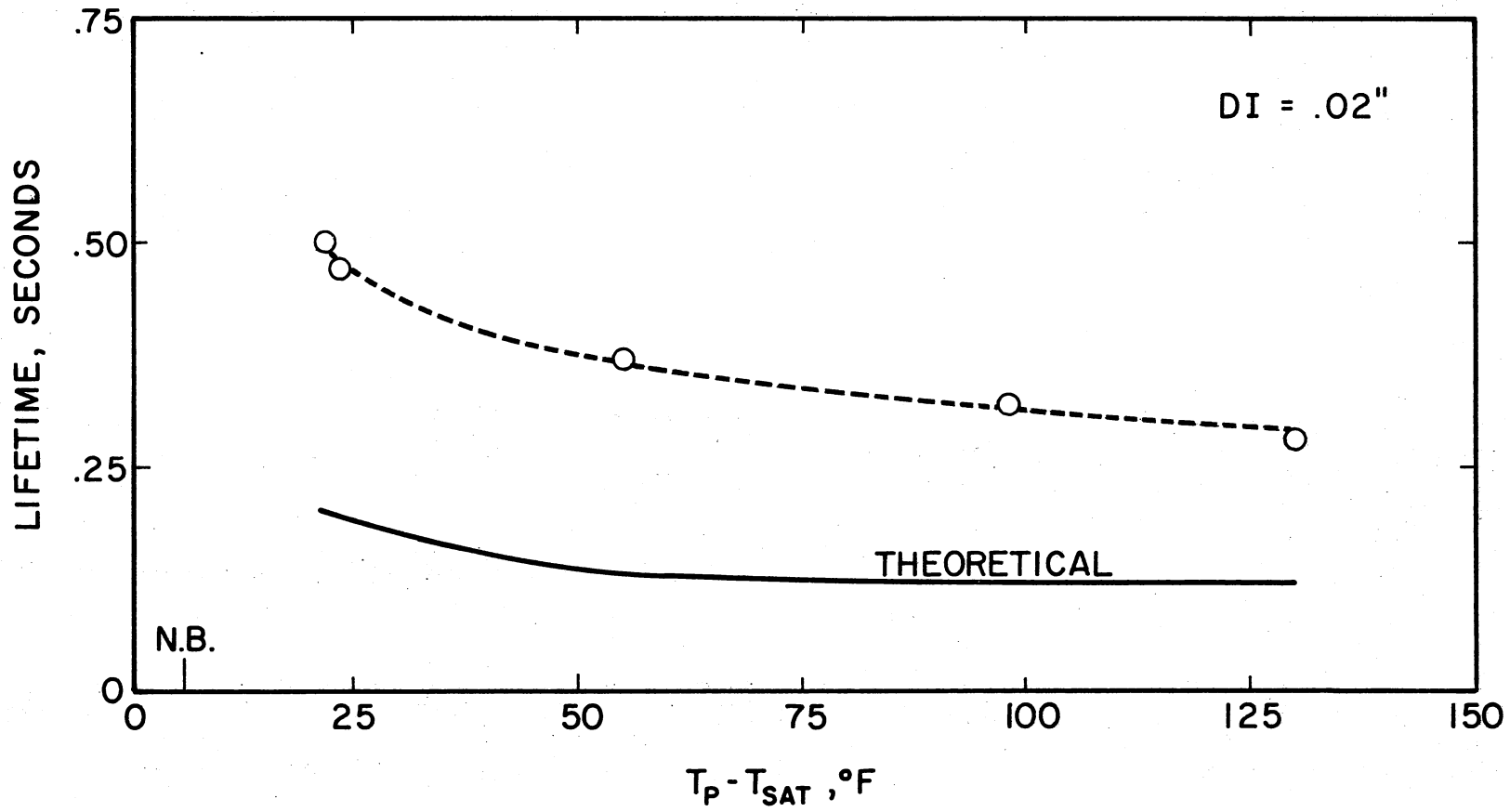

Figure 25. Freon-114 Drop Lifetime Curve, $P_r = 1$

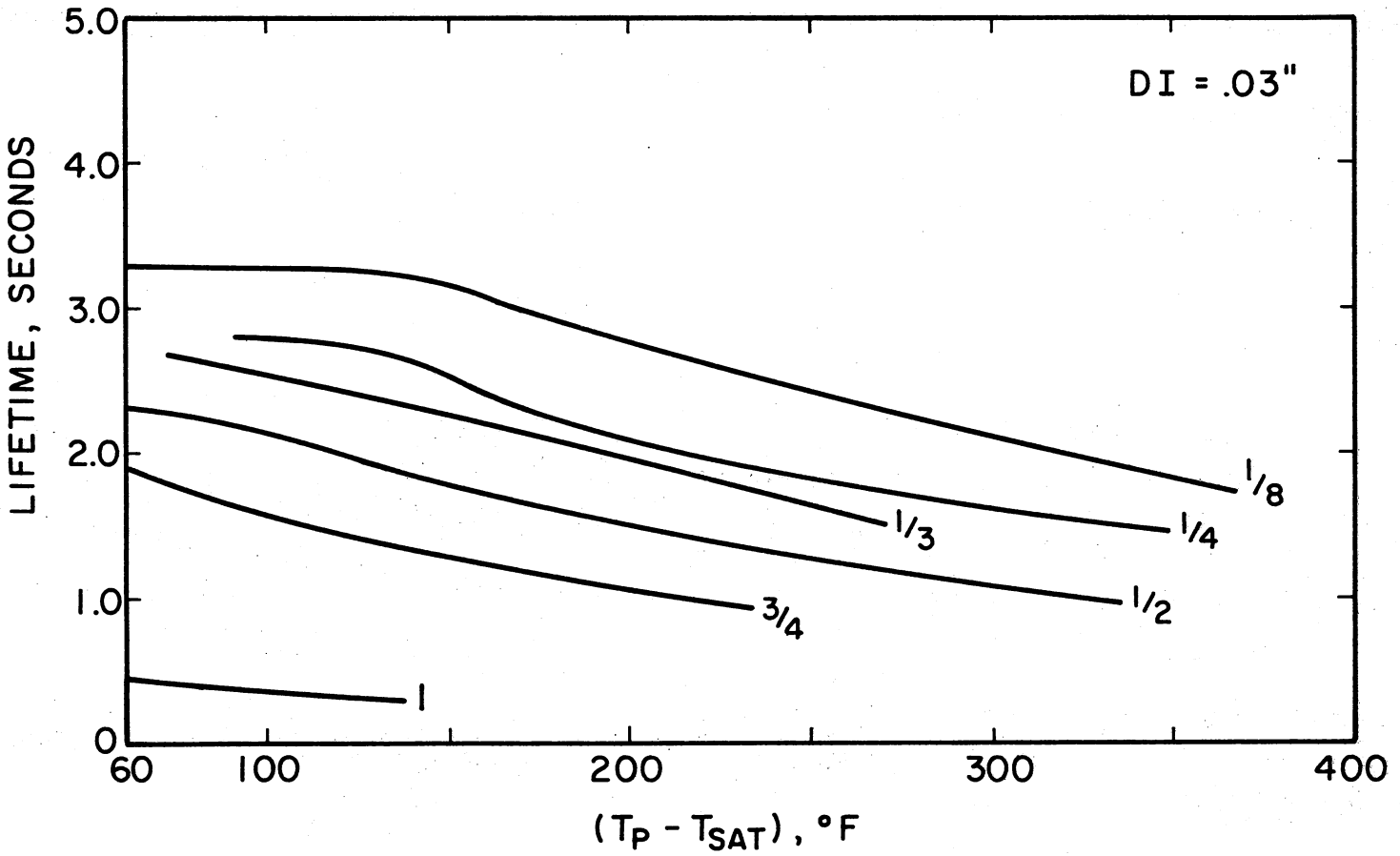

Figure 26. Drop Lifetime Behavior for Freon-114 at Various Reduced Pressures

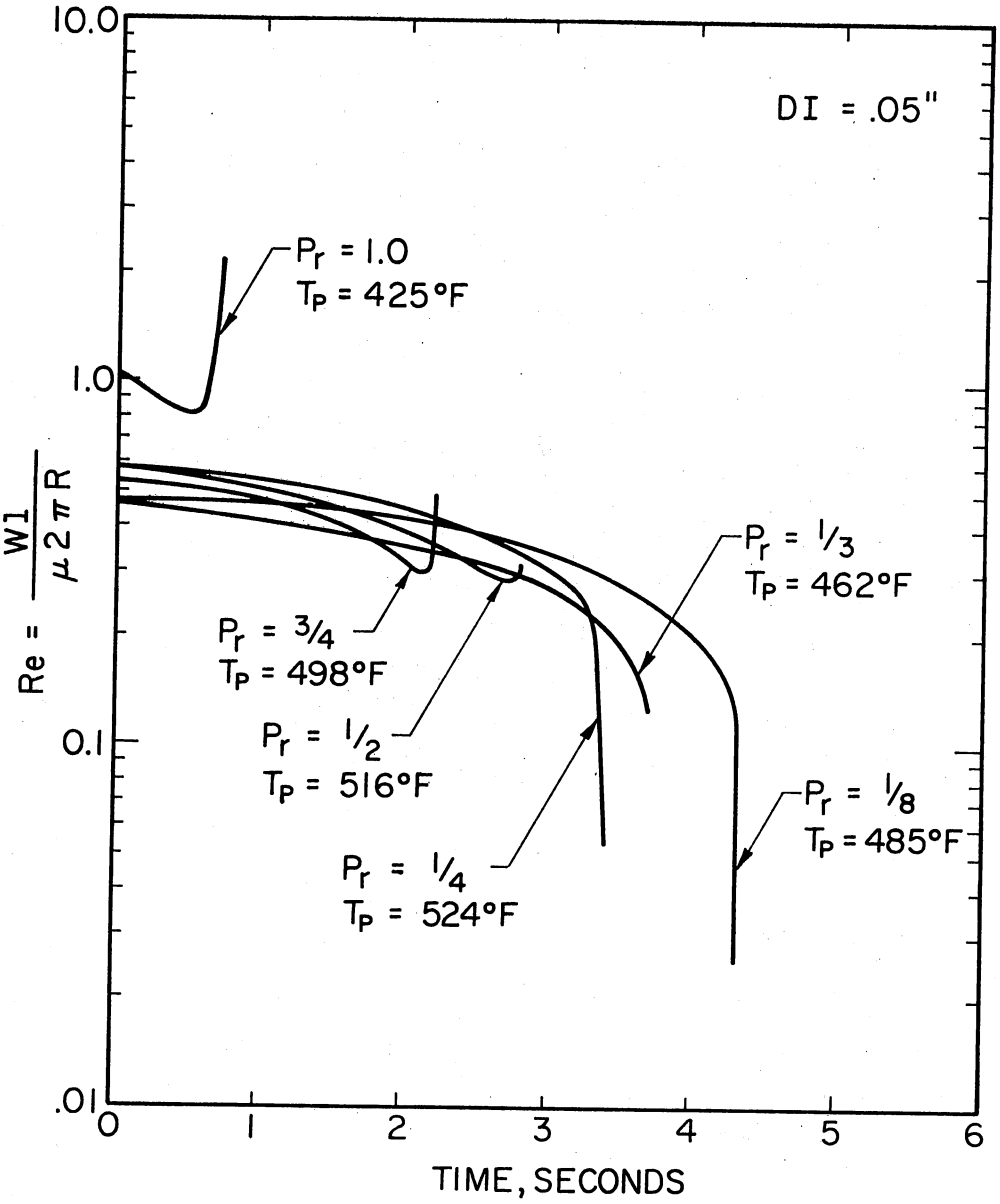

Figure 27. Reynolds Number vs. Time for Freon-114

Figures 28 and 29 show the heat flux history of typical water and Freon-114 drops. At the higher plate temperatures the radiant heat flux is about 6 percent the conductive heat flux for water and 7 percent for Freon-114. The radiant heat flux drops to 3 percent for water and 5 percent for Freon at the lower platt temperatures.

The mass fluxes, W_1/A_1 and W_2/A_2, from the top and bottom halves of the drop are shown in Figures 30 and 31 for water and Freon-114. A_1 is based on the projected area of the drop and A_2 is the surface area of the upper half of the drop. For both cases of the water drops the mass flux due to diffusion, W_2/A_2, is the same. For the entire temperature range of the water drops studied the mass loss due to diffusion predominates over W_1/A_1. The mass flux from the bottom half of the water drops goes through a minimum near the end of the drop lifetime. This behavior is accounted for by the fact that δ_1, the clearance at the bottom of the drop from the plate, passes through a minimum.

The behavior of the mass fluxes of the Freon is seen in Figure 31. At the higher plate temperature the mass flux from the lower surface is greater than the diffusive flux except near the end of the drop's lifetime. At the lower plate temperature the behavior is the same as seen for the water drops at the low temperature.

Above a certain size, a drop is no longer spherical. The model, which was derived for spherical drops, would not be valid for diameters in excess of this limit. Baumeister (4) has presented a criterion for the sphericity of drops as follows:

$$V^* \leq .8 \tag{47}$$

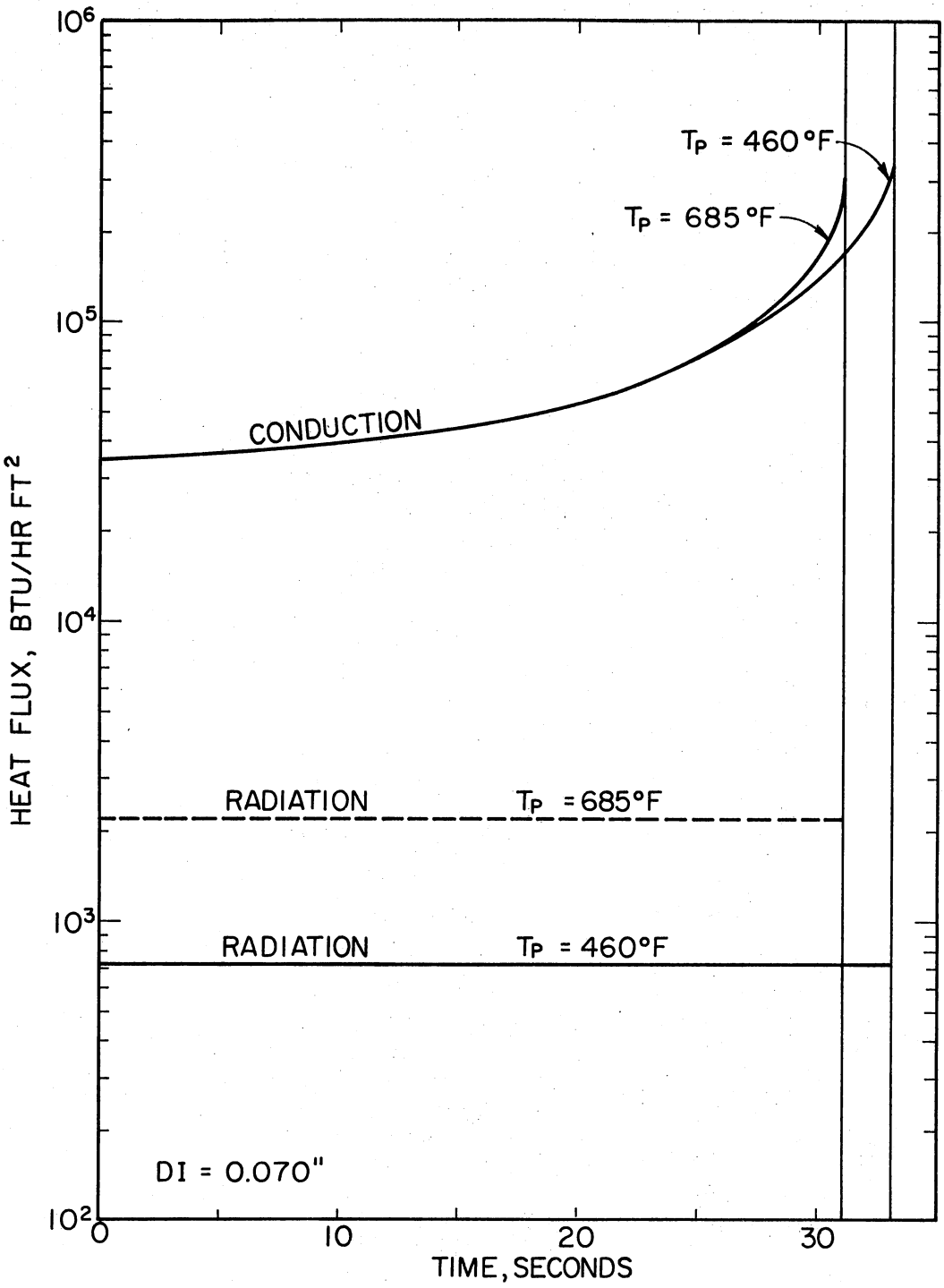

Figure 28. Heat Flux History of Water Drops

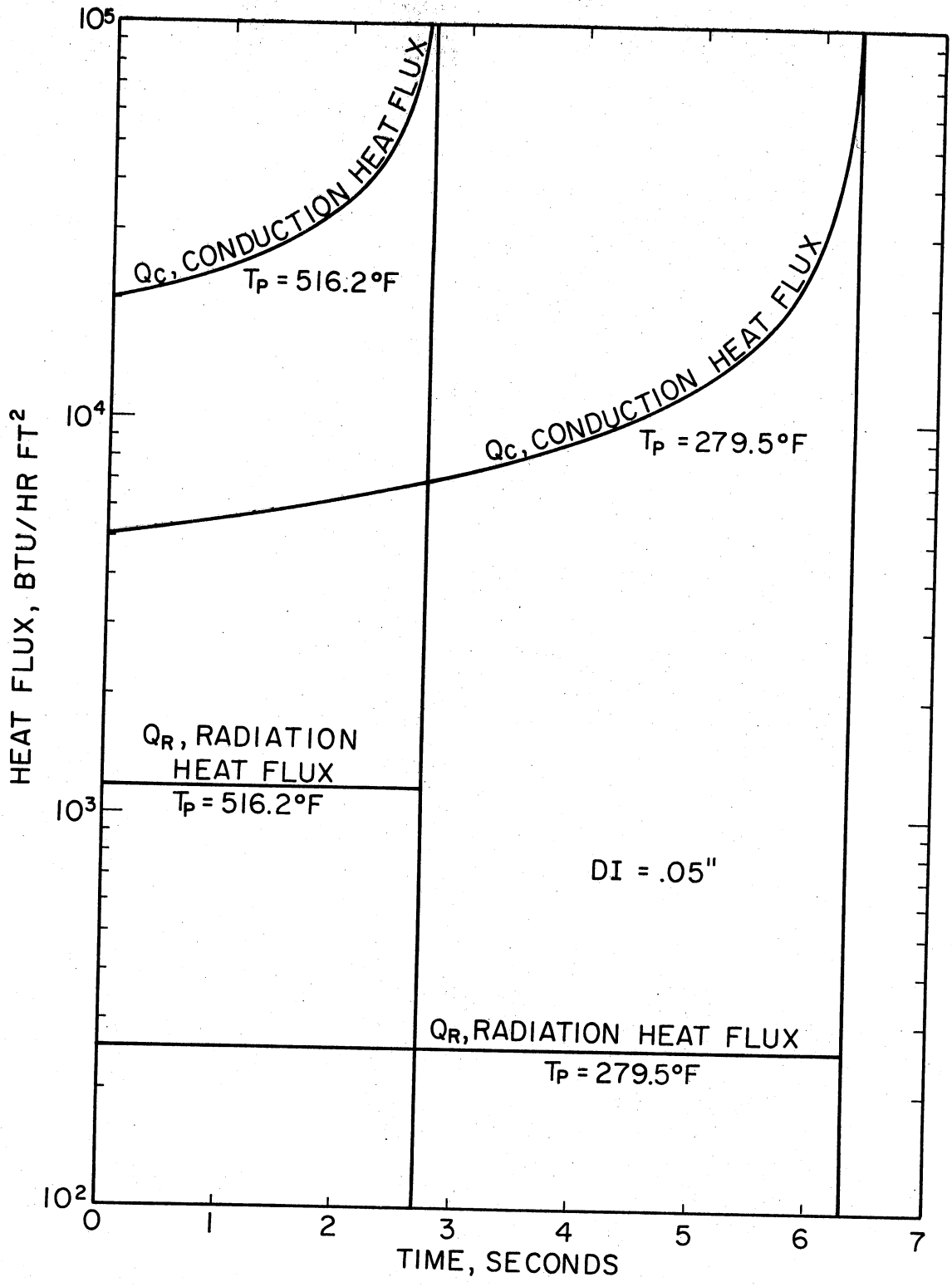

Figure 29. Heat Flux History of Freon-114 Drops, $P_r = 1/2$

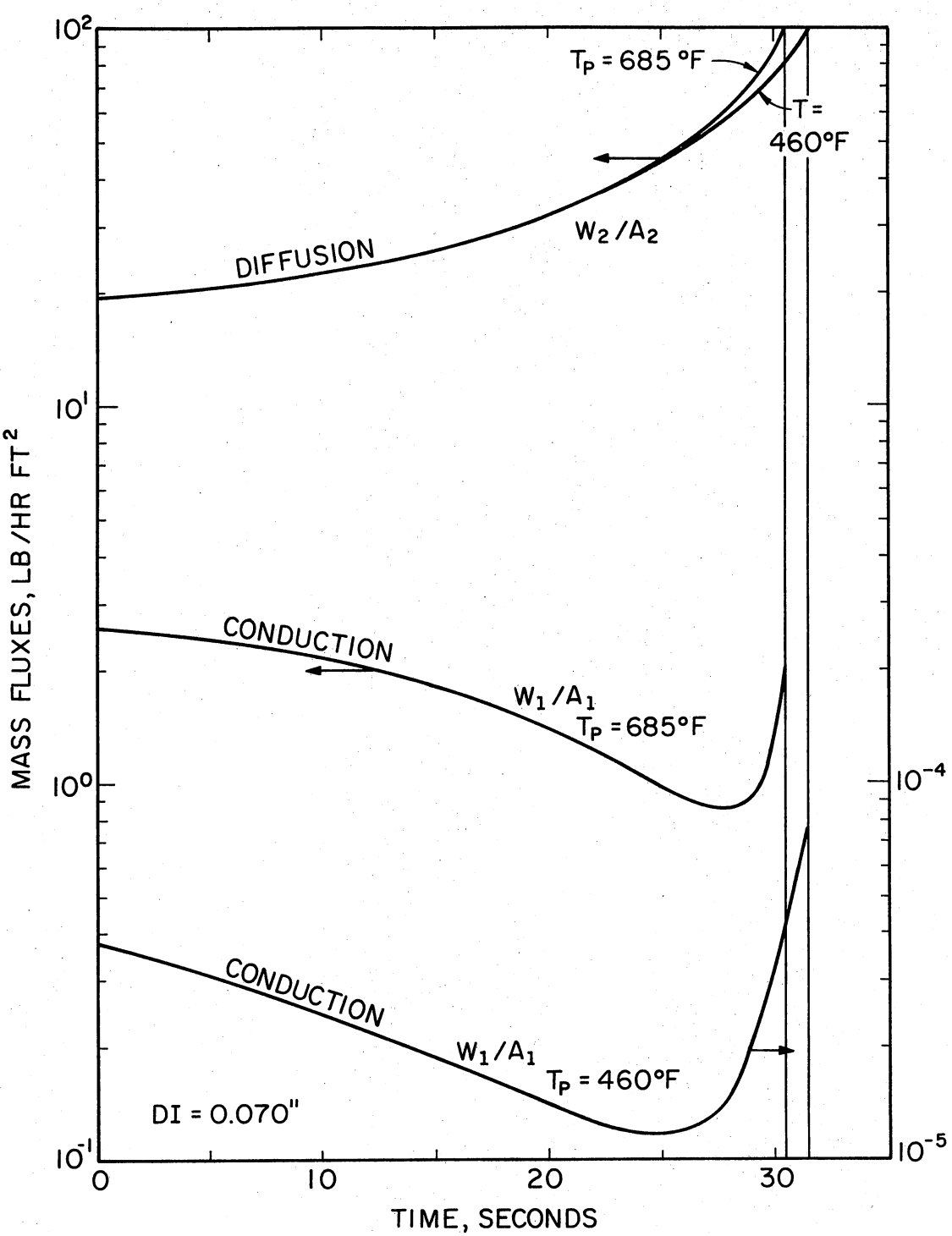

Figure 30. Mass Flux History for Water Drops

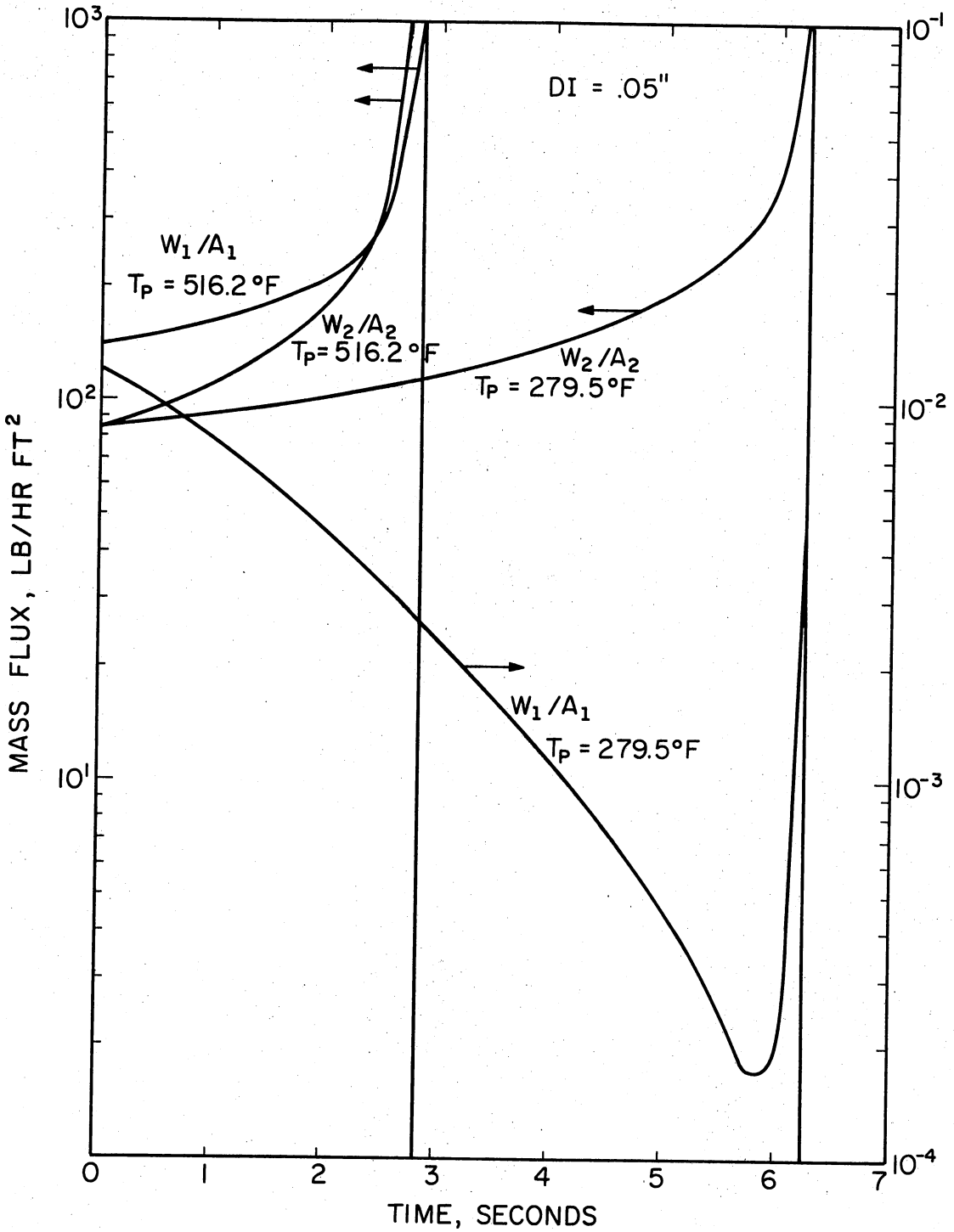

Figure 31. Mass Flux History of Freon-114 Drops at P_r = 1/2

where

$$V^* = \left(\frac{\sigma}{(\rho_L-\rho_V)g/g_c}\right)^{-3/2} * V \qquad (48)$$

As the reduced pressure is increased V^* becomes smaller due to lowering of the surface tension, σ. The behavior of the maximum diameter for sphericity is shown in Figure 32 for Freon-114.

The Reynolds number and drop height history for Freon-114 and water are shown in Figures 33 and 34. The Reynolds number goes through a minimum near the end of the water drop lifetime for both plate temperatures. The Reynolds number is directly proportional to the mass flux, W_1/A_1, from the bottom of the drop which goes through a minimum also. Thus, the behavior would be expected to be similar.

The Reynolds number behavior of the Freon-114 drops is similar to the water drop behavior except for magnitude. Both drops show a minimum in the Reynolds number curve near the end of the droplet lifetime.

The minima in the mass flux and Reynolds number curves are explained by the fact that δ_1, the drop height, goes through a minimum. The minimum occurs near the end of the drop lifetime. The cause of the minimum in δ_1 is the high rate of mass transfer, W_2/A_2, from the drop. W_2/A_2 takes heat from the heat balance equation in the model which much be replaced by a higher rate of heat conduction. The heat conduction is increased by shortening the distance through which the heat is conducted.

An analysis was made to determine the sensitivity of the Gottfried-Lee-Bell model to variations in the thermal conductivity and diffusivity for water drops. The values were allowed to vary 10 percent either side

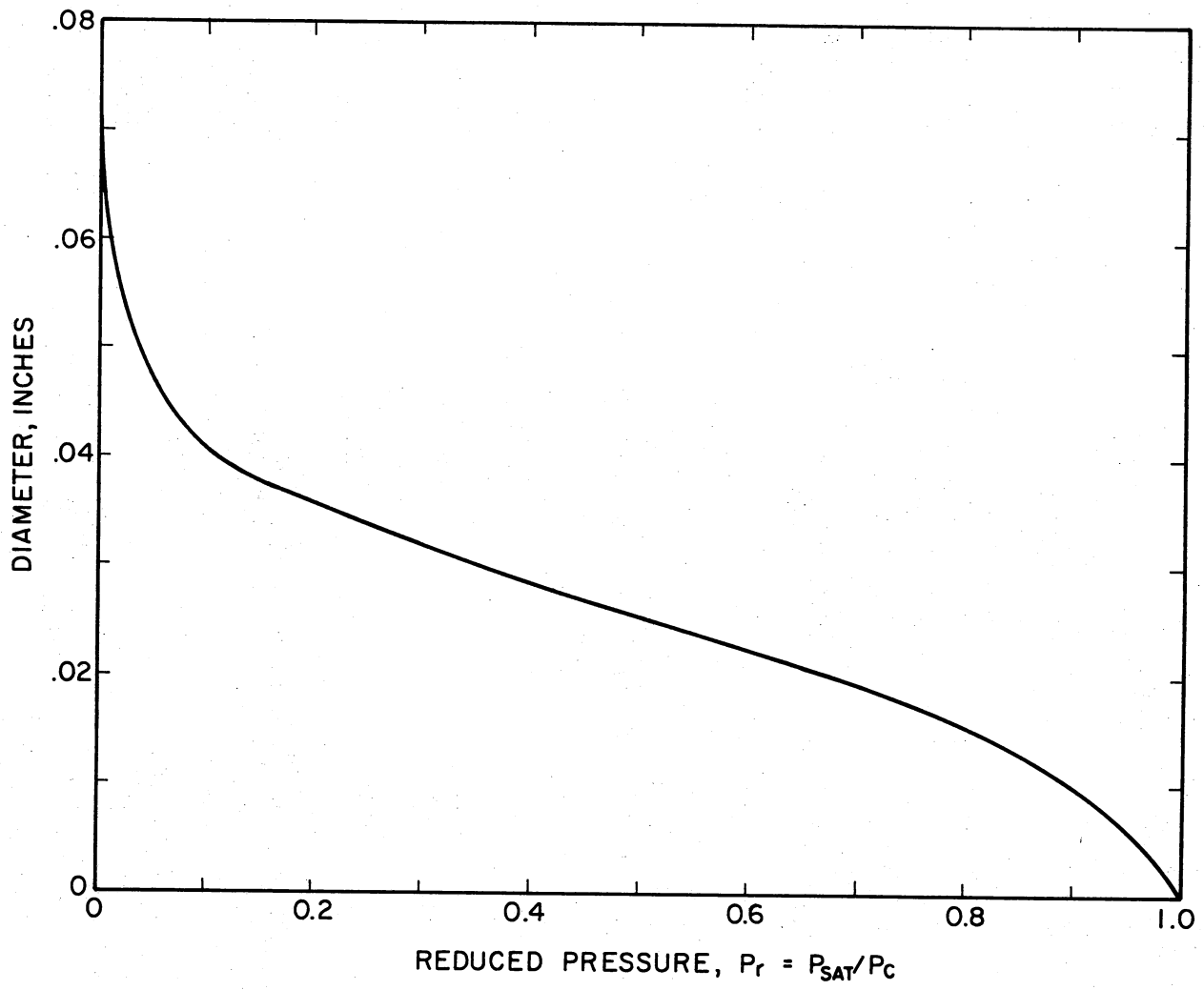

Figure 32. Drop Sphericity Criterion for Freon-114

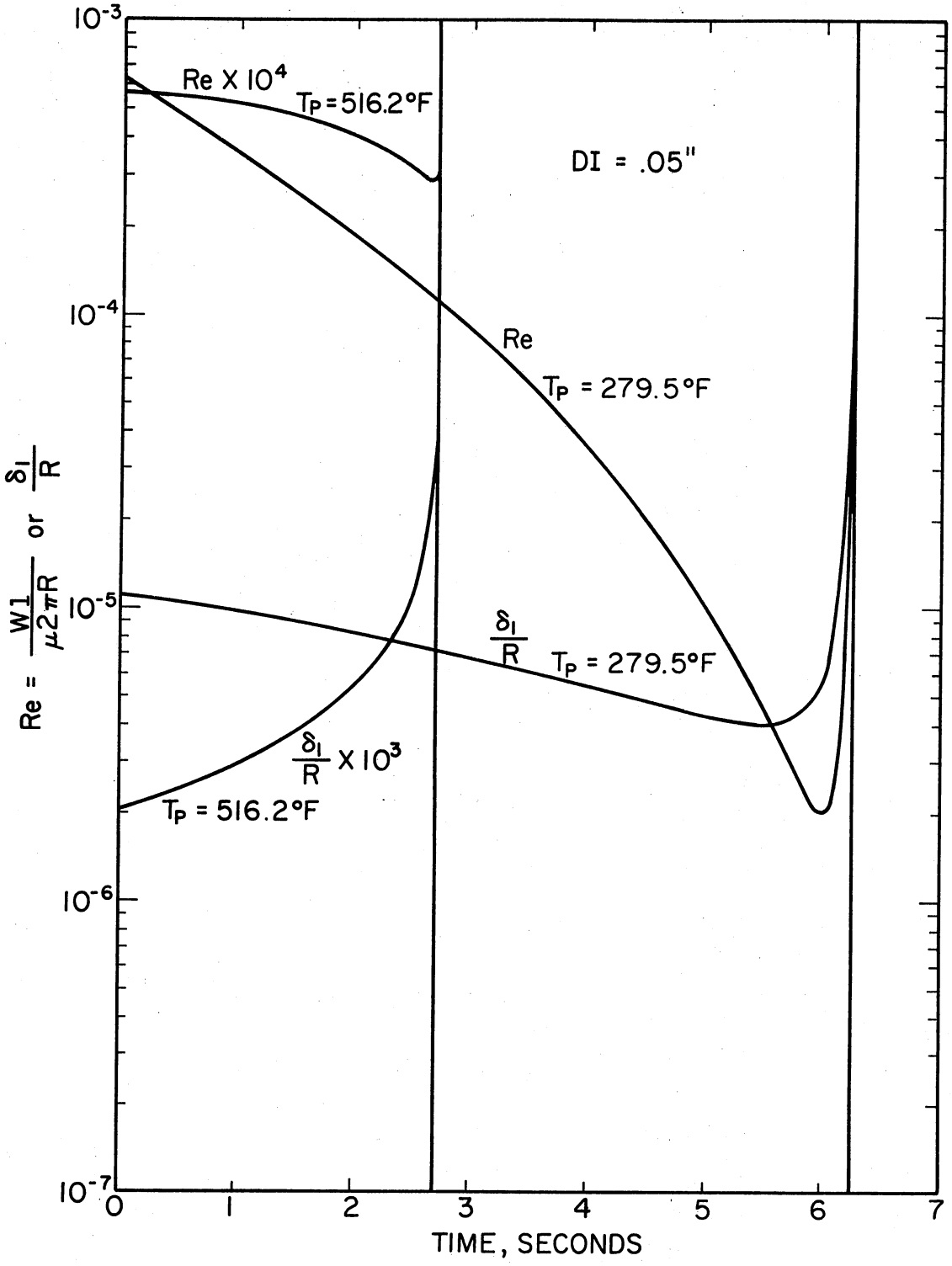

Figure 33. Reynolds Number History for Freon-114 Drops at $P_r = 1/2$

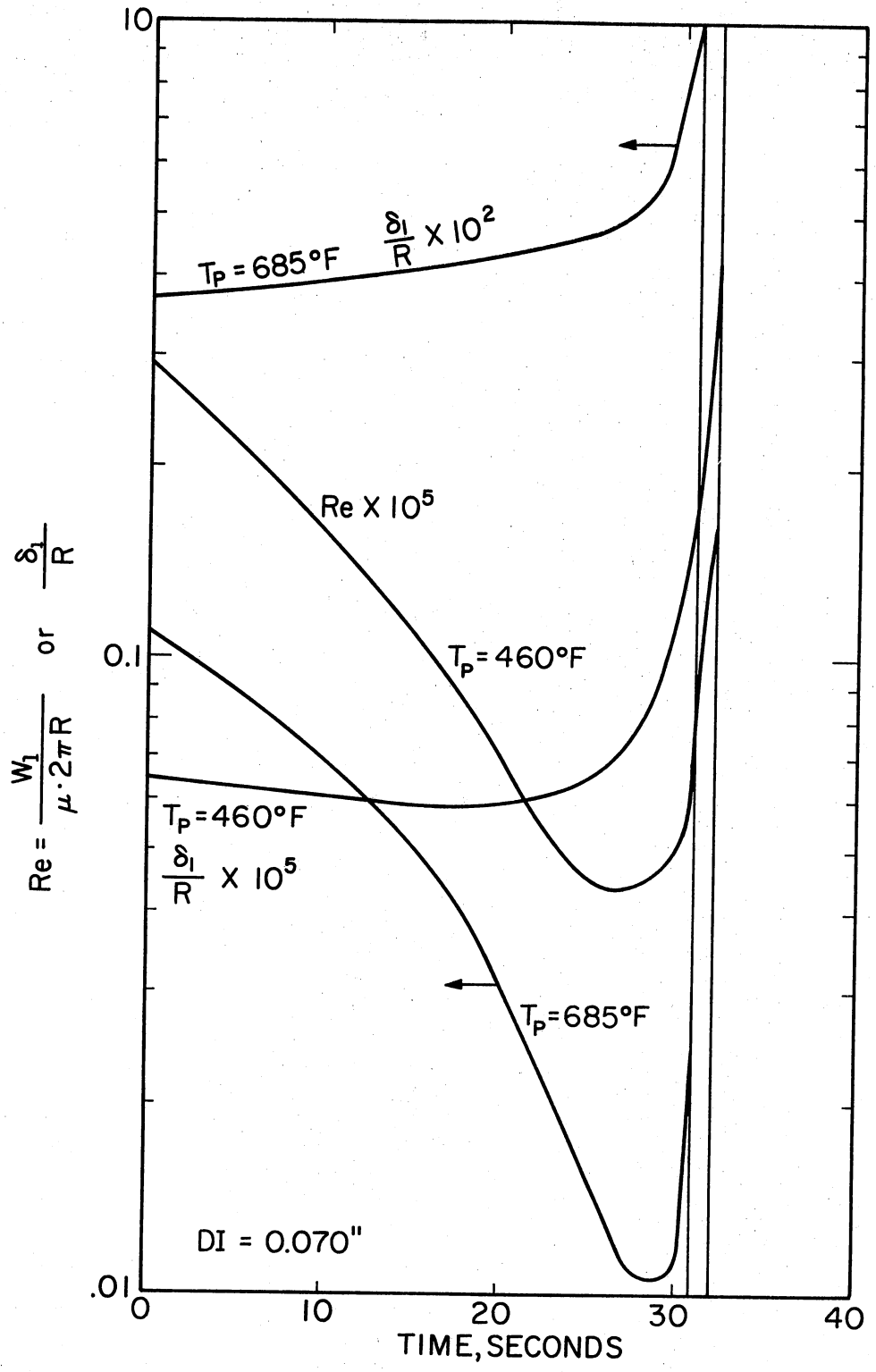

Figure 34. Reynolds Number vs. Time for Water

of the normal values. The results of the sensitivity analysis are shown in Figures 35 and 36. At the lower plate temperature the model is insensitive to changes in the thermal conductivity as seen in Figure 35. The model is, however, quite sensitive to changes in diffusivity. This is explained by the fact that the model is dominated by diffusion at low temperature difference. In Figure 36 the model is not as affected by the variations as the lower plate temperature. The changes in the diameter history curve indicate that variations in diffusion and conduction terms are approximately of the same order of importance.

The experimental diameter history can be compared to Lee's work (23). Figure 37 shows a plot of the diameter as function of time for water drops. The values taken from reference (23) are for a plate temperature of 662^{o}F, while the present work is for a plate temperature of 685^{o}F. While not the same plate temperatures exactly these were the closest drops for comparison. The agreement between the two is close, though the present data show a longer evaporation time even though the plate temperature is higher than for Lee's data.

A qualitative comparison can be made between the present work and the results of Temple-Pediani and the work of Sciance and Colver. Sciance and Colver show a plot of the Leidenfrost Point as a function of reduced pressure. From Temple-Pediani's work a similar plot was constructed. These results are shown in Figures 38 and 39, respectively. A plot of the Leidenfrost Point as a function of reduced pressure for Freon-114 from the present work is shown in Figure 40. A comparison of these results shows a similar behavior even though the compounds are different. A peak appears at the lower end of the reduced pressure scale in all three works. Though Temple-Pediani's work shows a sharp

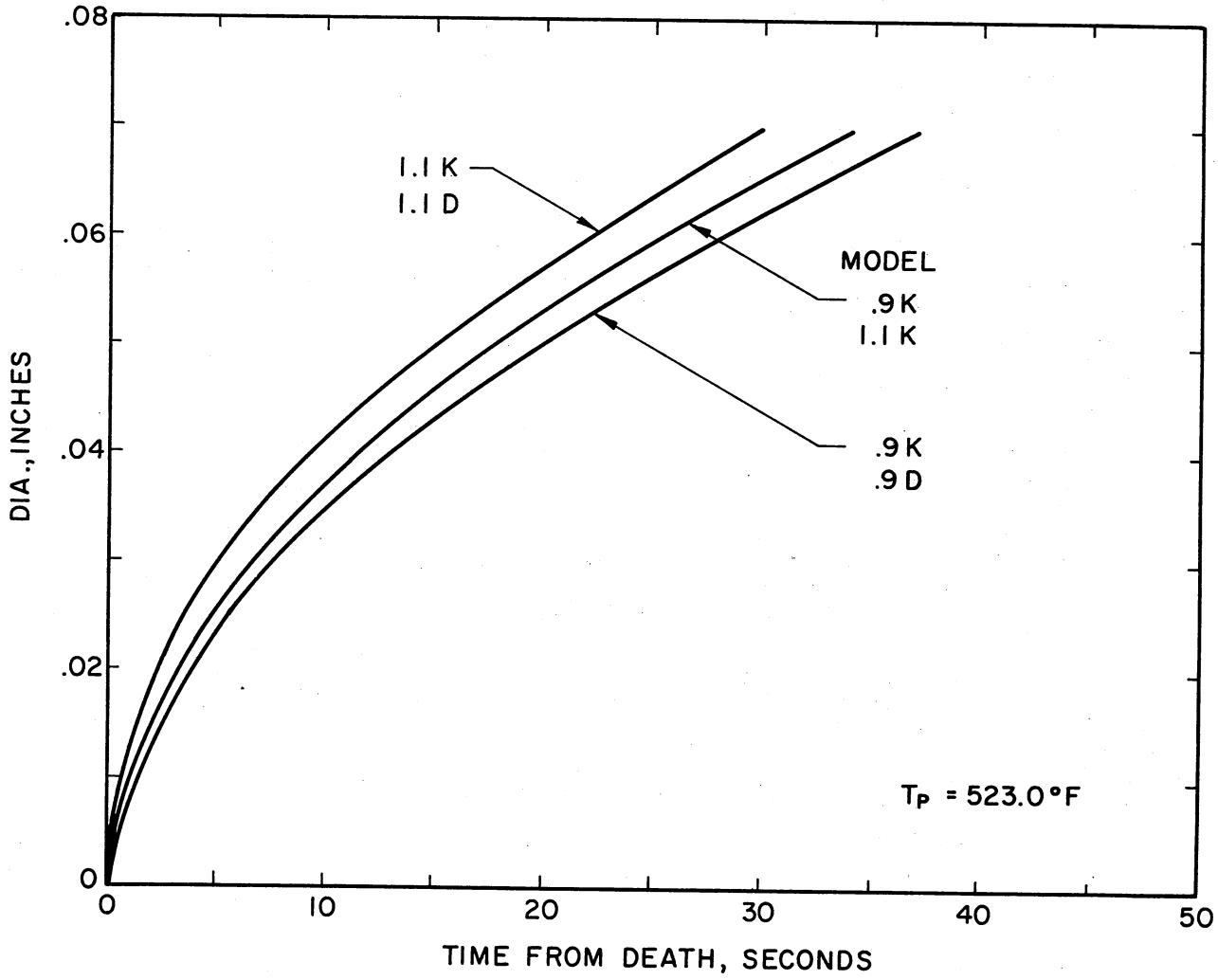

Figure 35. Sensitivity Analysis for Water drops, $T_p = 523^{o}F$

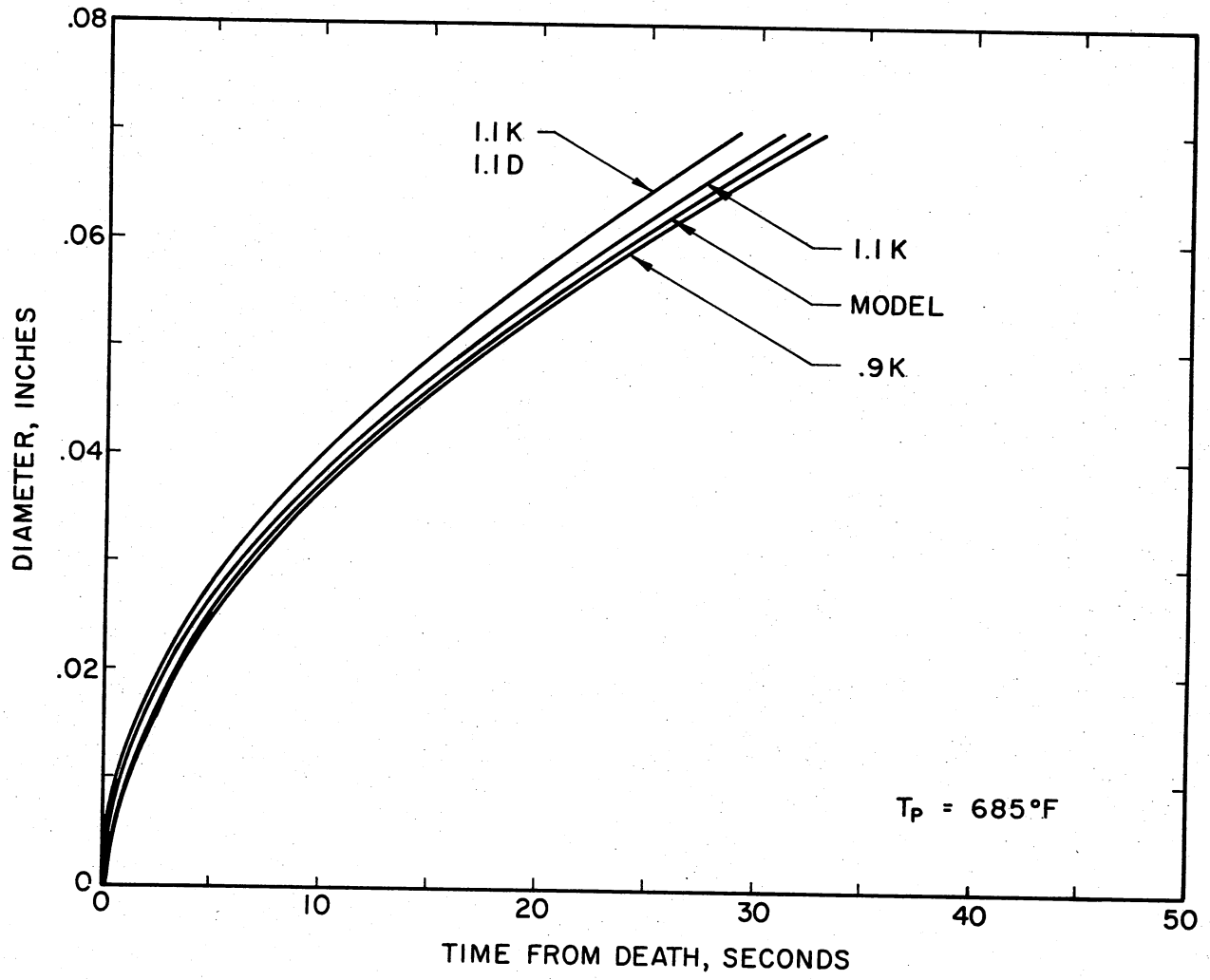

Figure 36. Sensitivity Analysis for Water Drops, $T_p = 685^{o}F$

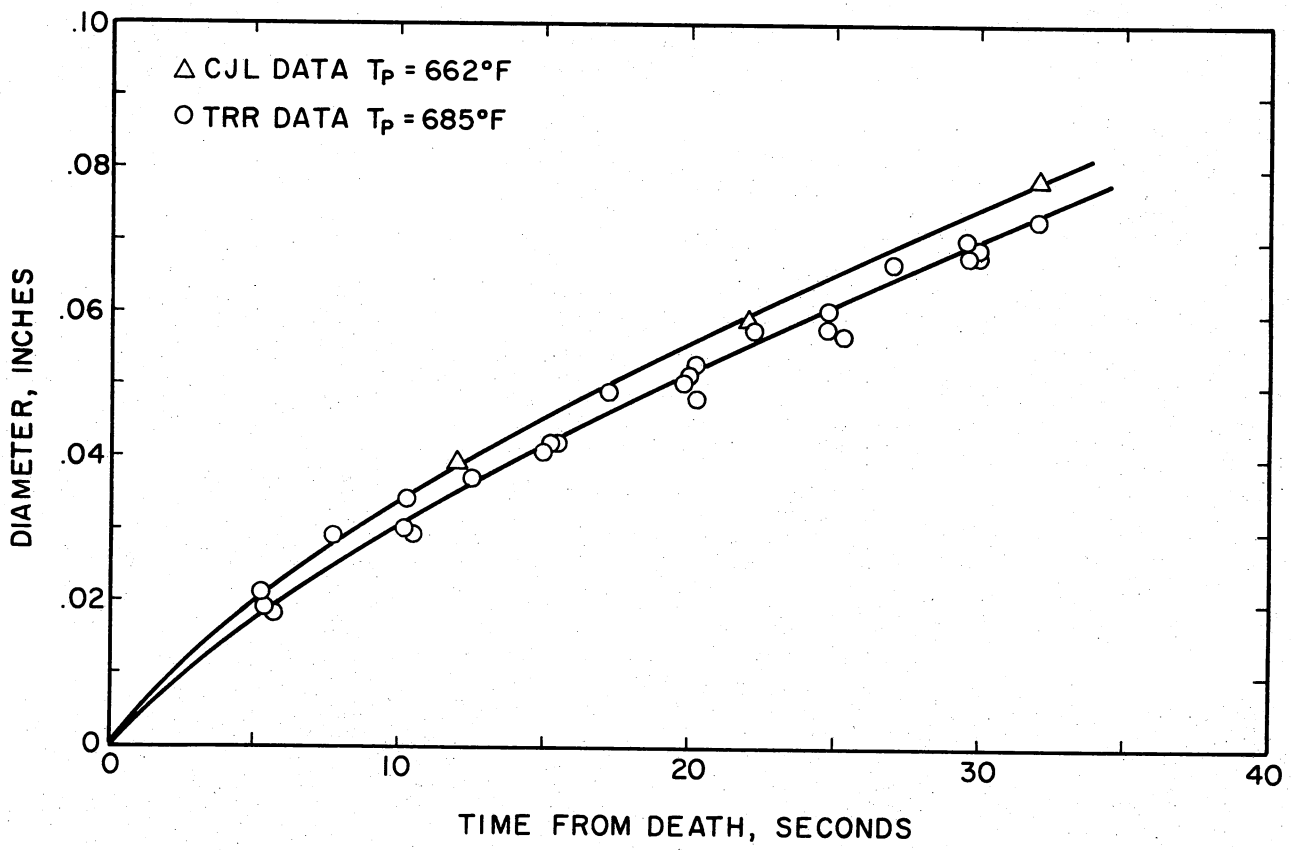

Figure 37. Diameter History of Water Drops

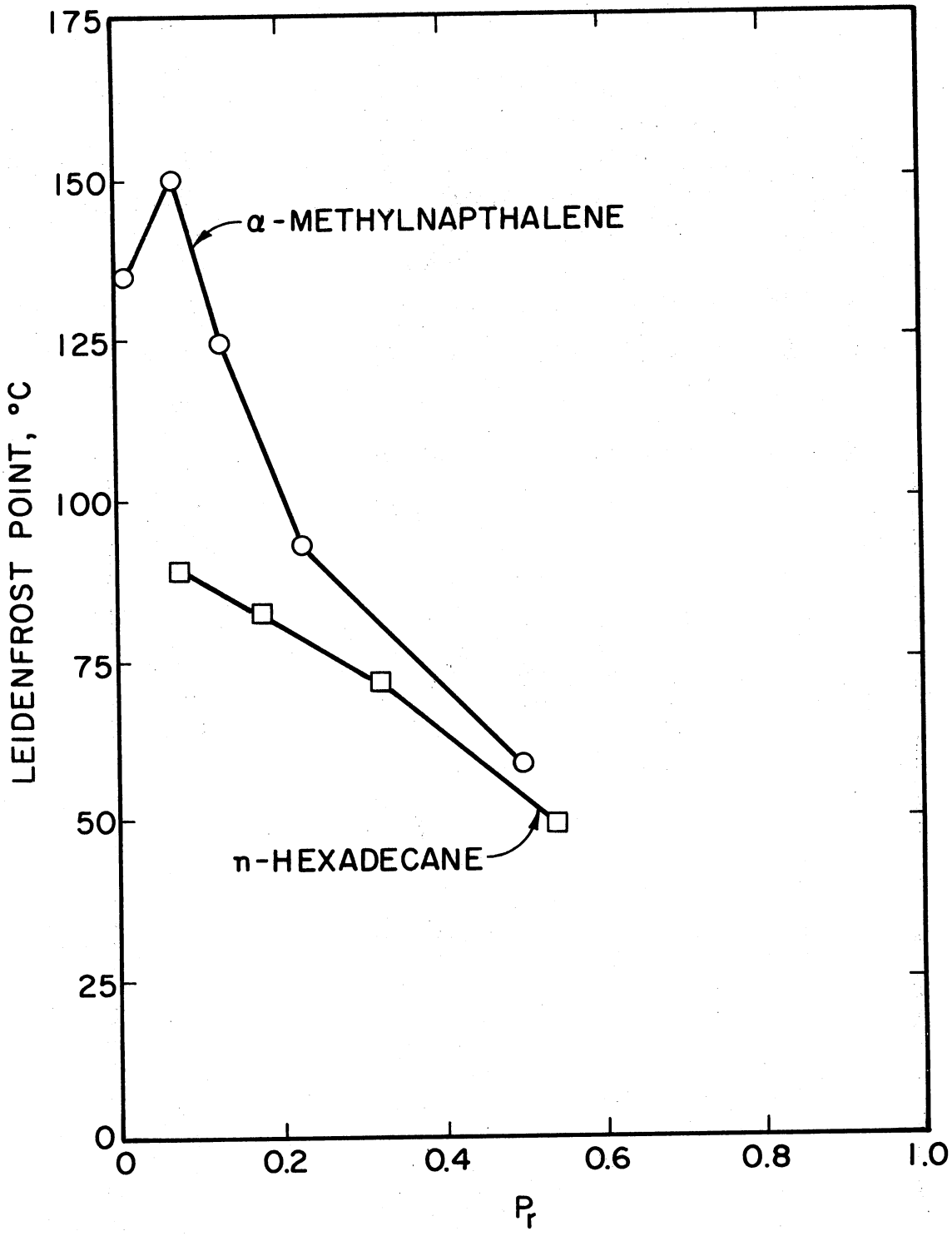

Figure 38. Leidenfrost Point vs. Reduced Pressure from Temple-Pediani

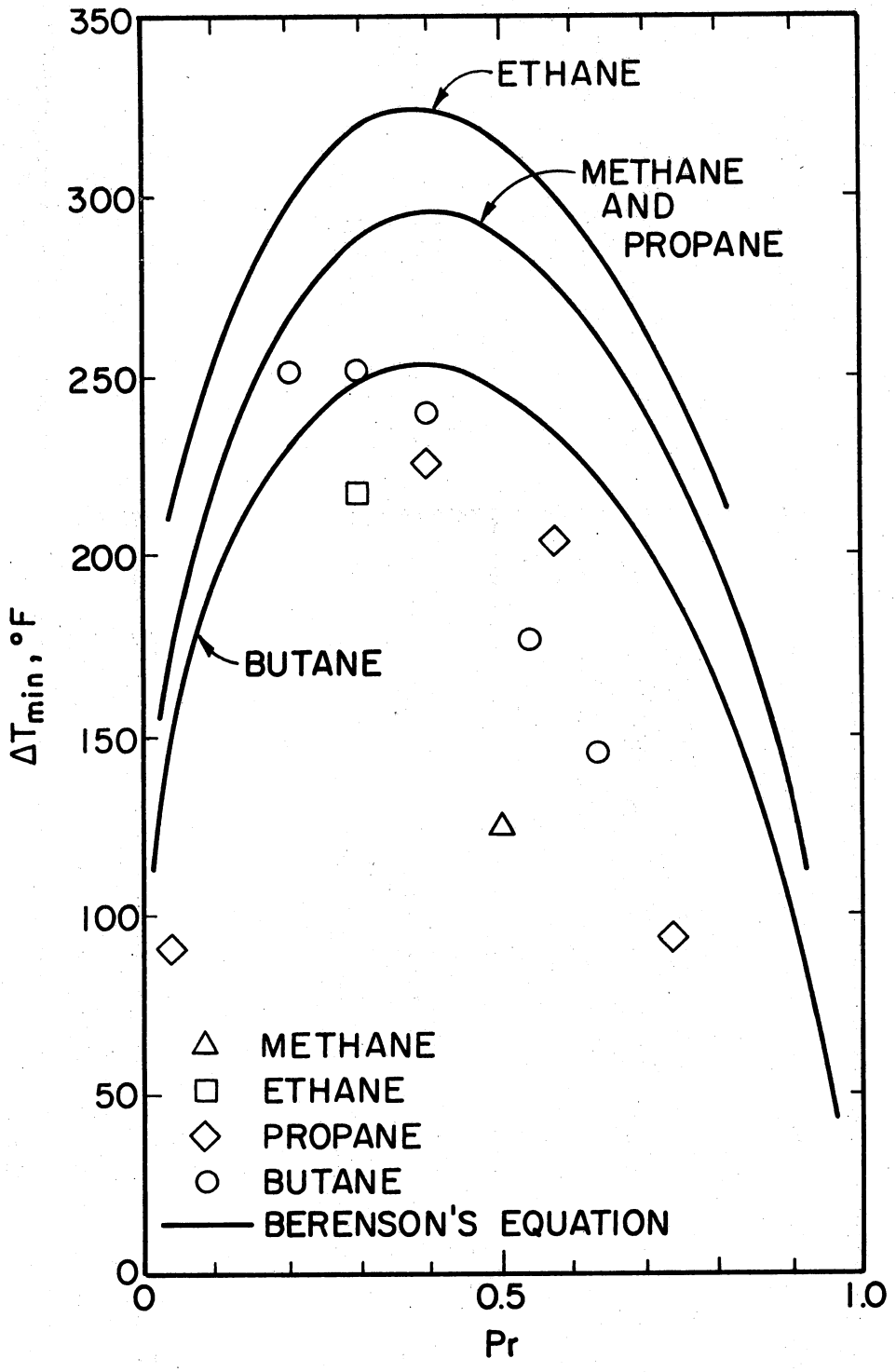

Figure 39. Leidenfrost Point vs. Reduced Pressure from Sciance and Colver

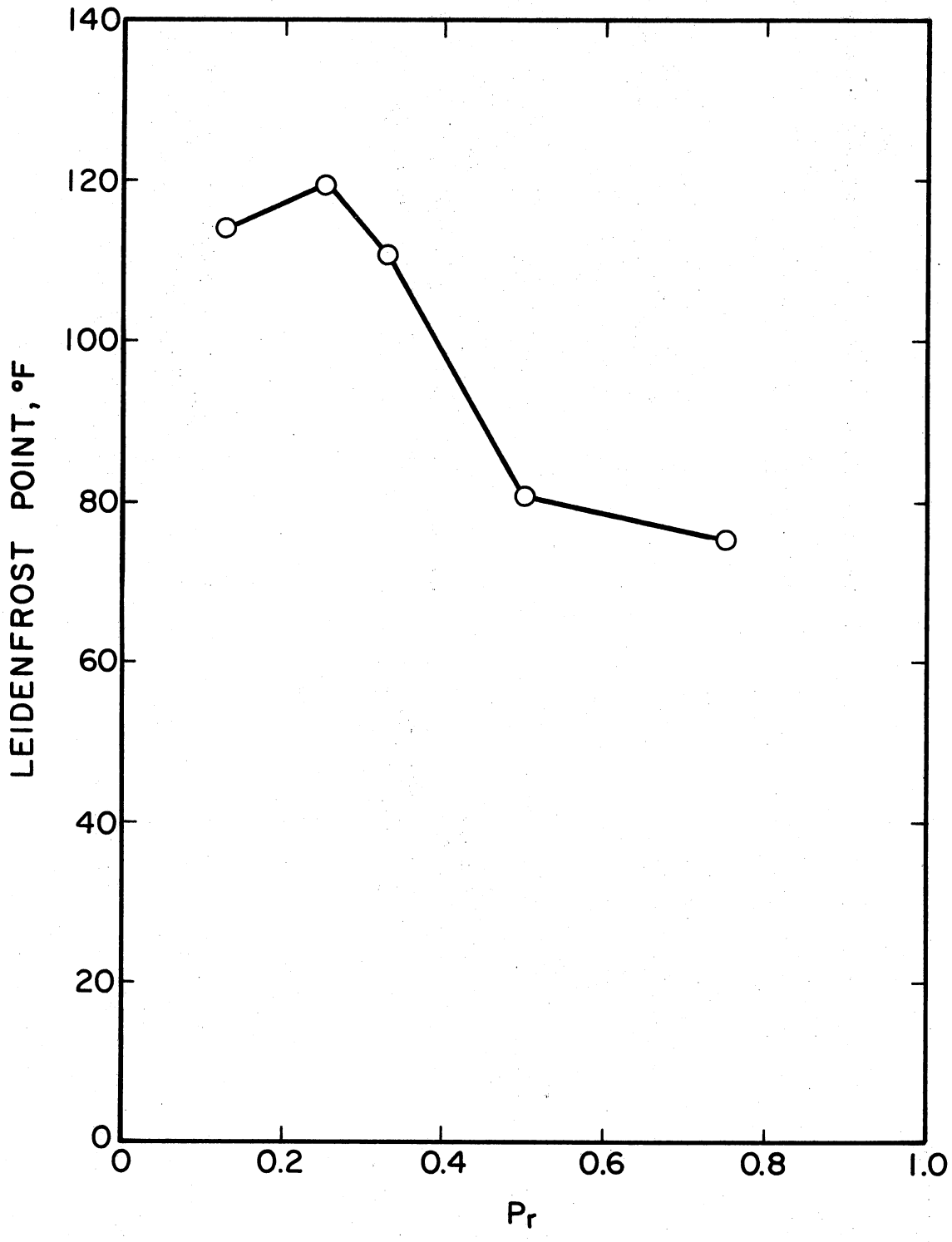

Figure 40. Leidenfrost Point vs. Reduced Pressure for Freon-114

peak, this may be explained by differences in compounds studied.

In the present work there is no well defined Leidenfrost Point at a reduced pressure of 1. Thus a complete curve cannot be drawn. However, nucleate boiling did persist $3^{o}C$ above the saturation temperature.

The present work is an extension of the Gottfried-Lee-Bell model for predicting the behavior of small drops undergoing film boiling. The model has been applied to two diverse fluids, in one case over an extreme range of pressure. In all cases the model predicted the qualitative behavior even if not in complete quantitative agreement.

The experimental data for water compared favorably with that of Lee in the one common case. The behavior of the Leidenfrost point agreed qualitatively with the results of two previous works.

CHAPTER VI

CONCLUSIONS AND RECOMMENDATIONS

Based on the previous discussion the following conclusions are drawn:

Experimental

1) The use of a relatively low speed movie camera to record drop histories was successful. This technique gives an opportunity to study each drop much more closely.
2) The data points for water in common with those of Lee (23) compare favorably quantitatively.
3) The Leidenfrost Point data of Freon-114 as a function of reduced pressure agree qualitatively with other workers.
4) The Freon-114 data exhibit a Leidenfrost Point at reduced pressures up to $P_r = .75$.
5) Nucleate boiling was observed at a temperature difference of $3^{o}C$ at the critical pressure. Film boiling was also observed at the critical pressure.

Theoretical

1) The Gottfried-Lee-Bell model predicts the behavior of Freon-114 drops qualitatively up to a reduced pressure of 3/4. At

reduced pressures of 3/4 and 1 the agreement is qualitative and of the same magnitude as the data.

2) The Gottfried-Lee-Bell model predicts the behavior of water drops at large differences between plate and saturation temperatures. The model is dominated by diffusion at the lower temperature differences.

3) The heat flux to the drop is dominated by the conductive-convective heat transfer between the plate and the drop.

The following recommendations for further work are suggested:

1) The physical and thermodynamic properties of Freon-114 need to be more accurately known, especially near the critical region.

2) Experimental data should be taken at pressures above the critical.

3) The Leidenfrost Point should be determined more precisely at a reduced pressure of one for Freon-114.

4) The theoretical model could be extended to other shapes such as ellipsoids.

5) Experimental measurements of film boiling behavior of other fluids such as water and cryogens under pressure would be useful.

6) The present experimental equipment could be used to investigate the behavior of extended masses under pressure.

SELECTED BIBLIOGRAPHY

1. Adadevoh, J. K., "Vaporization of a Fuel Droplet Contacting with a Hot Surface and Under Pressure," M.S. Thesis, Department of Mechanical Engineering, University of Wisconsin (1962).

2. Arpaci, Vedat S., Conduction Heat Transfer, Addison and Wesley, 550 (1966).

3. Baumeister, K. J., T. D. Hamill, F. L. Schwartz and G. J. Schoessow, "Film Boiling Heat Transfer to Water Drops on a Flat Plate," NASA TM X-52103 (1965).

4. Baumeister, K. J., T. D. Hamill and G. J. Schoessow, "A Generalized Correlation of Vaporization Times of Drops in Film Boiling on a Flat Plate," Proc. Third Int. Heat Transfer Conf., Chicago, 4, 66-75 (1966).

5. Baumeister, K. J., R. C. Hendricks and T. D. Hamill, "Metastable Leidenfrost States," NASA TN D-3226 (1966).

6. Baumeister, K. J., E. G. Keshock and D. A. Pucci, "Anamalous Behavior of Liquid Nitrogen Drops in Film Boiling," Advances in Cryogenic Engineering, 16, 445-454 (1970).

7. Baumeister, K. J., S. S. Papell and R. W. Graham, "Heat Transfer from an Incandescent Wire in Saturated Liquid Nitrogen from Atmospheric to the Critical Pressure," NASA (1971).

8. Baumeister, K. J. and G. J. Schoessow, "Creeping Flow Solution of Leidenfrost Boiling with a Moving Surface," Chemical Engineering Progress Symposium Series, 65, No. 92, 167-174 (1969).

9. Bell, K. J., "The Leidenfrost Phenomenon: A Survey," Chemical Engineering Progress Symposium Series, 63, No. 79, 73-82 (1967).

10. Berenson, P. J., "Film Boiling Heat Transfer from a Horizontal Surface," ASME Jour. Heat Transfer, 83, 3, 351-358 (1961).

11. Bird, R. B., W. E. Stewart and E. N. Lightfoot, Transport Phenomena New York: John Wiley and Sons, Inc. (1960).

12. Drew, T. B. and A. C. Mueller, Trans. Am. Inst. Chem. Engrs., 33, 449-471 (1937).

13. Emmerson, G. S., "The Effect of Pressure and Surface Material on the Leidenfrost Point of Discrete Drops of Water," Int. Jour. Heat Mass Transfer, 18, 381-386 (1975).

14. Farber, E. A. and R. L. Schorah, "Heat Transfer to Water Boiling Under Pressure," Trans. ASME, 70, 369-384 (1948).

15. Froessling, N., Gerlands Beitr. Geophys., 52, 170 (1938).

16. Gottfried, B. S., "The Evaporation of Small Drops on a Flat Plate in the Film-Boiling Regime," Ph.D. Thesis, Case Inst. of Technology (1962).

17. Gottfried, B. S., C. J. Lee and K. J. Bell, "The Leidenfrost Phenomenon: Film Boiling of Liquid Droplets on a Flat Plate," Int. Jour. Heat Mass Transfer, 9, 1167-1188 (1966).

18. Hendricks, R. C. and K. J. Baumeister, "Heat Transfer and Levitation of a Sphere in Leidenfrost Boiling," NASA TN D-5694 (1970).

19. Hendricks, R. C. and K. J. Baumeister, "Liquid or Solid on Liquid in Leidenfrost Film Boiling," Advances in Cryogenic Engineering, 16, 455-466 (1970).

20. Keshock, E. G., "Leidenfrost Film Boiling of Intermediate and Extended Bubbly Masses of Liquid Nitrogen," Ph.D. Thesis, School of Chemical Engineering, Oklahoma State University (1968).

21. Keshock, E. G. and K. J. Bell, "Heat Transfer Coefficient Measurement of Liquid Nitrogen Drops Undergoing Film Boiling," Advances in Cryogenic Engineering, 15 (1969).

22. Kovalev, S. A., "An Investigation of Minimum Heat Fluxes in Pool Boiling of Water," Int. Jour. Heat Mass Transfer, 9, 1219-1226 (1966).

23. Lee, C. J., "A Theoretical and Experimental Investigation of the Leidenfrost Phemonemon for Small Droplets," Ph.D. Thesis, School of Chemical Engineering, Oklahoma State University (1965).

24. Leidenfrost, J. G., "De Aquae Communis Nonnollis Qualitatibus Tractatus," Duisberg on Rhine (1756). This Treatise has been translated into English by Carolyn Wares and the pertinent portion published in Int. Jour. of Heat and Mass Transfer, 9, 115-1156 (1966).

25. Nikolayev, G. P., V. V. Bychenkov and V. P. Skripov, "Saturated Heat Transfer to Evaporating Droplets from a Hot wall at Different Pressures," Heat Transfer - Soviet Research, 6, No. 1, 128-132 (1974).

26. Patel, B. M., "The Leidenfrost Phenomenon for Extended Liquid Mass," Ph.D. Thesis, School of Chemical Engineering, Oklahoma State University (1965).

27. Reid, R. C. and T. K. Sherwood, The Properties of Gases and Liquids, New York: McGraw-Hill Book Company (1958).

28. Satcunanathan, S., "Evaporation Rates of Liquid Droplets Evaporating in the "Spherical" State on a Hot Surface," Jour. Mechanical Engineering Science, 10, No. 5, 438-441 (1968).

29. Schoessow, G. J. and K. J. Baumeister, "Mass Diffusivity Effects on Droplets in Film Boiling," AIChE Symp. Series - "Heat Transfer - Tulsa," 68, No. 118, 156-161 (1972).

30. Schoessow, G. J. and K. J. Baumeister, "Velocity Effects on Leidenfrost Bo ling in Various Liquids," Proceedings of the Fourth Int. Heat Transfer Conference, Versaille, France, Vol. V (1970).

31. Sciance, C. T. and C. P. Colver, "Minimum Film Boiling Point for Several Light Hydrocarbons," Trans. ASME, 92, 659-661 (1970).

32. Simoneau, R. J. and K. J. Baumeister, "Experimental Effects of Pressure, Subcooling, and Diameter on Thin Wire Film Boiling," Advances in Cryogenic Engineering, 16, 416-425 (1970),

33. Temple-Pediani, R. W., "Fuel Drop Vaporization Under Pressure on a Hot Surface," Proc. Instn. Mech. Engrs., 184, Pt. 1, No. 38, 677-696 (1969-1970).

34. Touloukian, Y. S., P. E. Liley and S. C. Saxena, Thermal Conductivity Nonmetallic Liquids and Gases, Thermophysical Properties of Matter, Plenum, 3, 207 (1970).

35. Touloukian, Y. S. and T. Makita, Specific Heat Nonmetallic Liquids on Gases, Thermophysical Properties of Matter, Plenum, 6, 228 (1970).

36. Wachters, L. H. J., H. Bonne and H. J. Van Nouhis, "The Heat Transfer from a Hot Horizontal Plate to Sessile Water Drops in the Spheroidal State," Chem. Eng. Sci., 21, 923-936 (1966).

37. Weibelt, John A., Engineering Radiation Heat Transfer, New York: Holt, Rinehart and Winston (1966).

APPENDIX A

VAPOR DIFFUSIVITY

VAPOR DIFFUSIVITY

The vapor diffusivity is calculated, at low pressure, by the Slattery and Bird correlation as presented by Reid and Sherwood (13) pages 530.

$$D_{12}P = 2.74x10^{-4}(m_1+m_2/m_1m_2)^{\frac{1}{2}}(P_{c_1}xP_{c_2})^{\frac{1}{3}}(T_{c_1}xT_{c_2})^{-.495}T^{1.823}\ \frac{atmcm^2}{sec}$$

where m_1, m_2, P_{c_1}, P_{c_2}, T_{c_1}, T_{c_2} are molecular weights, critical pressures in atmospheres, and critical temperatures in ^oK of the two gases. The temperature, T, is in ^oK and P is in atmospheres.

At high pressures the above equation is not strictly valid. Reid and Sherwood (13) give an equation, derived by Enskog, to correct for pressure effects:

$$\frac{D_{12}P}{z(D_{12}P)_0} = 1/x$$

where $(D_{12}P)_0$ is the value from the Slattery-Bird correlation, Z is the compressibility factor, and P is the pressure in atmospheres. x is approximately 1.0 for many systems. The correlation only gives rough values for high pressures, but is is the only one available.

DIFFUSIVITY SUBROUTINE, F=114

```
      SUBROUTINE DIFFUS(MW,TC,PC,PSAT,DP,Z)
      REAL MW
      CALLSATEM(PSAT,TSAT,3)
      DP0=2.74E-04*SQRT((MW+28.)/(MW*28.))*(PC*33.5)**(1./3.)/(TC*126.)
     1**.495*TSAT**(1.823)
      DP=DP0*Z*3.87
      RETURN
      END
```

APPENDIX B

VAPOR THERMAL CONDUCTIVITY

VAPOR THERMAL CONDUCTIVITY

The value of vapor thermal conductivity is necessary for the calculation of the heat flux to the bottom of the drop. The value used in the calculation is an average based on the values at the plate temperature and the saturation temperature.

$$K_{AVG.} = (K(TSAT) + K(TP))/2$$

The values of K for steam are taken from page 281 of the 1967 ASME Steam Tables. The values were curve fitted to the following equation

$$K = .6874617 \times 10^{-2} + .3217265 \times 10^{-4} T \text{ BTU/hr ft } ^{o}F$$

T = temperature in ^{o}F.

For F-114 Touloukian (17) presents an equation for the thermal conductivity at 1 atm as follows

$$KO = (3.79439-1.81602\times10^{-2}T+4.76397\times10^{-5}T^{2})\times10^{-5} \text{ cal/cmsec}^{o}C$$

However, at higher pressures the thermal conductivity must be corrected for the effect of pressure. The method of Stiel and Thodos as given by Reid and Sherwood (13) page 479 was used to correct KO. The equation given by Touloukian was combined with the pressure correlation into a FORTRAN subroutine called THERMK.

```
C          THERMAL CONDUCTIVITY SUBROUTINE, F=114
C
      SUBROUTINE THERMK(TC,PC,MW,RHOV,T,ZC ,K)
      REAL K1,K2
      REAL MW,KO,K
C     TC= DEG K,     PC= ATM
      RHOC=PC*MW/(.73*ZC*TC*1.8)
      GAMMA =TC**(1./6.)*SQRT(MW)/PC**(2./3.)
      RHOR=RHOV/RHOC
      KO=(3.79439-1.81602E-02*T+4.76397E-05*T*T)*1.E-05
      IF(RHOR.GT. .5) GOTO 10
      K=((14.E-08*(EXP(-.535*RHOR)-1.))/(GAMMA*ZC**5))+KO
      K=K*242.08
      GOTO 1
10    K=((13.1E-08*(EXP(.67*RHOR)-1.069))/(GAMMA*ZC**5))+KO
      K=K*242.08
1      CONTINUE
      RETURN
      END
```

APPENDIX C

ANALYSIS OF TEMPERATURE DISTRIBUTION IN THE WALL OF THE TEST CELL

ANALYSIS OF TEMPERATURE DISTRIBUTION IN THE WALL OF THE TEST CELL

Arpaci (2) makes an analysis of a skillet subjected to a uniform heat flux from below. The geometry of the test cell and the example solved by Arpaci is similar. From the results of the analysis the temperature distribution in the wall of the test cell is obtained. Once the temperature distribution in known then the radiation heat transfer from the wall to the drop can be obtained. The solution obtained is

$$\frac{T_w - T_\infty}{T_p - T_\infty} = \frac{\cosh(mz)}{\cosh(mL)} \tag{49}$$

where:

$m^2 = 2h\delta/K$

L = length of the wall

Z = distance from the top of the wall

δ = thickness of the wall

h = heat transfer coefficient from the wall to the surroundings

k = thermal conductivity of the wall material

Radiation Analysis for the Wall

The Stefan-Boltzmann equation for a given point x on the wall at temperature T_w can be written

$$Eb_w = \sigma T_w^4 \tag{50}$$

where Eb_w is the total emissive power of the wall in BTU/hr ft^2 ^oF. The average value of the total emissive power, $Eb_w(Z)$, is approximated by finding the weighted average value of the wall temperature. The analysis follows:

$$\theta = \frac{\cosh(mZ)}{\cosh(mL)}$$

from Equation (49). The Stefan-Boltzmann equation says that total emissive power at a given point is proportional to the temperature of that point to the fourth power. Thus, the average value of θ should be taken weighted as the fourth power

$$\theta^4_{AVG} = \frac{1}{L}\int_0^L \frac{\cosh^4(mZ)}{\cosh^4(mL)}\,dZ$$

$$= \frac{1}{L\cosh^4(mL)}\int_0^L \cosh^4(mZ)dZ$$

$$= \frac{1}{mL\cosh^4(mL)}\left[\frac{\sinh(4mZ)}{32} + \frac{\sinh(2mZ)}{4} + \frac{3mZ}{8}\right]_0^L$$

$$= \frac{1}{mL\cosh^4(mL)}\left[\frac{\sinh(4mL)}{32} + \frac{\sinh(2mL)}{4} + \frac{3mL}{8}\right]$$

For the typical value of K = 13 BTU/hr ft ^oF for stainless steel, δ = 1", L = 2.5" and a maximum value of h = 10 BTU/hr ft^2 ^oF.

$$mL \simeq 1$$

Thus,

$$\theta_{AVG} \doteq .736$$

or

$$T_w = T_p - .736(T_p - T_\infty)$$

The value of the weighted average wall temperature from the preceding analysis can be used to calculate the total emissive power of the entire wall from Equation (50).

For calculational simplicity in the radiation heat transfer analysis, the lid of the test cell is assumed to behave as if it were part of the wall. Thus, the droplet sees two sources of radiation, the plate (at T_p) and the surroundings, consisting of the wall and lid, at T_w.

APPENDIX D

INFRARED ABSORPTANCE FOR LIQUID F-114

INFRARED ABSORPTANCE FOR LIQUID F-114

The average value of the absorptance, α, was found by integrating the data by the following equation

$$\alpha_{AVG} = \frac{\int_{\lambda_1}^{\lambda_2} \alpha(\lambda)d\lambda}{\int_{\lambda_1}^{\lambda_2} d\lambda}$$

Due to the transmission and absorption bands the data were integrated over each band. The range of integration was from 2 to 14 microns.

The average absorptance was found to be

$$\alpha_{AVG} = .514$$

The source of the data was the API Research Project 44 serial number 1318. The data were contributed by the U. S. Navy Research Laboratory.

APPENDIX E

FORTRAN SUBROUTINES FOR HEAT CAPACITY AND SATURATION TEMPERATURE FOR FREON-114

```
    HEAT CAPACITY SUBROUTINE, F=114

SUBROUTINE SPHT(T,CP)
 CP IS IN BTU/LB- F ,  T IS IN DEG R
T=T/1.8
CP=-.022243+1.0849E-03*T-1.82865E-06*T*T+1.1592E-09*T*T*T
T=T*1.8
RETURN
END
```

```
C          SATURATION TEMPERATURE SUBROUTINE,F=114
C
      SUBROUTINE SATEM(PSAT,TSAT,NN)
      TSAT=5073.063/(12.87506-ALOG(PSAT))
      GOTO(1,2,3,4),NN
1     TSAT=TSAT-460.
2     TSAT=TSAT
      GOTO 5
3     TSAT=TSAT/1.8
      GOTO 5
4     TSAT=(TSAT/1.8)-273.16
5     RETURN
      END
```

APPENDIX F

DIAMETER HISTORY OF WATER DROPS

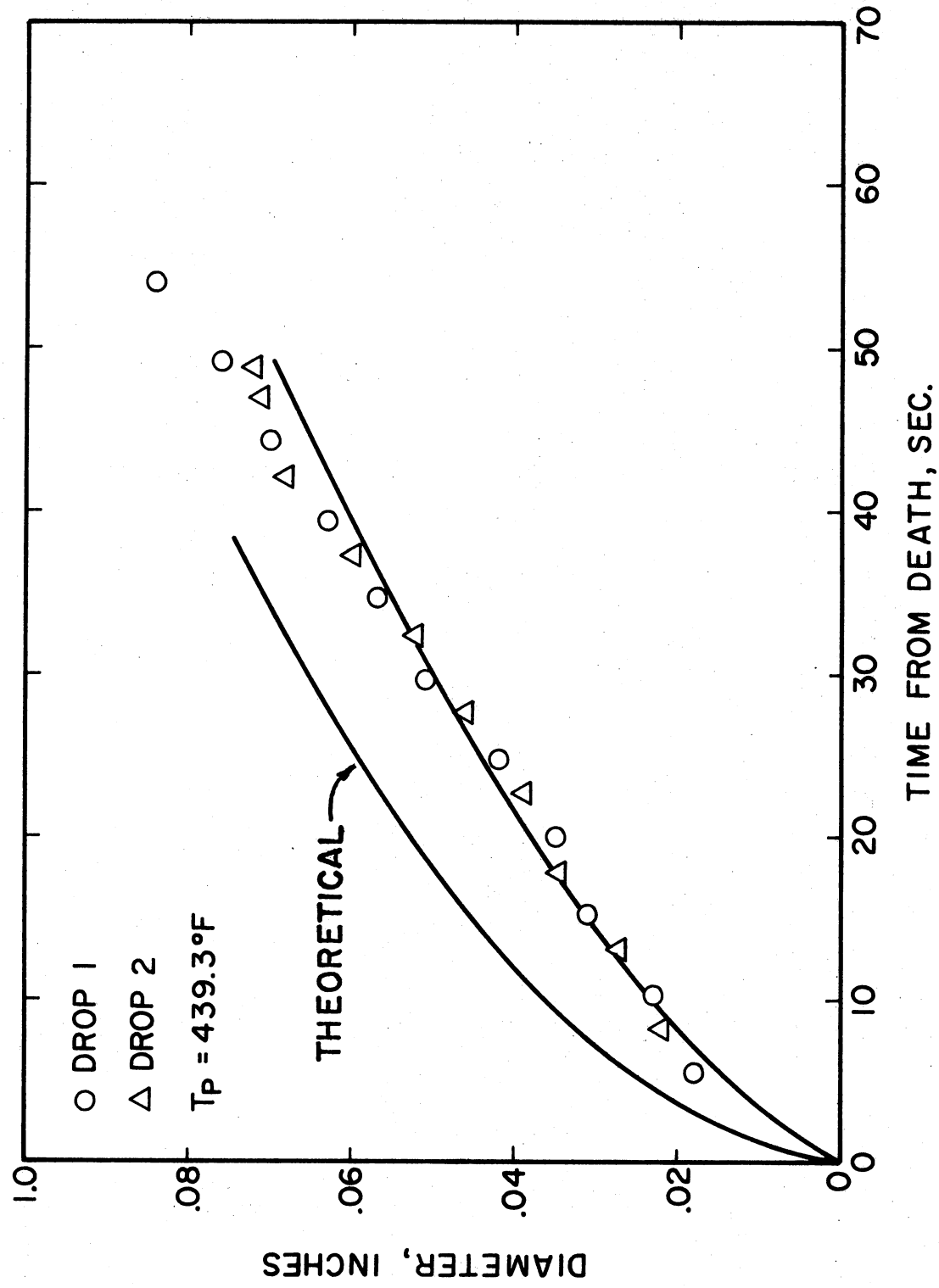
DIAMETER, INCHES
TIME FROM DEATH, SEC.
O DROP 1
Δ DROP 2
T_P = 439.3°F
THEORETICAL
0
10
20
30
40
50
60
70
.02
.04
.06
.08
1.0

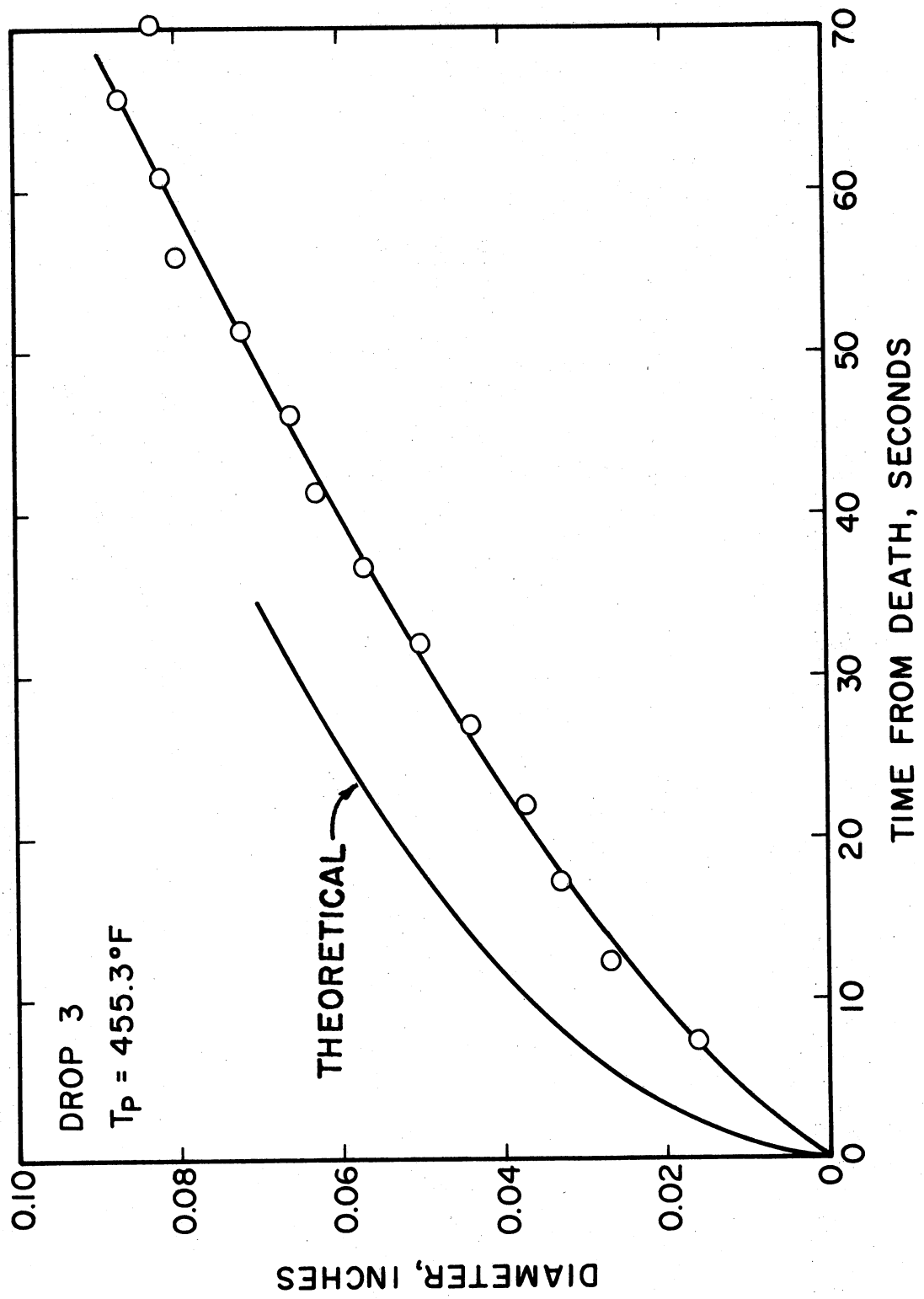
DIAMETER, INCHES
0.10
0.08
0.06
0.04
0.02
0
0
10
20
30
40
50
60
70
TIME FROM DEATH, SECONDS
DROP 3
T_P = 455.3°F
THEORETICAL

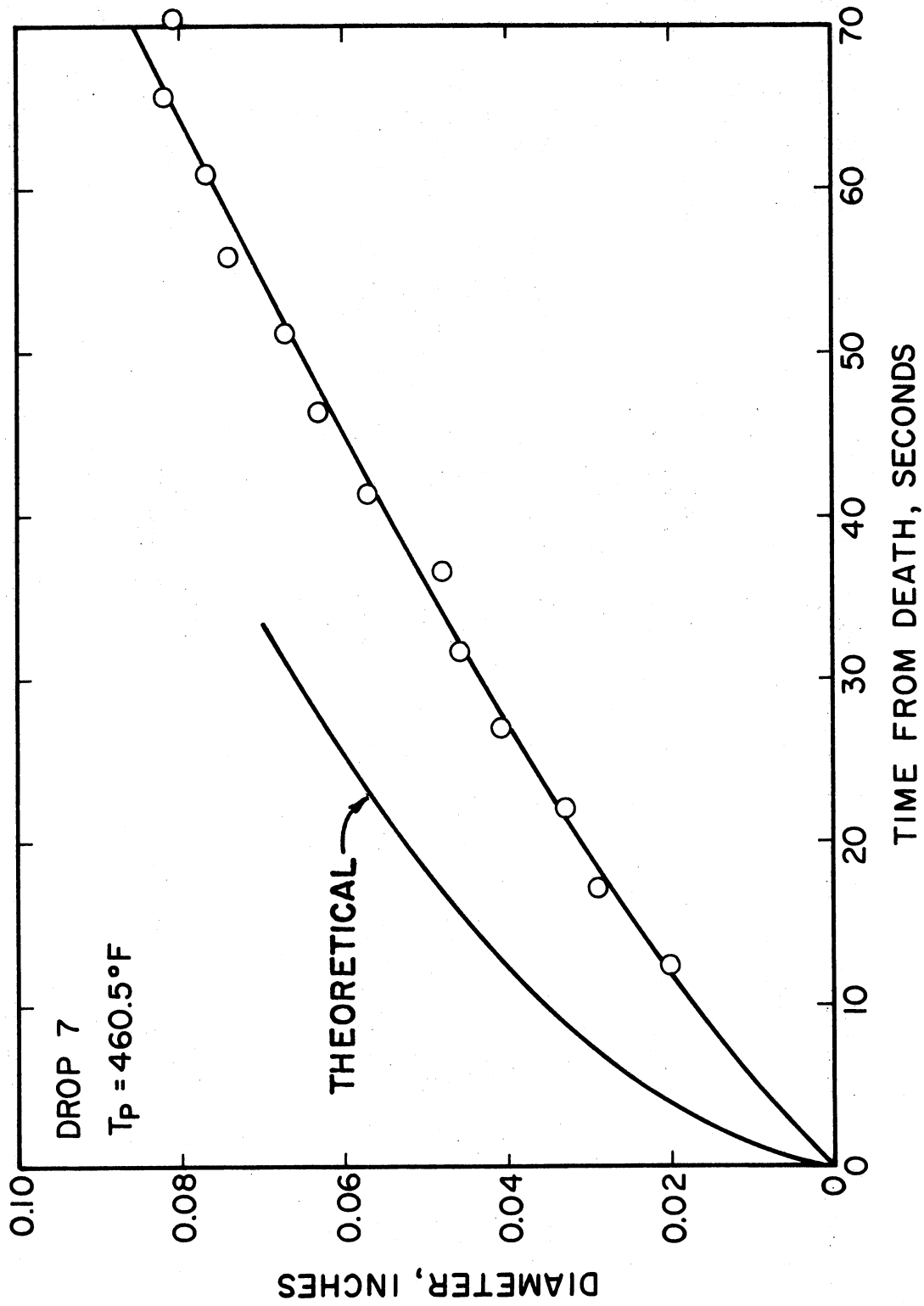
DROP 7
T_P = 460.5°F
THEORETICAL
DIAMETER, INCHES
TIME FROM DEATH, SECONDS
0.10
0.08
0.06
0.04
0.02
0
0
10
20
30
40
50
60
70

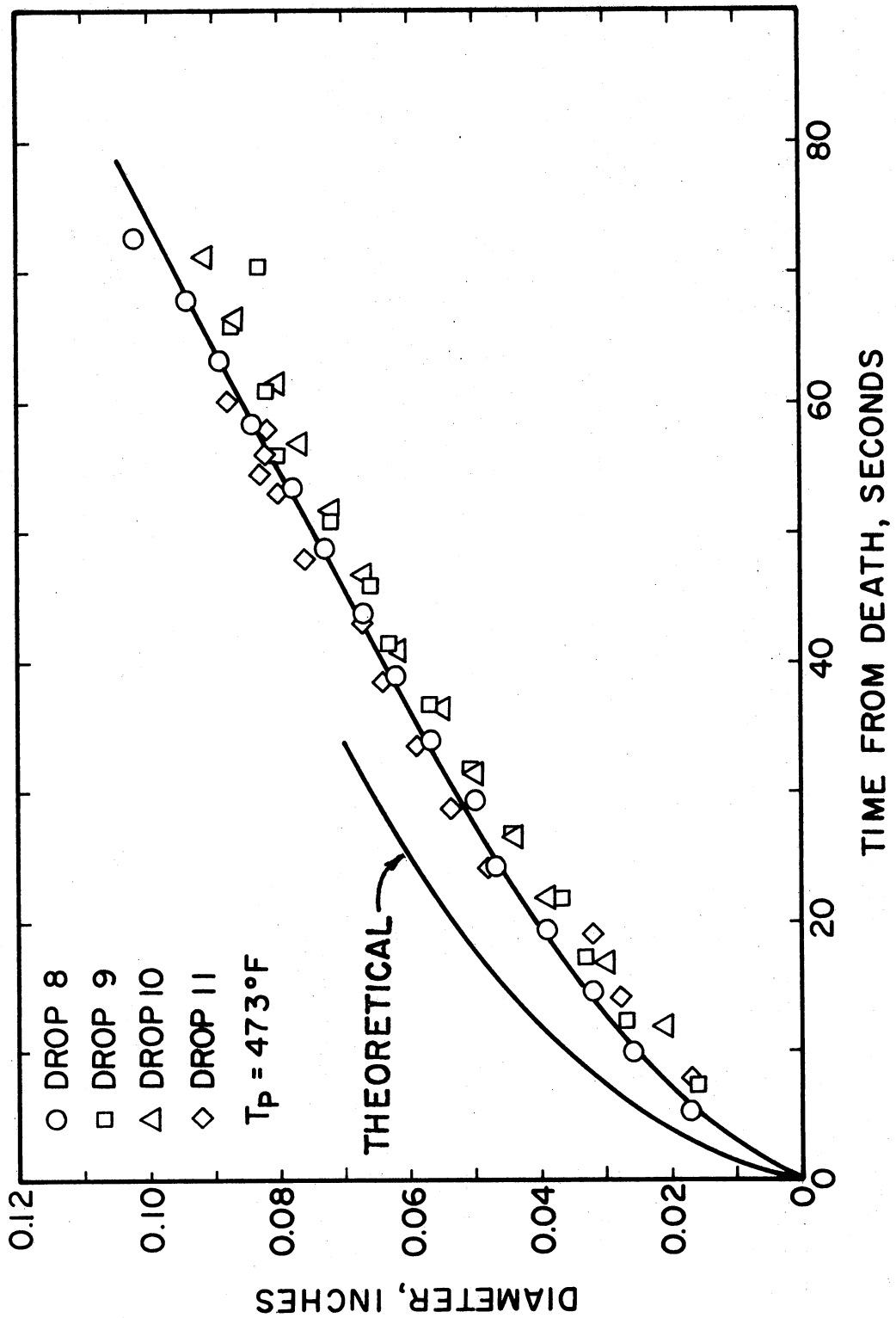
DIAMETER, INCHES
TIME FROM DEATH, SECONDS
0.12
0.10
0.08
0.06
0.04
0.02
0
0
20
40
60
80
○ DROP 8
□ DROP 9
△ DROP 10
◇ DROP 11
T_P = 473°F
THEORETICAL

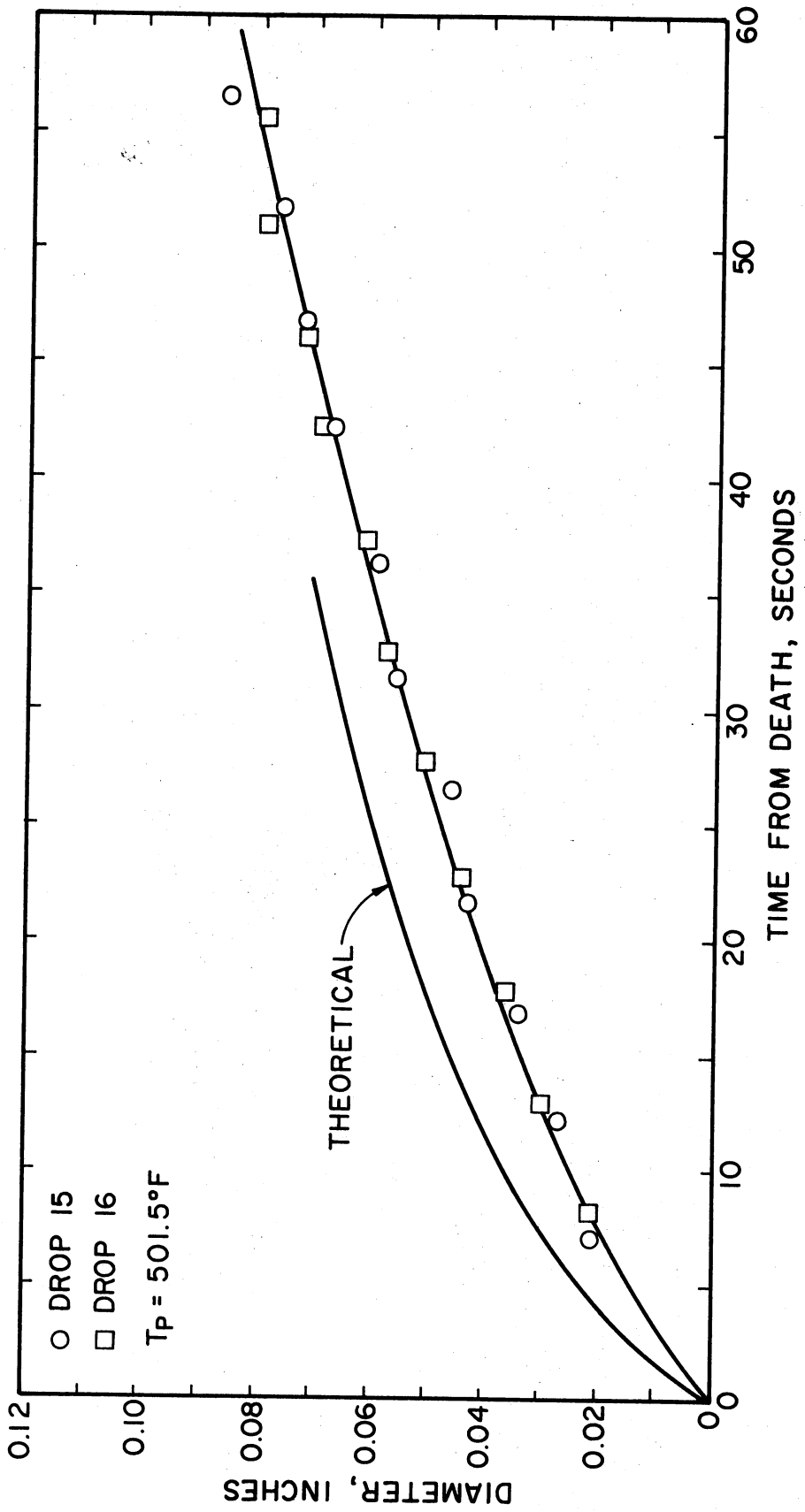
DIAMETER, INCHES
0.12
0.10
0.08
0.06
0.04
0.02
0
0
10
20
30
40
50
60
TIME FROM DEATH, SECONDS
THEORETICAL
○ DROP 15
□ DROP 16
T_P = 501.5°F

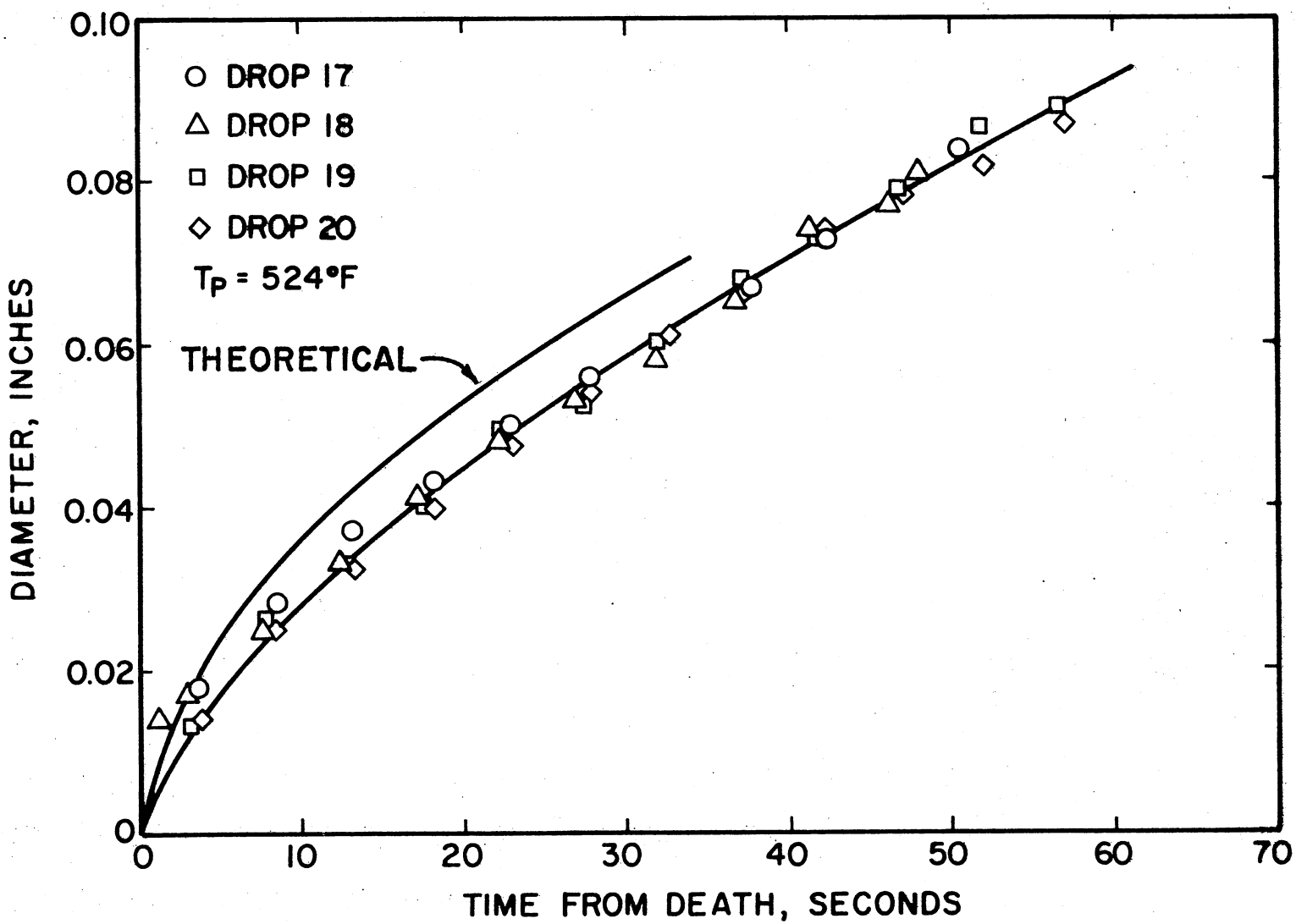
0.10
0.08
0.06
0.04
0.02
0
DIAMETER, INCHES
DROP 17
DROP 18
DROP 19
DROP 20
T_P = 524°F
THEORETICAL
0
10
20
30
40
50
60
70
TIME FROM DEATH, SECONDS

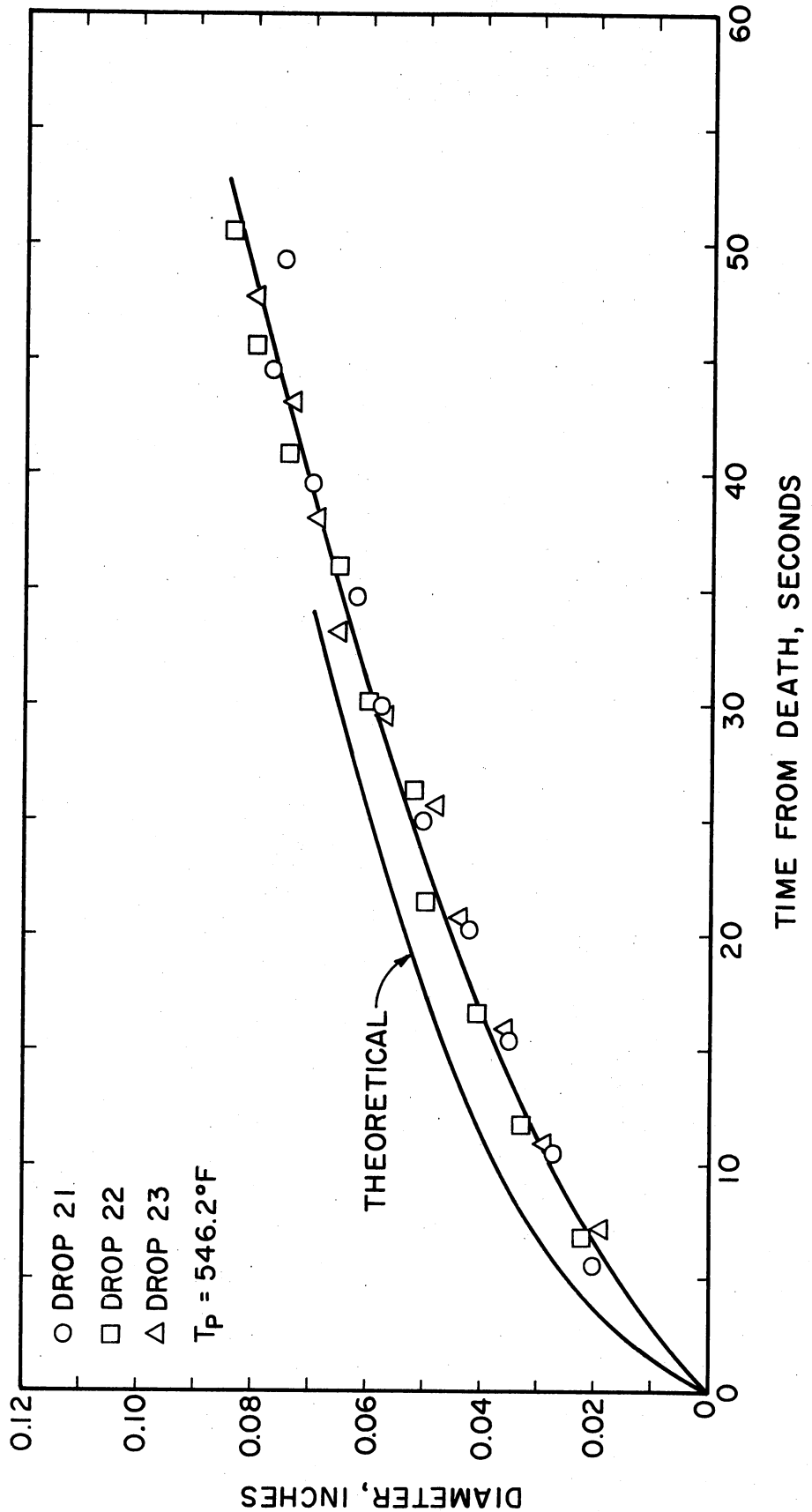
DIAMETER, INCHES
0.12
0.10
0.08
0.06
0.04
0.02
0
0
10
20
30
40
50
60
TIME FROM DEATH, SECONDS
○ DROP 21
□ DROP 22
△ DROP 23
T_P = 546.2°F
THEORETICAL

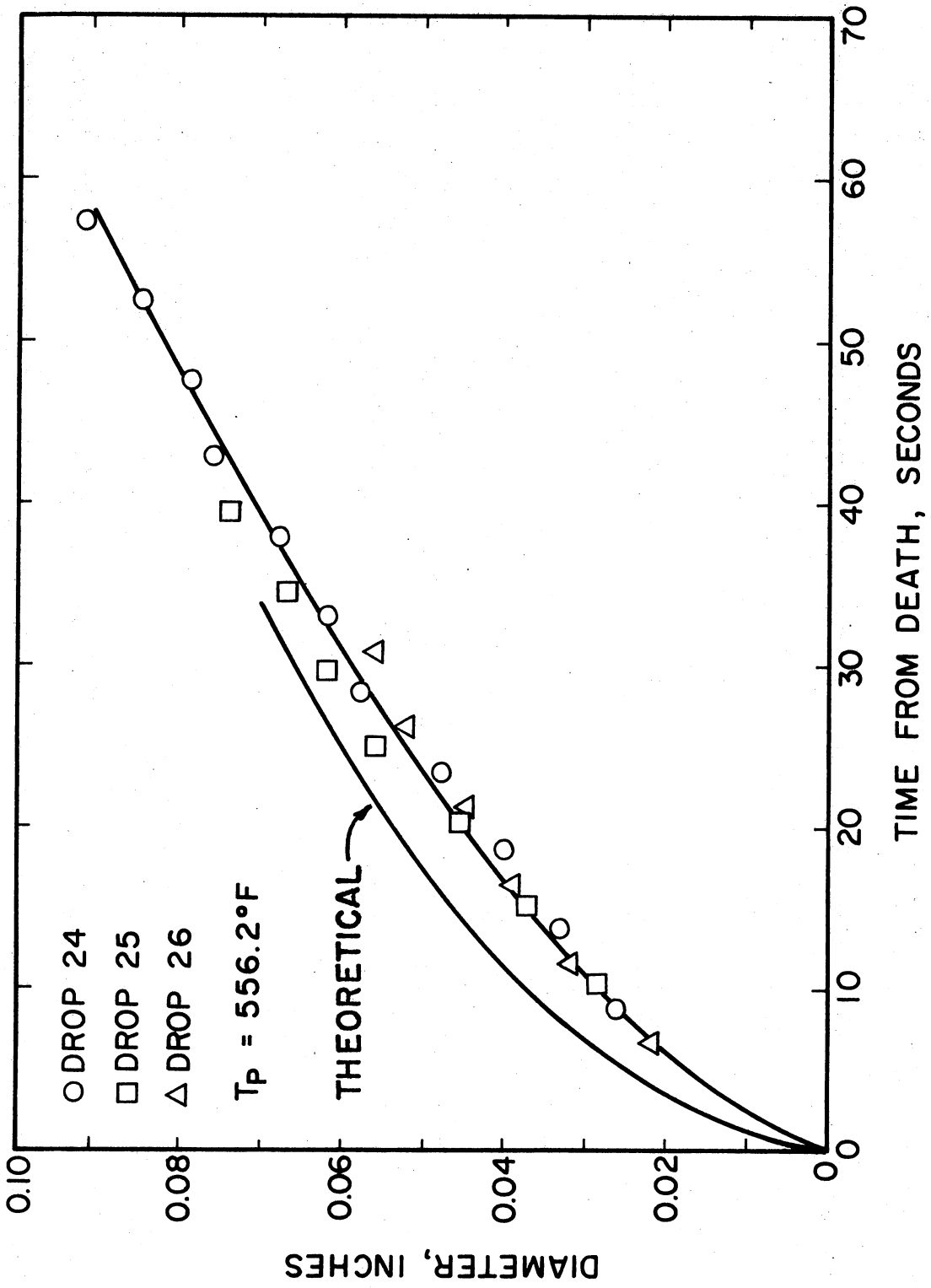
DIAMETER, INCHES
0.10
0.08
0.06
0.04
0.02
0
0
10
20
30
40
50
60
70
TIME FROM DEATH, SECONDS
○ DROP 24
□ DROP 25
△ DROP 26
T_P = 556.2°F
THEORETICAL

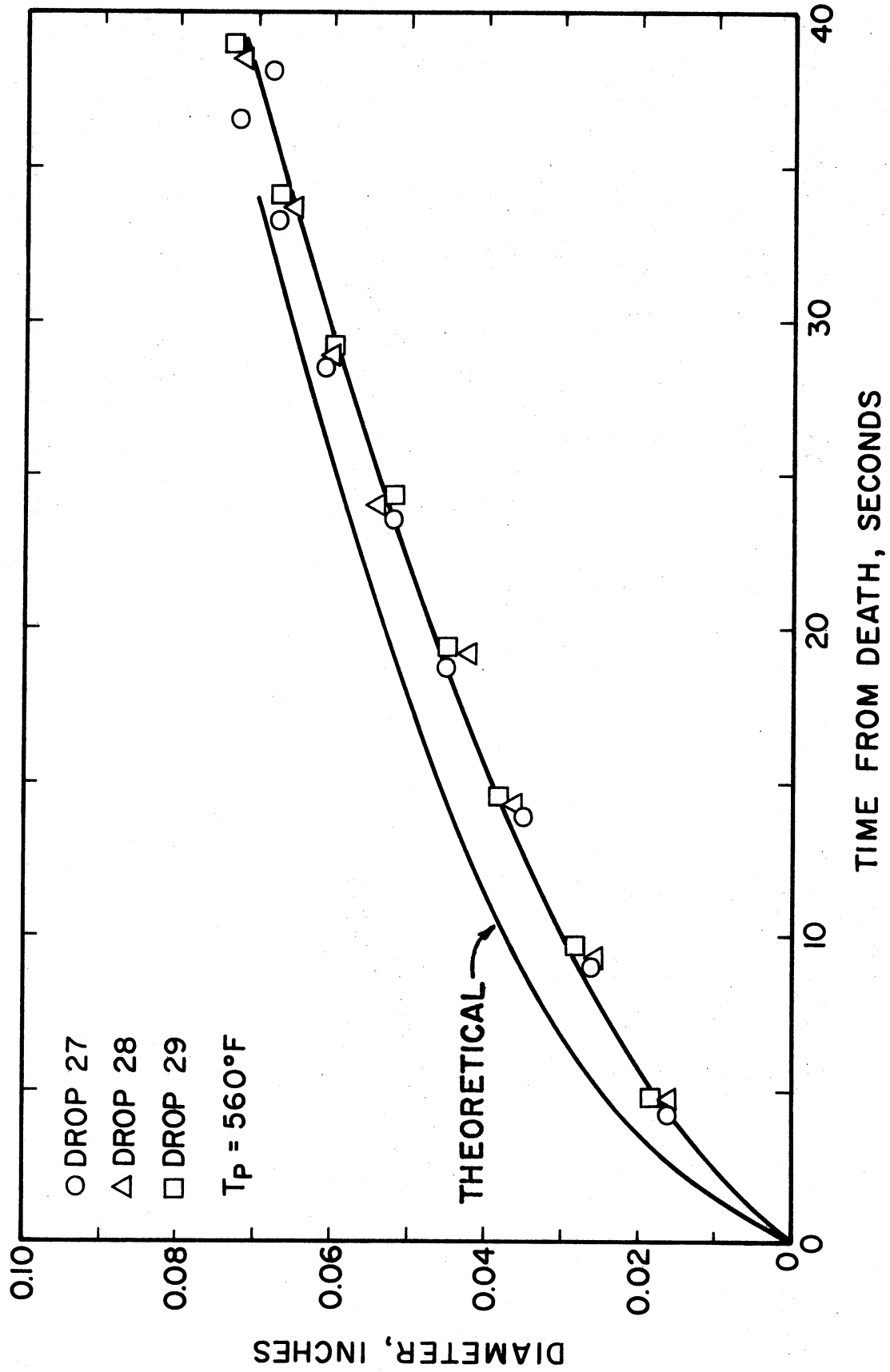
DIAMETER, INCHES
0.10
0.08
0.06
0.04
0.02
0
0
10
20
30
40
TIME FROM DEATH, SECONDS
○ DROP 27
△ DROP 28
□ DROP 29
T_P = 560°F
THEORETICAL

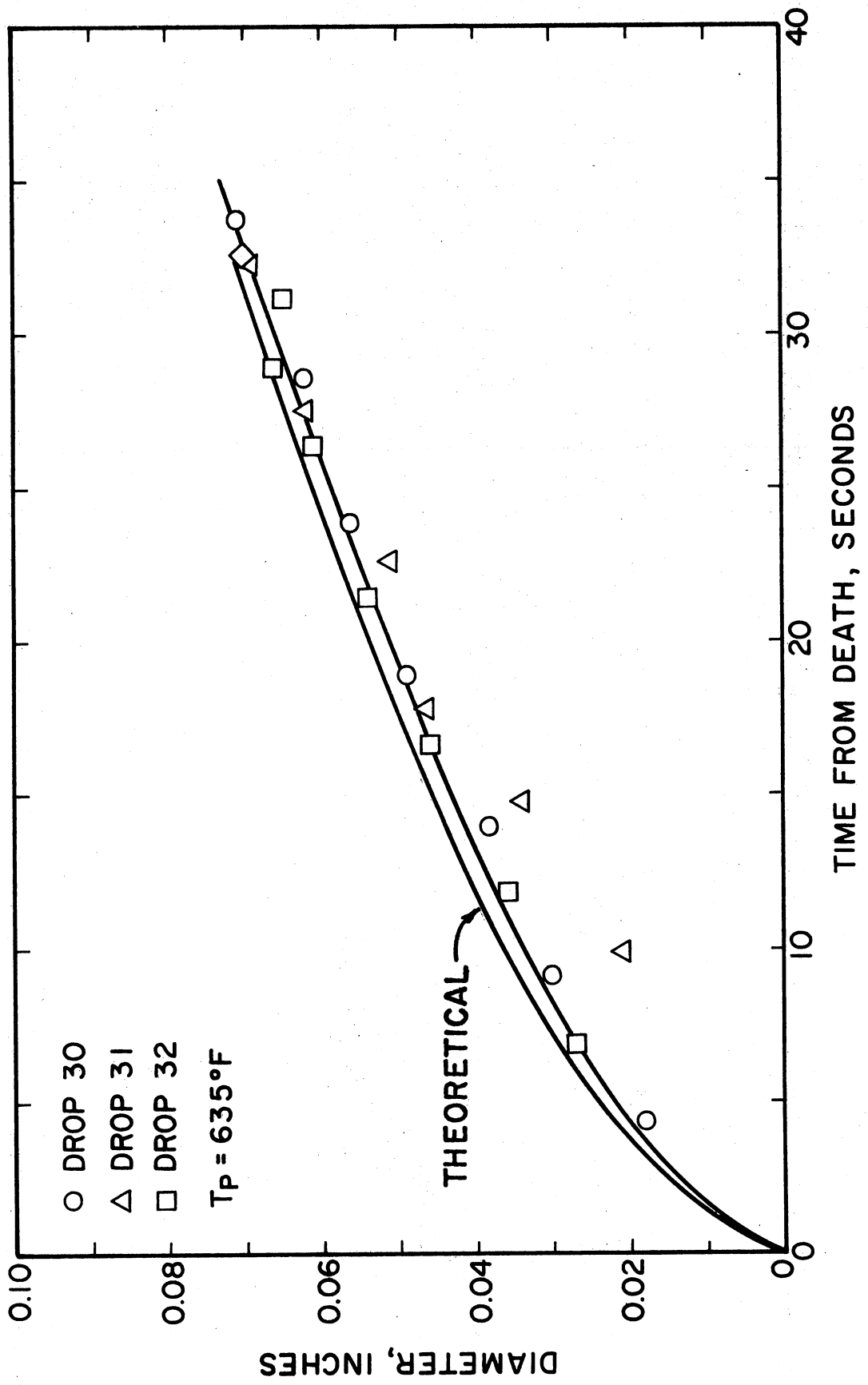
DIAMETER, INCHES
0.10
0.08
0.06
0.04
0.02
0
0
10
20
30
40
TIME FROM DEATH, SECONDS
○ DROP 30
△ DROP 31
□ DROP 32
T_P = 635°F
THEORETICAL

APPENDIX G

DIAMETER HISTORY OF FREON-114 DROPS

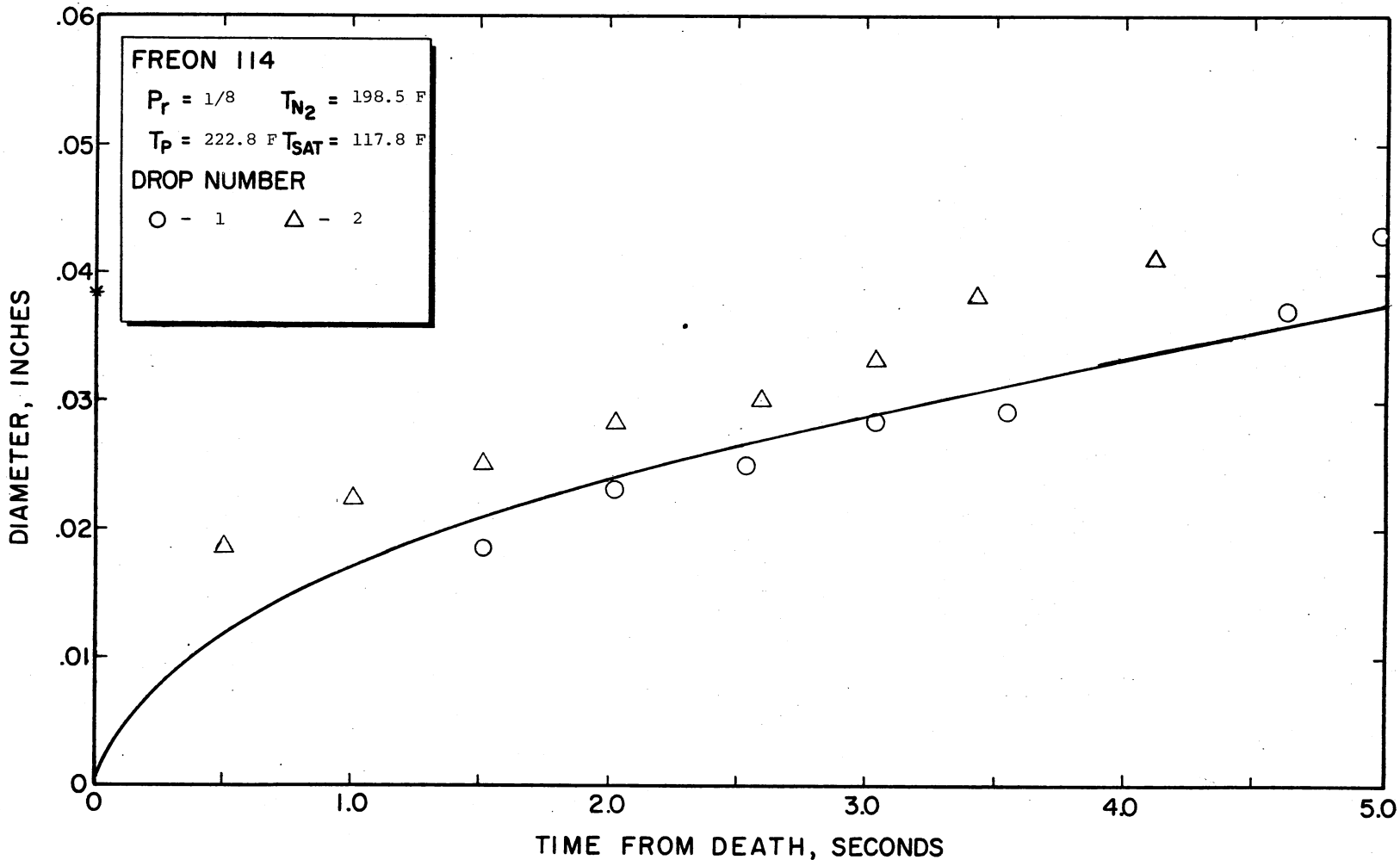
FREON 114
P_r = 1/8 T_{N_2} = 198.5 F
T_P = 222.8 F T_{SAT} = 117.8 F
DROP NUMBER
○ - 1 △ - 2
DIAMETER, INCHES
.06
.05
.04
.03
.02
.01
0
0
1.0
2.0
3.0
4.0
5.0
TIME FROM DEATH, SECONDS

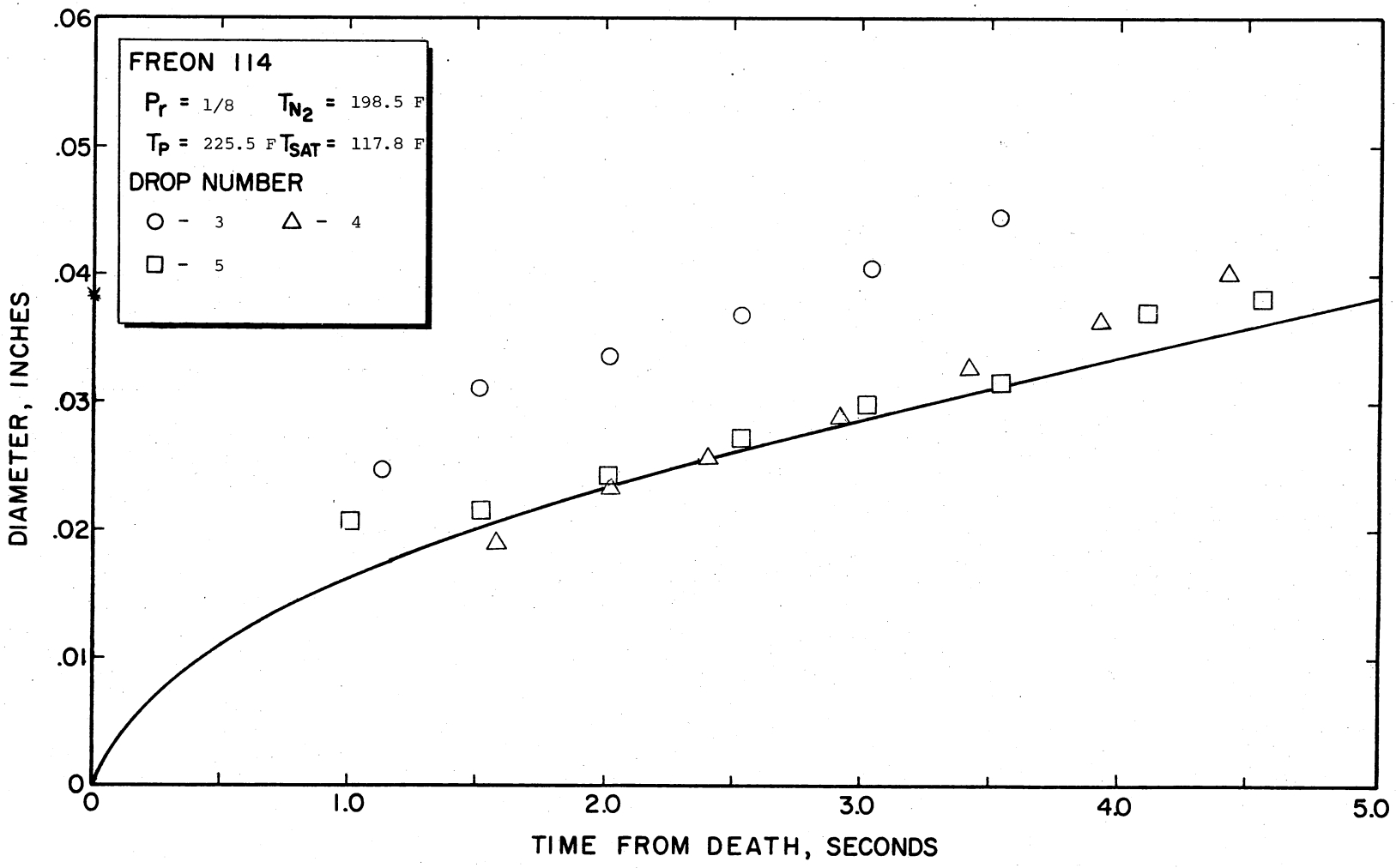
FREON 114
P_r = 1/8 T_{N_2} = 198.5 F
T_P = 225.5 F T_{SAT} = 117.8 F
DROP NUMBER
○ - 3 △ - 4
□ - 5
DIAMETER, INCHES
.06
.05
.04
.03
.02
.01
0
0
1.0
2.0
3.0
4.0
5.0
TIME FROM DEATH, SECONDS

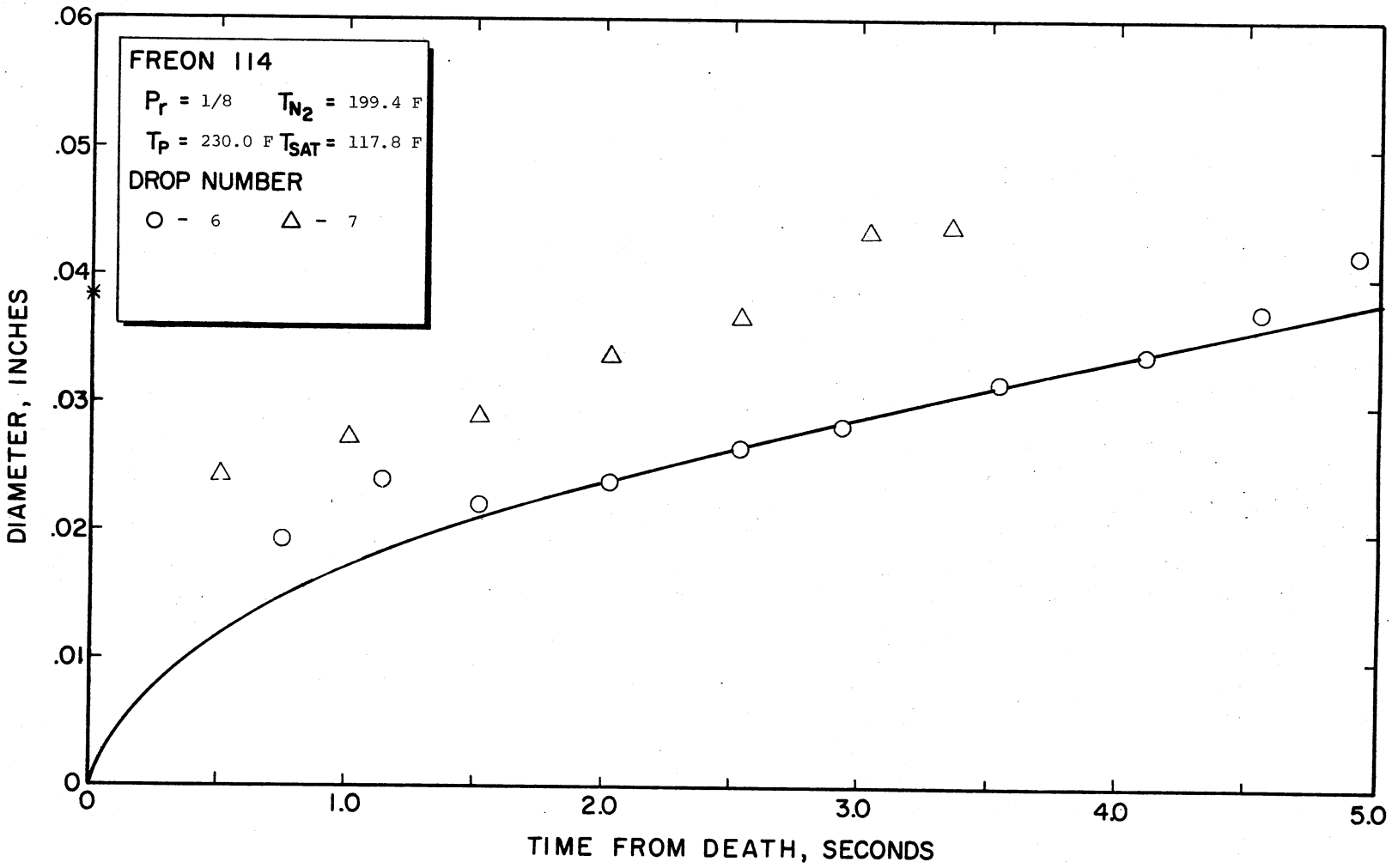
FREON 114
P_r = 1/8 T_{N_2} = 199.4 F
T_P = 230.0 F T_{SAT} = 117.8 F
DROP NUMBER
○ - 6 △ - 7
DIAMETER, INCHES
.06
.05
.04
.03
.02
.01
0
0
1.0
2.0
3.0
4.0
5.0
TIME FROM DEATH, SECONDS

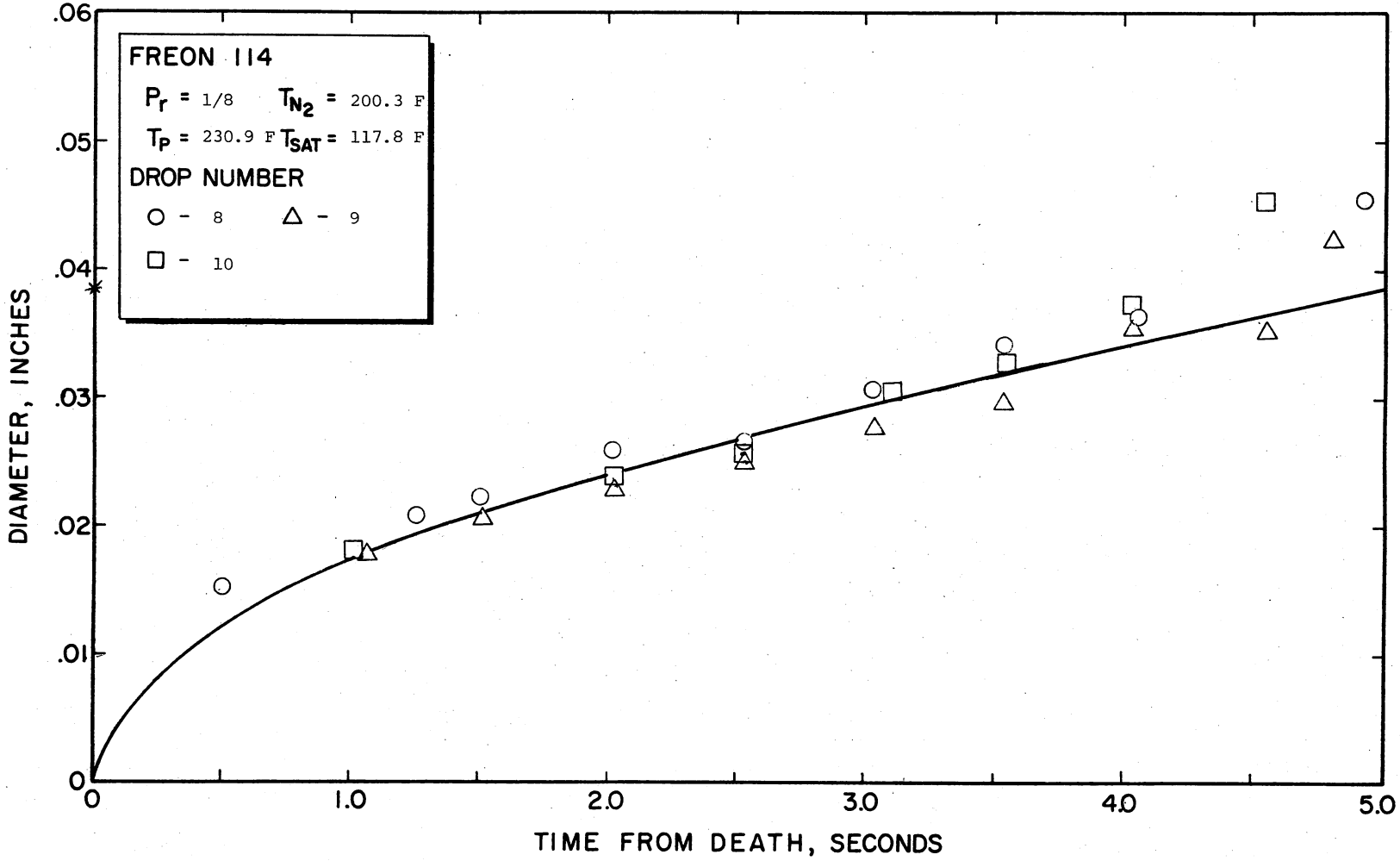
FREON 114
P_r = 1/8 T_{N_2} = 200.3 F
T_P = 230.9 F T_{SAT} = 117.8 F
DROP NUMBER
○ - 8 △ - 9
□ - 10
DIAMETER, INCHES
.06
.05
.04
.03
.02
.01
0
0
1.0
2.0
3.0
4.0
5.0
TIME FROM DEATH, SECONDS

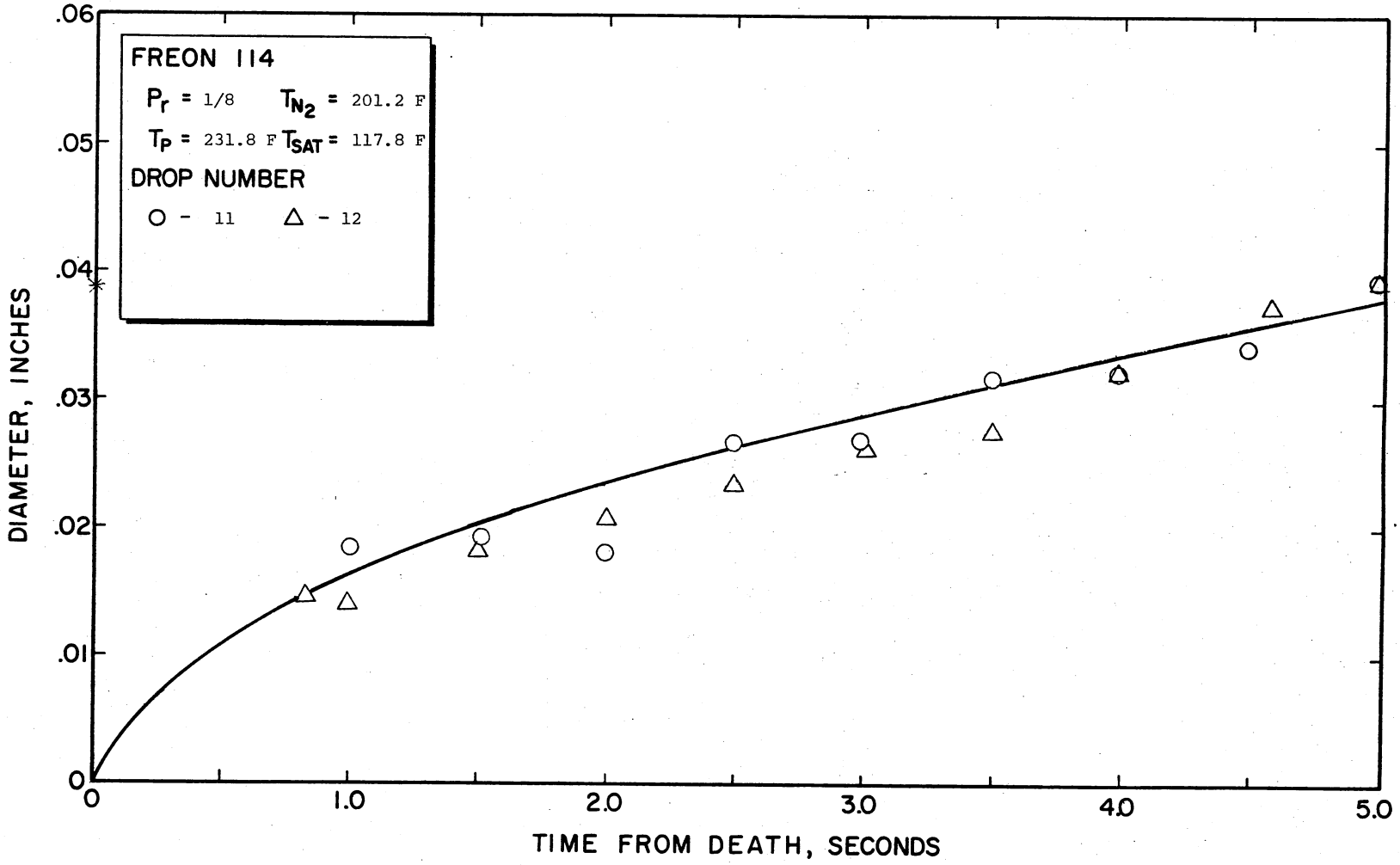
FREON 114
P_r = 1/8 T_{N_2} = 201.2 F
T_P = 231.8 F T_{SAT} = 117.8 F
DROP NUMBER
○ - 11 △ - 12
DIAMETER, INCHES
.06
.05
.04
.03
.02
.01
0
0
1.0
2.0
3.0
4.0
5.0
TIME FROM DEATH, SECONDS

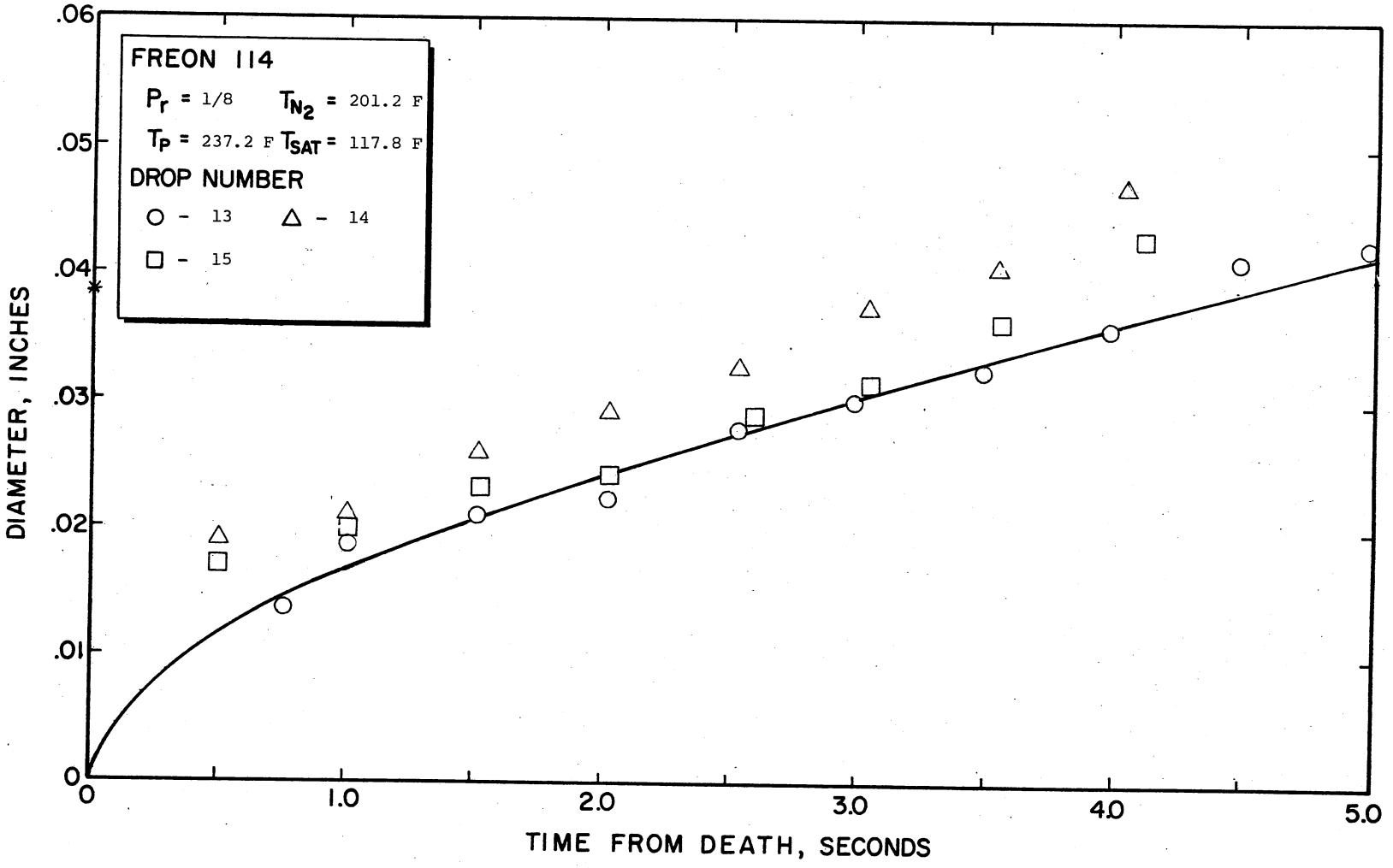
FREON 114
P_r = 1/8 T_{N_2} = 201.2 F
T_P = 237.2 F T_{SAT} = 117.8 F
DROP NUMBER
○ - 13 △ - 14
□ - 15
DIAMETER, INCHES
.06
.05
.04
.03
.02
.01
0
0
1.0
2.0
3.0
4.0
5.0
TIME FROM DEATH, SECONDS

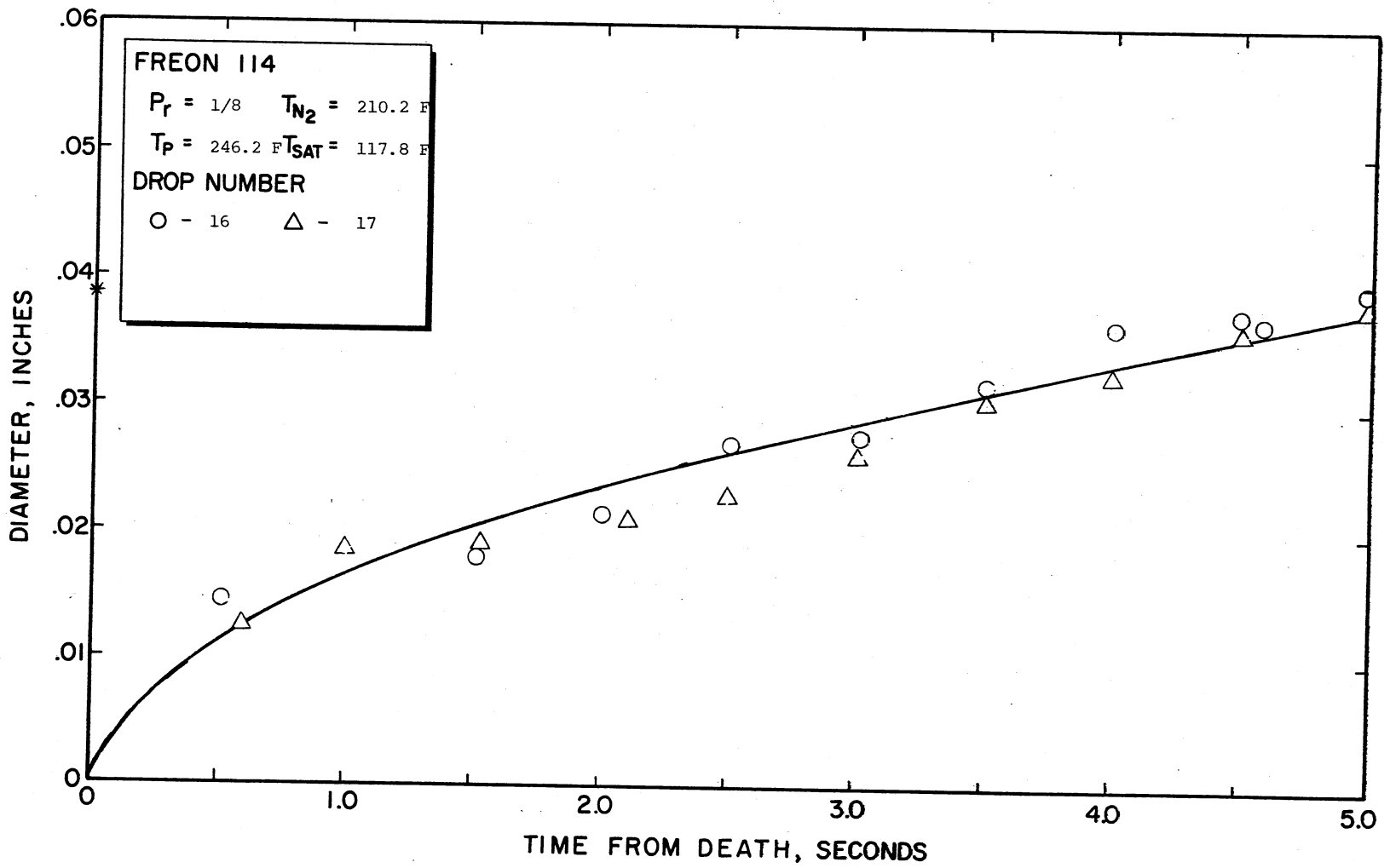
FREON 114
P_r = 1/8 T_{N_2} = 210.2 F
T_P = 246.2 F T_{SAT} = 117.8 F
DROP NUMBER
○ - 16 △ - 17
DIAMETER, INCHES
.06
.05
.04
.03
.02
.01
0
0
1.0
2.0
3.0
4.0
5.0
TIME FROM DEATH, SECONDS

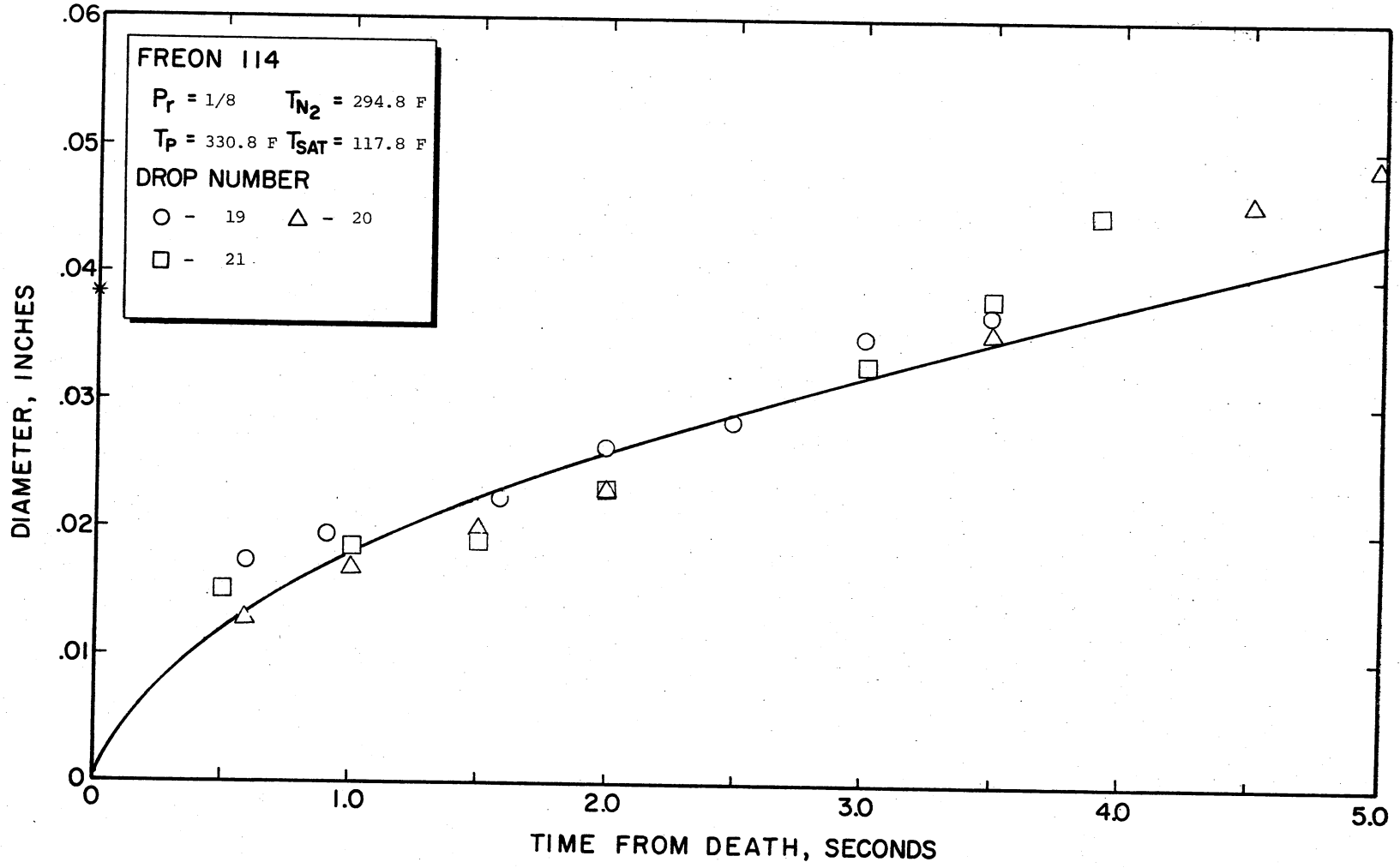
FREON 114
P_r = 1/8
T_{N_2} = 294.8 F
T_P = 330.8 F T_{SAT} = 117.8 F
DROP NUMBER
○ - 19
△ - 20
□ - 21
DIAMETER, INCHES
.06
.05
.04
.03
.02
.01
0
0
1.0
2.0
3.0
4.0
5.0
TIME FROM DEATH, SECONDS

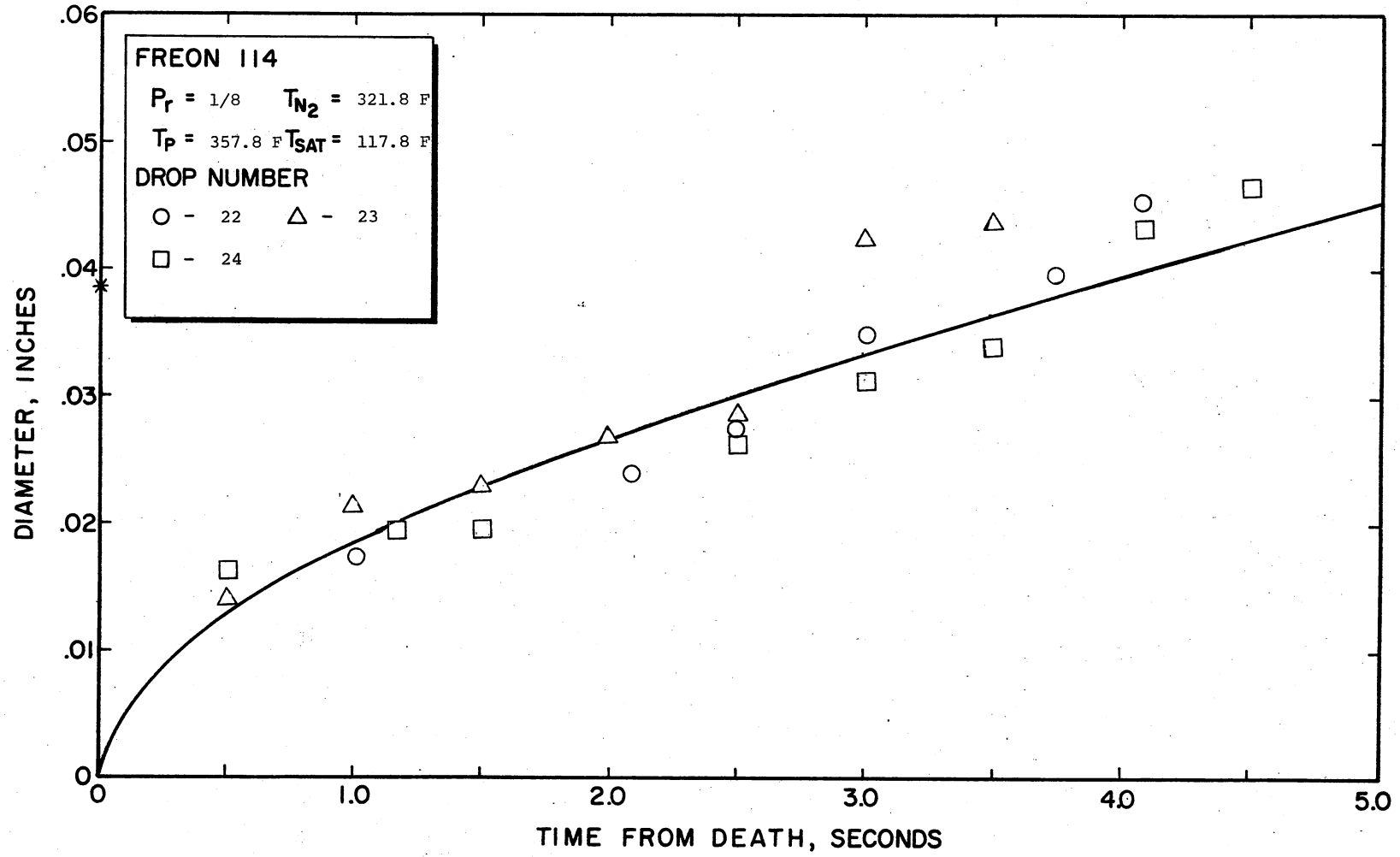
FREON 114
P_r = 1/8 T_{N_2} = 321.8 F
T_P = 357.8 F T_{SAT} = 117.8 F
DROP NUMBER
○ - 22 △ - 23
□ - 24
DIAMETER, INCHES
.06
.05
.04
.03
.02
.01
0
0
1.0
2.0
3.0
4.0
5.0
TIME FROM DEATH, SECONDS

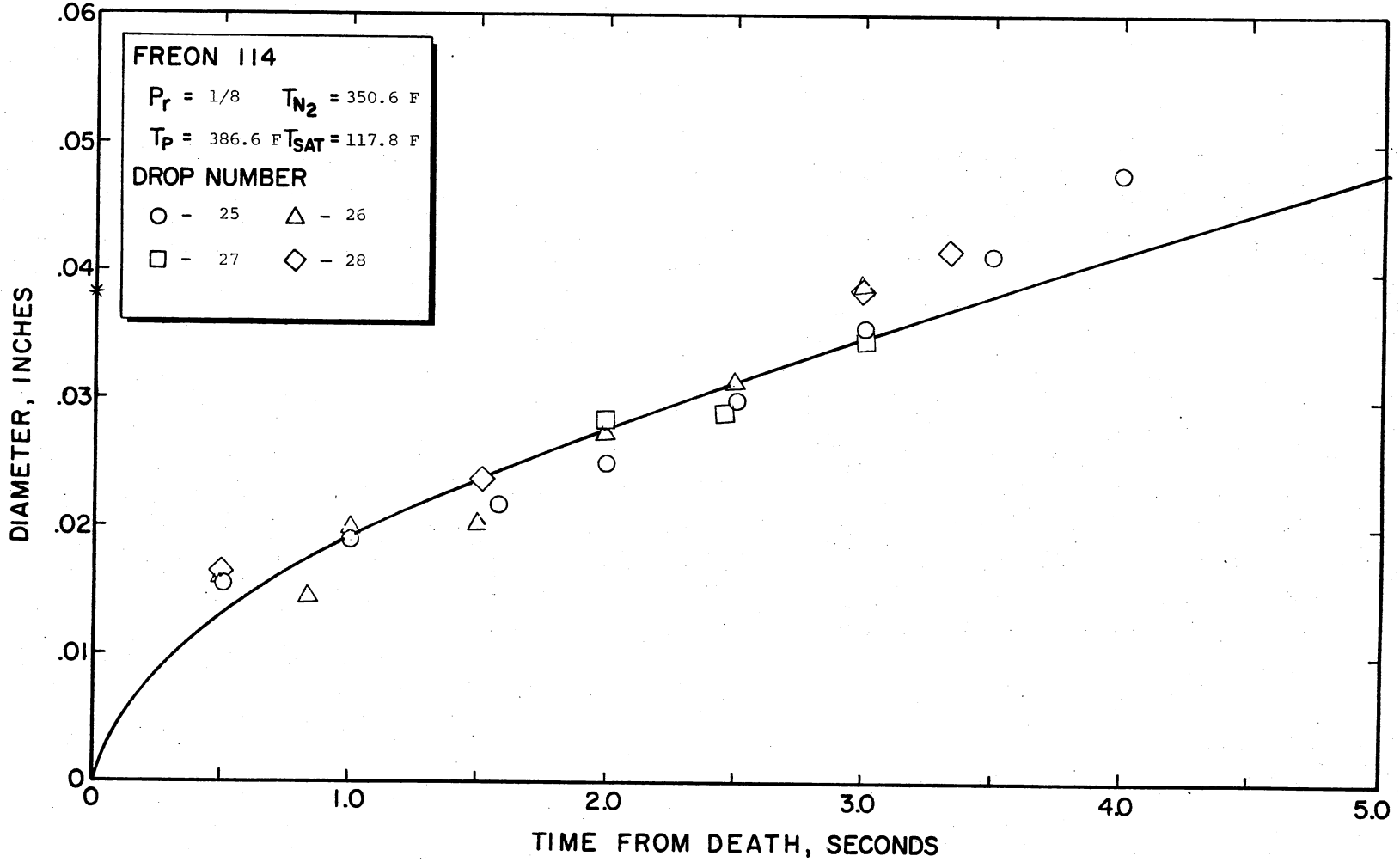
FREON 114
P_r = 1/8 T_{N_2} = 350.6 F
T_P = 386.6 F T_{SAT} = 117.8 F
DROP NUMBER
○ - 25 △ - 26
□ - 27 ◇ - 28
DIAMETER, INCHES
.06
.05
.04
.03
.02
.01
0
0
1.0
2.0
3.0
4.0
5.0
TIME FROM DEATH, SECONDS

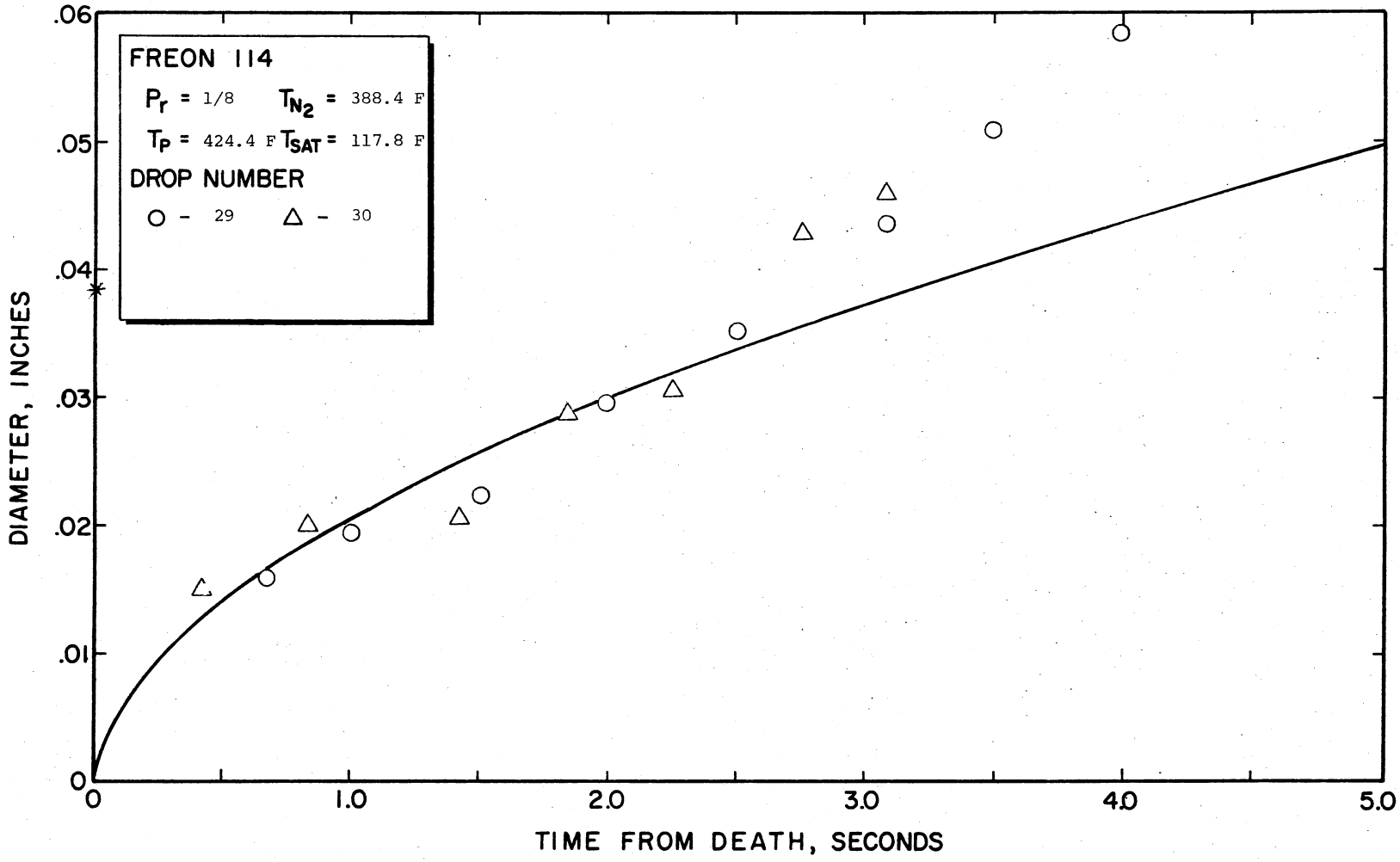
FREON 114
P_r = 1/8 T_{N_2} = 388.4 F
T_P = 424.4 F T_{SAT} = 117.8 F
DROP NUMBER
○ - 29 △ - 30
DIAMETER, INCHES
.06
.05
.04
.03
.02
.01
0
0
1.0
2.0
3.0
4.0
5.0
TIME FROM DEATH, SECONDS

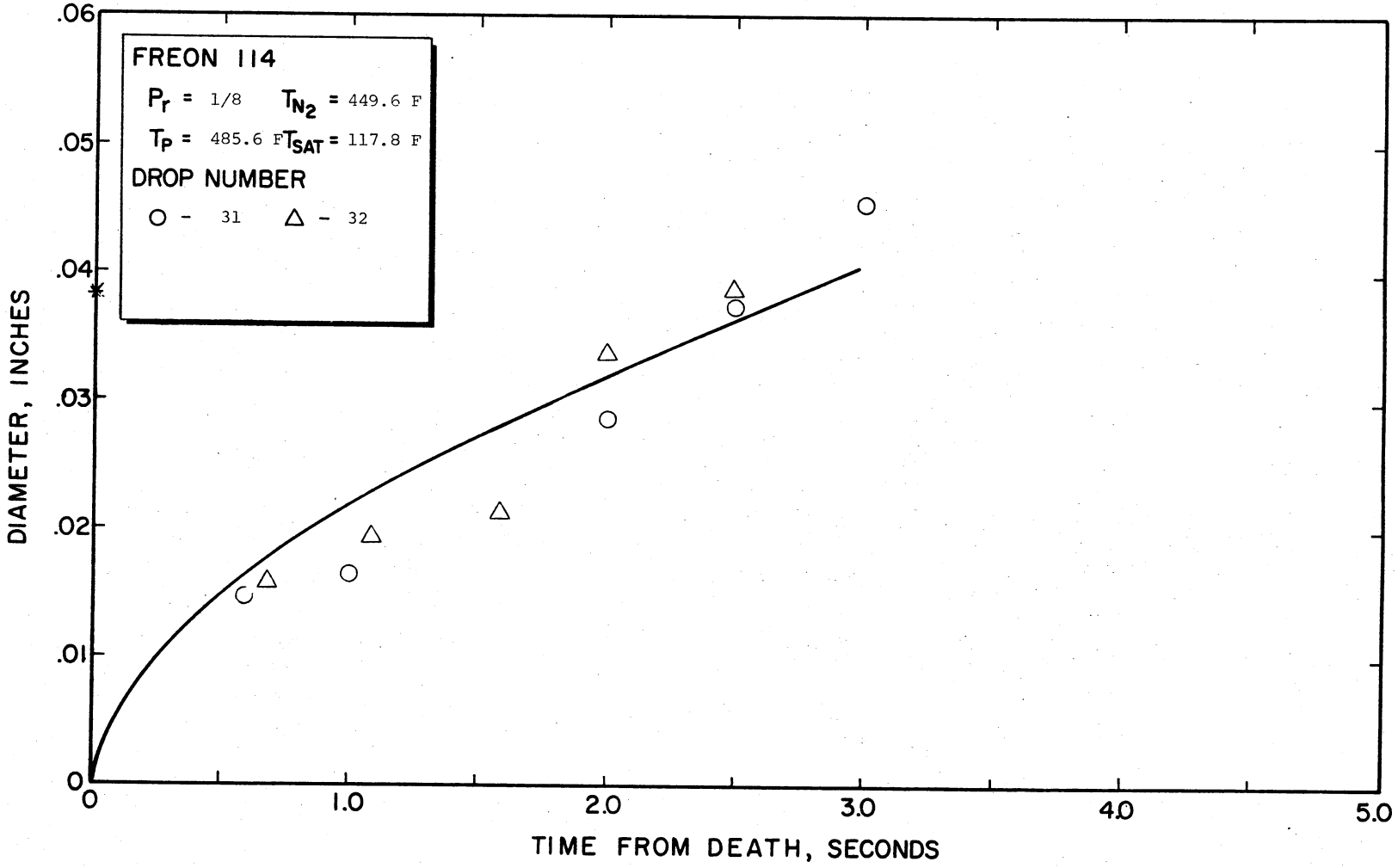
FREON 114
P_r = 1/8 T_{N_2} = 449.6 F
T_P = 485.6 F T_{SAT} = 117.8 F
DROP NUMBER
○ - 31 △ - 32
DIAMETER, INCHES
.06
.05
.04
.03
.02
.01
0
0
1.0
2.0
3.0
4.0
5.0
TIME FROM DEATH, SECONDS

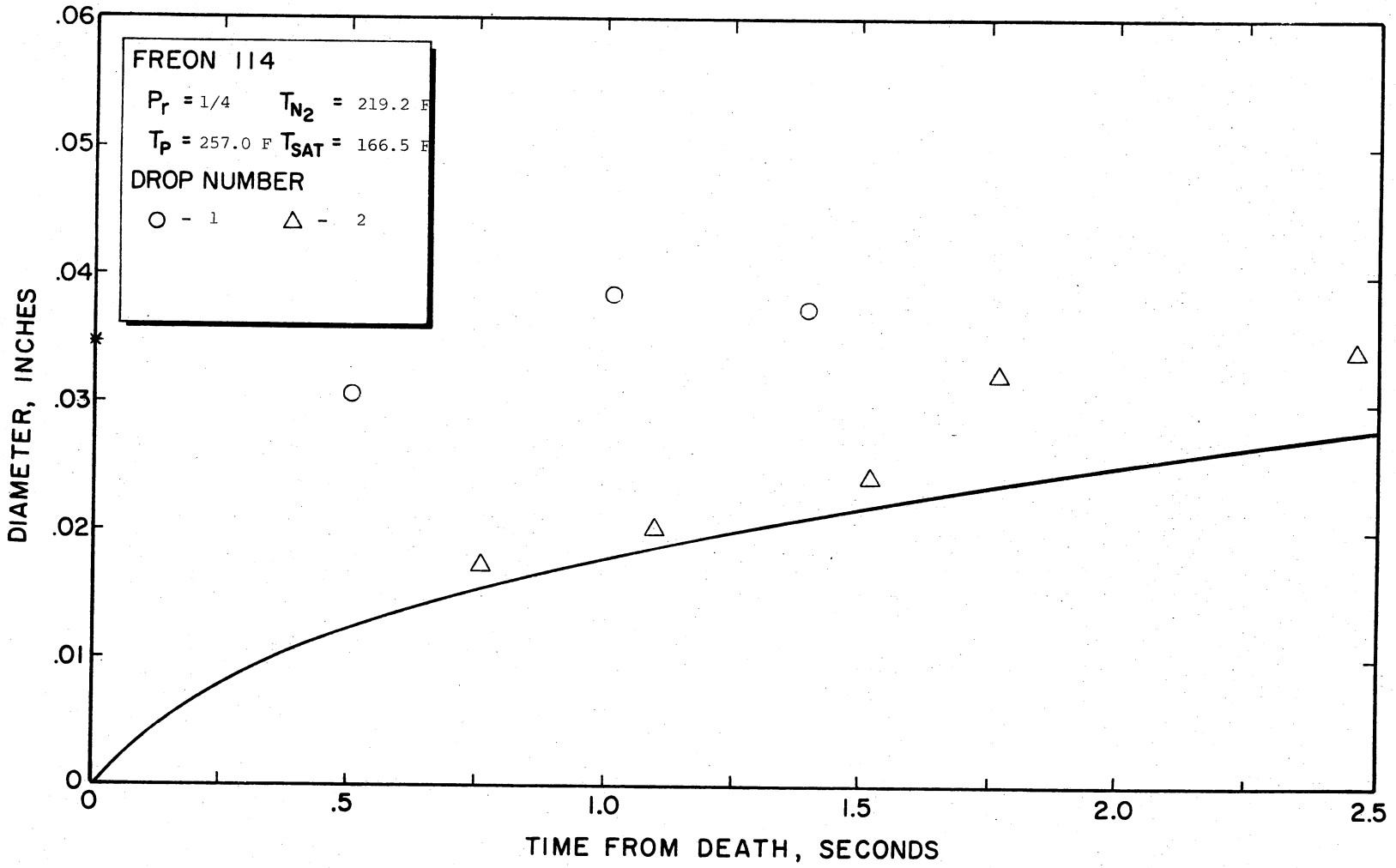
FREON 114
P_r = 1/4 T_{N_2} = 219.2 F
T_P = 257.0 F T_{SAT} = 166.5 F
DROP NUMBER
○ - 1 △ - 2
DIAMETER, INCHES
.06
.05
.04
.03
.02
.01
0
0
.5
1.0
1.5
2.0
2.5
TIME FROM DEATH, SECONDS

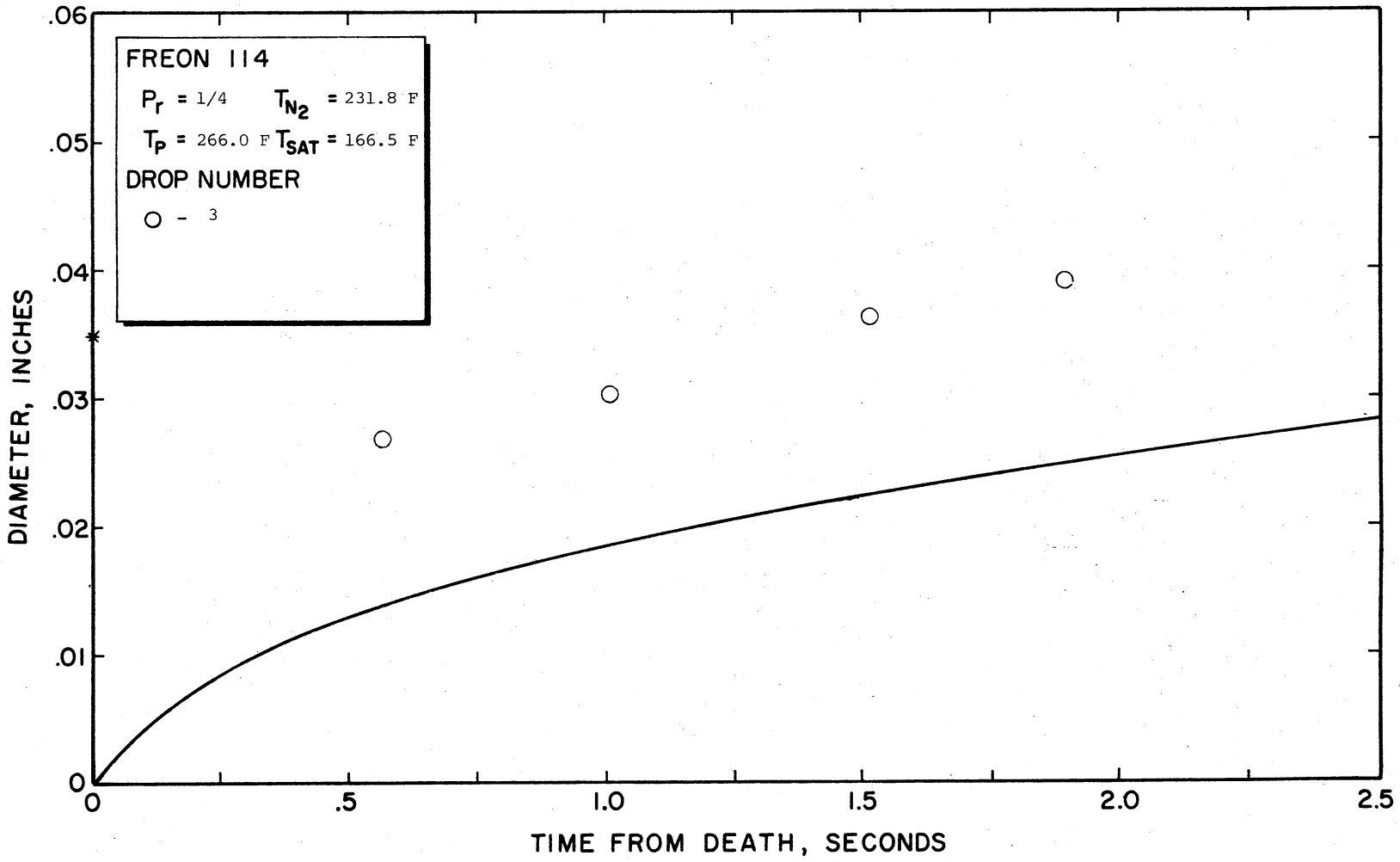
FREON 114
P_r = 1/4 T_{N_2} = 231.8 F
T_P = 266.0 F T_{SAT} = 166.5 F
DROP NUMBER
○ - 3
DIAMETER, INCHES
.06
.05
.04
.03
.02
.01
0
0
.5
1.0
1.5
2.0
2.5
TIME FROM DEATH, SECONDS

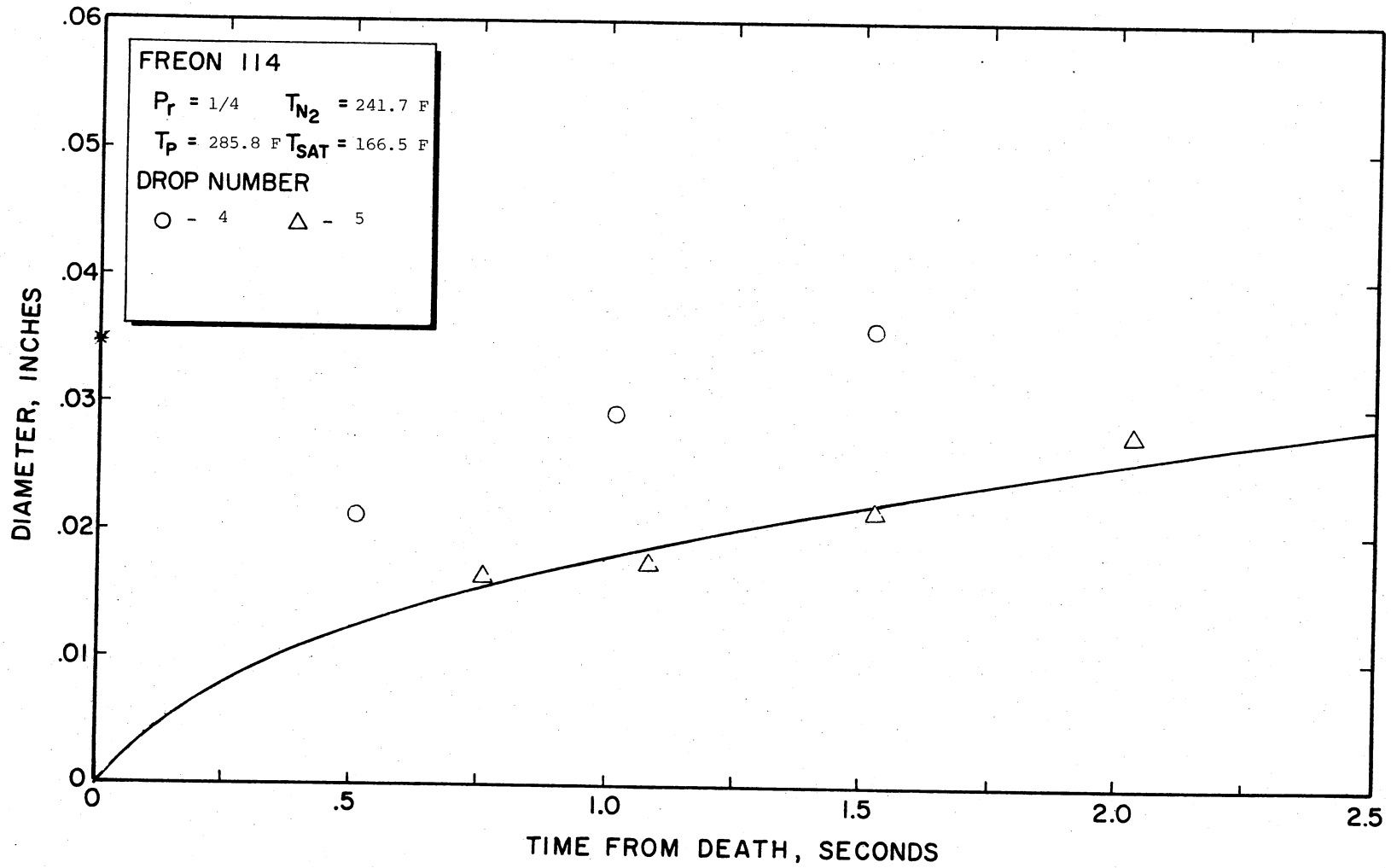
FREON 114
P_r = 1/4 T_{N_2} = 241.7 F
T_P = 285.8 F T_{SAT} = 166.5 F
DROP NUMBER
○ - 4 △ - 5
DIAMETER, INCHES
.06
.05
.04
.03
.02
.01
0
0
.5
1.0
1.5
2.0
2.5
TIME FROM DEATH, SECONDS

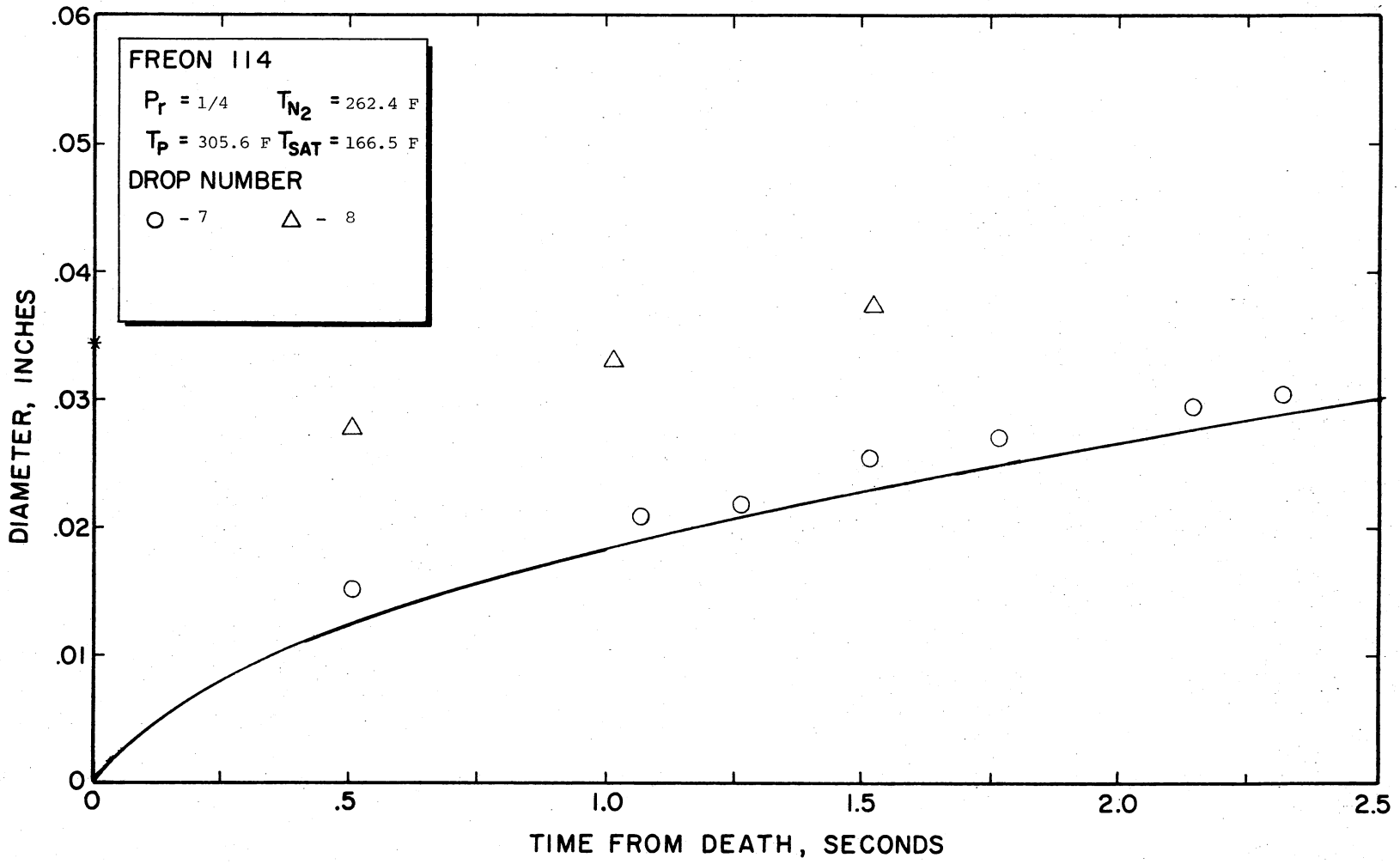
FREON 114
P_r = 1/4 T_{N_2} = 262.4 F
T_P = 305.6 F T_{SAT} = 166.5 F
DROP NUMBER
○ - 7 △ - 8
DIAMETER, INCHES
.06
.05
.04
.03
.02
.01
0
0
.5
1.0
1.5
2.0
2.5
TIME FROM DEATH, SECONDS

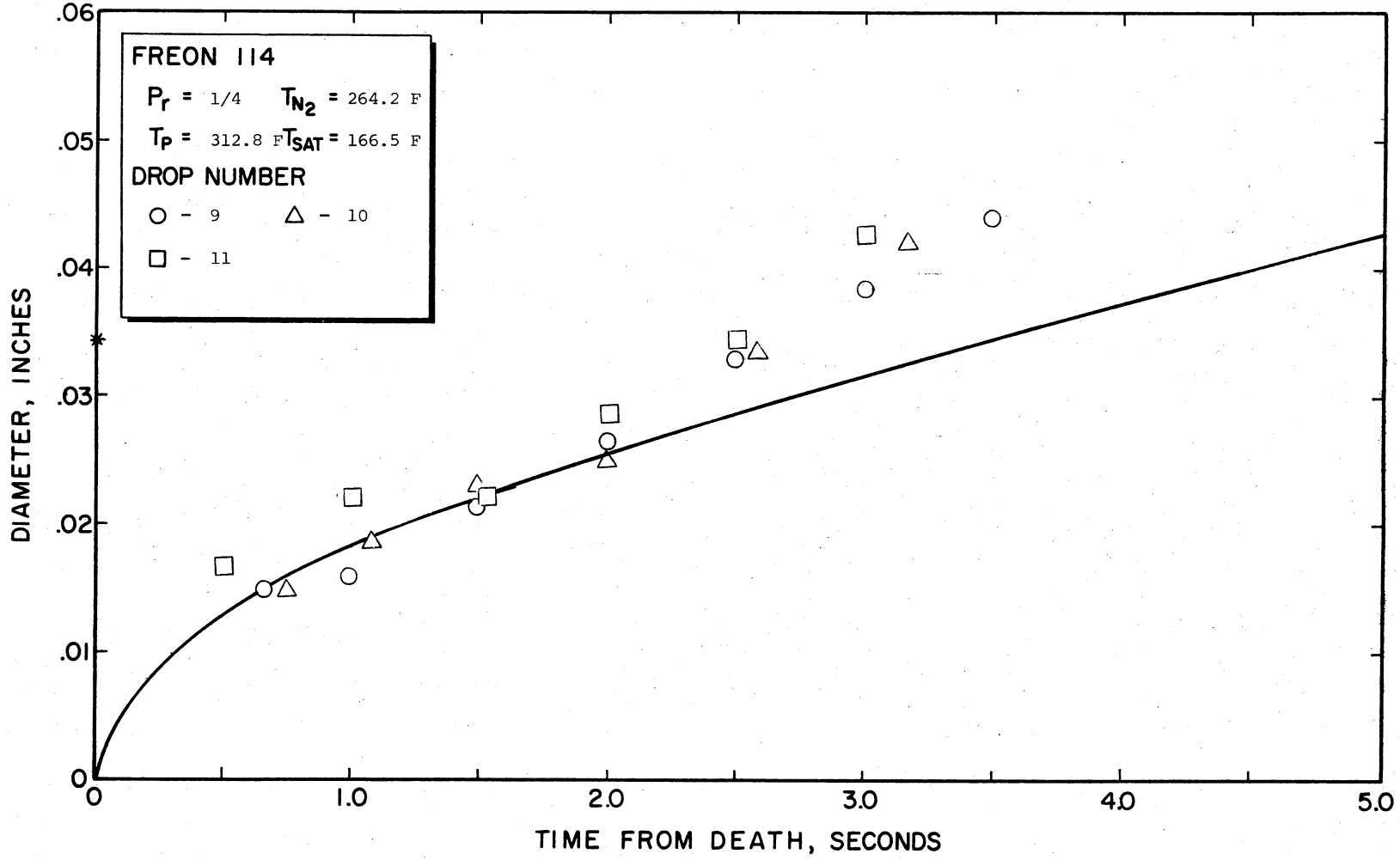
FREON 114
P_r = 1/4 T_{N_2} = 264.2 F
T_P = 312.8 F T_{SAT} = 166.5 F
DROP NUMBER
○ - 9 △ - 10
□ - 11
DIAMETER, INCHES
.06
.05
.04
.03
.02
.01
0
0
1.0
2.0
3.0
4.0
5.0
TIME FROM DEATH, SECONDS

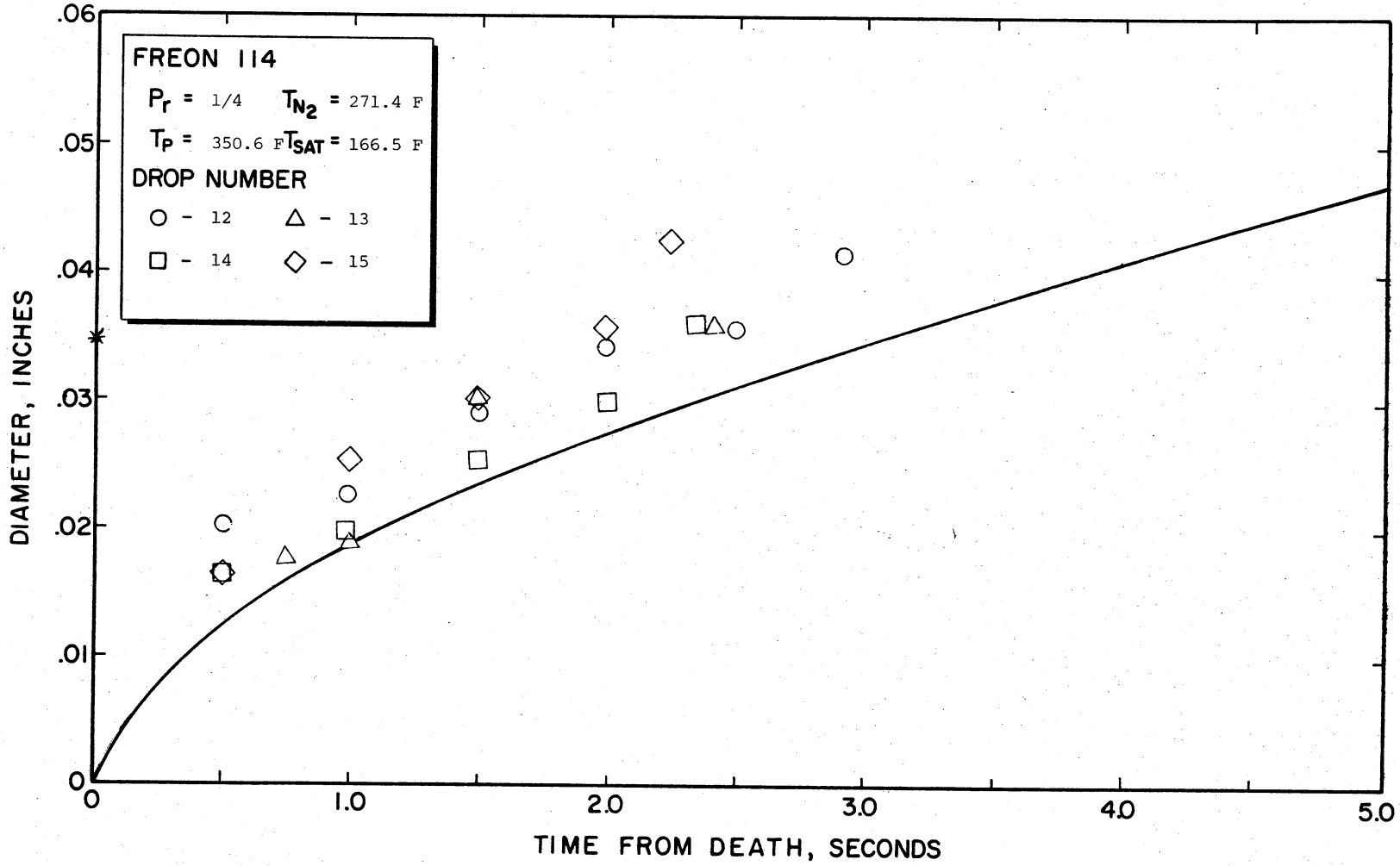
FREON 114
P_r = 1/4 T_{N_2} = 271.4 F
T_P = 350.6 F T_{SAT} = 166.5 F
DROP NUMBER
○ - 12 △ - 13
□ - 14 ◇ - 15
DIAMETER, INCHES
.06
.05
.04
.03
.02
.01
0
0
1.0
2.0
3.0
4.0
5.0
TIME FROM DEATH, SECONDS

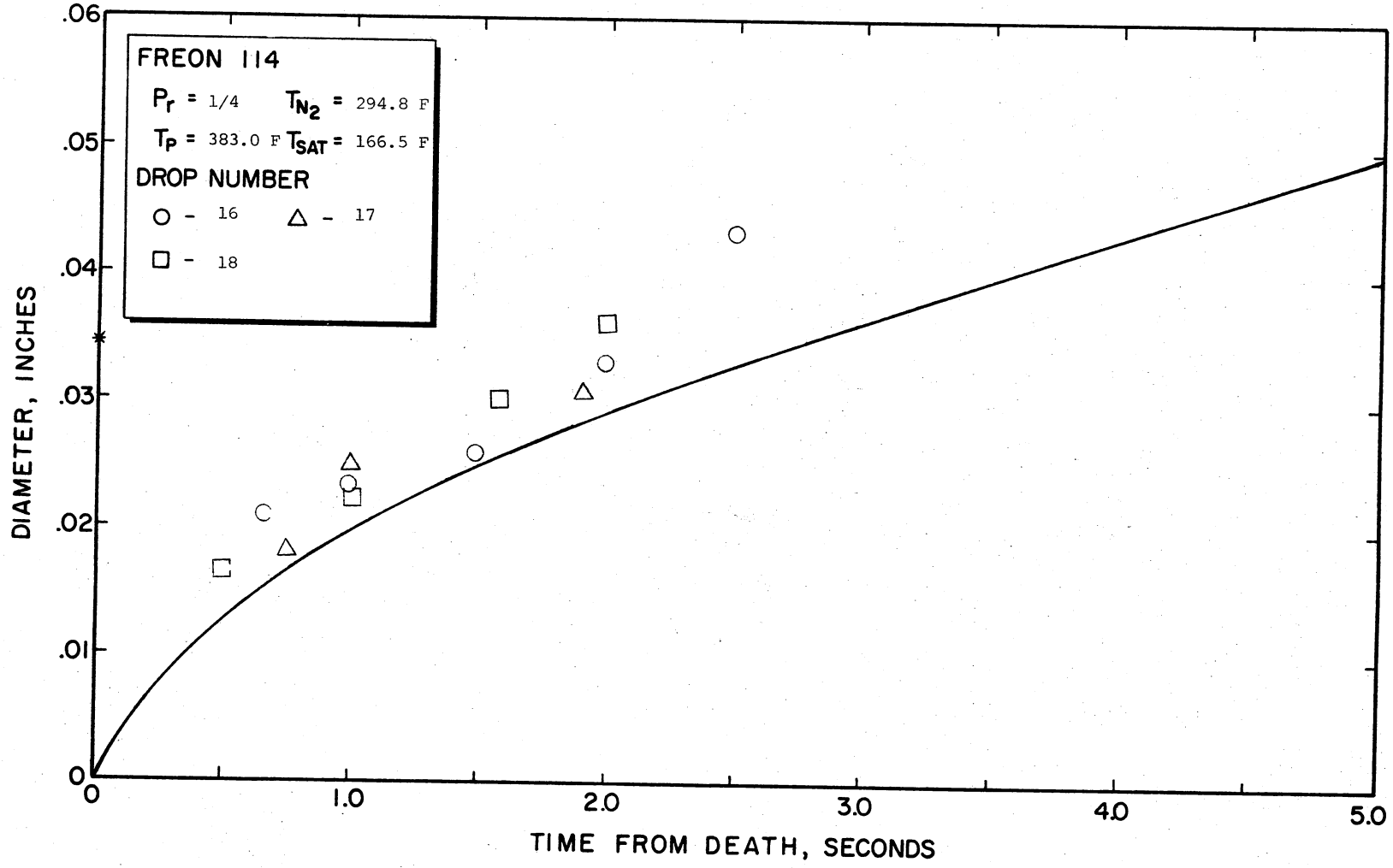
FREON 114
P_r = 1/4 T_{N_2} = 294.8 F
T_P = 383.0 F T_{SAT} = 166.5 F
DROP NUMBER
○ - 16 △ - 17
□ - 18
DIAMETER, INCHES
.06
.05
.04
.03
.02
.01
0
0
1.0
2.0
3.0
4.0
5.0
TIME FROM DEATH, SECONDS

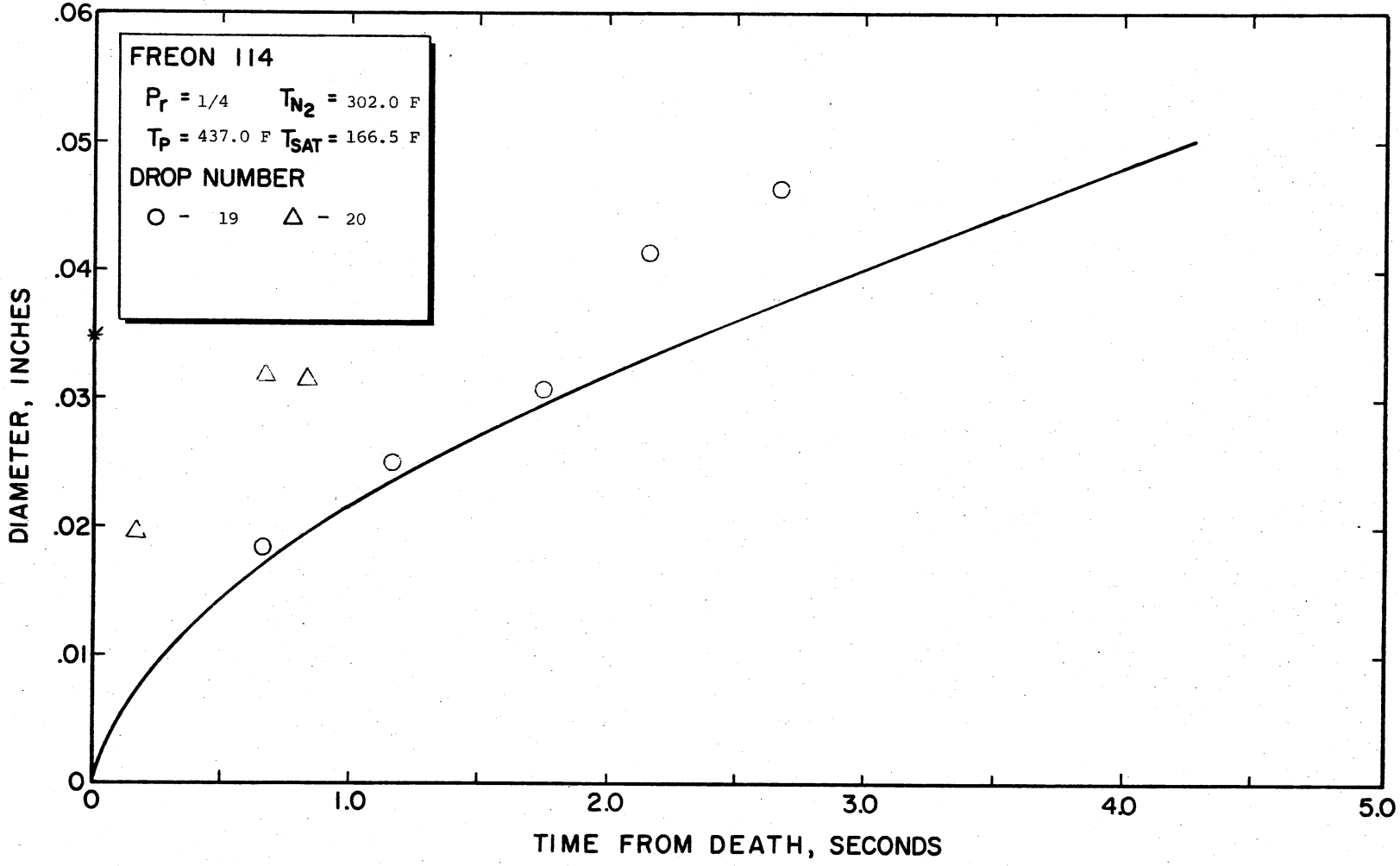
FREON 114
P_r = 1/4 T_{N_2} = 302.0 F
T_P = 437.0 F T_{SAT} = 166.5 F
DROP NUMBER
O - 19 Δ - 20
DIAMETER, INCHES
.06
.05
.04
.03
.02
.01
0
0
1.0
2.0
3.0
4.0
5.0
TIME FROM DEATH, SECONDS

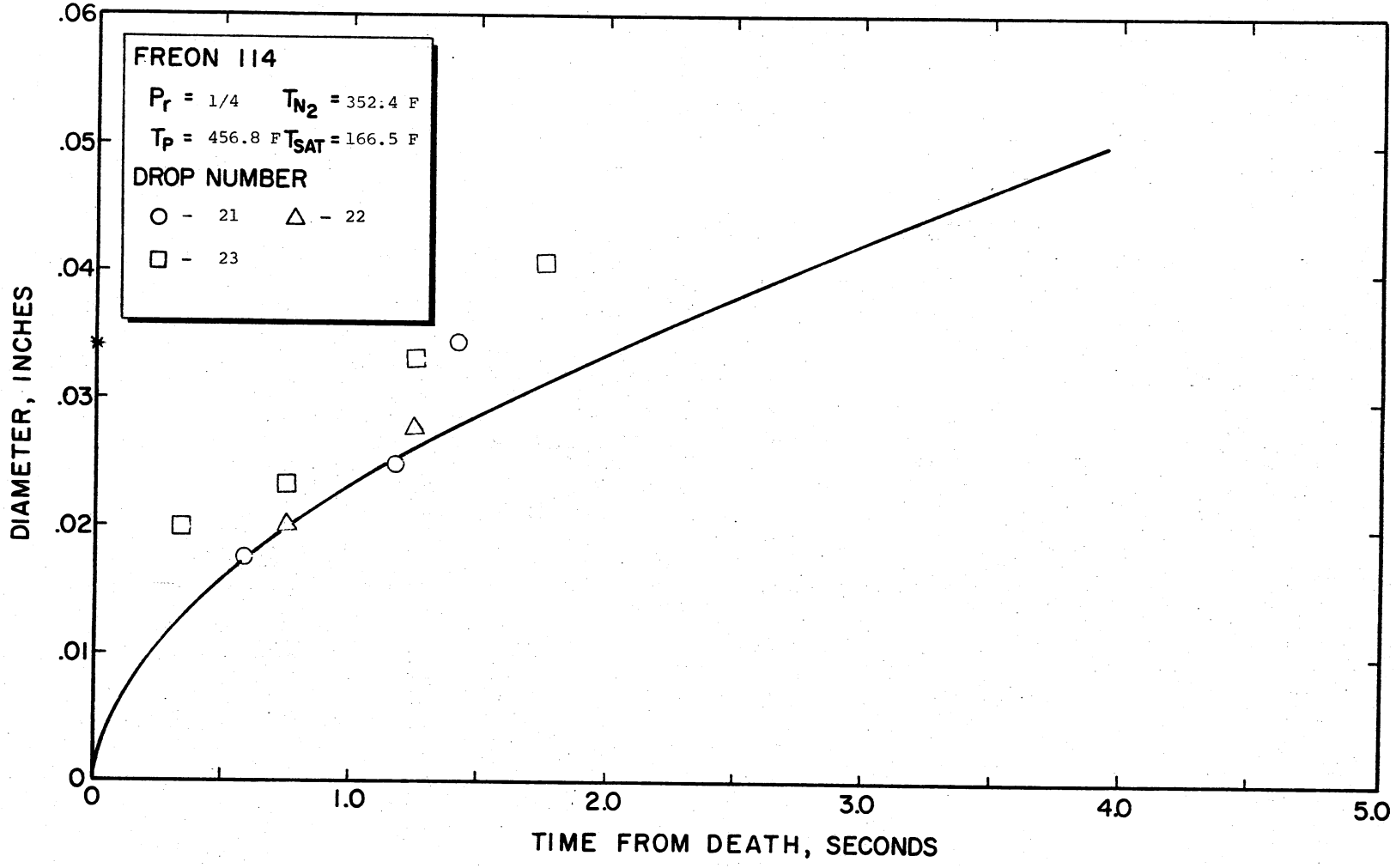
FREON 114
P_r = 1/4 T_{N_2} = 352.4 F
T_P = 456.8 F T_{SAT} = 166.5 F
DROP NUMBER
○ - 21 △ - 22
□ - 23
DIAMETER, INCHES
.06
.05
.04
.03
.02
.01
0
0
1.0
2.0
3.0
4.0
5.0
TIME FROM DEATH, SECONDS

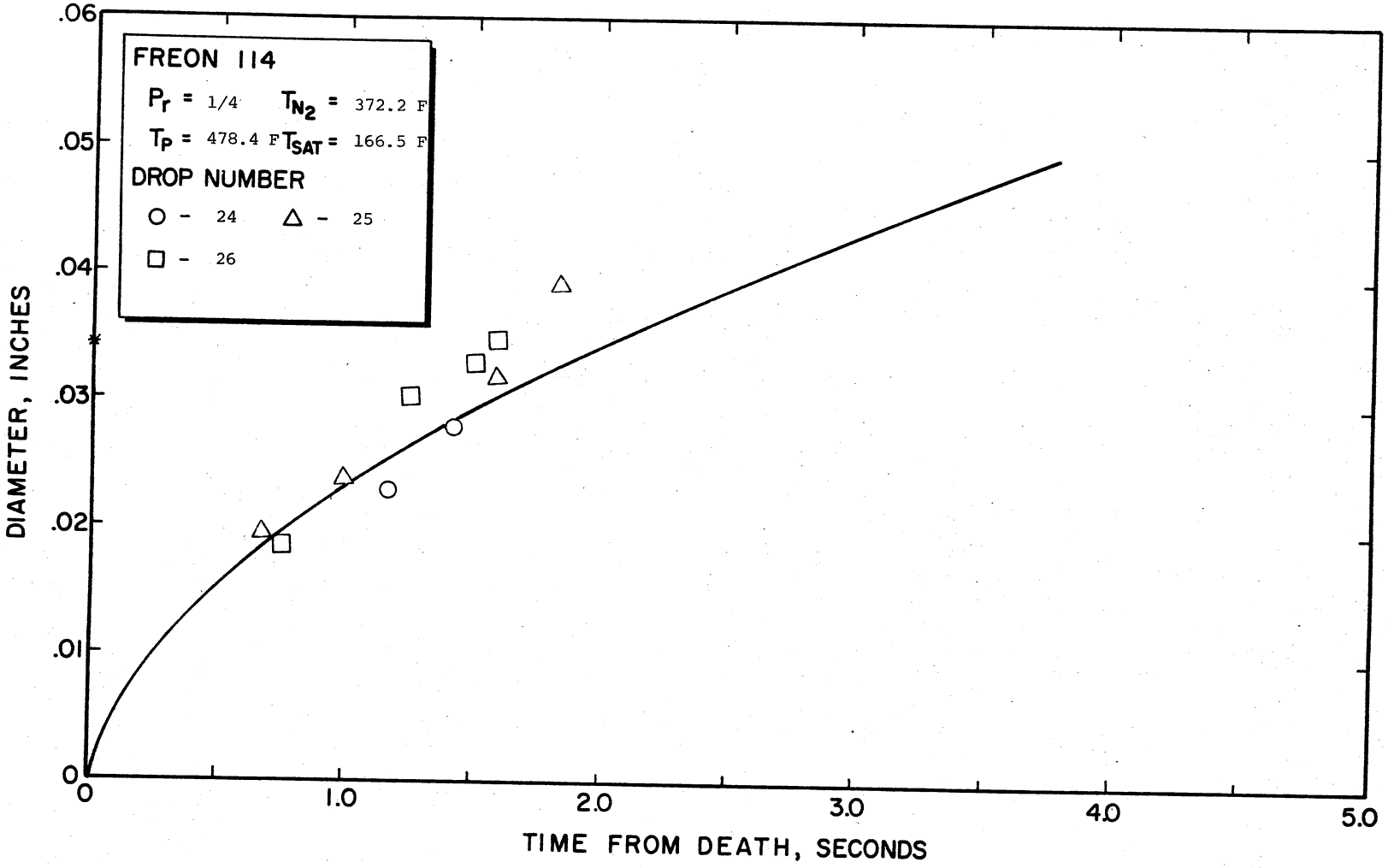
FREON 114
P_r = 1/4 T_{N_2} = 372.2 F
T_P = 478.4 F T_{SAT} = 166.5 F
DROP NUMBER
○ - 24 △ - 25
□ - 26
DIAMETER, INCHES
.06
.05
.04
.03
.02
.01
0
0
1.0
2.0
3.0
4.0
5.0
TIME FROM DEATH, SECONDS

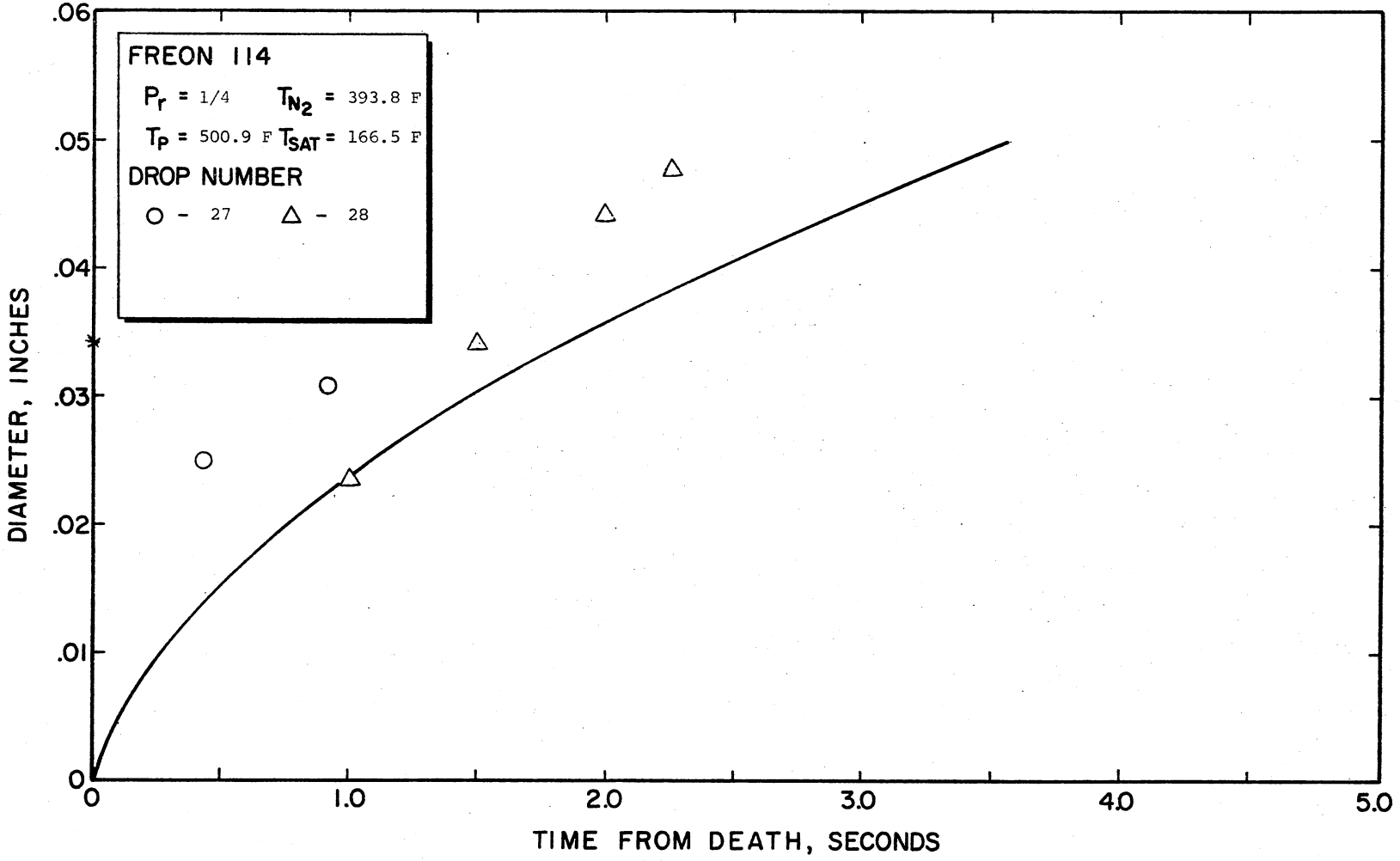
FREON 114
P_r = 1/4 T_{N_2} = 393.8 F
T_P = 500.9 F T_{SAT} = 166.5 F
DROP NUMBER
○ - 27 △ - 28
DIAMETER, INCHES
.06
.05
.04
.03
.02
.01
0
0
1.0
2.0
3.0
4.0
5.0
TIME FROM DEATH, SECONDS

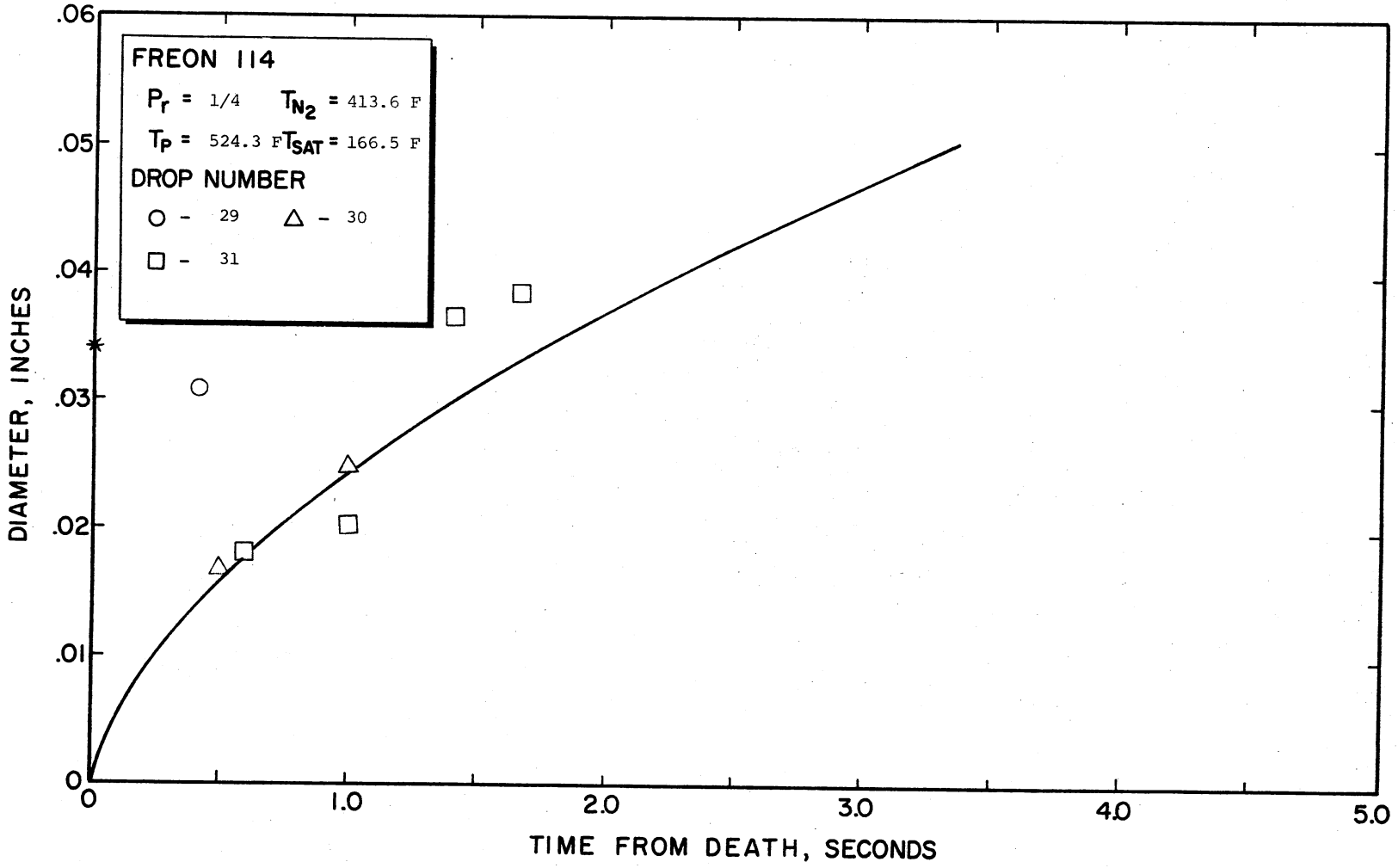
FREON 114
P_r = 1/4 T_{N_2} = 413.6 F
T_P = 524.3 F T_{SAT} = 166.5 F
DROP NUMBER
○ - 29 △ - 30
□ - 31
DIAMETER, INCHES
.06
.05
.04
.03
.02
.01
0
0
1.0
2.0
3.0
4.0
5.0
TIME FROM DEATH, SECONDS

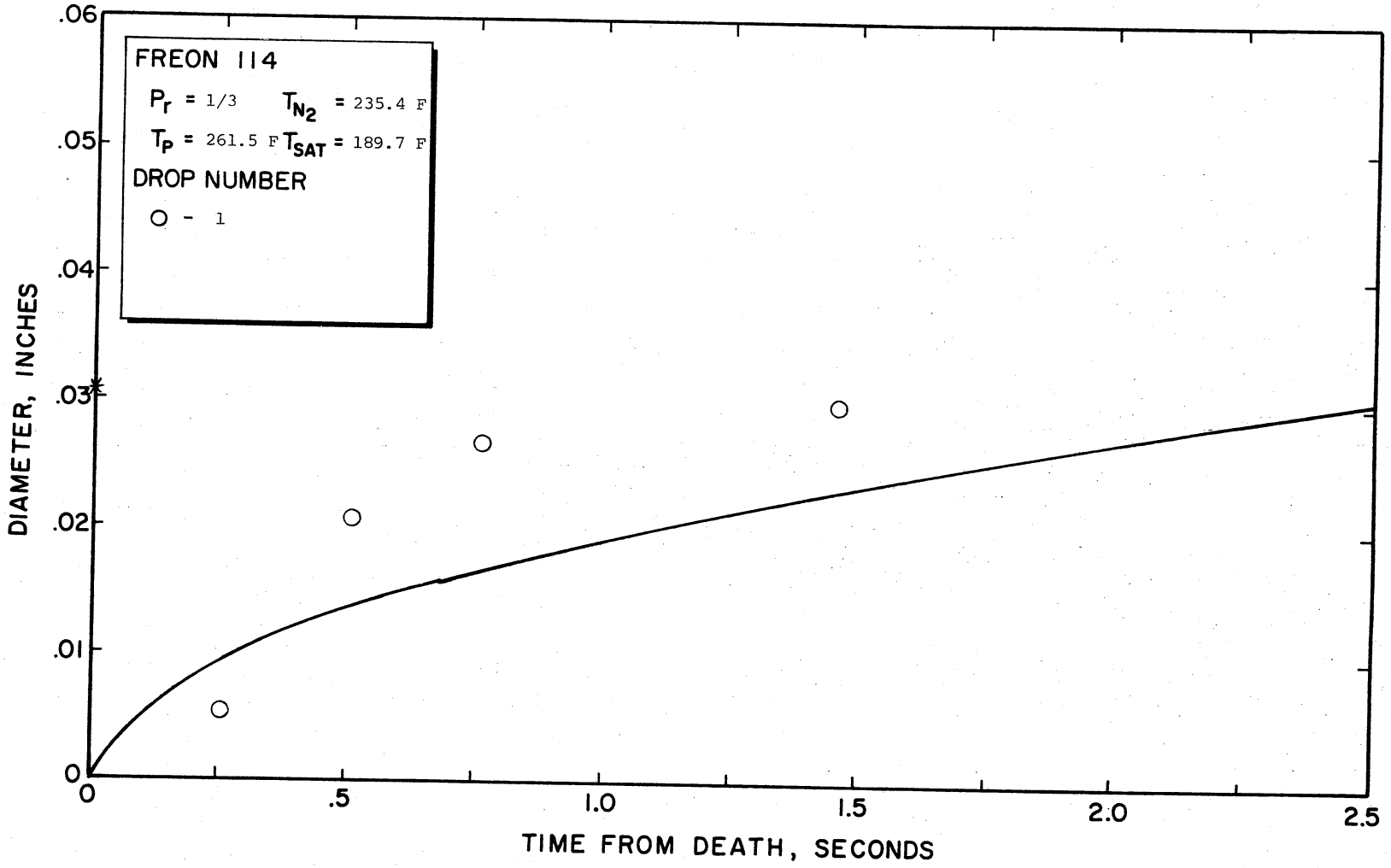
FREON 114
P_r = 1/3 T_{N_2} = 235.4 F
T_P = 261.5 F T_{SAT} = 189.7 F
DROP NUMBER
○ - 1
DIAMETER, INCHES
.06
.05
.04
.03
.02
.01
0
0
.5
1.0
1.5
2.0
2.5
TIME FROM DEATH, SECONDS

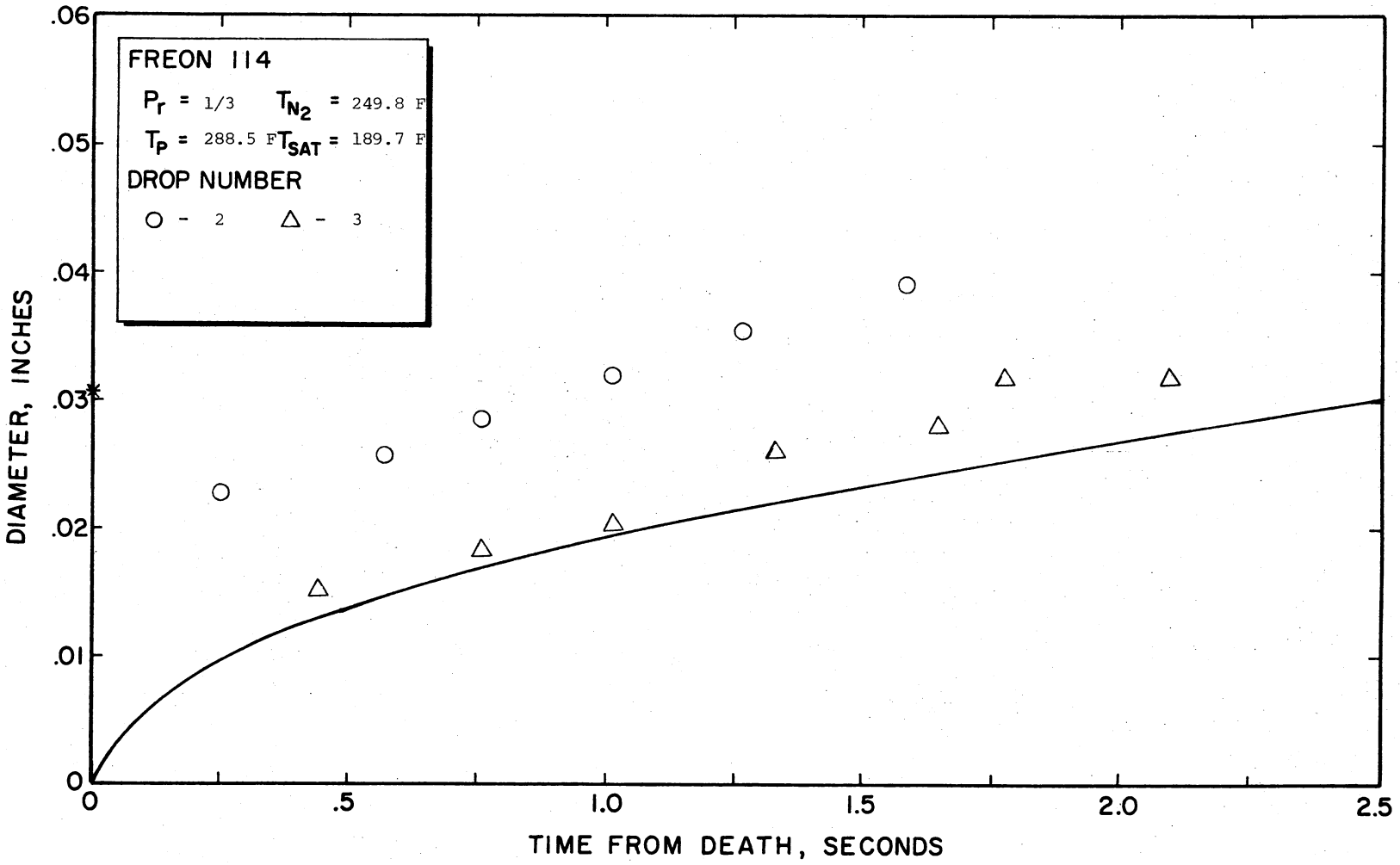
FREON 114
P_r = 1/3 T_{N_2} = 249.8 F
T_P = 288.5 F T_{SAT} = 189.7 F
DROP NUMBER
○ - 2 △ - 3
DIAMETER, INCHES
.06
.05
.04
.03
.02
.01
0
0
.5
1.0
1.5
2.0
2.5
TIME FROM DEATH, SECONDS

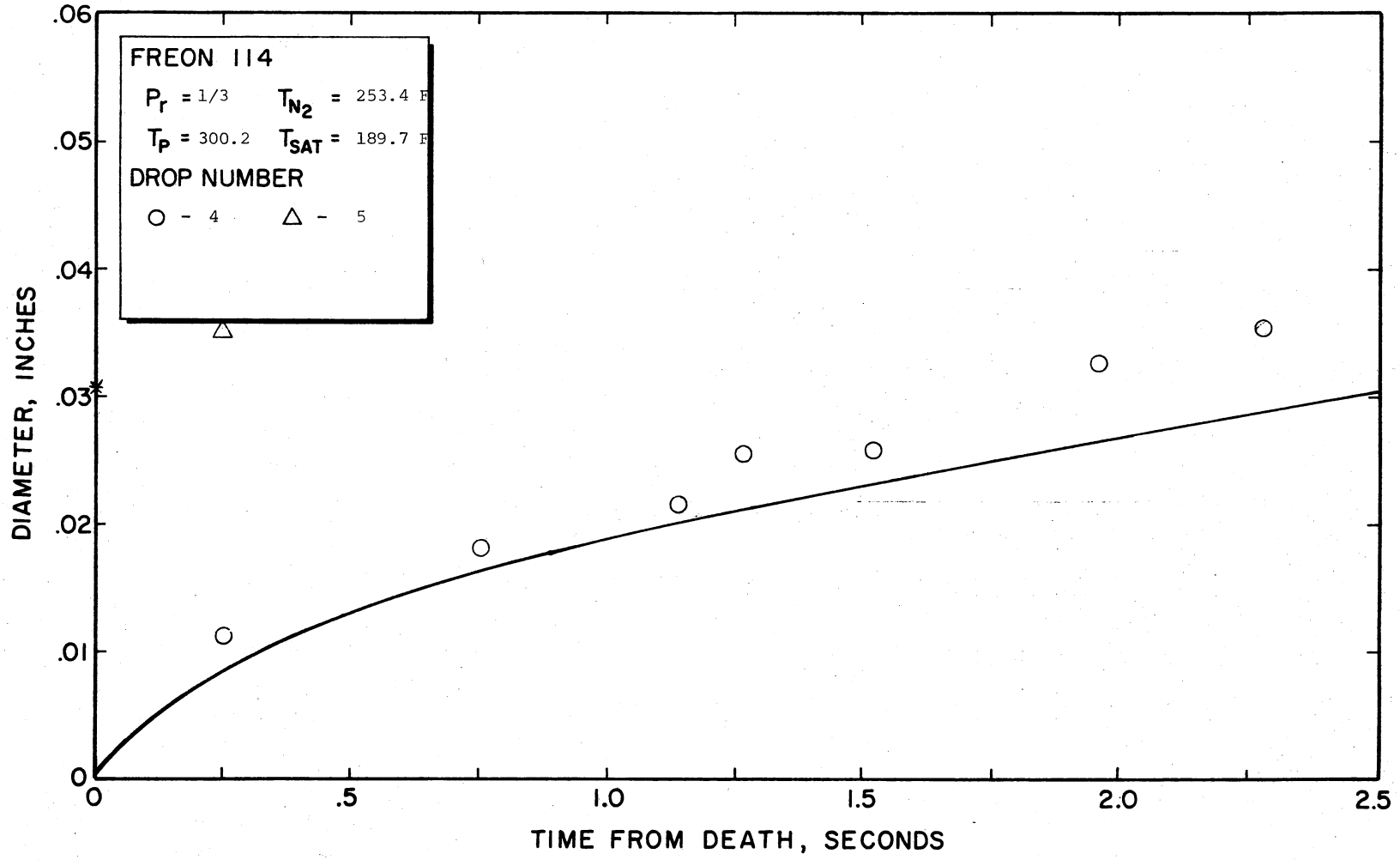
FREON 114
P_r = 1/3
T_{N_2} = 253.4 F
T_P = 300.2
T_{SAT} = 189.7 F
DROP NUMBER
○ - 4
△ - 5
DIAMETER, INCHES
.06
.05
.04
.03
.02
.01
0
0
.5
1.0
1.5
2.0
2.5
TIME FROM DEATH, SECONDS

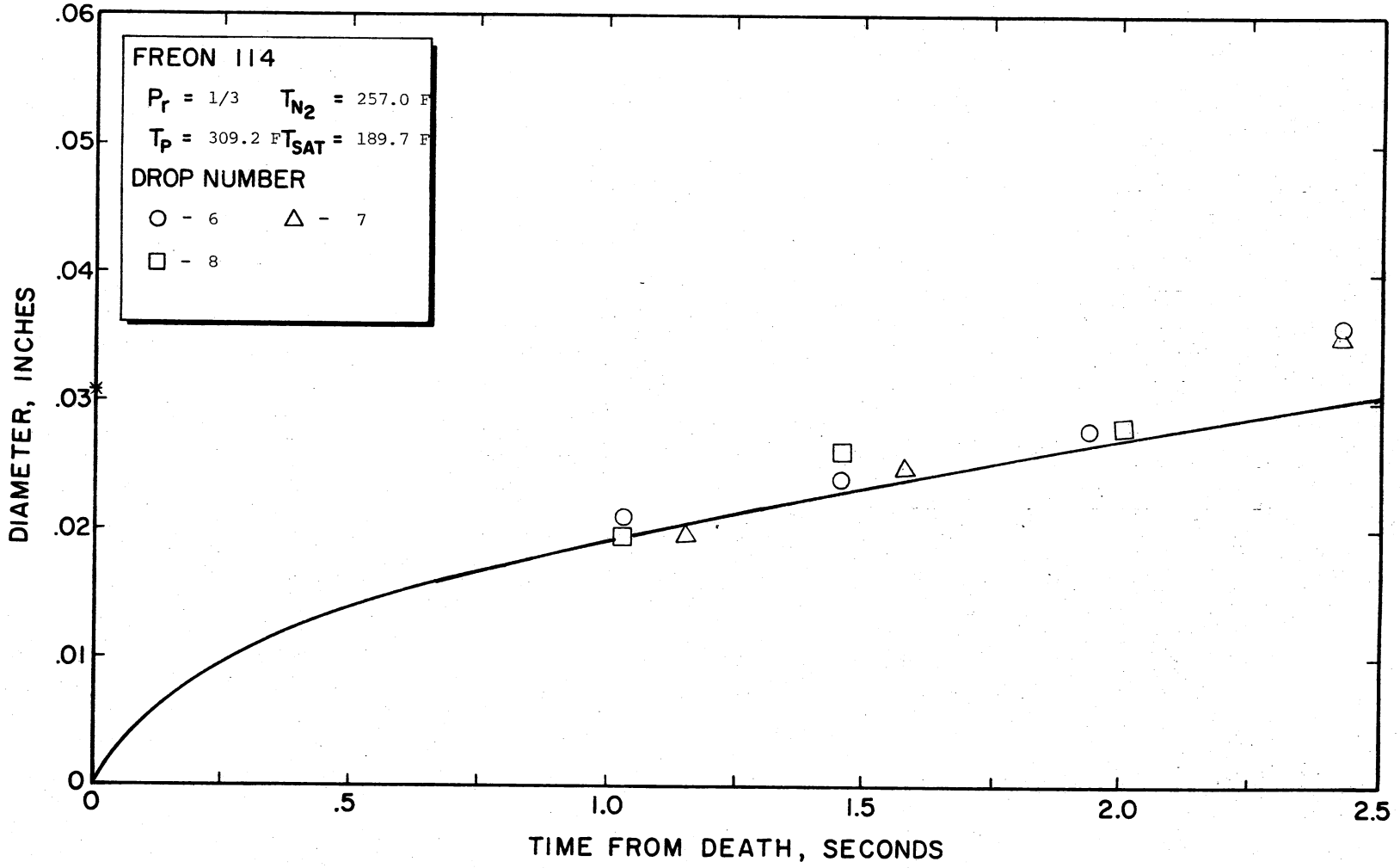
FREON 114
P_r = 1/3 T_{N_2} = 257.0 F
T_P = 309.2 F T_{SAT} = 189.7 F
DROP NUMBER
○ - 6
△ - 7
□ - 8
DIAMETER, INCHES
.06
.05
.04
.03
.02
.01
0
0
.5
1.0
1.5
2.0
2.5
TIME FROM DEATH, SECONDS

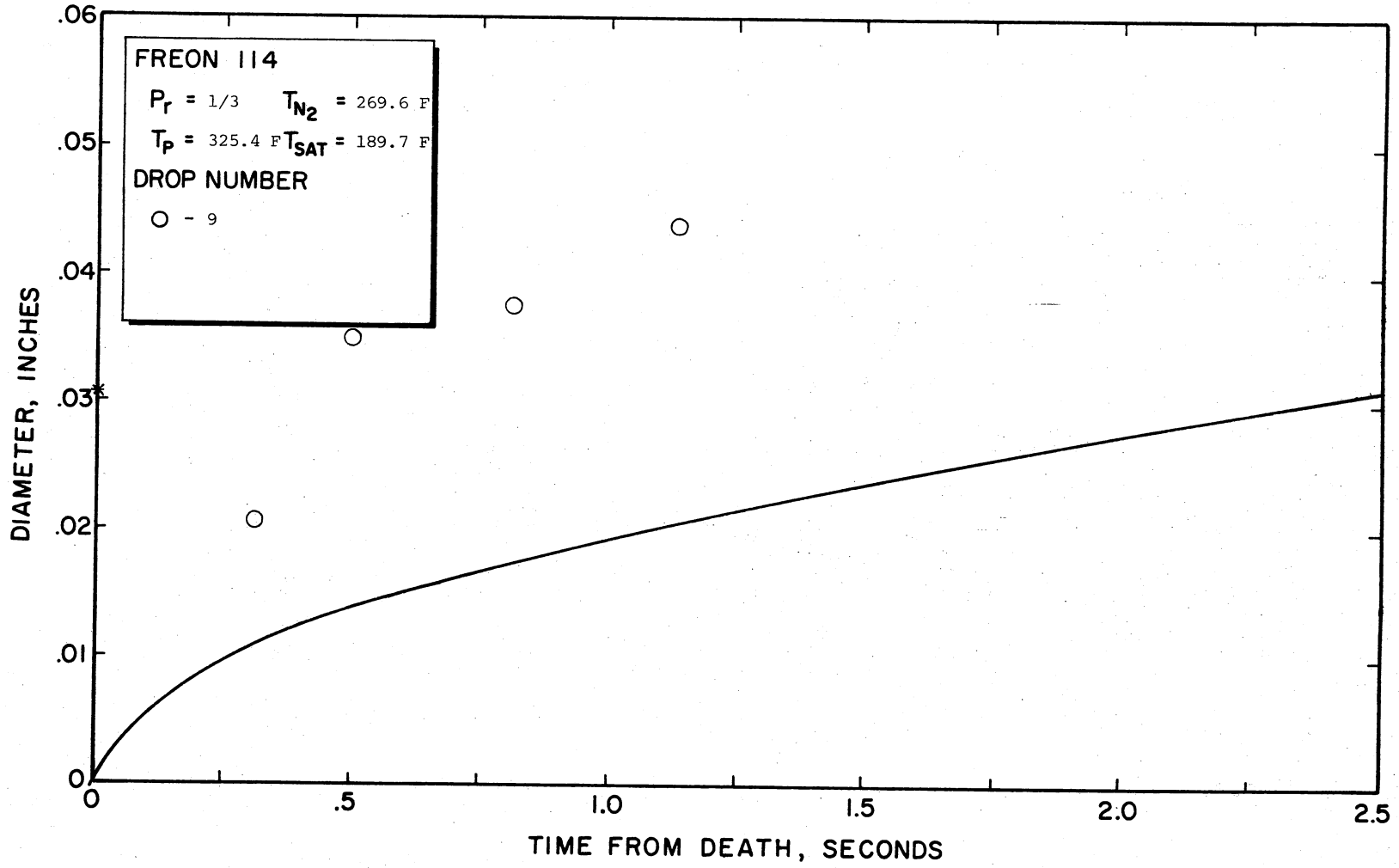
FREON 114
P_r = 1/3 T_{N_2} = 269.6 F
T_P = 325.4 F T_{SAT} = 189.7 F
DROP NUMBER
O - 9
DIAMETER, INCHES
.06
.05
.04
.03
.02
.01
0
0
.5
1.0
1.5
2.0
2.5
TIME FROM DEATH, SECONDS

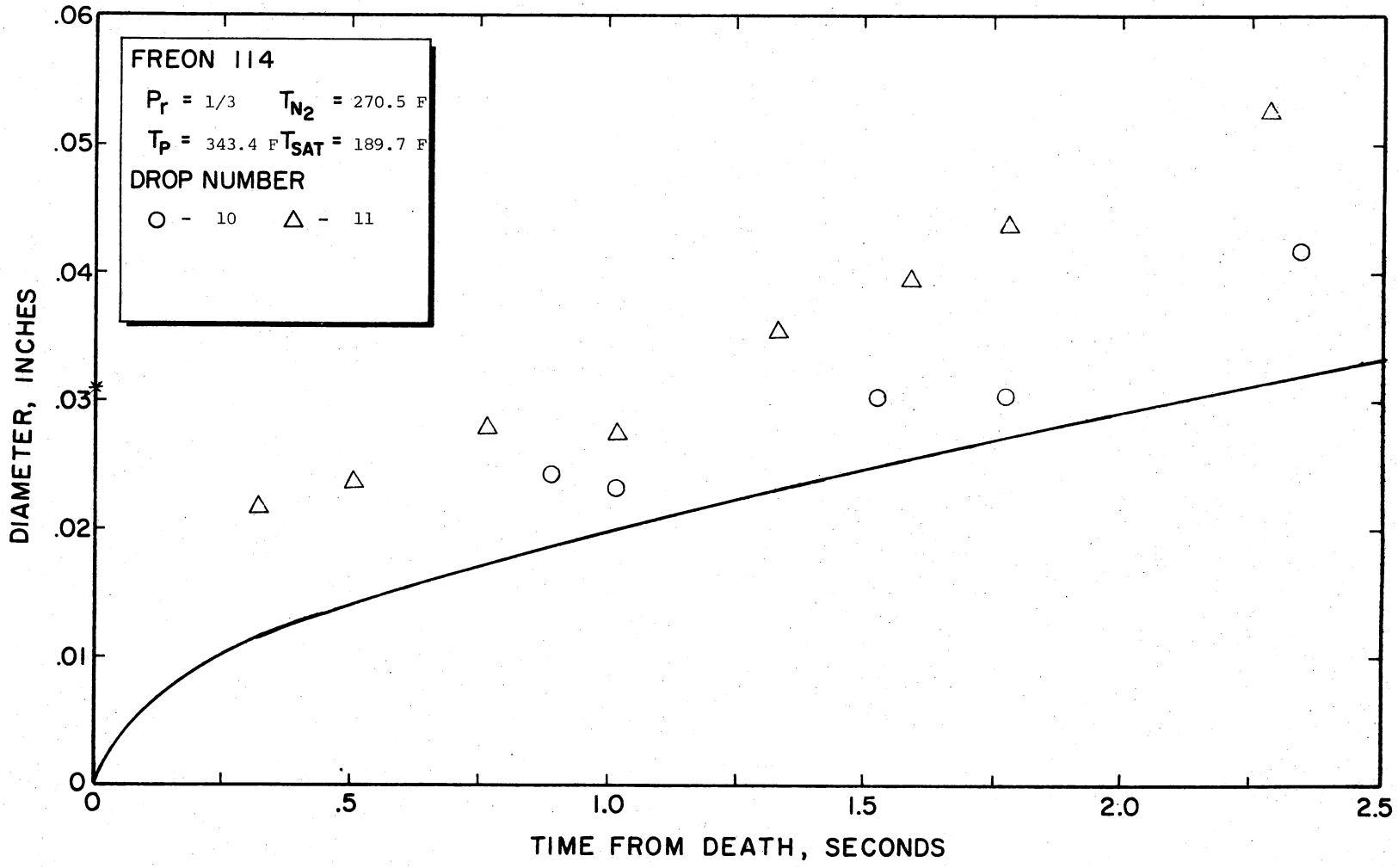
FREON 114
P_r = 1/3 T_{N_2} = 270.5 F
T_P = 343.4 F T_{SAT} = 189.7 F
DROP NUMBER
○ - 10 △ - 11
DIAMETER, INCHES
.06
.05
.04
.03
.02
.01
0
0
.5
1.0
1.5
2.0
2.5
TIME FROM DEATH, SECONDS

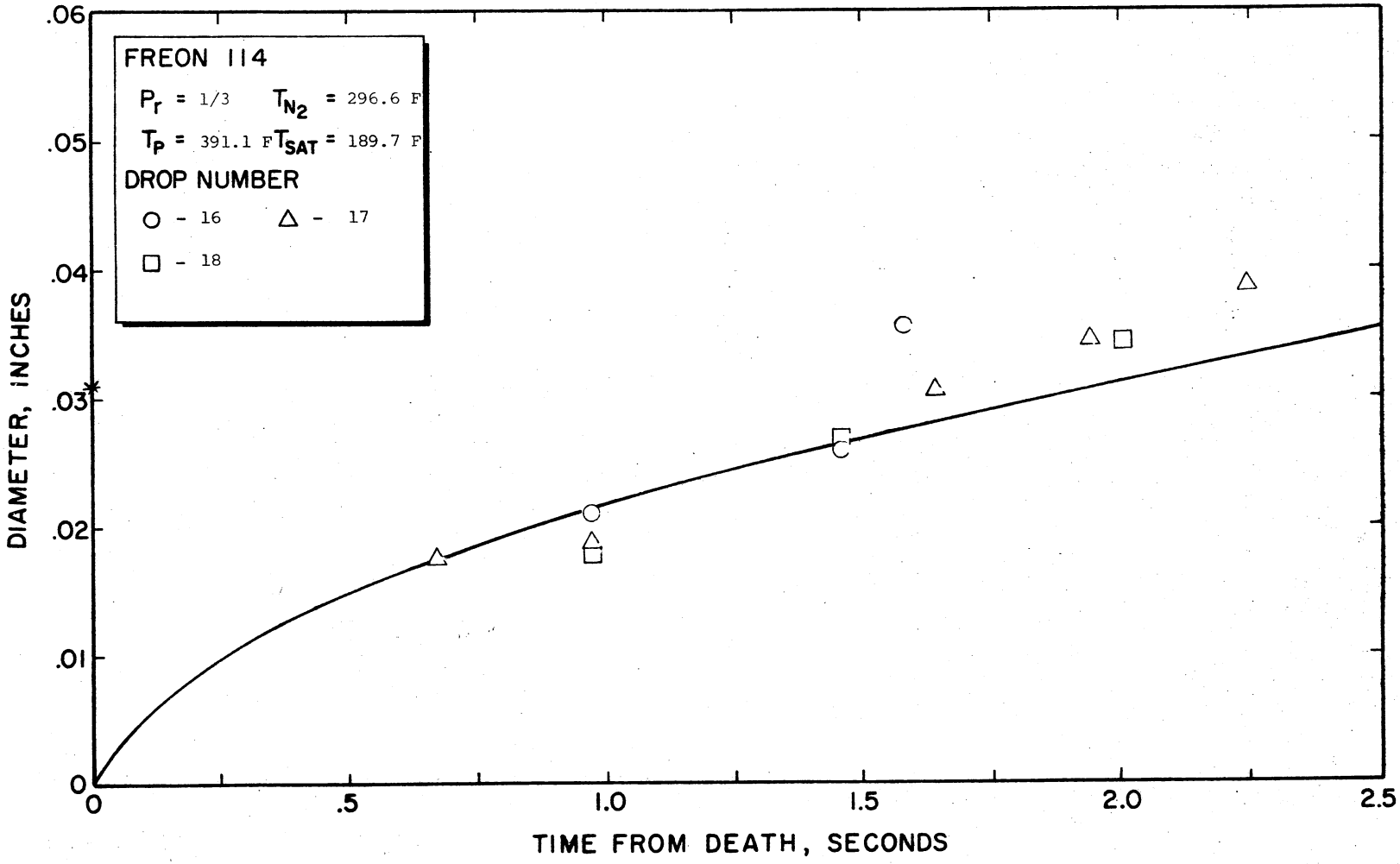
FREON 114
P_r = 1/3 T_{N_2} = 296.6 F
T_P = 391.1 F T_{SAT} = 189.7 F
DROP NUMBER
○ - 16 △ - 17
□ - 18
DIAMETER, INCHES
.06
.05
.04
.03
.02
.01
0
0
.5
1.0
1.5
2.0
2.5
TIME FROM DEATH, SECONDS

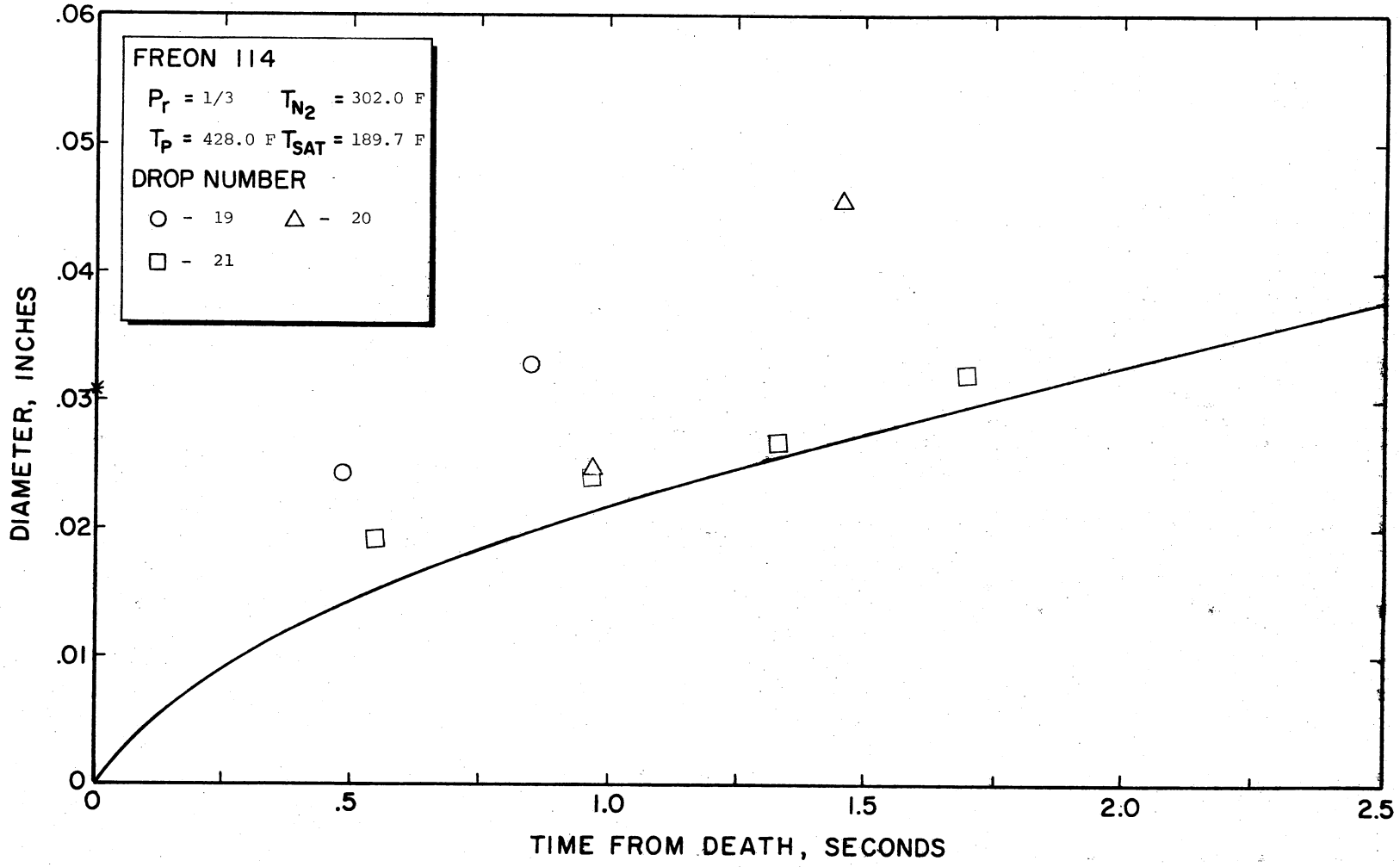
FREON 114
P_r = 1/3 T_{N_2} = 302.0 F
T_P = 428.0 F T_{SAT} = 189.7 F
DROP NUMBER
○ - 19 △ - 20
□ - 21
DIAMETER, INCHES
.06
.05
.04
.03
.02
.01
0
0
.5
1.0
1.5
2.0
2.5
TIME FROM DEATH, SECONDS

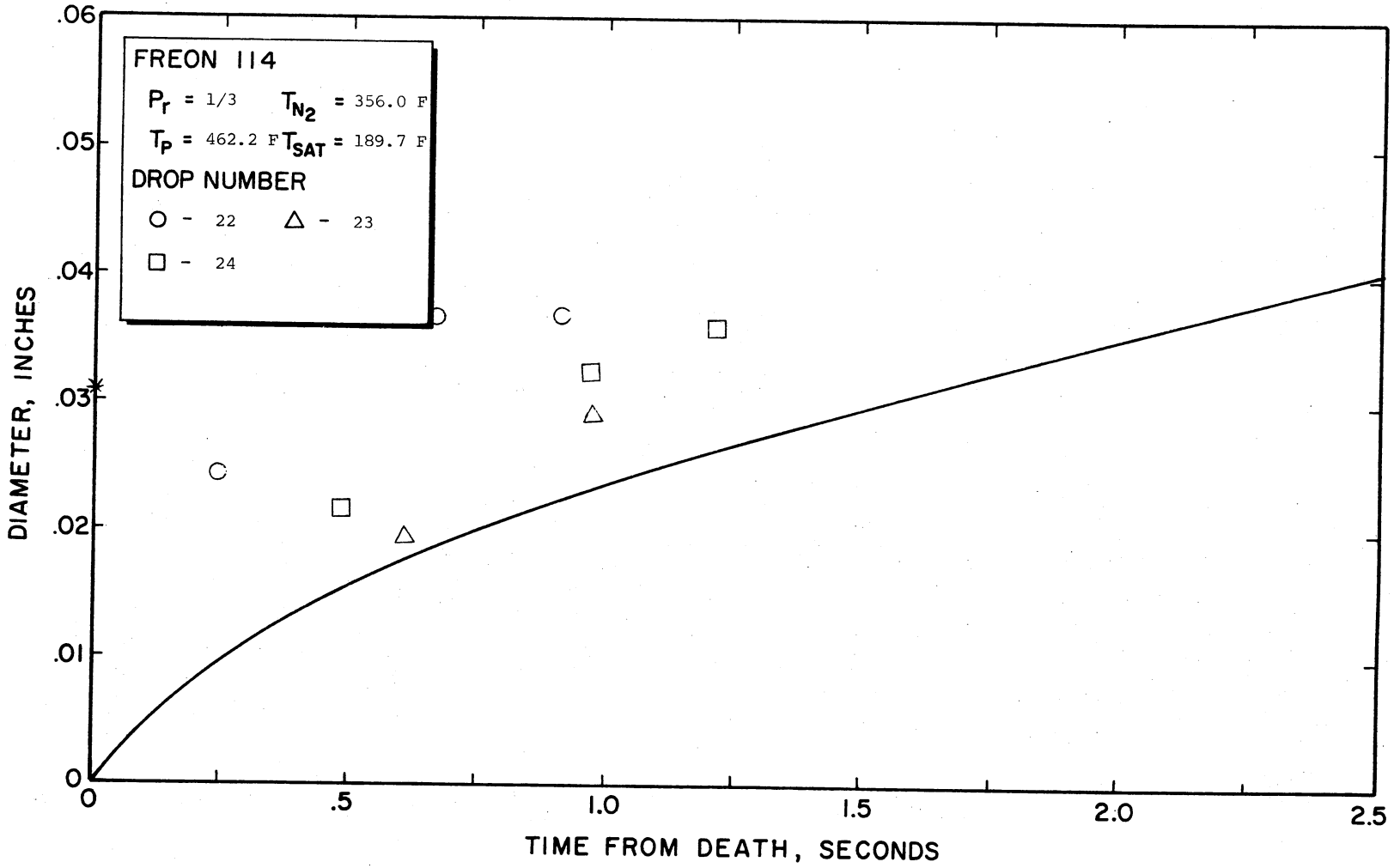
FREON 114
P_r = 1/3 T_{N_2} = 356.0 F
T_P = 462.2 F T_{SAT} = 189.7 F
DROP NUMBER
○ - 22 △ - 23
□ - 24
DIAMETER, INCHES
.06
.05
.04
.03
.02
.01
0
0
.5
1.0
1.5
2.0
2.5
TIME FROM DEATH, SECONDS

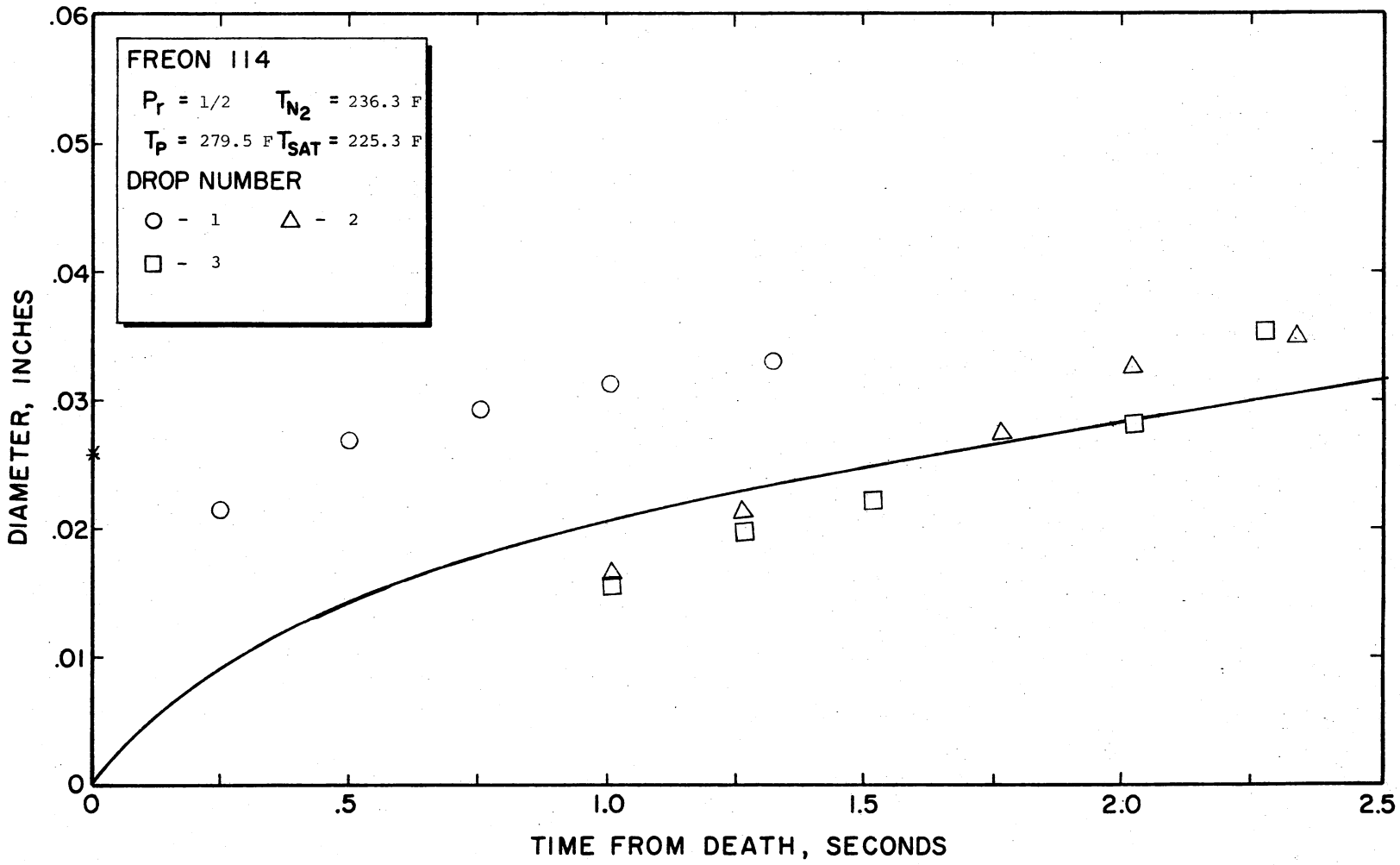
FREON 114
P_r = 1/2 T_{N_2} = 236.3 F
T_P = 279.5 F T_{SAT} = 225.3 F
DROP NUMBER
○ - 1 △ - 2
□ - 3
DIAMETER, INCHES
.06
.05
.04
.03
.02
.01
0
0
.5
1.0
1.5
2.0
2.5
TIME FROM DEATH, SECONDS

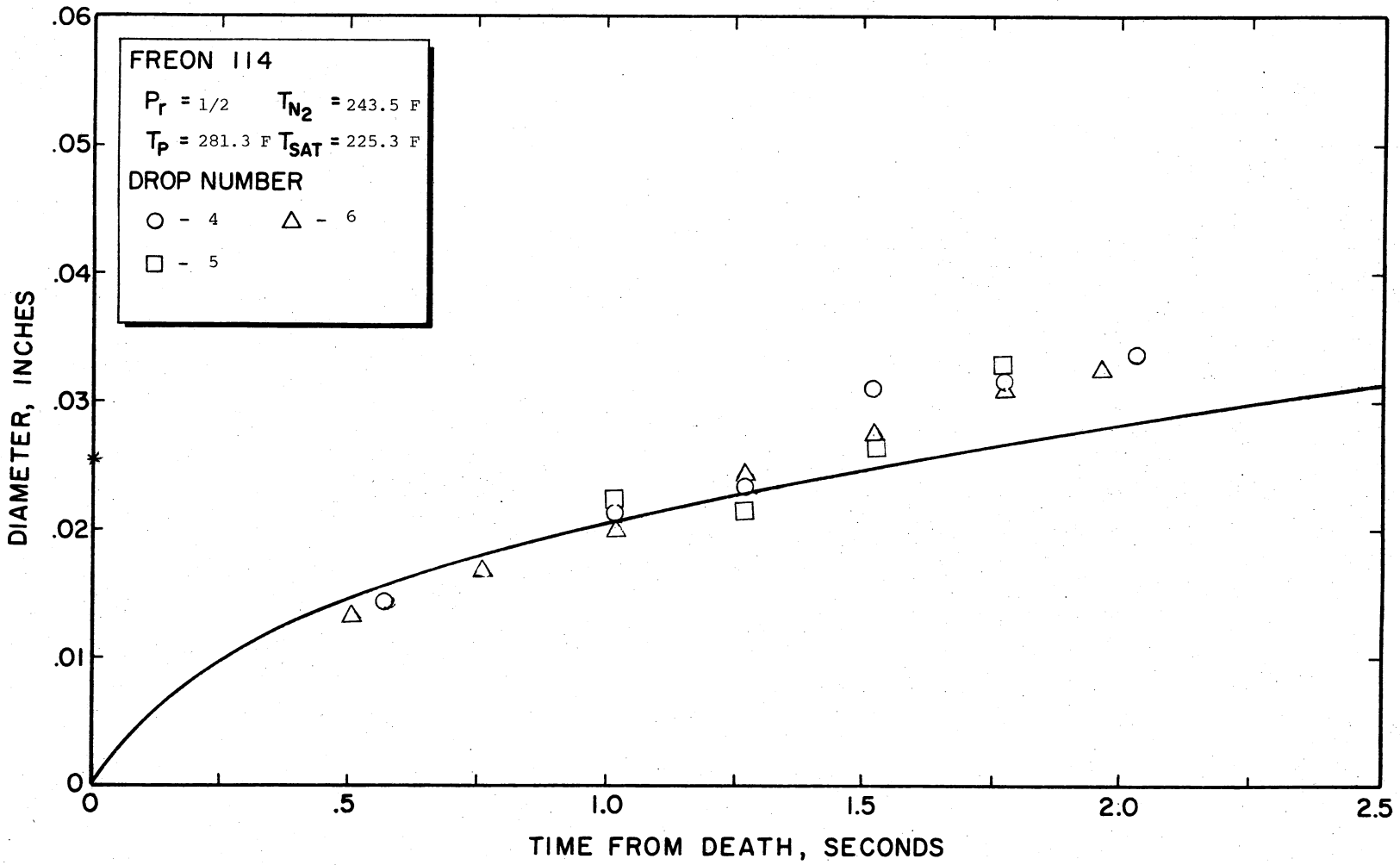
FREON 114
P_r = 1/2 T_{N_2} = 243.5 F
T_P = 281.3 F T_{SAT} = 225.3 F
DROP NUMBER
○ - 4 △ - 6
□ - 5
DIAMETER, INCHES
.06
.05
.04
.03
.02
.01
0
0
.5
1.0
1.5
2.0
2.5
TIME FROM DEATH, SECONDS

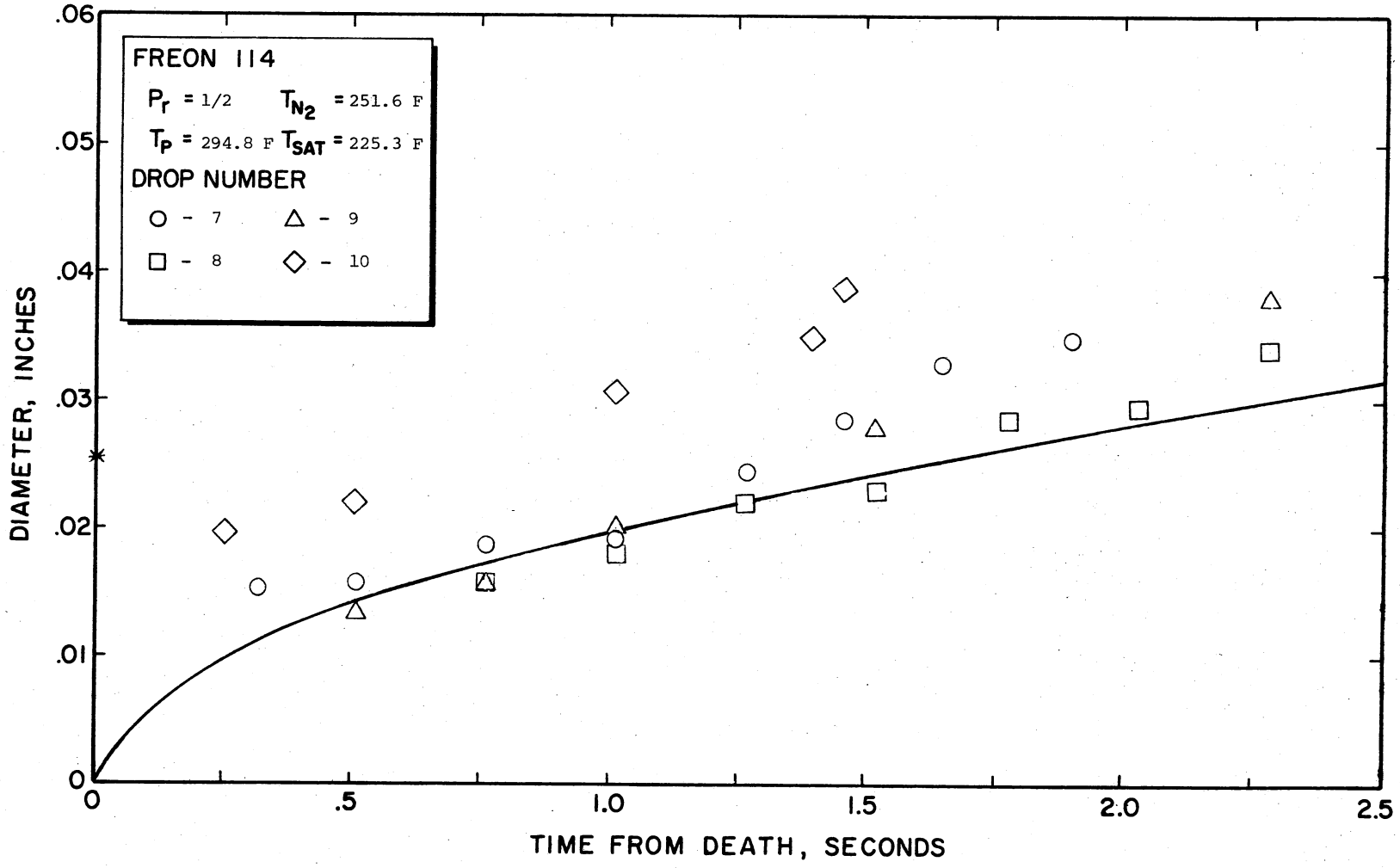
FREON 114
P_r = 1/2 T_{N_2} = 251.6 F
T_P = 294.8 F T_{SAT} = 225.3 F
DROP NUMBER
○ - 7 △ - 9
□ - 8 ◇ - 10
DIAMETER, INCHES
.06
.05
.04
.03
.02
.01
0
0
.5
1.0
1.5
2.0
2.5
TIME FROM DEATH, SECONDS

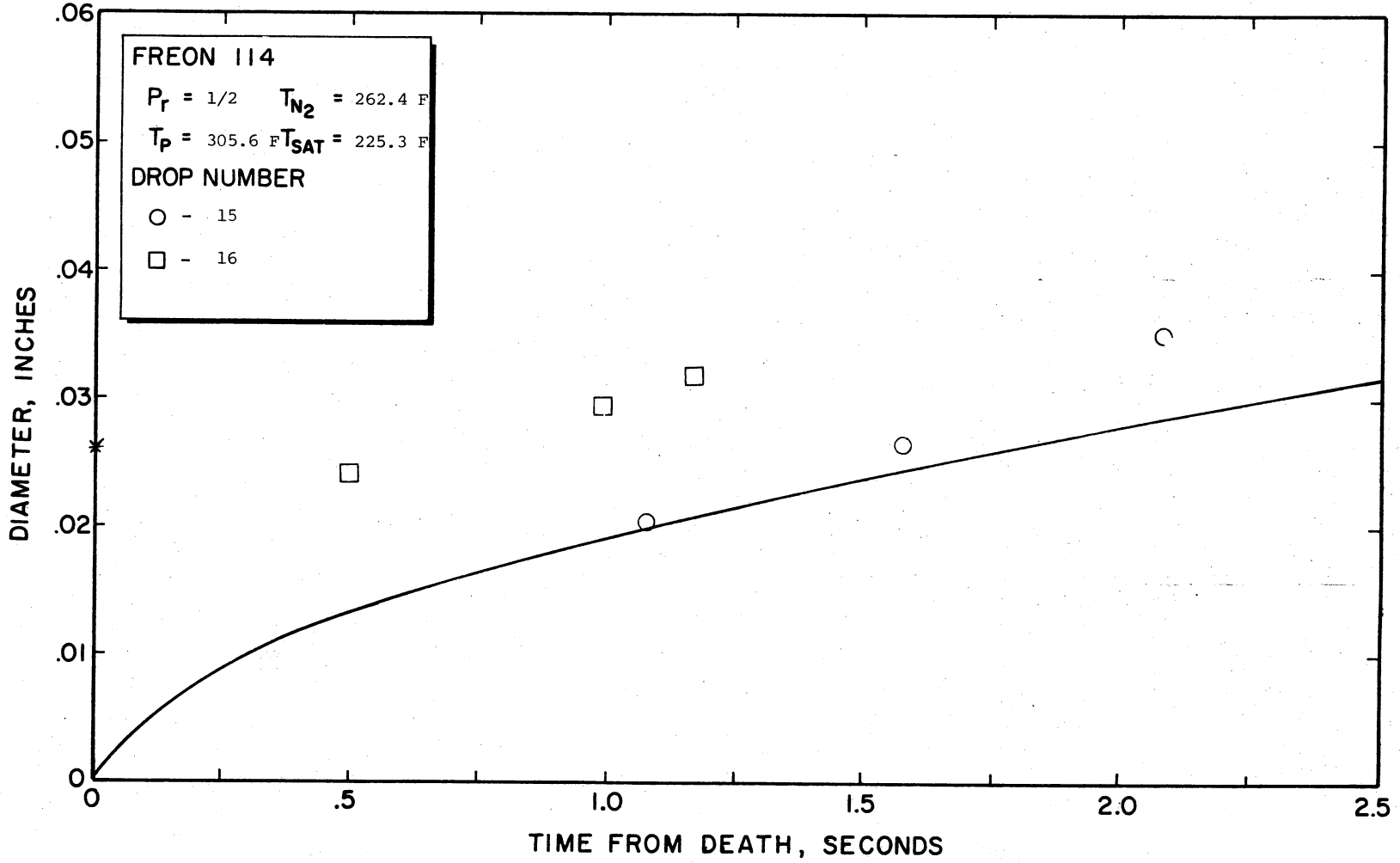
FREON 114
P_r = 1/2 T_{N_2} = 262.4 F
T_P = 305.6 F T_{SAT} = 225.3 F
DROP NUMBER
○ - 15
□ - 16
DIAMETER, INCHES
.06
.05
.04
.03
.02
.01
0
0
.5
1.0
1.5
2.0
2.5
TIME FROM DEATH, SECONDS

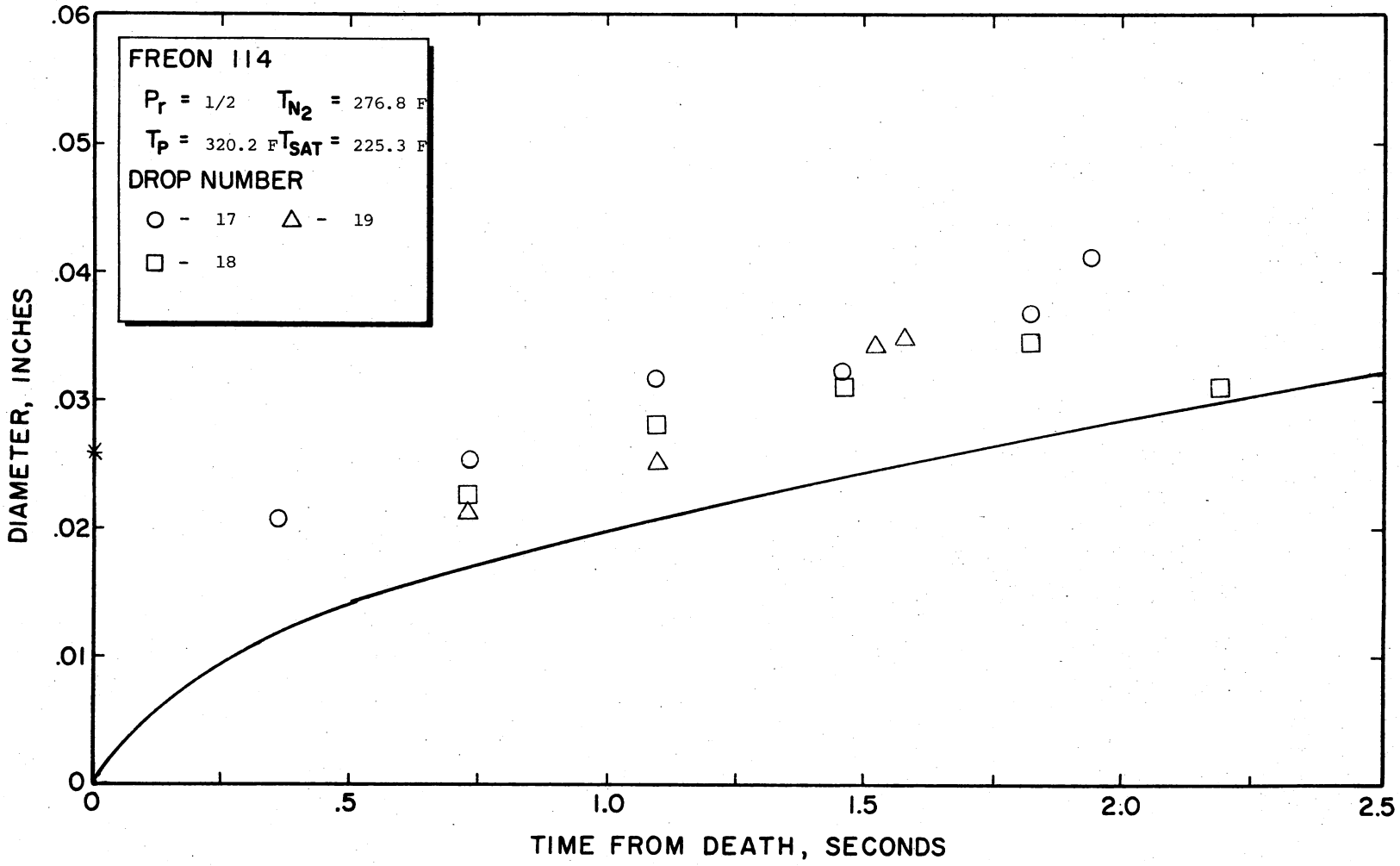
FREON 114
P_r = 1/2 T_{N_2} = 276.8 F
T_P = 320.2 F T_{SAT} = 225.3 F
DROP NUMBER
○ - 17 △ - 19
□ - 18
DIAMETER, INCHES
.06
.05
.04
.03
.02
.01
0
0
.5
1.0
1.5
2.0
2.5
TIME FROM DEATH, SECONDS

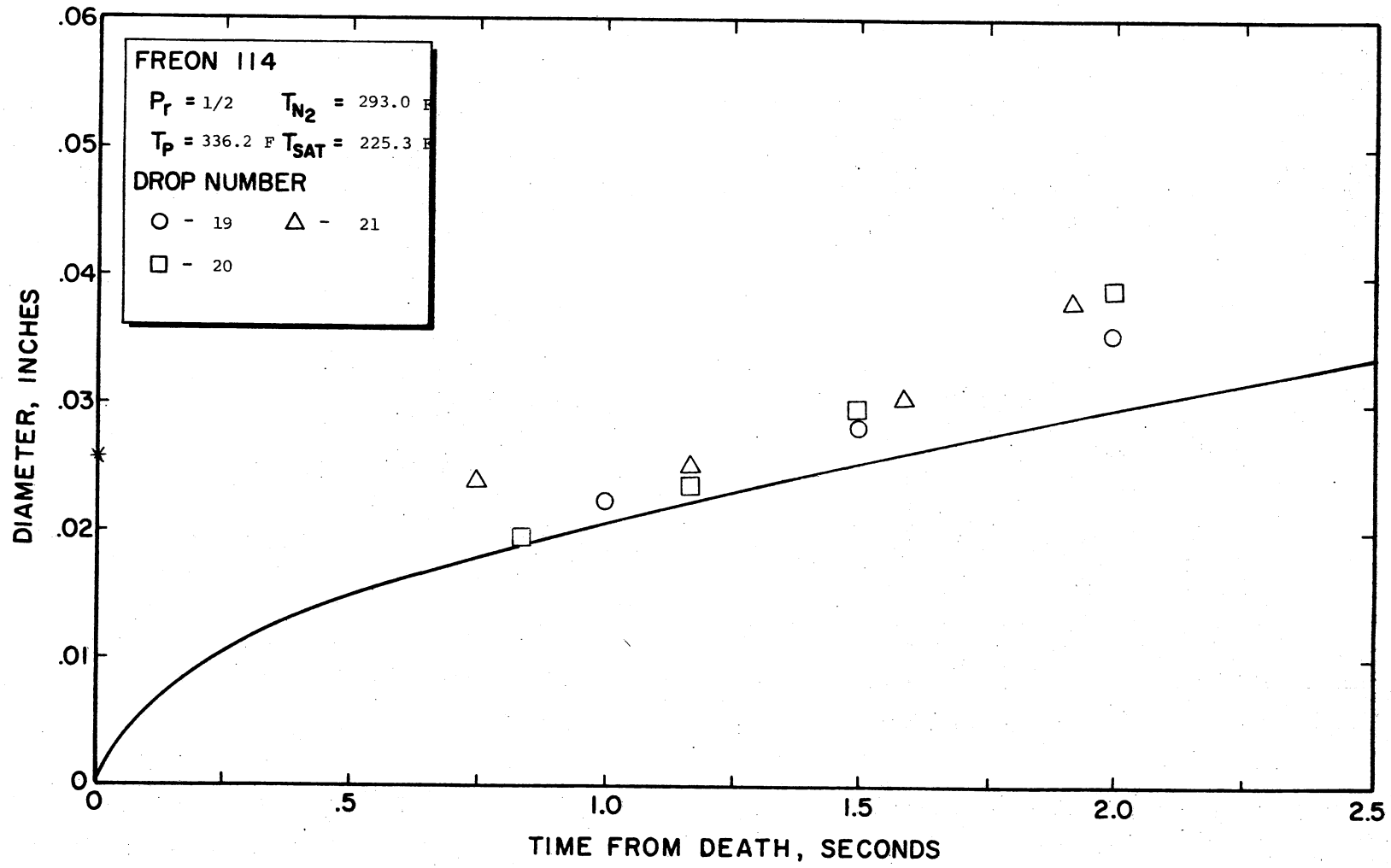
FREON 114
P_r = 1/2 T_{N_2} = 293.0 F
T_P = 336.2 F T_{SAT} = 225.3 F
DROP NUMBER
○ - 19 △ - 21
□ - 20
DIAMETER, INCHES
.06
.05
.04
.03
.02
.01
0
0
.5
1.0
1.5
2.0
2.5
TIME FROM DEATH, SECONDS

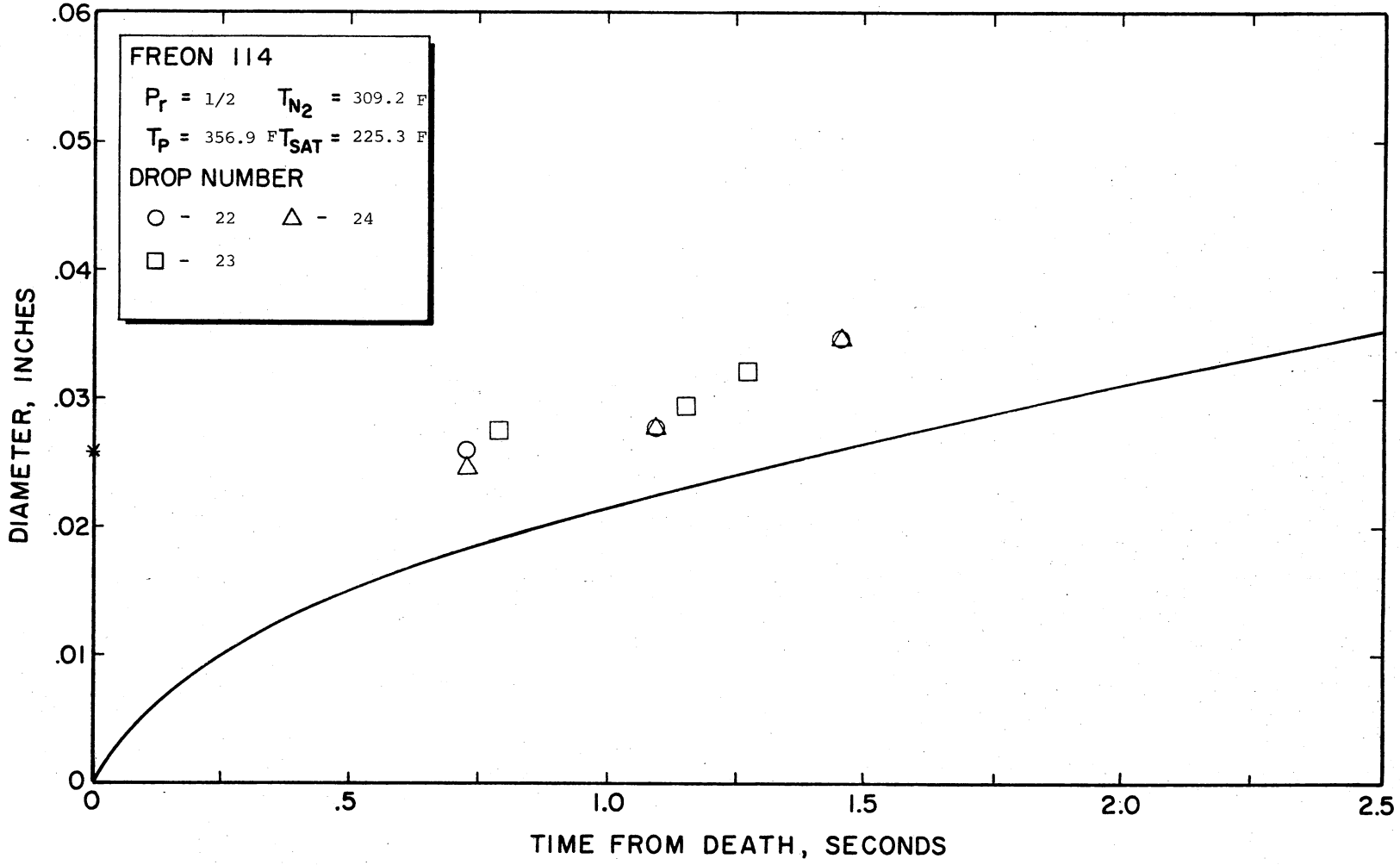
FREON 114
P_r = 1/2 T_{N_2} = 309.2 F
T_P = 356.9 F T_{SAT} = 225.3 F
DROP NUMBER
○ - 22 △ - 24
□ - 23
DIAMETER, INCHES
.06
.05
.04
.03
.02
.01
0
0
.5
1.0
1.5
2.0
2.5
TIME FROM DEATH, SECONDS

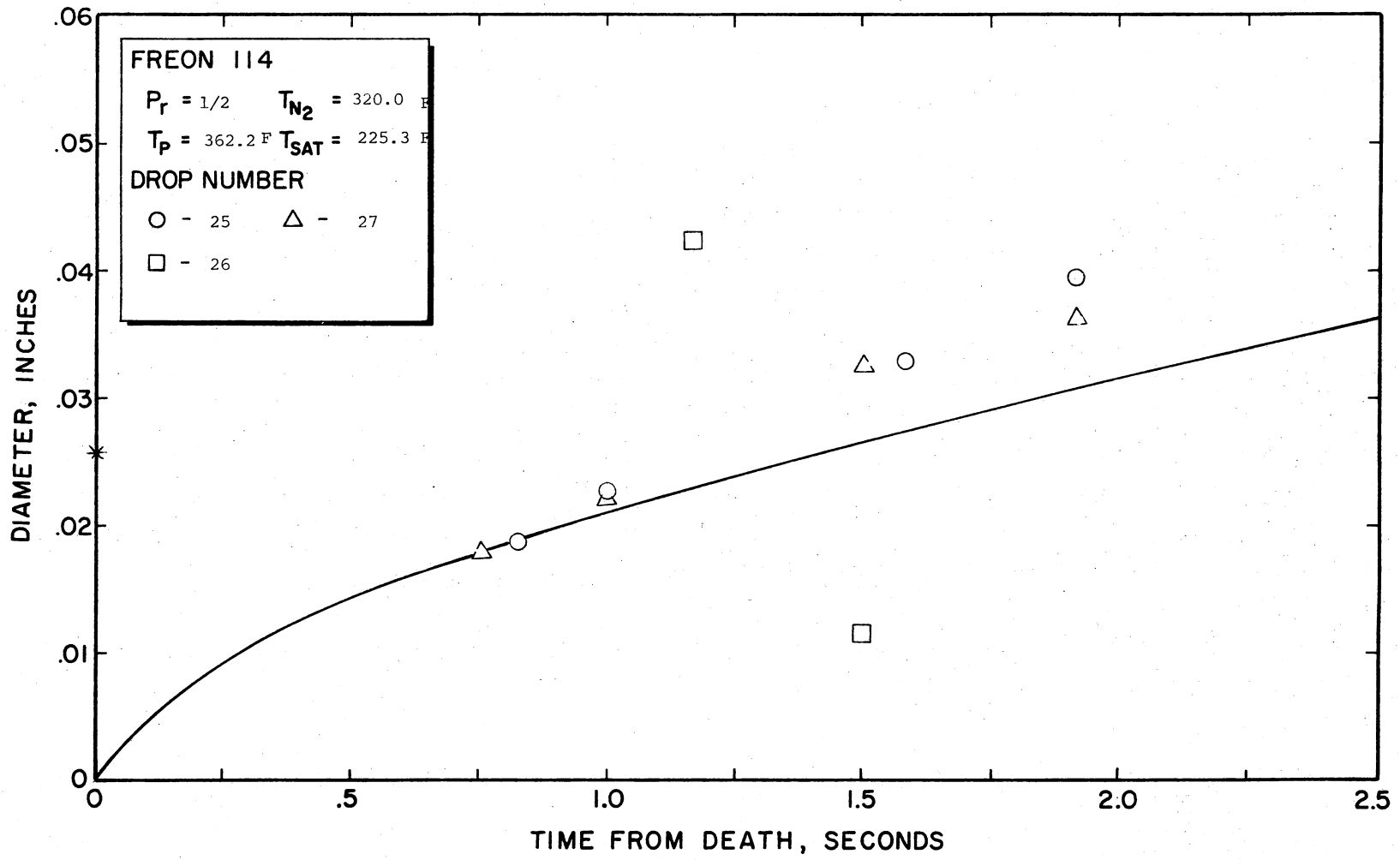
FREON 114
P_r = 1/2 T_{N_2} = 320.0 F
T_P = 362.2 F T_{SAT} = 225.3 F
DROP NUMBER
○ - 25 △ - 27
□ - 26
DIAMETER, INCHES
.06
.05
.04
.03
.02
.01
0
0
.5
1.0
1.5
2.0
2.5
TIME FROM DEATH, SECONDS

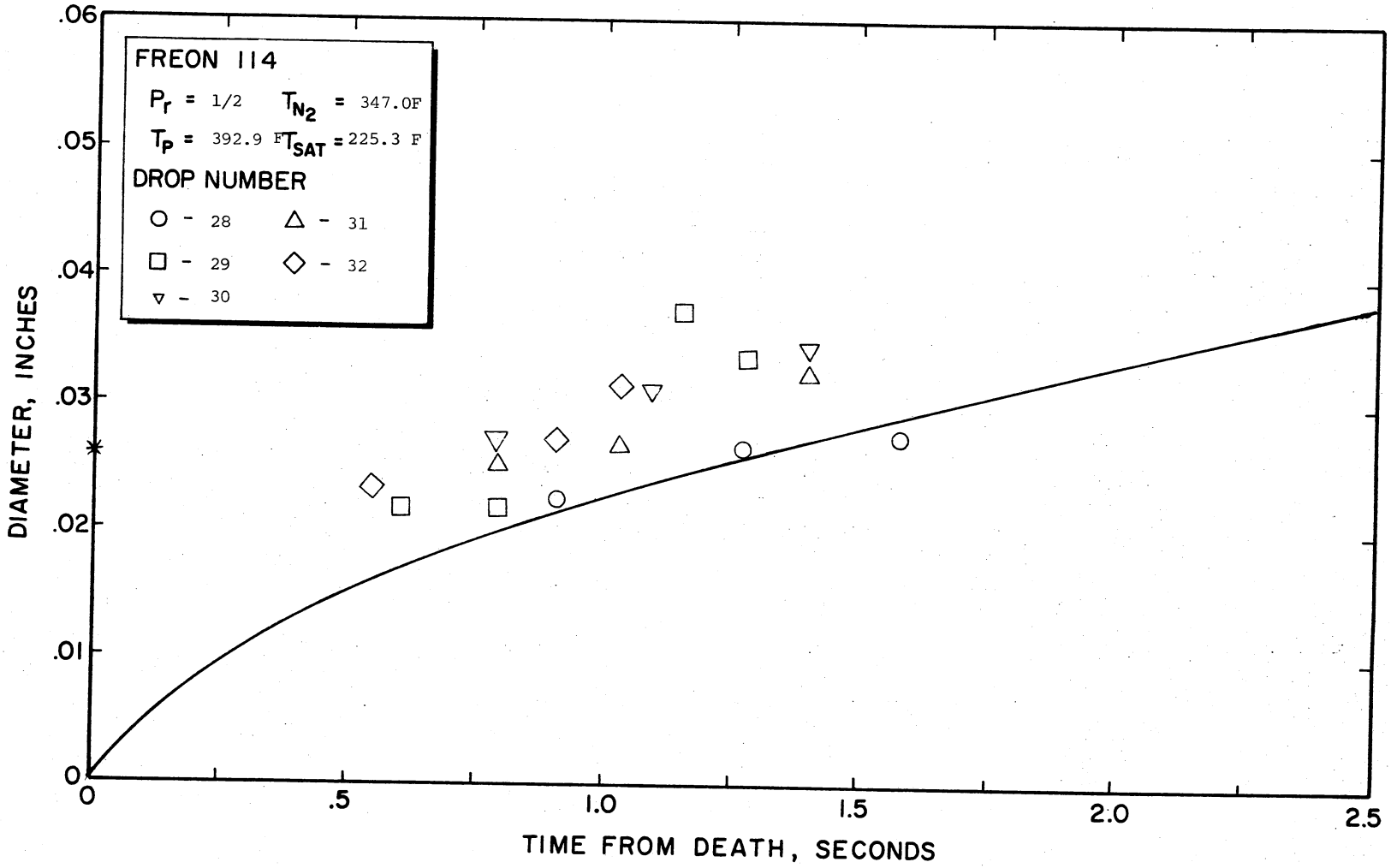
FREON 114
P_r = 1/2 T_{N_2} = 347.0F
T_P = 392.9 F T_{SAT} = 225.3 F
DROP NUMBER
○ - 28 △ - 31
□ - 29 ◇ - 32
▽ - 30
DIAMETER, INCHES
.06
.05
.04
.03
.02
.01
0
0
.5
1.0
1.5
2.0
2.5
TIME FROM DEATH, SECONDS

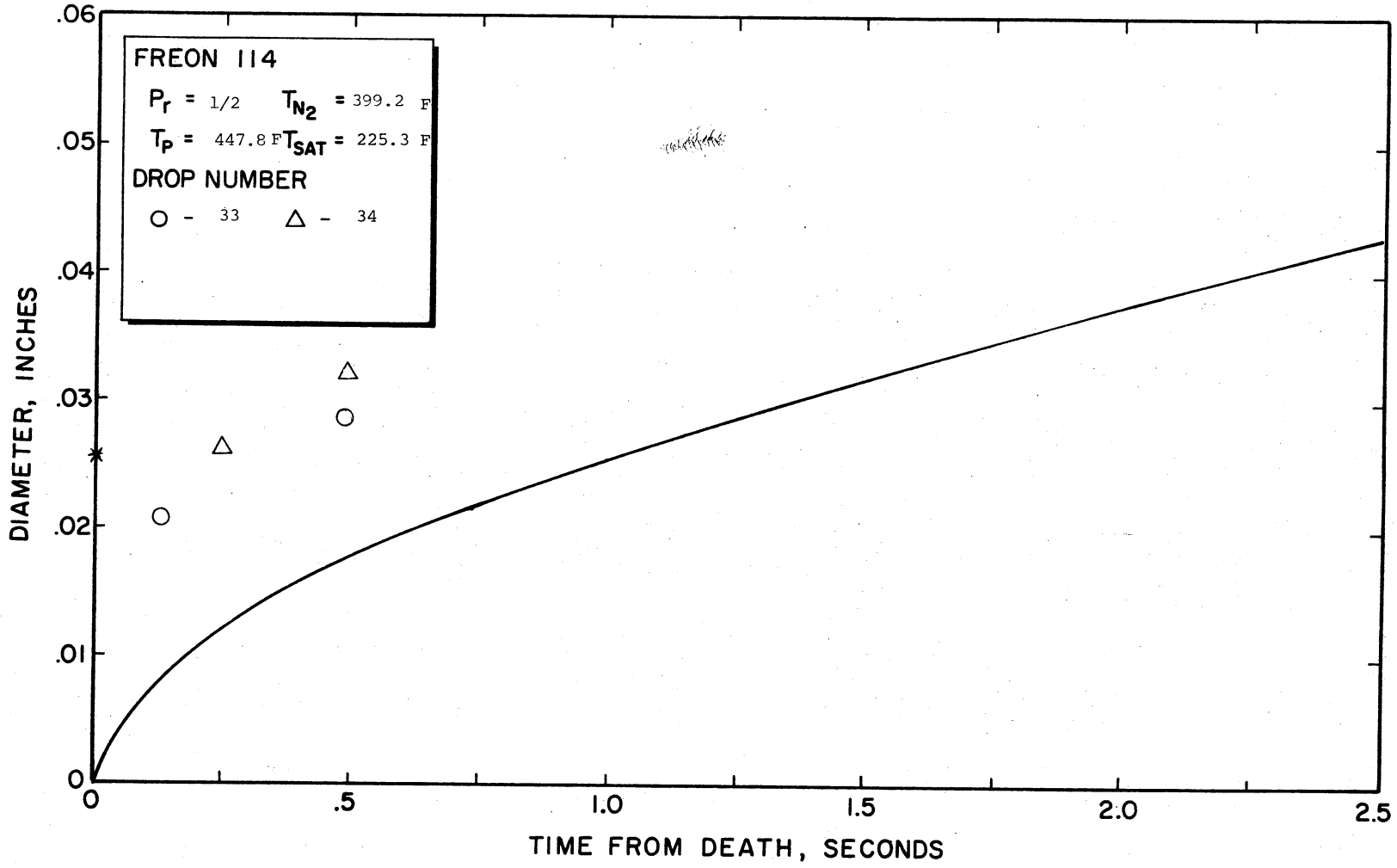
FREON 114
P_r = 1/2 T_{N_2} = 399.2 F
T_P = 447.8 F T_{SAT} = 225.3 F
DROP NUMBER
○ - 33 △ - 34
DIAMETER, INCHES
.06
.05
.04
.03
.02
.01
0
0
.5
1.0
1.5
2.0
2.5
TIME FROM DEATH, SECONDS

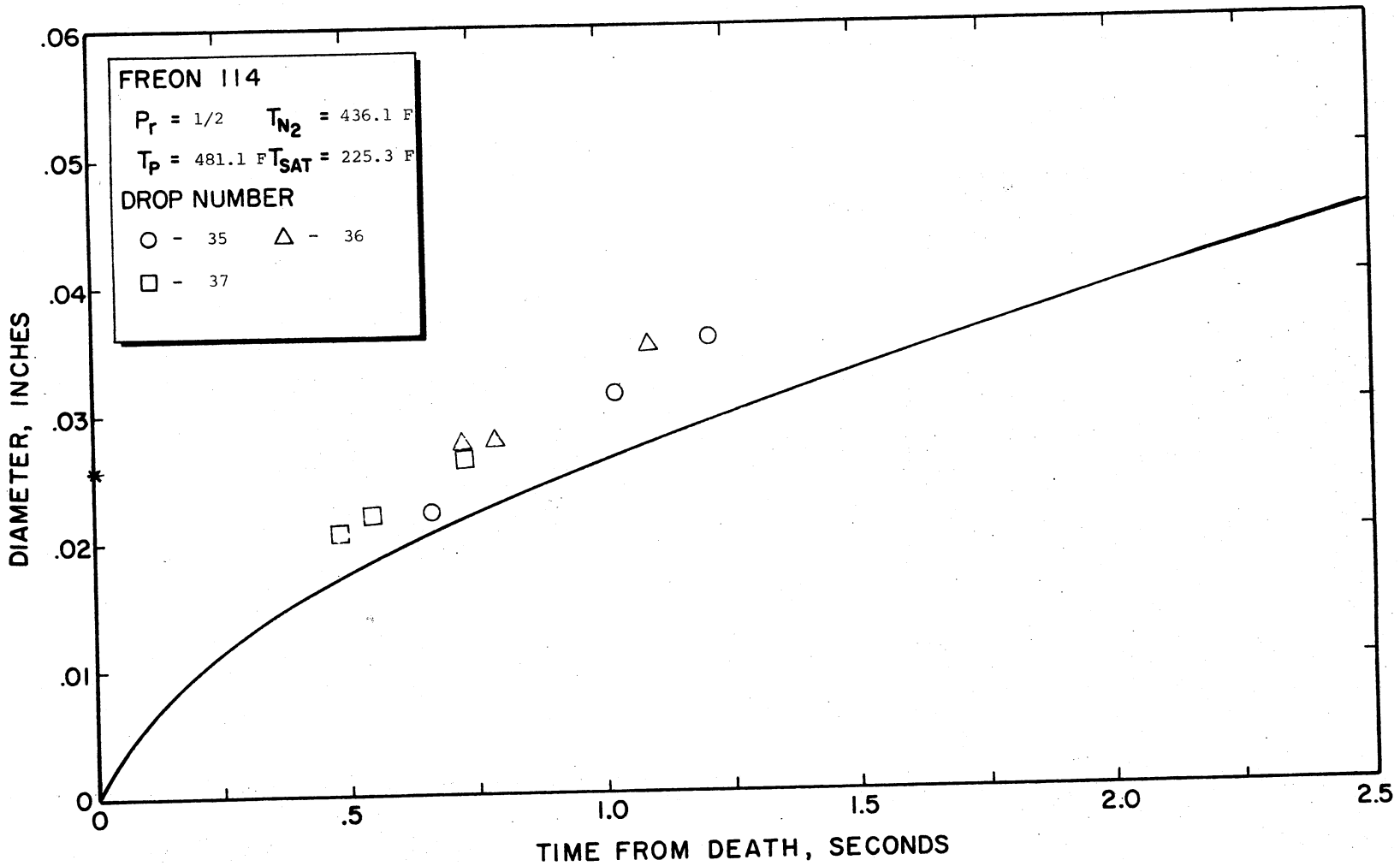
FREON 114
P_r = 1/2 T_{N_2} = 436.1 F
T_P = 481.1 F T_{SAT} = 225.3 F
DROP NUMBER
○ - 35 △ - 36
□ - 37
DIAMETER, INCHES
.06
.05
.04
.03
.02
.01
0
0
.5
1.0
1.5
2.0
2.5
TIME FROM DEATH, SECONDS

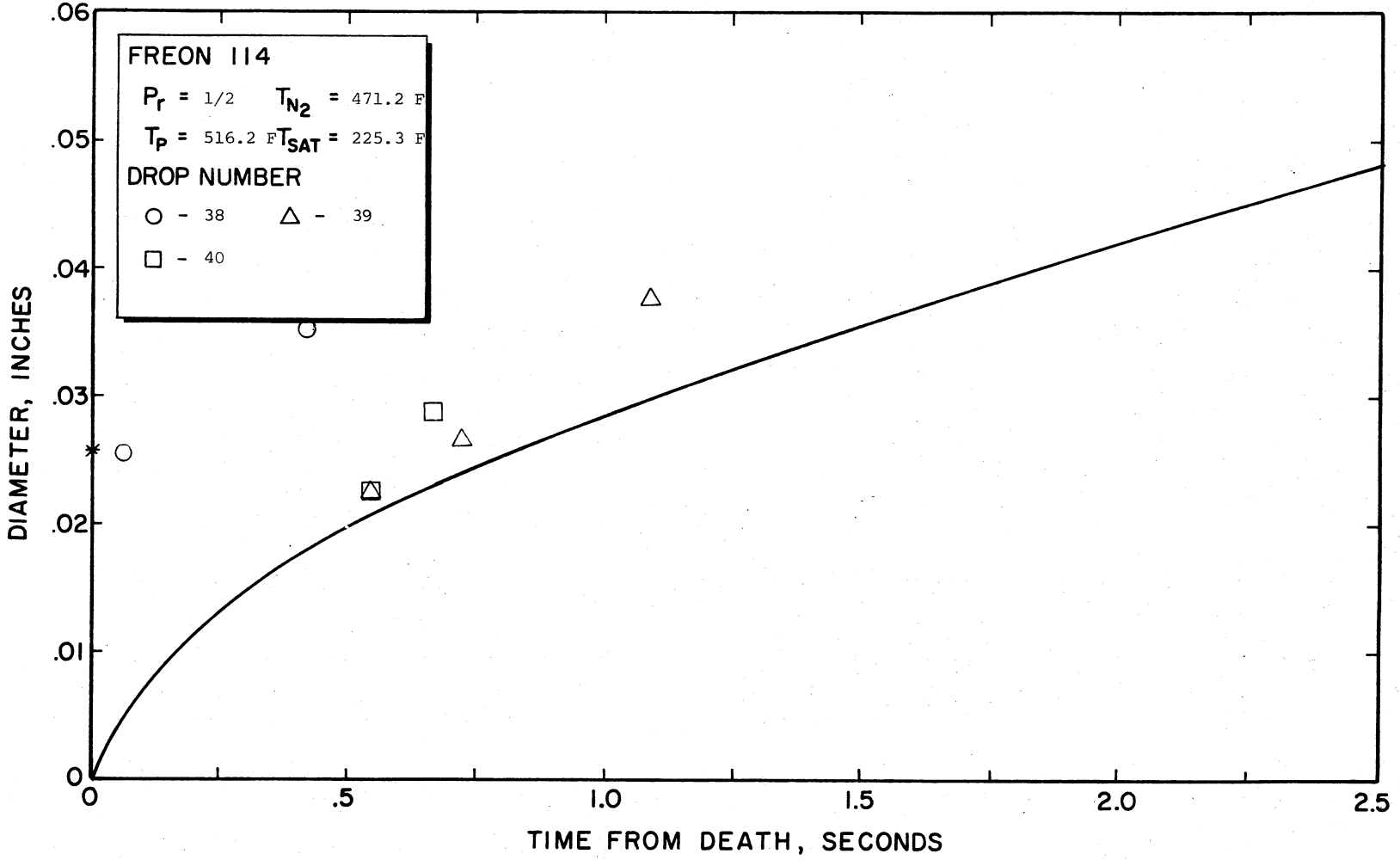
FREON 114
P_r = 1/2 T_{N_2} = 471.2 F
T_P = 516.2 F T_{SAT} = 225.3 F
DROP NUMBER
○ - 38 △ - 39
□ - 40
DIAMETER, INCHES
.06
.05
.04
.03
.02
.01
0
0
.5
1.0
1.5
2.0
2.5
TIME FROM DEATH, SECONDS

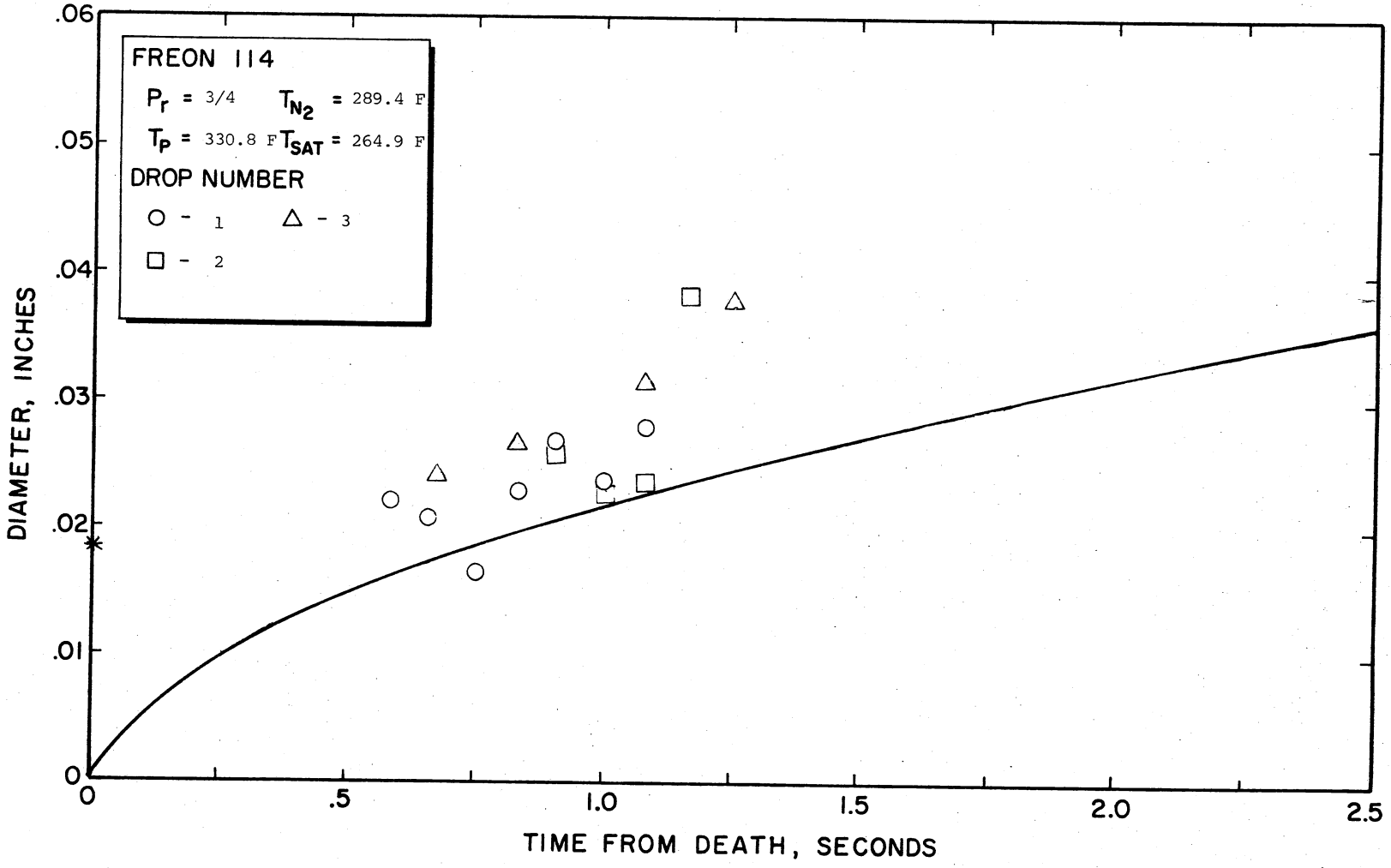
FREON 114
P_r = 3/4 T_{N_2} = 289.4 F
T_P = 330.8 F T_{SAT} = 264.9 F
DROP NUMBER
○ - 1
△ - 3
□ - 2
DIAMETER, INCHES
.06
.05
.04
.03
.02
.01
0
0
.5
1.0
1.5
2.0
2.5
TIME FROM DEATH, SECONDS

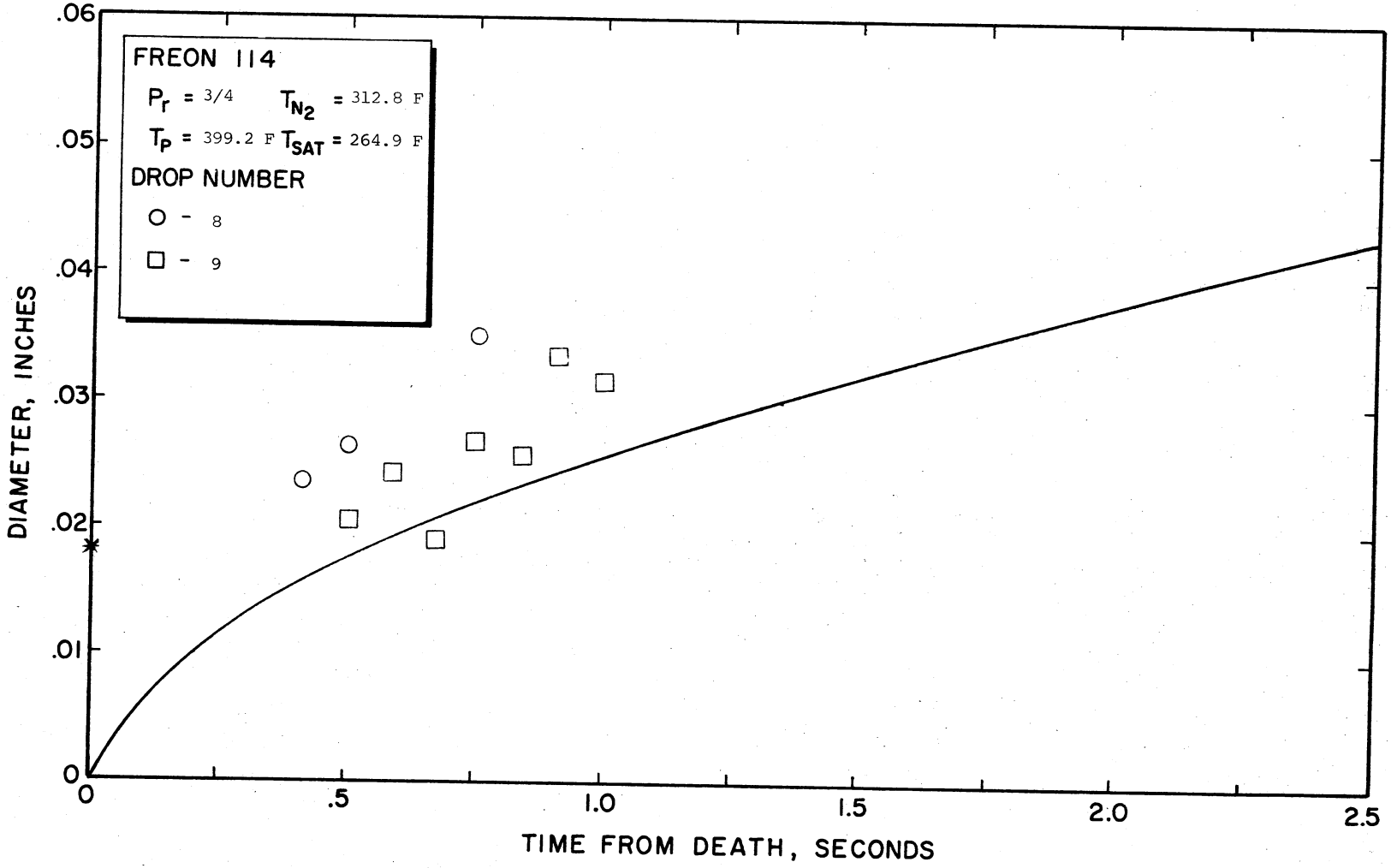
FREON 114
P_r = 3/4 T_{N_2} = 312.8 F
T_P = 399.2 F T_{SAT} = 264.9 F
DROP NUMBER
○ - 8
□ - 9
DIAMETER, INCHES
.06
.05
.04
.03
.02
.01
0
0
.5
1.0
1.5
2.0
2.5
TIME FROM DEATH, SECONDS

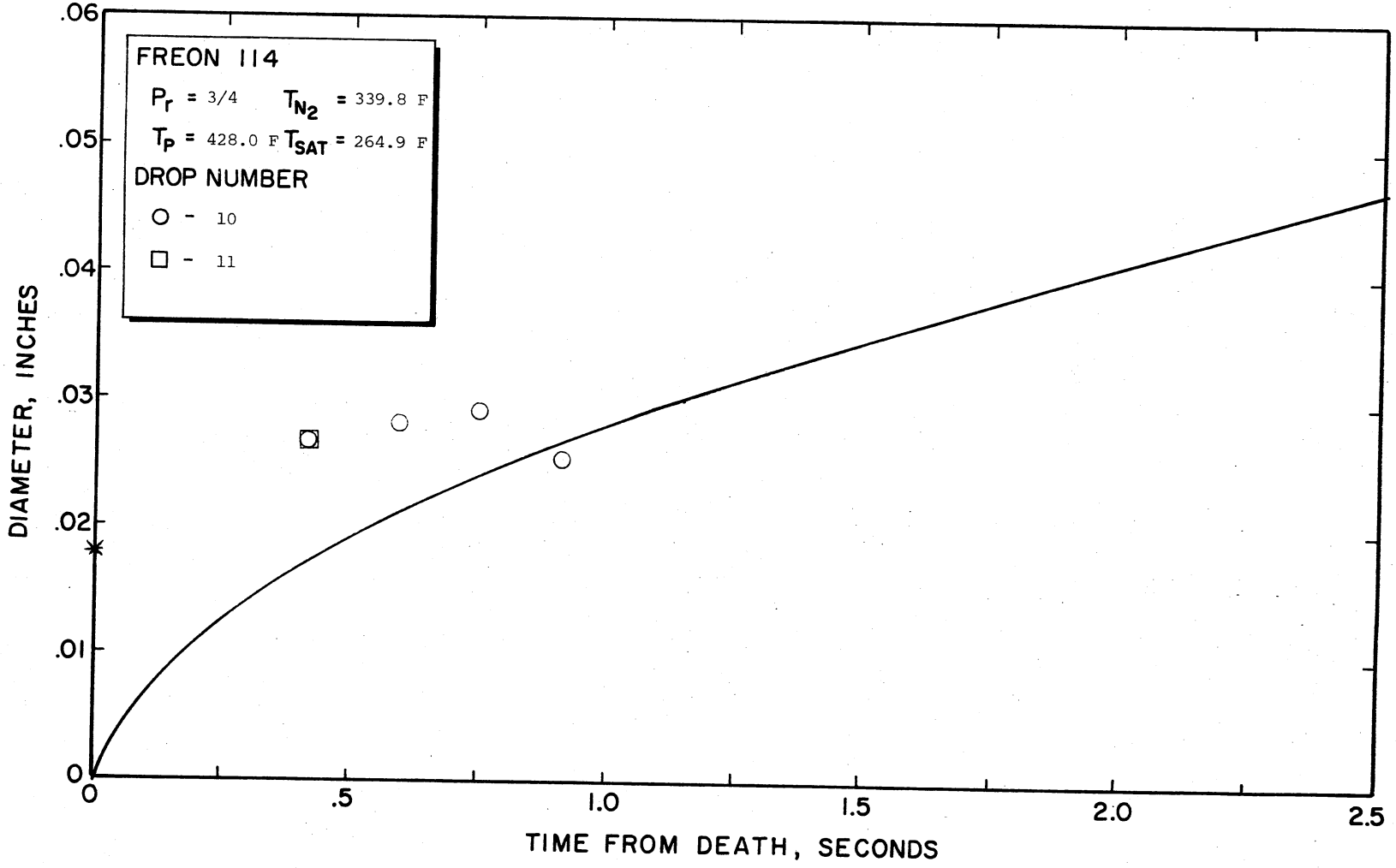
FREON 114
P_r = 3/4 T_{N_2} = 339.8 F
T_P = 428.0 F T_{SAT} = 264.9 F
DROP NUMBER
○ - 10
□ - 11
DIAMETER, INCHES
.06
.05
.04
.03
.02
.01
0
0
.5
1.0
1.5
2.0
2.5
TIME FROM DEATH, SECONDS

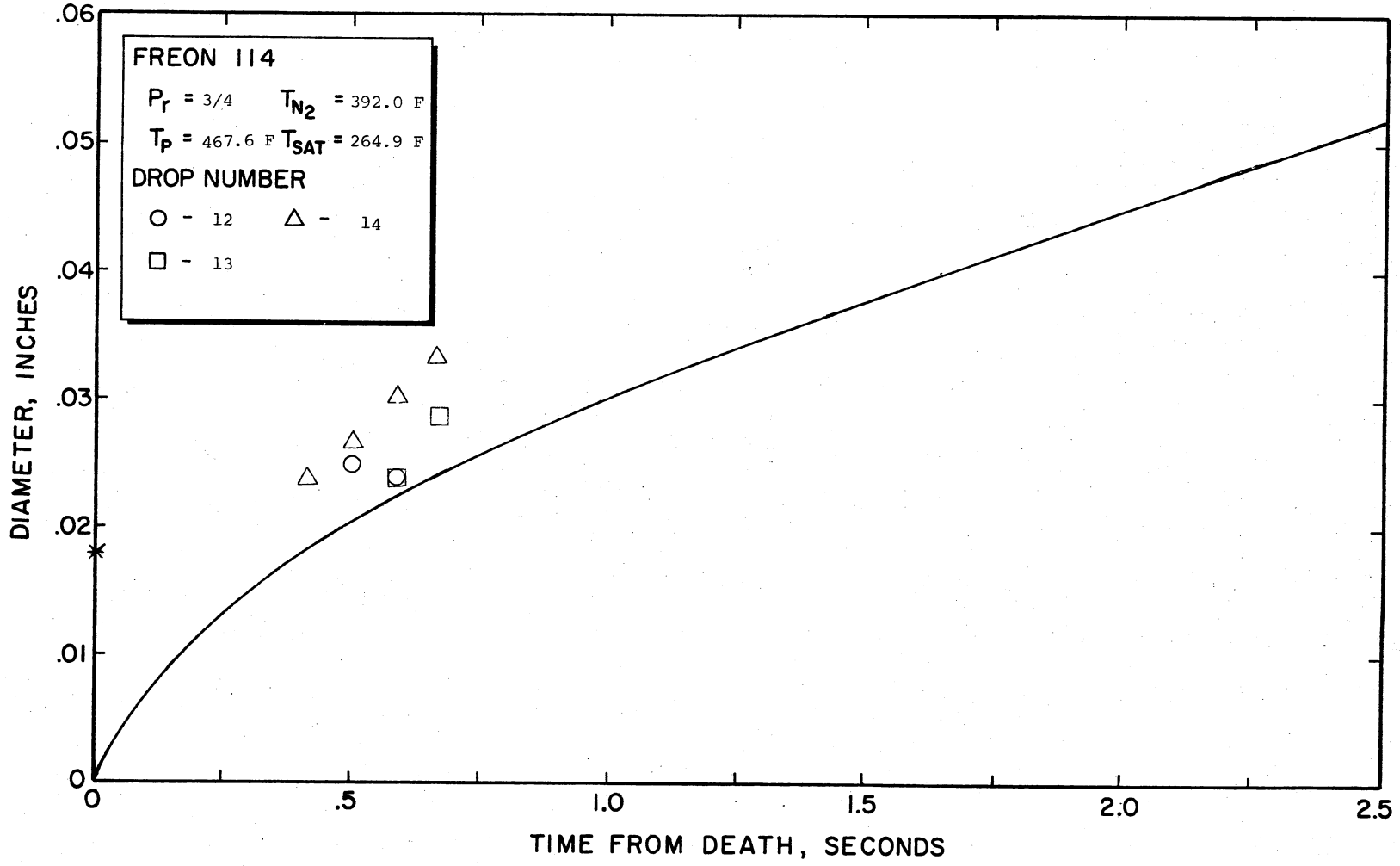
FREON 114
P_r = 3/4 T_{N_2} = 392.0 F
T_P = 467.6 F T_{SAT} = 264.9 F
DROP NUMBER
○ - 12 △ - 14
□ - 13
DIAMETER, INCHES
.06
.05
.04
.03
.02
.01
0
0
.5
1.0
1.5
2.0
2.5
TIME FROM DEATH, SECONDS

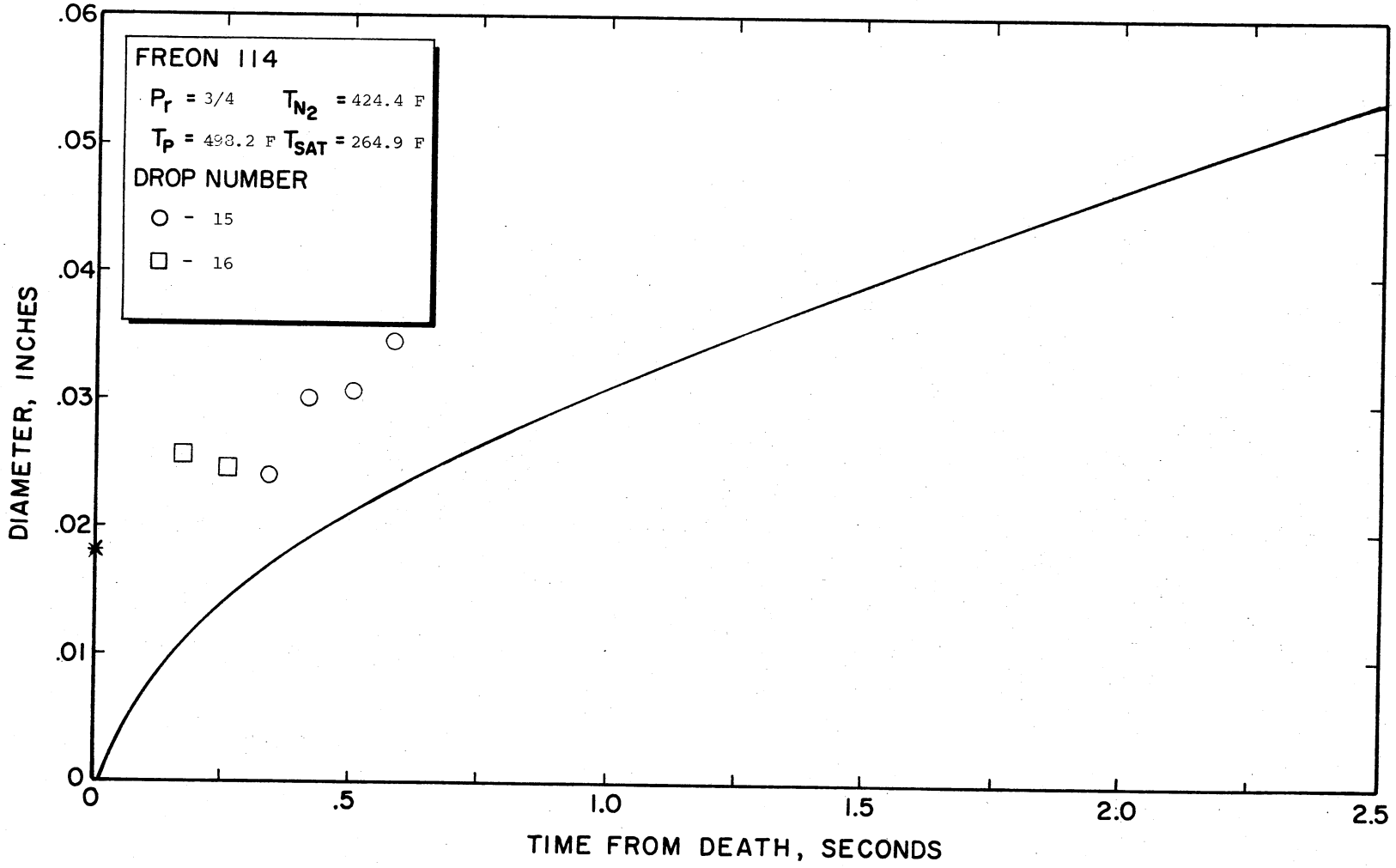
FREON 114
P_r = 3/4 T_{N_2} = 424.4 F
T_P = 498.2 F T_{SAT} = 264.9 F
DROP NUMBER
○ - 15
□ - 16
DIAMETER, INCHES
.06
.05
.04
.03
.02
.01
0
0
.5
1.0
1.5
2.0
2.5
TIME FROM DEATH, SECONDS

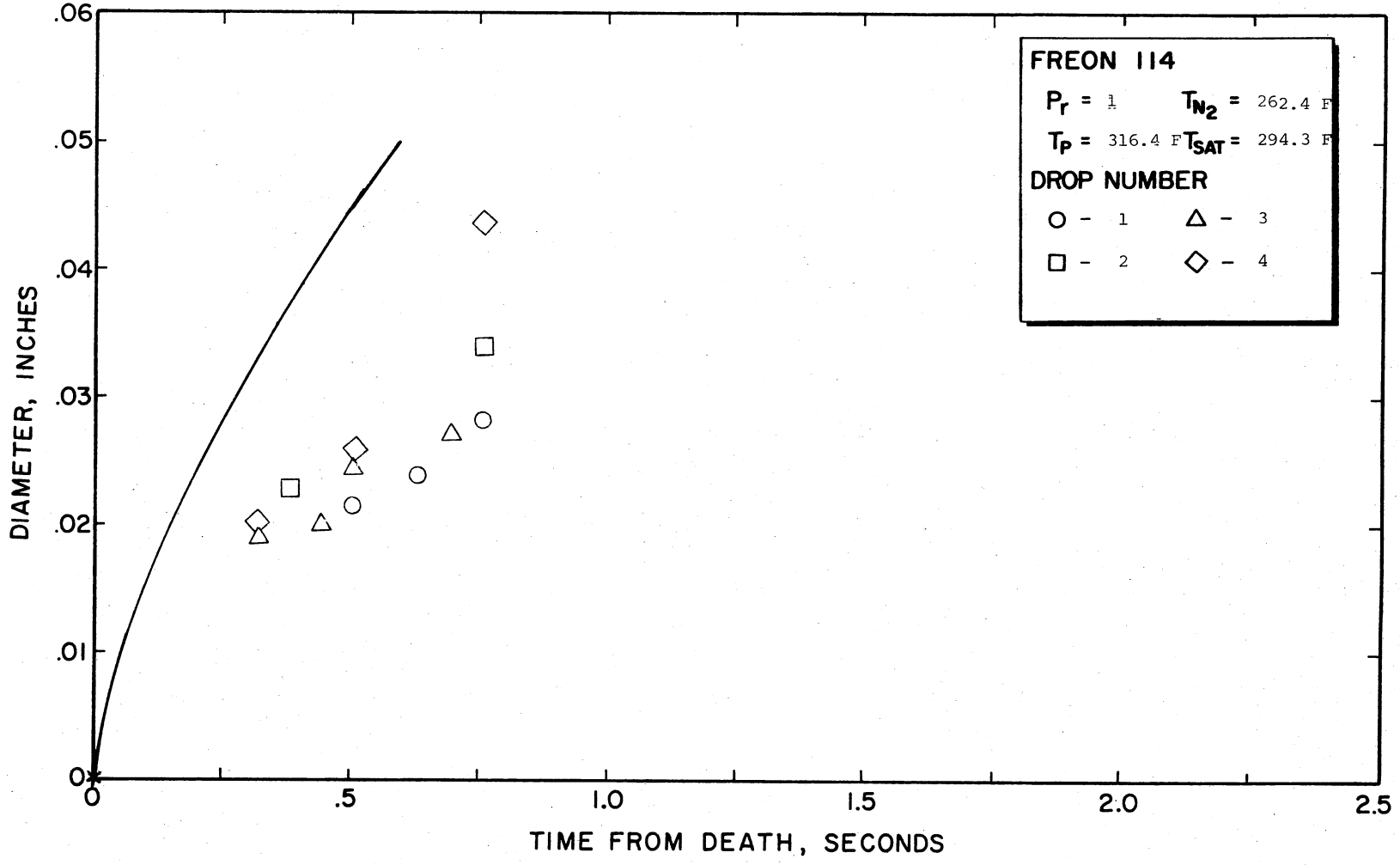
FREON 114
P_r = 1 T_{N_2} = 262.4 F
T_P = 316.4 F T_{SAT} = 294.3 F
DROP NUMBER
○ - 1 △ - 3
□ - 2 ◇ - 4
DIAMETER, INCHES
.06
.05
.04
.03
.02
.01
0
0
.5
1.0
1.5
2.0
2.5
TIME FROM DEATH, SECONDS

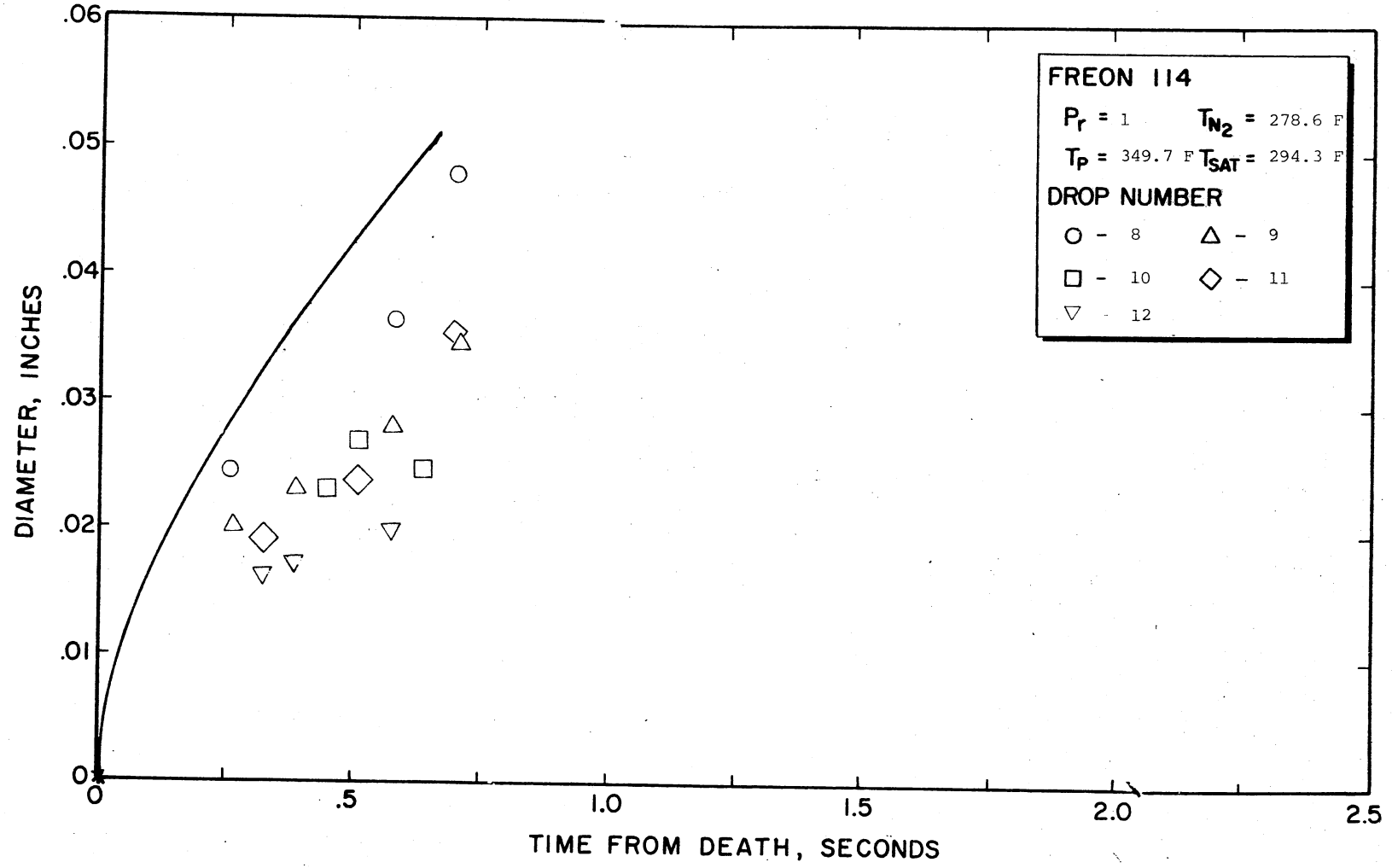
FREON 114
P_r = 1
T_{N_2} = 278.6 F
T_P = 349.7 F
T_{SAT} = 294.3 F
DROP NUMBER
○ - 8
△ - 9
□ - 10
◇ - 11
▽ - 12
DIAMETER, INCHES
.06
.05
.04
.03
.02
.01
0
0
.5
1.0
1.5
2.0
2.5
TIME FROM DEATH, SECONDS

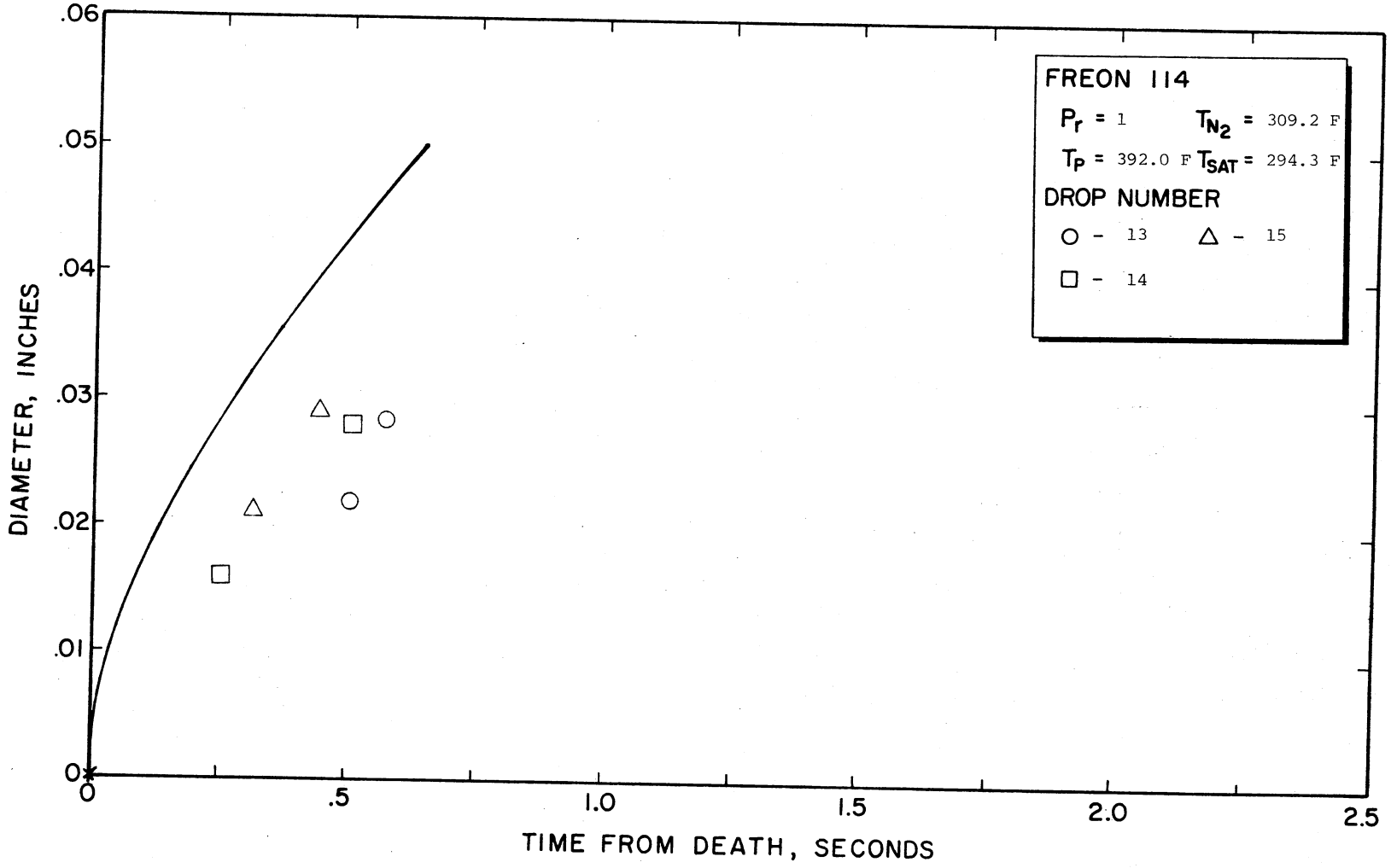
FREON 114
P_r = 1
T_{N_2} = 309.2 F
T_P = 392.0 F
T_{SAT} = 294.3 F
DROP NUMBER
○ - 13
△ - 15
□ - 14
DIAMETER, INCHES
.06
.05
.04
.03
.02
.01
0
0
.5
1.0
1.5
2.0
2.5
TIME FROM DEATH, SECONDS

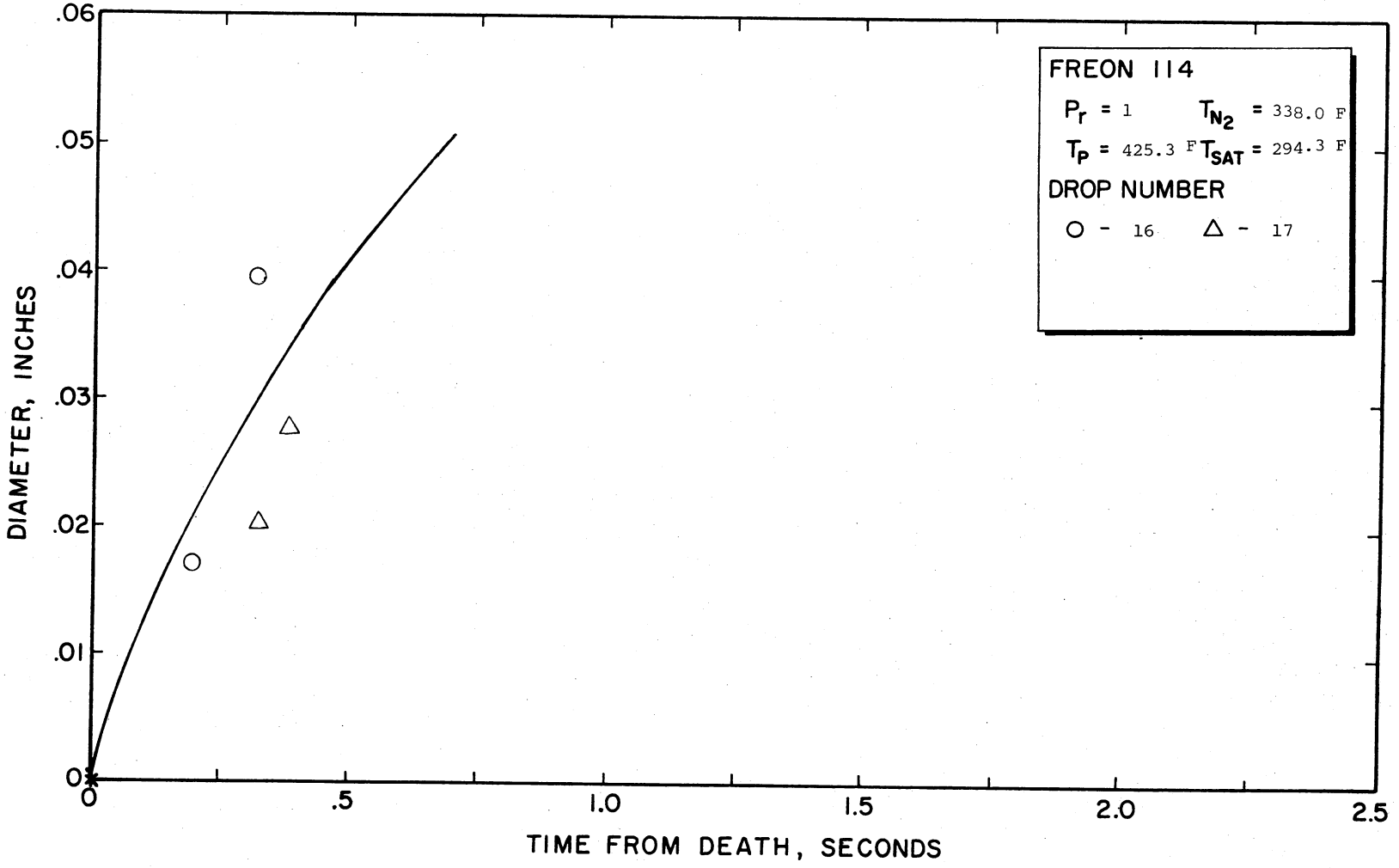
FREON 114
P_r = 1
T_{N_2} = 338.0 F
T_P = 425.3 F
T_{SAT} = 294.3 F
DROP NUMBER
○ - 16
△ - 17
DIAMETER, INCHES
.06
.05
.04
.03
.02
.01
0
0
.5
1.0
1.5
2.0
2.5
TIME FROM DEATH, SECONDS

APPENDIX H

THERMOCOUPLE CALIBRATION

To calibrate the thermocouples a Leeds and Northrup platinum resistance thermometer (no. 1613906) was used. Thermocouple number 5 was placed in a Hoskins furnace with the platinum resistance thermometer. The results are shown in Table II. Thermocouples 1, 2, 3, 4, and 6 were then cross checked against thermocouple 5. These results are seen in Table III.

TABLE II

CALIBRATION OF THERMOCOUPLE 5

Thermocouple 5		Platinum Resistance Thermometer	
Reading, mv	Temperature, ^{o}C	Ratio	Temperature, ^{o}C
4.110	100.25	1.3171	99.75
4.775	116.44	1.455847	116.37
6.049	147.98	1.576886	147.97
7.775	191.13	1.740106	191.09
10.188	250.70	1.964382	251.25
11.693	287.08	2.103733	289.24
11.775	289.44	2.111500	291.37
11.886	292.15	2.121676	294.16
12.120	297.75	2.142578	299.90
14.250	349.00	2.328456	351.48
16.504	402.51	2.519110	405.31
18.350	446.75	2.670193	448.66
19.480	473.75	2.760999	474.02
20.320	492.25	2.827539	494.49

TABLE III

CALIBRATION OF THERMOCOUPLES 1, 2, 3, 4, 6

	Thermocouple Number					
Reading,	5	1	2	3	4	6
millivolts	.921	.921	.921	.921	.921	.920
	5.112	5.095	5.085	5.090	5.100	5.030
	6.543	6.536	6.534	6.534	6.534	6.591
	8.702	8.702	8.691	8.700	8.696	8.766
	10.759	10.776	10.756	10.774	10.774	10.845
	13.288	13.304	13.294	13.335	13.356	13.487
	16.120	16.146	16.135	16.186	16.209	16.325
	18.786	18.795	18.762	18.785	18.785	18.891
	4.050	4.050	4.050	4.050	4.046	4.060

The experimental cell was filled with ethyl alcohol to a depth of ½ inch. Heat was applied to the cell from the electric heaters. The temperature of the cell was lowered by reducing the heat input. As the alcohol ceased nucleate boiling the thermocouples were read and recorded.

Atmospheric pressure = 740 mm Hg; T_{BP} = 77.8°C.

TABLE IV

CALIBRATION IN SITU

Thermocouple Number	Thermocouple Reading, mv	Temperature, °C
1	3.168	77.75
2	3.170	77.75
3	3.120	76.5
4	3.181	78.0
5	3.175	78.0

APPENDIX I

PRESSURE GAUGE CALIBRATION

PRESSURE GAUGE CALIBRATION

A Marsh and an ACCO Helicoid gauge were used for pressure measurements in the cell. The Marsh gauge had a pressure range of 0-100 psig, and the ACCO gauge had a range of 0-1000 psig.

The two gauges were calibrated on a Budenburg Dead Weight Gauge, which has an accuracy of 0.05%.

TABLE V

CALIBRATION OF PRESSURE GAUGES

Helicoid Gauge		Marsh Gauge	
Dead Weight Tester	Gauge psig	Dead Weight Tester	Gauge psig
20	20	20	20
40	41	40	40
50	51	50	50
60	61	60	60
100	101	100	100
200	201		
300	300		
400	400		
500	500		
600	600		
700	701		
800	802		
900	902		
1000	1004		

APPENDIX J

COMPUTER PROGRAM AND FORTRAN SUBROUTINES

```
C          FREON-114  MAIN PROGRAM
C
      DIMENSION BVAL(5)
      COMMON AC,AB,CC,BB
      EXTERNAL F
      REAL NU1,NU2,K1,K2,LAMDA,KE,KASS,KAVG
      REAL INT,INTA,NU,MW
1     FORMAT(1X,7(E15.7,3X))
100   FORMAT(5F10.1)
101   FORMAT(5F10.1)
102   FORMAT(F5.1,F5.1)
110   FORMAT(1X,'DIA,INCHES',9X,'TIME,SEC',12X,'W1,LB/HR',12X,'W2,LB/HR
     9',12X,'QC,BTU/HR',11X,'QR1,BTU/HR',10X,'QR2,BTU/HR')
      READ(5,100)TC,PC,MW,ZC,ALPHAD
      READ(5,101)DI,PSAT,RH0L,VSAT,LAMDA
99    READ(5,102)TP,TN2
      PRINT,TP,TN2
      WRITE(6,110)
      TSUR=TN2+.736*(TP-TN2)
      TP=TP+460.
      TSUR=TSUR+460.
      RH0VS=1./VSAT
      RH0C=PC*MW/(ZC*TC*.73*1.8)
      CALL SATEM(PSAT,TSAT,2)
      CALLRK(TP,PSAT,RH0V,TC,PC,Z,MW)
      RH0AVG=(RH0VS+RH0V)/2.
      TP=TP/1.8
      CALL THERMK(TC,PC,MW,RH0V,TP,ZC,K2)
      TP=TP*1.8
      TSAT=TSAT/1.8
      CALL THERMK(TC,PC,MW,RH0VS,TSAT,ZC,K1)
      TSAT=TSAT*1.8
      KAVG=(K1+K2)/2.
      CALL SATEM(PSAT,TSAT,2)
      CALL SPHT(TSAT,CP1)
      CALL SPHT(TP,CP2)
      CPAVG=(CP1+CP2)/2.
      PLAMDA=LAMDA+CPAVG*(TP-TSAT)/2.
      Z=PSAT*VSAT/(10.73*TSAT)*MW
      CALL DIFFLS(MW,TC,PC,PSAT,DP,Z)
      CALL SATEM(PSAT,TSAT,2)
      CALL VISC(TC,PC,MW,TSAT,NU1,RH0VS,ZC)
      CALL VISC(TC,PC, MW,TP,NU2,RH0V,ZC)
      ANU=(NU1+NU2)/2.
      G=32.2*3600.**2
      R0=DI/2.
      R0=R0/12.
      T=0.0
      TIN=0.0
      TINC=.05/3600.
      KASS=KAVG
14    R=R0
      TIN=T
      I=1
      AB=R0**4*G*(RH0L-RH0AVG)*PLAMDA*6.28/(18.*.125*ANU)
      AC=KAVG*6.28*R0*(TP-TSAT)
9     NC=1
      W2 =DP*RH0VS*R0*6.28*14.696/PSAT
      QR1=.5*.9*1.71E-09*TP**4-.5*ALPHAD* 1.71E-09*TSAT**4
      QR1=QR1*12.56*R0*R0
      QR2=.5*.9*1.71E-09*TSUR**4-.5*ALPHAD*1.71E-09*TSAT**4
      QR2=QR2*12.56*R0*R0
      CC=QR1+QR2
      BB=W2*LAMDA
      XL=.1E-15
      XR=.05
      CALL BISEC(F,.0000001,100,6,-1,NFAIL,XL,XR)
      DELR=(XL+XR)/2.
      W1=AB*DELR**2*(-1.+(1.+DELR)*ALOG((1.+DELR)/DELR))/PLAMDA
10    CONTINUE
1000  FUNC=-(W1+W2)/(12.5664*RH0L*R0*R0)
      BVAL(I)=TINC*FUNC
      GOTO(20,21,22,23),I
20    T=TIN+.5*TINC
      R0=R+.5*BVAL(1)
```

```
      I=I+1
      GOTO 9
21    T=TIN+.5*TINC
      R0=R+.5*BVAL(2)
      I=I+1
      GOTO 9
22    T=TIN+TINC
      R0=R+BVAL(3)
      I=I+1
      GOTO 9
23    I=I+1
      R0=R+(BVAL(1)+2.*BVAL(2)+2.*BVAL(3)+BVAL(4))/6.
      QC=W2*LAMDA+W1*PLAMDA-QR1-QR2
      QC=QC/(3.1416*R0*R0)
      QR=(QR1+QR2)/(12.56*R0*R0)
      W1=W1/(6.28*R0*R0)
      W2=W2/(6.28*R0*R0)
      T=TIN+TINC
      TT=T*3600.
      RR=R0*24.
      WRITE(6,1) RR,TT,W1,W2,QC,QR,RE
      IF(RR.LT.0.0) GOTO 999
      IF(W2.LT.0.0) GOTO 999
      GOTO 14
999   GOTO 99
      STOP
      END
      SUBROUTINE RK(T,P,RHOV,TCR,PCR,Z,MW)
      REAL MW
C     THIS SUBROUTINE WRITTEN BY DR. J.H. ERBAR
      DIMENSION XV(10),ARK(10),BRK(10),PC(10),TC(10)
      TC(1)=TCR*1.2
      PC(1)=PCR*14.696
      AMIX=0.0
      BMIX=0.0
      XV(1)=1.
      DO 1 I=1,1
      CONA=T/TC(I)
      ARK(I)=SQRT(.42748/(PC(I)*CONA**2.5))
      BRK(I)=.08664035/(PC(I)*CONA)
      BMIX=BMIX+BRK(I)*XV(I)
      AMIX=AMIX+ARK(I)*XV(I)
1     CONTINUE
      EX=1./3.
      CONB=BMIX*P
      AOB=AMIX*AMIX/BMIX
      QQQ=CONB*(AOB-1.-CONB)
      RRR=-AOB*CONB**2
      AAA=QQQ-EX
      BBB=QQQ/3.-2./27.+RRR
      TEST=(AAA**3)/27.+(BBB**2)/4.
      IF(TEST)140,150,150
150   CA=SQRT(TEST)-BBB/2.
      CB=-CA-BBB
      CAPA=SIGN((ABS(CA)**EX),CA)
      CAPB=SIGN((ABS(CB)**EX),CB)
      Z=CAPA+CAPB
      IF(TEST)160,160,1000
160   Z=AMAX1(Z,(-Z/2.))
      GOTO 1000
140   THET=ATAN(SQRT(-TEST)/(-BBB/2.))/3.
      TERM=2.*SQRT(-AAA/3.)
      X4=TERM*COS(THET)
      X2=TERM*COS(THET+2.0944)
      X3=TERM*COS(THET+4.1888)
      Z=AMAX1(X4,X2,X3)
1000  Z=Z+EX
      IF(Z-.259)200,200,201
200   Z=.259
201   CONTINUE
      RHOV=P*MW/(Z*10.73*T)
      RETURN
      END
      SUBROUTINE BISEC(F,EPS,MAXIT,IO,NPR,NFAIL,XL,XR)
C
C     SUBROUTINE BISEC,  EDITION ONE   9/12/73
```

```
C     WRITTEN IN A.N.S.I. STANDARD FORTRAN
C     WRITTEN BY DAVID DAUTENHAHN,  OKLAHOMA STATE UNIVERSITY
C     THIS SUBROUTINE WILL FIND THE ROOT OF AN EQUATION BY THE METHOD OFBISEC  6
C     INTERVAL HALVING                                                 BISEC  7
C     REFERENCE                                                        BISEC  8
C     NUMERICAL METHODS WITH FORTRAN IV CASE STUDIES                   BISEC  9
C     BY WILLIAM S. DORN, AND DANIEL MCCRACKEN  -  PAGE 3-17           BISEC 10
C                                                                      BISEC 11
C     THE REQUIRED INPUT PARAMETERS ARE                                BISEC 12
C                                                                      BISEC 13
C     IO = THE LOGICAL UNIT NUMBER OF THE PRINTER                      BISEC 14
C     MAXIT = THE MAXIMUM NUMBER OF ITERATIONS TO BE PERFORMED         BISEC 15
C     EPS = THE TOLERENCE OF ACCURACY BETWEEN XL AND XR                BISEC 16
C     XL = THE LEFT BRACKET OF THE ROOT                                BISEC 17
C     XR = THE RIGHT BRACKET OF THE ROOT
C     NPR = THE PRINT SWITCH
C           IF NPR.GT.0 PRINT EACH ITERATION
C           IF NPR.EQ.0 PRINT ONLY INITIAL AND FINAL VALUES            BISEC 21
C           IF NPR.LT.0 PRINT NOTHING
C     F = THE NAME OF THE FUNCTION SUBPROGRAM
C
C     A FUNCTION SUBPROGRAM IS REQUIRED IN THE FOLLOWING FORM FOR PROPERBISEC 25
C     EXECUTION
C     FUNCTION F(X)
C     F = X**2. - 4.0
C     RETURN
C     END
C
C     AN EXTERNAL STATEMENT IS REQUIRED AT THE BEGINING OF THE MAIN    BISEC 32
C     PROGRAM.  THIS ALLOWS OTHER FUNCTIONS TO BE EVALUATED IN THE SAME BISEC 33
C     COMPILATION
C
C     THE OUTPUT PARAMETERS ARE
C
C     XL = THE LEFT BRACKET OF THE ROOT
C     XR = THE RIGHT BRACKET OF THE ROOT
C     NFAIL = WILL BE NON ZERO IF MAXIT ITERATIONS WERE PERFORMED BEFOREBISEC 45
C     EPS TOLERENCE WAS ACHEIVED, AND IF XL AND XR DID NOT BRACKET A ROOBISEC 46
C     ROOT.
C
C     FOR DOUBLE PRECISION ACTIVATE THE FOLLOWING CARD, AND ALL OTHERS WITH
C     CD IN COLUMNS 1-2
CD    DOUBLE PRECISION F,XL,XR,EPS,TWO,YR,YL,Y,X,DELTA                 BISEC 52
C
C     ****** THE PROGRAM STARTS HERE *****
C
      XLI = XL
      XRI = XR
CD    TWO = 2.0D0
      TWO = 2.0
      ICNT = 0
C
C      TEST FOR XL GREATER THAN XR, AND REVERSE THEM IF TRUE           BISEC 62
C
      IF(XR-XL)970,971,971
  970 XR=XLI
      XL=XRI
  971 CONTINUE
      YR = F(XR)
      YL = F(XL)
      IF(NPR)901,901,902
  902 WRITE(IO,903)
  901 CONTINUE
C
C     TEST FOR XL AND XR BRACKETING A ROOT.  IF THEY DO  NOT THEN STOP AND SET
C     NFAIL  = 1
C
      IF(YR)301,950,950
  950 IF(YL) 300,951,951
  301 IF(YL)951,951,300
  951 NFAIL = 1
      GO TO 704
  300 CONTINUE
C
C     CHECK WHETHER THE ITERATION COUNTER HAS BEEN EXCEEDED
C     IF SO THEN STOP AND SET NFAIL = 2
```

```
C
      IF (MAXIT-ICNT      ) 85,85,86
   85 NFAIL = 2
      IF (NPR) 704,704,912
  912 WRITE(IE,88)EPS,MAXIT
      GO TO 704
   86 X = (XL + XR)/TWO
C
C     TEST FOR X NOT LYING STRICTLY BETWEEN XL AND XR. THIS IS A TEST FOR THE
C     COMPUTERS ACCURACY TO A FIXED NUMBER OF DECIMAL PLACES, AND WOULD BE
C     TERMED A CONVERGENCE SUCESS.
C
      IF(XR-X)704,704,989
  989 IF(X-XL)704,704,988
  988 CONTINUE
      Y = F(X)
      ICNT = ICNT + 1
      DELTA = XR-XL
      IF (NPR)62,62,66
   66 WRITE(IE,701) ICNT,XL,YL,XR,YR,X,Y,DELTA
   62 CONTINUE
C
C     THIS TEST KEEPS XL AND XR BRACKETING THE ROOT
C
      IF(YL) 960,704,962
  960 IF(Y) 80,704,60
  962 IF(Y) 60,704,80
   60 XR = X
      YR = Y
      GO TO 90
   80 XL = X
      YL = Y
C
C     IF EPS TOLERENCE HAS NOT BEEN ACHIEVED THEN TRY AGAIN
C
   90 IF ( DELTA-EPS) 704,704,300
  704 CONTINUE
      IF(NPR)91,92,92
   92 WRITE(IE,93) XLI,XRI,XL,XR,ICNT
   91 CONTINUE
C
C     FOR DOUBLE PRECISION ALL E20.8 SHOULD BE CHANGED TO D20.8
C
   88 FORMAT(//38H THE SUBROUTINE BISEC DID NOT ACHIEVE ,E15.4,2X17H TOL
     1ERENCE AFTER ,I5,2X10HITERATIONS )
   93 FORMAT(//1X36HTHE INITIAL VALUES FOR XL AND XR ARE,2E20.8,/40H THE
     1 FINAL VALLE FOR THE ROOT IS BETWEEN,E20.8,5H AND ,E20.8,///,I5,27H
     2 ITERATIONS WERE PREFORMED )
  701 FORMAT(I4,7E16.8)
  903 FORMAT(1H19HITERATION3X2HXL14X2HYL14X2HXR14X2HYR15X1HX15X1HY12X5HX
     1R=XL///)
      RETURN
      END
      FUNCTION F(DELR)
      COMMONAC,AB,CC,BB
      F=(AB+DELR**2=AC)*(=1.+(1.+DELR)*ALOG((1.+DELR)/DELR))=CC+BB
      RETURN
      END
```

```
C          VISCOSITY SUBROUTINE, F=114
C
      SUBROUTINE VISC(TC,PC,MW,T,NU,RHOV,ZC)
C     T IN DEG R, NU IS IN FT*FT/HR
      REAL NU1,NU2
      REAL MW,MU,MUO,NU
      A=(TC/PC**4)**(1./6.)/SQRT(MW)
      MUO=.1777433E-04*T+.1974139E-02
      T=T/1.8
      RHOC=PC*MW/(.73*ZC*TC*1.8)
      TR=T/TC
      RHOR=RHOV/RHOC
      IF(RHOR.GE. .3) GOTO 3
      MU=(11.*EXP(1.584*RHOR)-11.)*1.E-05/A+MUO
      NU=MU*2.42/RHOV
      GOTO 4
3     MU=(23.12*EXP(1.079*RHOR)-25.)*1.E-05/A+MUO
      NU=MU*2.42/RHOV
4     CONTINUE
      T=T*1.8
      RETURN
      END
```

APPENDIX K

ORDER OF MAGNITUDE ANALYSIS

ORDER OF MAGNITUDE ANALYSIS

Due to the complexity of Equations (4) and (5), simplification is necessary. To perform the order of magnitude analysis an additional equation is necessary, continuity (11):

$$\frac{1}{r}\frac{\partial(rV_r)}{\partial r} + \frac{\partial V_z}{\partial z} = 0$$

Rewriting the momentum balance equations (4, 5)

$$\rho\left[\frac{\partial V_r}{\partial t} + V_r\frac{\partial V_r}{\partial r} + \frac{V_\theta}{r}\frac{\partial V_r}{\partial \theta} - \frac{V_\theta}{r} + V_z\frac{\partial V_r}{\partial z}\right] = -\frac{\partial p}{\partial z} + \rho g_r$$

$$+\mu\left[\frac{\partial}{\partial r}\left(1/r\,\frac{\partial(rV_r)}{\partial r}\right) + 1/r^2\,\frac{\partial^2 V_r}{\partial \theta^2} + \frac{2}{r^2}\frac{\partial^2 V_\theta}{\partial \theta^2} + \frac{\partial^2 V_r}{\partial z^2}\right] \qquad (4)$$

$$\rho\left[\frac{\partial V_z}{\partial t} + V_r\frac{\partial V_z}{\partial r} + \frac{V_\theta}{r}\frac{\partial V_z}{\partial \theta} \quad V_z\frac{\partial V_z}{\partial z}\right] = -\frac{\partial p}{\partial r}\,g_c + \rho g_z$$

$$+\mu\left[1/r\,\frac{\partial}{\partial r}\left(\frac{r\partial V_z}{\partial r}\right) + 1/r^2\,\frac{\partial^2 V_z}{\partial \theta^2} + \frac{\partial^2 V_z}{\partial z^2}\right] \qquad (5)$$

Some terms in (4) and (5) may be eliminated on physical grounds.

1) The gravitational terms can be omitted. There is no component of gravity in the z direction since the plate is horizontal. The maximum change in height in the z direction is roughly equal to the radiums hence the g_z term is negligible.

2) The terms involving V_θ can be deleted since there is no fluid motion in the θ direction or any force to induce a rotational motion. A manifestation of a rotational motion in the vapor field would be a rotation of the drop; none is observed experimentally.

3) Gradients of velocity in the θ direction are zero since there is azimuthal or angular symmetry. The flow in the r and z directions is the same no matter what angle θ they are viewed. If there were gradients in the θ direction there would be a net force to cause a lateral motion of the drop. The drop is assumed quiescent and lateral motion is usually only observed experimentally when the drop is disturbed by an external force.

4) The transient terms are assumed to be the same order of magnitude as the convective terms. There are no sudden pressure waves during the lifetime of the drop to cause a sudden acceleration.

5) The physical properties are treated as constant values evaluated as the mean of the values at each boundary.

Equations (4) and (5) can now be simplified as a result of the previous reasoning.

$$\rho\left[\frac{\partial V_r}{\partial t} + V_r\frac{\partial V_r}{\partial r} + V_z\frac{\partial V_r}{\partial z}\right] = -g_c\frac{\partial P}{\partial r} + \mu\left[\frac{\partial\left(1/r\,\frac{\partial(rV_r)}{\partial r}\right)}{\partial r} + \frac{\partial^2 V_r}{\partial z^2}\right] \qquad (52)$$

$$\rho\left[\frac{\partial V_z}{\partial t} + V_r\frac{\partial V_z}{\partial r} + V_z\frac{\partial V_z}{\partial z}\right] = -g_c\frac{\partial P}{\partial z} + \mu\left[\frac{1}{r}\frac{\left(\partial\, r\,\frac{\partial V_z}{\partial r}\right)}{\partial r} + \frac{\partial^2 V_z}{\partial z^2}\right] \qquad (53)$$

Equations (52) and (53) are still much too complex for an analytical solution. Further simplification can be effected by an order of magnitude analysis.

Referring to Figure 6, the boundary conditions for the flow beneath the drop may be written as follows:

1) $V_z = 0$ at $Z = \delta$

2) $V_r = V_z = 0$ at $Z = 0$

Consider V_r in boundary conditions 1 and 2. From the information either V_r is uniformly zero or goes through a maxima at some intermediate value of Z. Obviously, there is a maximum value of V_r, V_{rmax}, at some point on the velocity profile.

For convenience nondimensionalize equations (52) and (53) and the boundary conditions as below:

Velocity	Coordinates	Pressure	Time
$V_r/V_{rmax} = V_r^*$	$r/R = r^*$	$P^* = \frac{Pg_c}{\rho V_{rmax}^2}$	$\frac{tV_{rmax}}{R} = \theta$
$V_Z/V_{rmax} = V_Z^*$	$z/R = Z^*$		

Substituting these expressions into (52) and (53) and the boundary conditions yields:

Boundary Conditions:

$$V_r^* = 0 \text{ @ } Z^* = \delta/R = \delta^*$$

$$V_r^* = V_Z^* = 0 \text{ @ } Z^* = 0$$

Momentum:

$$\left[\frac{\partial V_r^*}{\partial \theta} + V_r^* \frac{\partial V_r^*}{\partial r^*} + V_z^* \frac{\partial V_r^*}{\partial z^*}\right] = -\frac{\partial P^*}{\partial r^*} + \frac{1}{R_e}\left[\frac{\partial \; 1/r^* \dfrac{\partial (r^* V_r^*)}{\partial r}}{\partial r} + \frac{\partial^2 V_r^*}{\partial z^{*2}}\right] \quad (52)$$

$$\left[\frac{\partial V_z^*}{\partial \theta} + V_r^* \frac{\partial V_z^*}{\partial r^*} + V_z^* \frac{\partial V_z^*}{\partial z^*}\right] = -\frac{\partial P^*}{\partial z^*} + \frac{1}{R_e}\left[\frac{1}{r^*} \frac{\partial \; r^* \dfrac{\partial V_r^*}{\partial r^*}}{\partial r^*} + \frac{\partial^2 V_z^*}{\partial z^{*2}}\right] \quad (53)$$

where $Re = \dfrac{RV_{rmax}\rho}{\mu}$

Continuity:

$$\frac{1}{r^*} \frac{\partial (rV_r^*)}{\partial r^*} + \frac{\partial V_Z^*}{\partial Z^*} = 0$$

Examining the continuity equation, assign an order of magnitude to the radial gradient as follows:

$$\frac{1}{r^*} \frac{\partial (r^* V_r^*)}{\partial r^*} \simeq 0(1) \text{ at point } r^* \text{ in the flow field}$$

This implies that

$$\frac{\partial V_z^*}{\partial Z^*} \simeq 0(1)$$

To find the magnitudes of V_r^* and V_z^* an approximate method can be used.

$$\frac{\partial V_z^*}{\partial z^*} \simeq \frac{dV_z^*}{dz^*} \simeq 0(1)$$

integrating

$$\int_0^{V_z^*} dV_z^* \simeq O(1) \int_0^{z^*} dz^*$$

$$V_z^* = O(1)\ z^*$$

The maximum value of z^* is δ^*, thus

$$V_z^* \simeq O(\delta^*)$$

Similarly for V_r^*

$$\frac{1}{r^*} \frac{\partial(r^* V_r^*)}{\partial r^*} \simeq \frac{1}{r^*} \frac{d(r^* V_r^*)}{dr^*} \simeq O(1)$$

Integrating

$$\int_0^{r^* V_r^*} (r^* V_r^*) = O(1) \int_0^{r^*} r^* dr^*$$

$$r^* V_r^* = O(1) \frac{r^{*2}}{2}$$

$$V_r^* = O(1) \frac{r^*}{2}$$

the maximum value of r^* is 1, thus

$$V_r^* \simeq O(1)$$

To find the magnitude of the gradient of V_r^* in the z direction the following approximation is necessary:

$$\frac{\partial V_r^*}{\partial z^*} \simeq \frac{\Delta V_r^*}{\Delta z^*} \times \frac{(V_r^*)_{max} - 0}{\delta^*/2 - 0} \simeq \frac{1-0}{\delta^*/2} \simeq 0(\frac{1}{\delta^*})$$

Similarly for the second derivative

$$\frac{\partial^2 V_r^*}{\partial z^{*2}} \simeq \frac{\Delta V_r^*}{(\Delta z^*)^2} \simeq \frac{(V_r^*)_{max} - 0}{(\delta^*/2 - 0)^2} \simeq \frac{1}{(\delta^*/2)^2} \simeq (\frac{1}{\delta^{*2}})$$

An integral approach can be used to find the following partials

$$\frac{\partial}{\partial r^*} (1/r^* \frac{\partial (r^* V_r^*)}{\partial r^*}) \simeq 0(x) \text{ where x is unknown}$$

Integrate

$$\int_0^{0(1)} (1/r^* \frac{\partial (r^* V_r^*)}{\partial r^*}) = 0(x) \int_0^{r^*} dr^*$$

$$0(1) - 0 = 0(x)\ r^*,\ r^* \simeq 0(1)$$

$$0(x) \simeq 0(1)/0(1) \simeq 0(1)$$

Similarly for the gradient of V_z^* in the z^* direction

$$\frac{\partial}{\partial z^*} (\frac{\partial V_r^*}{\partial z^*}) = \frac{\partial^2 V_z^*}{\partial z^{*2}} = 0(x)$$

Integrating

$$\int_0^{0(1)} d(\frac{\partial V_z^*}{\partial z^*}) = 0(x) \int_0^{\delta^*} dz^*$$

$$0(1) - 0 = 0(x)(\delta^* - 0)$$

$$0(x) \simeq 0(1)/\delta^* \simeq 0(1/\delta^*)$$

$$\frac{\partial^2 V_z^*}{\partial z^{*2}} \simeq 0(1/\delta^*)$$

To find the gradients of V_z^* in the r^* direction an integral approach is convenient.

$$\frac{\partial V_z^*}{\partial r^*} \simeq \frac{dV_z^*}{dr^*} \simeq 0(x)$$

Integrating

$$\int_0^{V_z^*} dV_z^* = 0(x) \int_0^{r^*} dr^*$$

$$V_z^* = 0(x)\ r^*$$

but $r^* \simeq 0(1)$ and $V_z^* \simeq 0(\delta^*)$, thus $0(x) \simeq 0(\delta^*)$

$$\frac{\partial V_z^*}{\partial r^*} = 0(\delta^*)$$

Similarly for the second partial

$$\frac{\partial}{\partial r^*} \left(r^* \left(\frac{\partial V_z^*}{\partial r^*} \right) \right) \simeq \frac{d}{dr^*} \left(r^* \frac{\partial V_z^*}{\partial r^*} \right) \simeq 0(x)$$

Integrating

$$\int_0^{r^*} \frac{\partial V_r^*}{\partial r^*}\, d\left(r^* \frac{\partial V_z^*}{\partial r^*}\right) = O(x) \int_0^{r^*} dr^*$$

$$r^* \frac{\partial V_z^*}{\partial r^*} = O(x)\ r^*$$

previously,

$$\frac{\partial V_z^*}{\partial r^*} \simeq O(\delta^*) = O(x)$$

thus

$$\frac{\partial}{\partial r^*}\left(r^* \frac{\partial V_z}{\partial r^*}\right) \simeq O(\delta^*)$$

The order of magnitude of all the terms in equations (52) and (53) have been determined. Simplification of (52) and (53) by the relative magnitude of term is as follows:

$$\frac{\partial V_r^*}{\partial \theta} + V_r^* \frac{\partial V_r^*}{\partial r^*} + V_z^* \frac{\partial V_r^*}{\partial z^*} = -\frac{\partial P^*}{\partial r^*} + \frac{1}{Re}\left[\frac{\partial}{\partial r^*}\left(1/r^* \frac{\partial (r^* V_r^*)}{\partial r^*}\right) + \frac{\partial^2 V_r^*}{\partial z^{*2}}\right] \quad (52)$$

$$O(1)\ O(1)\ O(1)\ O(\delta^*)\ O(1/\delta^*)\ O(\delta^{*2})\ O(1)\ O(1/\delta^{*2})$$

$$\frac{\partial V_z^*}{\partial \theta} + V_r^* \frac{\partial V_z^*}{\partial r^*} + V_z^* \frac{\partial V_z^*}{\partial z^*} = -\frac{\partial P^*}{\partial z^*} + \frac{1}{Re}\left[\frac{1}{r^*}\frac{\partial (r^* \partial V_z^*}{\partial r^*}\frac{}{\partial r^*}) + \frac{\partial^2 V_z^*}{\partial z^{*2}}\right] \quad (53)$$

$$O(\delta^*)\ O(1)\ O(\delta^*)\ O(1)\ O(\delta^*)\ O(\delta^2)\ 1/O(1)\ O(1/\delta^*)$$

From Equation (52) the viscous and inertial forces are of the same magnitude when

$$\frac{1}{Re} \simeq O(\delta^{*2})$$

(52) may be simplified by neglecting the inertial and transient terms on the L.H.S. and the radial gradient in the viscous term by their order of magnitude. Compared to (52) all the terms are $O(\delta^*)$ or less, hence negligible. The pressure gradient in the z direction $\partial P^*/\partial Z^*$ is of $O(\delta^*)$. The pressure increase which would be obtained by integrating (53) would be of $O(\delta^{*2})$, which is very small. Thus, the pressure in the direction normal to the plate is practically constant.

Equation (52) now becomes

$$\frac{dP^*}{dr^*} = \frac{1}{Re} \frac{\partial^2 V_r^*}{\partial z^{*2}} \text{ when } Re < 1/\delta^{*2} \tag{54}$$

with boundary conditions

$$V_r^* = 0 \text{ @ } Z^* = 0$$

$$V_r^* = 0 \text{ @ } Z^* = \delta^*$$

APPENDIX L

CONFIGURATION FACTOR ANALYSIS

CONFIGURATION FACTOR ANALYSIS

The unit sphere method, as presented by Weibelt (37) is used to determine the pointwise configuration factor on the surface of the drop. Consider the geometry of the drop and plate as illustrated in Figure 41. The unit sphere is placed at an arbitrary angle θ. By examining the unit sphere the pointwise configuration factor may be derived. Consider the unit sphere as seen in Figure 42. For the case under consideration the configuration factor for a differential area at angle θ is

$$F_{dA\rightarrow plate} = \frac{\text{Area of Darkened Portion Projected onto the Base of the Hemisphere}}{\text{Surface Area of Hemisphere Projected onto the Base of the Hemisphere}} \tag{55}$$

The projection onto the base of the hemisphere of the darkened portion is seen also in Figure 42. Equation (55) can be reduced to:

$$F_{dA\rightarrow plate} = \frac{\frac{1}{2}\pi(1)^2 + \frac{1}{2}(\text{Area of ellipse})}{\pi(1)^2} \tag{56}$$

where the area of an ellipse is

$$\text{Area} = \pi AB$$

A and B are the lengths of the semi-axes. Equation (52) may now be simplified to the following expression for the pointwise configuration factor:

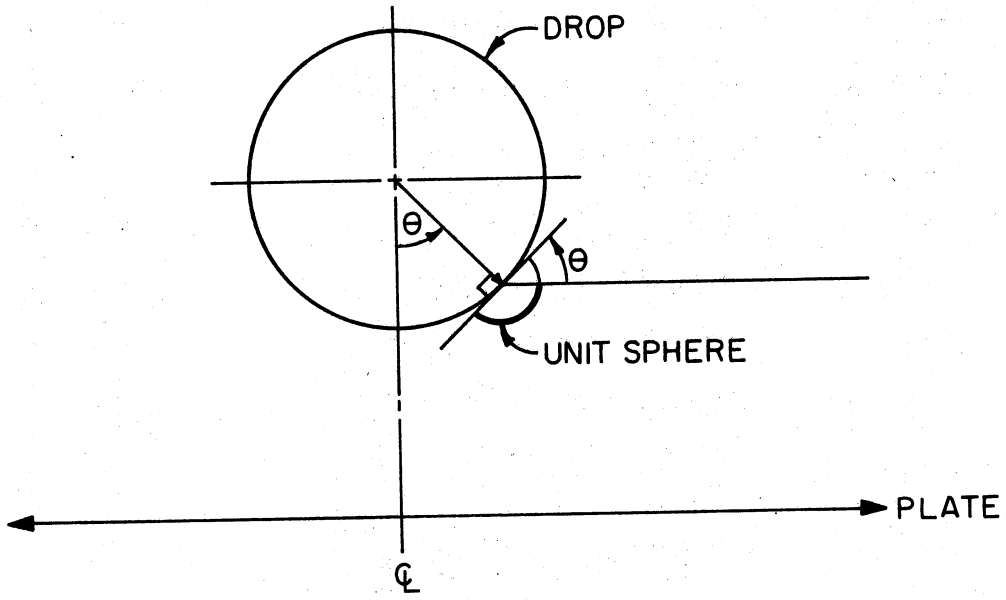

Figure 41. Unit Sphere

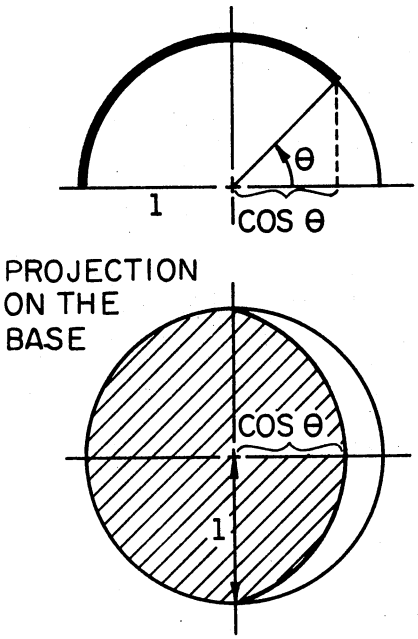

$$F_{dA \rightarrow Plate} = \frac{\text{surface area of hemisphere of darkened portion projected onto base of hemisphere}}{\text{surface area of hemisphere projected onto the base of the hemisphere}}$$

$$= \frac{1/2\,\pi(1)^2 + 1/2\,(\text{area of ellipse})}{\pi(1)^2}$$

$$\text{Area of Ellipse} = \pi A B$$

$$B \text{ \& } A = \text{lengths of semi-axes}$$

$$F_{dA \rightarrow Plate} = \frac{\pi/2 + \frac{\pi(1)(\cos\theta)}{2}}{\pi}$$

$$= \frac{1 + \cos\theta}{2}$$

Figure 42. Configuration Factor

$$F_{dA\rightarrow plate} = \frac{\pi/2 + \frac{\pi(1)(\cos\theta)}{2}}{\pi} = \frac{1 + \cos\theta}{2} \qquad (57)$$

A plot of equation (57) is seen in Figure 43. The average configuration factor over the top and bottom halves of the drop may be determined by the following procedure:

$$F_{A\rightarrow plate} = \frac{1}{A}\int_{A} F_{dA\rightarrow plate}\, dA \qquad (58)$$

where, $dA = 2\pi R^2 \sin\theta d\theta$.

The analysis for the bottom half of the drop is as follows:

$$F_{A1\rightarrow plate} = \frac{1}{2\pi R^2}\int_{0}^{\pi/2} \left[\frac{1+\cos\theta}{2}\right] 2\pi R^2 \sin\theta d\theta$$

$$= \tfrac{1}{2}\int_{0}^{\pi/2} \sin\theta d\theta + \tfrac{1}{2}\int_{0}^{\pi/2} \sin\theta\cos\theta d\theta$$

$$= .75$$

A similar analysis for the top half of the drop yields

$$F_{A1\rightarrow plate} = .25$$

where the limits of integration are from $\pi/2$ to π.

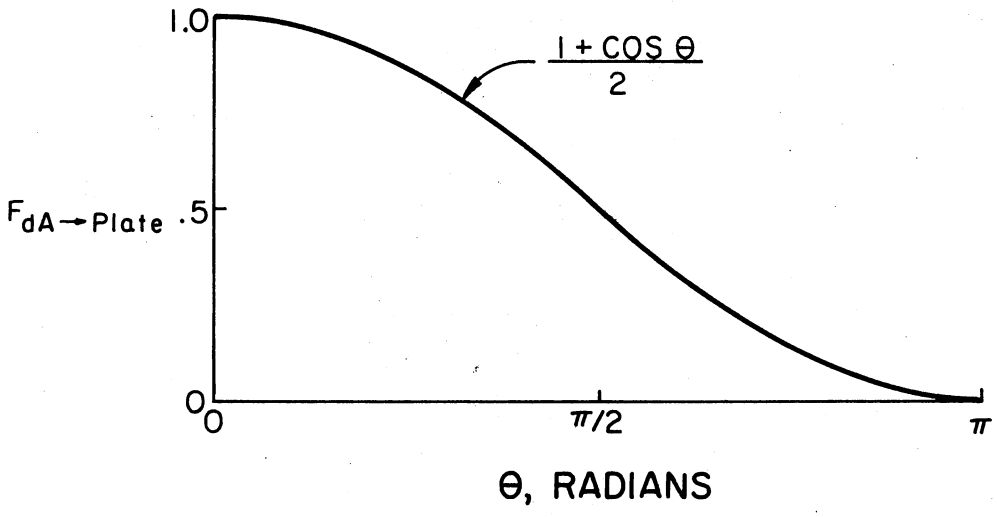

Figure 43. Average F Over Each Hemisphere

APPENDIX M

ERROR ANALYSIS

APPENDIX M

ERROR ANALYSIS

There are several possible sources of error that could affect the experimental observations. Errors in measuring the temperature and pressure in the cell have been minimized by calibrating the thermocouples and pressure gauges. These calibrations are found in Appendices H and I.

The movie camera was timed after each experimental run to determine the filming speed. The process consisted of filming an electric stop clock for a given period of time. The number of frames per second could then be calculated by measuring the elapsed time between a given number of frames.

Errors in measurement of drop diameters were minimized by using the Vanguard Motion Analyzer. The moveable cross hairs were readable to .001". Drop diameter measurements were taken in the x and y directions on the screen. The diameters determined in the x and y directions were obtained by differences which helps to reduce errors. The arithmetic average of these values were used in plotting the data to further eliminate errors.

The largest source of error in determining drop diameter histories was foreign material on the plate surface. A speck of material could penetrate the vapor film beneath the drop and alter the boiling mechanism. In the most dramatic cases the drop could be observed to "hang up" on a spot and rapidly disappear. This was usually a clue to the experimenter

that it was time to clean the surface again. Other times the behavior was not quite so noticeable, in which case, the deviant behavior could be observed in the diameter versus time plots. The curve would have the same general shape as the other drop curves except the deviant curve would appear to be shifted to the left of the plots. The only way to eliminate these bad points was to take data on several drops at a given plate temperature. Thus, a drop with suspicious behavior could be compared to other hopefully better behaved drops.

The other source of experimental error of drop diameter histories was determination of the end of a drop's lifetime. During the filming the drop was observed by the experimenter through a telescope. When the drop had totally evaporated the camera was shut off as an indication of the death of a drop. Reaction time of the observer and inertia of the camera mechanism would cause the filming to go slightly past the end of the drop's lifetime. When the film was analyzed, the drop's death could be detected to within three frames. Thus, the uncertainty in the drop lifetime can be expressed as

$$\Delta t = 3/(\text{frames per second}), \text{ sec}$$

At the lowest filming speed of 12 fps for F-114, the uncertainty, Δt, would be 1/4 second. The lower film speeds were used at low pressure where the drop lifetimes were relatively long. At the critical region, film speeds of 64 fps were used since lifetimes were short. This yields an uncertainty of approximately 1/20 of a second, which is small compared to the drop's lifetime.